University of Southampton

Faculty of Medicine

Clinical and Experimental Sciences

Mechanism of Triterpenoid Saponin Mediated Augmentation of Saporin Based Immunotoxin Cytotoxicity

DOI: 10.5258/SOTON/D1148

by

Harrison James Wensley

ORCID ID 0000-0002-9634-5462

Thesis for the degree of Doctor of Philosophy

December 2019

University of Southampton

Abstract

Faculty of Medicine

Clinical and Experimental Sciences

Thesis for the degree of Doctor of Philosophy

Mechanism of Triterpenoid Saponin Mediated Augmentation of Saporin Based Immunotoxin Cytotoxicity

Harrison James Wensley

Immunotoxins are hybrid molecules comprised of a protein toxin molecule and a monoclonal antibody that selectively delivers the toxin to antigen expressing cells. These therapeutics are under investigation as agents for the treatment of cancers, but their clinical development has been hampered by a number of off-target, dose limiting toxicities particularly vascular leak syndrome. A number of plant derived triterpenoid saponins significantly augment the cytotoxicity of saporin based immunotoxins, possibly by increasing the endolysosomal escape of the toxin into the cytosol. This would have the effect of quantitatively increasing toxin availability to target ribosomes whilst avoiding its degradation by lysosomes. This may help to widen the therapeutic window of immunotoxin therapy.

The primary objective of the work presented in this thesis was to investigate the mechanism(s) by which saponin augments immunotoxin cytotoxicity against lymphoma and leukaemia cells. The work focuses primarily on the potential roles that different endocytic processes and the endolysosomal escape of the immunotoxin into the cytosol play in the augmentation process. The work in this thesis presents evidence for the possible involvement of various endocytic pathways in saponin mediated augmentation of immunotoxin cytotoxicity and suggests that an acidic endolysosomal lumen is a requirement for augmentation. Also presented is evidence that membrane repair processes are not involved in the augmentation of immunotoxin cytotoxicity.

Part of this thesis describes the development of a novel flow cytometric method to measure the endolysosomal escape of a fluorescently labelled immunotoxin into the cytosol. This assay revealed that treatment of target cells with saponin increased the endolysosomal escape of the immunotoxin into the cytosol and allowed a quantitative assessment of the effects of pharmacological inhibitors of endocytic processes on this escape. The effect of these agents on the saponin mediated endolysosomal escape of the immunotoxin correlated with their effect on the augmentation of immunotoxin cytotoxicity by saponin. This offers further evidence that endolysosomal escape is at least one of the mechanisms by which augmentation occurs.

Table of Contents

Table of Tables

Table of Figures

Table of Figures

List of Accompanying Materials

Dataset DOI: 10.5258/SOTON/D1148

Research Thesis: Declaration of Authorship

Print name:	HARRISON JAMES WENSLEY
Title of thesis:	Mechanism of Triterpenoid Saponin Mediated Augmentation of Saporin Based Immunotoxin Cytotoxicity

I declare that this thesis and the work presented in it are my own and has been generated by me as the result of my own original research.

I confirm that:

1. This work was done wholly or mainly while in candidature for a research degree at this University;
2. Where any part of this thesis has previously been submitted for a degree or any other qualification at this University or any other institution, this has been clearly stated;
3. Where I have consulted the published work of others, this is always clearly attributed;
4. Where I have quoted from the work of others, the source is always given. With the exception of such quotations, this thesis is entirely my own work;
5. I have acknowledged all main sources of help;
6. Where the thesis is based on work done by myself jointly with others, I have made clear exactly what was done by others and what I have contributed myself;
7. Parts of this work have been published as:-

Smith W, Johnston D, Holmes S, **Wensley H**, Flavell S, Flavell D. Augmentation of Saporin-Based Immunotoxins for Human Leukaemia and Lymphoma Cells by Triterpenoid Saponins: The Modifying Effects of Small Molecule Pharmacological Agents. Toxins. Multidisciplinary Digital Publishing Institute; 2019 Feb;11(2):127–21.

Wensley H, Johnston D, Smith W, Holmes S, Flavell S, Flavell D. A Flow Cytometric Method to Quantify the Endosomal Escape of a Protein Toxin to the Cytosol of Target Cells. Pharmaceutical Research. (Accepted for Publication Oct 2019)

Signature: Date:

Acknowledgements

This research would not have been possible without the generous contribution of Leukaemia Busters. I would like to gratefully acknowledge the funding received through the charity which has allowed me to undertake this PhD.

To my supervisor Dr David Flavell, I would like to express my gratitude for providing me with the opportunity to be involved with this study. Thank-you for your continuous support over the last three years of research and the writing of this thesis. Your encouragement and guidance have been invaluable. Thanks also to Dr Andrew Walls for his role as co-supervisor, your outside perspective on this work was greatly appreciated.

I would like to thank my colleagues in the Simon Flavell Leukaemia Research Unit, Dr Wendy Smith, Suzanne Holmes and Dr Bee Flavell for their teaching, assistance and comments. Thank-you for your patience when listening to my ideas, our discussions have been immensely helpful throughout this project.

To Dr David Johnston, Dr Elizabeth Angus and the other staff at the BIU, I am grateful for you sharing your experience with me. Thank-you for going above and beyond to help with all the out-of-hours imaging and troubleshooting my experiments.

To my parents, thank-you for always having faith in me, even when I didn't have it myself. Your support, not just for the last few years, but throughout my life has been amazing and this would not have been possible without you.

Finally, to Katherine, you are the best thing that ever happened to me. Thank-you for your patience and understanding, and for being there for me when I needed it.

Definitions and Abbreviations

a2MR	Alpha-2 Macroglobulin Receptor
ACT	Adoptive Cell Therapy
ADC	Antibody Drug Conjugate
ADCC	Antibody Dependent Cell-mediated Cytotoxicity
AF488	Alexa Fluor 488
ALL	Acute Lymphoblastic Leukaemia
AOP1	Anti-oxidant Protein 1
BCA	Bicinchoninic Acid
BiTEs	Bispecific T Cell Engagers
BSA	Bovine Serum Albumin
BsAb	Bispecific Antibody
CAR	Chimeric Antigen Receptor
CFD10	Ca^{2+} Depleted D10
CLL	Chronic Lymphocytic Leukaemia
CME	Clathrin Mediated Endocytosis
CRS	Cytokine Release Syndrome
D10	DMEM supplemented with 10% FCS and 2 mM glutamine and 2 mM sodium pyruvate
DHE	Dehydroergosterol
DMEM	Dulbecco's modified Eagle's Medium
DT	Diphtheria Toxin
DTA	Diphtheria Toxin A Chain
DTT	1,4-Dithiothreitol
EC_{50}	50% Maximum Effective Concentration
EF2	Elongation Factor 2
EGTA	Ethylene glycol-bis(β-aminoethyl ether)-*N*,*N*,*N*',*N*'-tetraacetic acid
EGF	Epidermal Growth Factor
EGFR	Epidermal Growth Factor Receptor
EIPA	Ethylisopropylamiloride
ELISA	Enzyme-Linked Immunosorbent Assay
ERAD	Endoplasmic Reticulum-associated protein degradation
ETA	Pseudomonas Exotoxin A
FCS	Foetal Calf Serum

FITC	Fluorescein isothiocyanate
FITC-H	Pulse Height of the signal recorded by a 525/40 nm bandpass filter
FITC-W	Pulse Width of the signal recorded by a 525/40 nm bandpass filter
FSC	Forward Scatter
HCL	Hairy Cell Leukaemia
HER2	Epidermal Growth Factor Receptor 2
HPLC	High Performance Liquid Chromatography
HRP	Horseradish Peroxidase
IL-2	Interleukin 2
IP	Isoelectric Point
IT	Immunotoxin
LAK	Lymphokine Activated Killer Cells
LMP	Lysosomal Membrane Permeabilisation
mAb	Monoclonal Antibody
MEND	Massive Endocytosis
MFI	Mean Fluorescence Intensity
MHC	Major Histocompatibility Complex
MVB	Multivesicular Body
MWCO	Molecular Weight Cut Off
NHE1	Na^+/H^+ Exchanger
NHL	Non-Hodgkin's Lymphoma
NK cell	Natural Killer Cell
OKSAP-AF	Alexa Fluor 488 conjugated OKT10-SAP
PARP	Poly(ADP-ribose) polymerase
PBS	Phosphate Buffered Saline
PE	Phycoerythrin
PI	Propidium Iodide
PMS	Phenazine-methosulphate
PRIT	Pre-Targeted Radioimmunotherapy
RIP	Ribosome Inactivating Protein
R10	RMPI-1640 medium supplemented with 10% FCS and 2 mM glutamine and 2 mM sodium pyruvate
ROS	Reactive Oxygen Species
RPMI	Roswell Park Memorial Institute Medium
RTA	Ricin A-chain
SA	Saponinum Albumin

SA2E	Saporin-adapter- Epidermal Growth Factor
SAP-AF	Saporin-Alexa Fluor 488
SAPK	Stress Activated Protein Kinases
scFv	Single Chain Variable Fragment
SDS-PAGE	Sodium Dodecyl Sulphate-Polyacrylamide Gel Electrophoresis
SE	Saporin-Epidermal Growth Factor
SEM	Scanning Electron Microscopy
SLO	Streptolysin O
SPR	Surface Plasmon Resonance
SSC	Side Scatter
TCR	T-Cell Receptor
TEM	Transmission Electron Microscopy
TIL	Tumour Infiltrating Lymphocytes
TT	Targeted Toxin
VEGF	Vascular Endothelial Growth Factor
VLS	Vascular Leak Syndrome
XTT	2,3-Bis-(2-Methoxy-4-Nitro-5-Sulfophenyl)-2H-Tetrazolium-5-Carboxanilide

Chapter 1 Introduction

1.1 Advances in Cancer Therapy

Chemotherapeutic agents for the treatment of cancers were first discovered in the 1940s with the introduction of nitrogen mustard[1]. Since then great progress has been made in the development of a range of potent, small-molecule anticancer drugs. These include alkylating agents, anti-metabolites, anti-microtubule agents and anti-tumour antibiotics[2]. These agents act systemically to disrupt the cell cycle and are particularly cytotoxic in rapidly dividing cells such as tumour cells. Alongside surgical excision and radiotherapy, chemotherapy is a central pillar of cancer therapy and plays a major role in the treatment of haematological malignancies and primary or metastatic cancers. However, despite decades of research most of these drugs are non-specifically toxic and also affect non-cancerous, rapidly dividing cells. This gives them a narrow therapeutic window and results in side effects which limit their efficacy. The requirement for prolonged treatment at lower dose levels can also lead to the development of resistance.

In recent years there have been exciting advances in two areas of cancer therapy, targeted therapy and immunotherapy. Immunotherapy involves the stimulation and targeting of the patients own immune response to clear tumours. These can involve cancer vaccinations, cell-based therapies such as chimeric antigen receptor (CAR) T cells and the use of monoclonal antibodies (mAb) in immune checkpoint inhibition[3]. Targeted therapy involves the specific targeting of tumour cells with reduced effects upon normal tissues. These include tyrosine kinase inhibitors such as imatinib[4], which inhibit the deregulated protein kinases involved in the proliferation of certain cancers, and mAb therapies. A brief review of CAR-T cell and mAb therapeutics is presented here.

1.1.1 CAR-T Cells

CAR-T cell therapy is a form of adoptive cell therapy (ACT) where immune cells are taken from the patient, expanded *in vitro* and then reinfused back into the patient to improve the immune response to a tumour. Early successes with ACT came with the use of lymphokine activated killer (LAK) cells, cytotoxic effector lymphocytes activated in the presence of interleukin-2 (IL-2), in patients with metastatic melanoma, colon cancer and renal cell carcinoma[5]. The identification of a subpopulation of tumour antigen-specific T cells isolated from within tumours offered increased therapeutic potency. These cells, known as tumour infiltrating lymphocytes (TIL) were extracted from a patient's excised tumour and expanded in IL-2 before being injected back into

the patient[6]. Trials with TILs have shown promising responses in patients with metastatic melanoma[7].

The aim behind the development of CAR-T cells was to combine the effector functions of T cells with the antigen targeting specificity and greater affinity of an antibody[8]. Autologous T cells are extracted from the patient and isolated by leukapheresis. These cells are genetically modified by viral or non-viral methods to express the CAR, expanded and then infused back into the patient. The CAR consists of an extracellular antigen-binding single chain variable fragment (scFv), a fusion of the variable heavy (V_H) and light (V_L) chains of a humanized monoclonal antibody, connected via a peptide spacer to an intracellular signaling domain responsible for T cell activation. In the first generation of CAR-T cells the intracellular domain was composed of the T-cell receptor (TCR) CD3-ζ fragment which is sufficient to activate downstream signalling pathways[9]. Whilst the signal strength from CD3-ζ alone was enough to stimulate lytic activity it was insufficient to drive a cytokine response, patients were given exogenous IL-2[10], or to elicit T cell expansion. As a result, the persistence of first-generation CAR-T cells was poor in most patients[11]. The second generation of CAR-T cells incorporated a co-stimulatory molecule such as CD28 or 4-1BB into the intracellular domain which improved the proliferation, cytotoxicity and lifespan of the cells[12] [13]. Third generation CAR-T cells have combined multiple signaling domains but have not yet demonstrated improved patient outcomes over second generation CAR-T cells[14]. CARs allow T cell recognition of surface bound antigens without the need for processing and presentation via the major histocompatibility complex (MHC). This enables recognition of a wider range of target antigens including carbohydrate and glycolipid structures and, by bypassing MHC class restriction, means that $CD4^+$ and $CD8^+$ CAR-T cells can be recruited[15]. Removing the requirement for MHC presentation also means that CAR-T cells are not affected by tumour cell MHC depletion.

The clinical efficacy of CAR-T cells has so far been demonstrated most in haematological malignancies. Trials of anti-CD19 CAR-T cells in Acute Lymphoblastic Leukaemia (ALL), Chronic Lymphocytic Leukaemia (CLL) and B-cell Non-Hodgkin's Lymphoma (NHL) have shown high rates of complete remission[16-18]. Reduced levels of success have been seen in solid tumours. This is likely due to the immunosuppressive microenvironment of the tumour, tumour heterogeneity, poor infiltration of CAR-T cells into the tumour and loss of target antigens[19,20]. The problem of antigen loss and the development of tumour escape variants has also been observed in leukaemias treated with anti-CD19 CAR-T cells. CD19 epitope loss is estimated to occur in 10-20% of pediatric B-cell ALL patients resulting in resistant tumour populations[21,22]. The use of CAR-T cell therapy has also been limited by a number of potentially severe toxicities. The most common of these are cytokine release syndrome (CRS) and a range of neurotoxicities[23].

1.1.2 Monoclonal Antibody Therapies

The development of monoclonal antibody (mAb) therapies to selectively target cancer hopes to realise Paul Ehrlich's concept of a ''magic bullet'', conceived over 100 years ago[24,25]. This was initially made possible by the production of mAbs by hybridomas[26]. These antibodies were murine in nature and their clinical utility was limited by their immunogenicity and poor immune effector recruitment in humans[27,28]. The subsequent development of humanisation processes[29] that graft murine variable domains or complementarity determining regions onto human IgG produced chimeric or humanised antibodies respectively. Incorporating a human Fc domain, these antibodies have largely overcome the problems that were initially encountered with murine mAb.

MAb therapies have been developed to act on a range of therapeutic targets. MAbs can target tumour specific antigens in order to effect cell death or block the activity of growth factors. They can also be used to target the more general tumour microenvironment or immune cells to combat tumour induced immunosuppression via immune checkpoint blockade. Modified antibodies including bispecific antibodies and antibody conjugates further expand their potential therapeutic effects.

1.1.2.1 Cytotoxicity of Tumour Cells

By targeting tumour cell specific surface antigens mAbs present the opportunity for a therapy that can specifically target and kill cancer cells with minimal systemic toxicity. The therapeutic effect of these antibodies is primarily exerted by engaging immune effectors. Antibody-dependent cellular cytotoxicity (ADCC), antibody dependent cell phagocytosis (ADCP) [30], complement-dependent cytotoxicity (CDC) and complement-dependent cell mediated cytotoxicity have all been implicated in the immune response to these mAbs [31-33].

For ADCC mediated immunotherapy, the binding of IgG mAb to surface antigens enables the targeting of innate immune effector cells including: Natural killer (NK) cells, macrophages and neutrophils to kill tumour cells. Of these, NK cells are the primary ADCC effectors and kill their target cells via exocytosis of cytotoxic granules containing perforin and granzymes or via the engagement of death receptors on the target cell, such as Fas, resulting in apoptotic cell death[34].

ADCC is activated by the interaction of bound mAbs to Fc receptors on effector cells. Fc receptors include the high affinity FcγRI (CD64) and lower affinity FcγRIIa (CD32a), FcγRIIc (CD32c) and FcγRIIIa (CD16a). Multiple FcγR are expressed by macrophages, neutrophils, eosinophils and

dendritic cells, although FcγRIIc is only expressed in 7-15% of the population[35,36]. FcγRIIIa is the key receptor activating NK cells [37-39]. ADCC has been demonstrated to play a role in the anti-tumour activities of the anti-CD20 mAb rituximab, used in the treatment of Non-Hodgkin's lymphoma and CLL and of trastuzumab which targets anti-HER2/neu for the treatment of breast cancer[40-42].

ADCP has been shown to be a major mechanism by which macrophages contribute to the anti-tumour effect of mAbs [30]. Gül et al used intravital imaging of a murine melanoma model to demonstrate that mAb opsonised tumour cells were phagocytosed by Kupffer cells [43]. This phagocytosis was shown to be dependent on FcγRI. ADCP has been shown to be a contributing factor to the effector mechanisms of a number of therapeutic antibodies against a range of antigenic targets [30], including anti-CD20 rituximab [44,45].

In addition to the activation of cellular effectors, IgG molecules also activate the classical complement pathway. This effect is highly dependent on the IgG isotype. IgG3 shows the greatest complement fixing activity, followed by IgG1 and IgG2, with IgG4 being unable to fix complement [46,47]. Surface bound IgG recruits C1q to its Fc domain, initiating the complement cascade that results in the formation of the membrane attack complex and subsequent lysis of the tumour cell. Complement cascades also produce the chemotactic agents C3a and C5a which help recruit leukocytes to the tumour location[48]. CDC plays a role in the clinical efficacy of many mAb including rituximab[49,50].

In the absence of immune effector mechanisms some mAbs have been shown to be capable of cytotoxic activity. A number of *in vitro* studies with malignant B-cell lines demonstrate that rituximab and other anti-CD20 antibodies can induce apoptosis[51,52]. Binding of rituximab to CD20 leads to cross-linking and activation of protein tyrosine kinases. These in turn activate phospholipase Cγ (PLCγ) resulting in Ca^{2+} release from the endoplasmic reticulum, activation of caspase 3 and initiation of apoptosis.

1.1.2.2 Ligand Binding and Signal Blockade

Members of the epidermal growth factor receptor (EGFR) family are often overexpressed in solid tumours. These tyrosine kinases are important for cell growth and their upregulation can be critical for abnormal proliferation of malignant cells. The anti-EGFR mAb cetuximab is used for the treatment of metastatic colorectal cancer. Cetuximab binding to the EGFR extracellular domain prevents binding of its activating ligands and promotes EGFR internalisation[53,54]. Blockade of EGFR signalling in this way results in cell cycle arrest in G1[55].

Another member of the EGFR family, HER2, is overexpressed in 20-30% of breast cancers and is associated with poor clinical outcomes[56]. HER2 has no known ligands and is instead activated by receptor homo- or hetero-dimerisation leading to its autophosphorylation and the subsequent triggering of several downstream pathways including the PI3K/Akt regulator of cell growth and survival. The anti-HER2 mAb trastuzumab can interfere with HER2 dimerisation and trigger receptor internalisation and degradation. This inhibits PI3K/Akt and MAPK pathways and leads to cell cycle arrest and a reduction in cell growth[57].

1.1.2.3 Targeting the Tumour Microenvironment

The specific, targeted nature of mAbs means that they can also be used to target aspects of the tumour microenvironment. An example that has made its way into clinical practice revolves around tumour angiogenesis. Many solid tumours secrete vascular endothelial growth factor (VEGF) in response to hypoxia[58]. VEGF binds to its receptor on the vascular endothelium to stimulate new blood vessel growth and its upregulation is associated with poorer prognosis. The mAb Bevacizumab selectively binds to circulating VEGF and prevents it binding to its receptor. This reduces the growth of blood vessels into the tumour limiting its blood supply[59]. As a tumouristatic agent, Bevacizumab is approved for combination use with chemotherapy in a number of solid tumours including metastatic colon cancer[60,61].

1.1.2.4 Targeting the Immune System: Immune Checkpoint Blockade

The aim of immune checkpoint blockade is the removal of inhibitory signals that regulate T cell activation and are responsible for T cell exhaustion. This enhances the patient's own T cell mediated anti-tumour responses[62]. Two immune checkpoint receptors have so far been targeted by clinical therapies, CTLA4 and PD-1. The first immune checkpoint inhibitor, ipilimumab, which targets the T cell negative costimulatory molecule CTLA4, was approved by the FDA in 2011 for the treatment of metastatic melanoma. Since then, a number of immune checkpoint blockade therapies targeting the PD-1/PD-L1 system have been approved for a range of different cancer types.

CTLA4 is upregulated to the T cell membrane in response to T-cell receptor stimulation[63]. Here it competes with the positive co-stimulatory molecule CD28 for its ligands on antigen presenting cells; B7-1 (CD80) and B7-2 (CD86)[64]. CTLA4 binds with a higher affinity and avidity to these ligands than CD28[65]. By competing with CD28, CTLA4 reduces its activation of downstream signalling via PI3K and AKT[66,67] and therefore attenuates the effect of CD28 on T cell activation. CTLA4 is crucial for tolerance and the regulation of T cell activation. This is

demonstrated in Ctla4 knockout mice which exhibit massive and lethal lymphoproliferation [68,69]. CTLA4 primarily exerts its immunosuppressive effect via synergistic downregulation of $CD4^+$ helper T cells and activation of regulatory T cell activity[70]. Blockade of CTLA4 by the humanised antibody ipilimumab prevents its binding to B7[71] and enables CD28 positive co-stimulation allowing for increased effector T cell activation. Ipilimumab treatment also results in a depletion of intratumoural regulatory T cells[72] and this combination of effects leads to an enhancement of T cell anti-tumour activity. Ipilimumab treatment has shown significant improvements in overall survival in patients with metastatic melanoma[73].

In contrast to CTLA4, PD-1 acts primarily in the periphery to regulate local T cell responses and minimise tissue damage[74,75]. PD-1 expression is induced in T cells upon their activation[76]. Its ligands, PD-L1 and PD-L2 are widely expressed in non-lymphoid tissues in response of IFN-γ and act to inhibit T cell activation[77,78]. Activation of PD-1 by its ligands directly inhibits T cell activation by recruitment of the phosphatase SHP2 which dephosphorylates CD28 and inactivates its signaling [79,80]. Persistent PD-1 signaling leads to T cell exhaustion via metabolic restriction[81], resulting in poor effector function and preventing tumour clearance[82].

There are currently six FDA approved PD-1/PD-L1 axis inhibitors: pembrolizumab, nivolumab and cemiplimab target PD-1 whilst atezolizumab, avelumab and durvalumab target PD-L1. Agents are approved for a range of tumour types including melanoma, non-small cell lung cancer, renal cell carcinoma and Hodgkin's lymphoma[83]. PD-1/PD-L1 axis blockade prevents activation of the downstream negative signaling pathway and can lead to the reinvigoration of subsets of the exhausted T cell population[84] re-enabling immune mediated anti-tumour responses.

Both CTLA-4 and PD-1 blockade are associated with a number of inflammatory side effects known as immune-related adverse events[85,86]. These events can affect a wide variety of different organs and include colitis, hepatitis, pneumonitis and dermatitis. It is thought that these events are related to the mechanism of action of these drugs. By blockading inhibitory signals which play an important role in immune tolerance and T-cell regulation, these therapies may increase the opportunity for autoimmune response in normal tissues.

The distinct mechanisms by which CTLA4 and PD-1 inhibit T cell activation allows for synergistic combination treatment. Blockade of both pathways results in improved therapeutic efficacy compared to individual therapies[87,88]. A recent 4 year follow up to a phase III trial in advanced melanoma reported a 53% overall survival rate for a combined ipilimumab and nivolumab therapy[89]. However, the use of combination therapy has been shown to increase the likelihood

of patients developing immune-related adverse events which may lead to the discontinuation of treatment [90,91].

1.1.2.5 Bispecific T cell Engagers

Bispecific antibodies possess two distinct variable regions each targeting a different antigen. By simultaneously targeting epitopes on tumour and immune cells, bispecific antibodies can direct the effector function of NK cells, macrophages and T cells. Those that target T cells are known as Bispecific T cell engagers (BiTEs) [92]. BiTEs enable T cell activation without the requirement for TCR-MHC interaction. This allows activation of T cells even in the face of MHC downregulation, a common mechanism of tumour cell immune escape and means that T cell immune responses are no longer dependent on the generation of specific T cell clones. BiTEs have been shown to activate both $CD8^+$ cytotoxic T cells and $CD4^+$ cells, in which there is upregulation of granzyme B[93]. Clinical success has been seen with the CD19/CD3 BiTE blinatumomab in the treatment of non-Hodgkin's lymphoma and ALL[94,95].

1.1.2.6 Antibody Conjugates

There is now a well described stable of naked antibodies against defined targets such as CD20 that exert cytotoxicity against antigen expressing target cells. However, many naked antibodies lack any obvious cytotoxic activity. Malignant cells are often resistant to apoptosis and immunocompromised patients lack the necessary competent immune effectors for effective treatment. This has been a major limiting factor in their development[96]. One way to confer on or potentially improve on the therapeutic action of mAbs is to directly link them to a radioisotope, cytotoxic drug or protein toxin. These conjugates offer the specificity of an antibody but aim to provide a greater potency.

Radioimmunoconjugates, consist of a mAb conjugated with a radioisotope such as yttrium 90. These aim to deliver a high dose of radiation directly to a tumour with minimal off target toxicities. Trials with radioimmunoconjugates showed impressive results in B-cell lymphomas including good responses in non-Hodgkin lymphoma patients that did not otherwise respond to unconjugated antibodies or chemotherapy [97,98]. Two radiolabelled antibodies have received FDA approval but have not found widespread use in clinical practice due to requirements for specialists in nuclear medicine to administer the therapy and concerns about dose limiting toxicities including prolonged myelosuppression [99,100]. More recently, advancements in pre-targeted radioimmunotherapy (PRIT), which offers improvements in therapeutic index, hope to overcome these problems. PRIT involves a multistage delivery of reagents, starting with administration of a bispecific antibody or an antibody-streptavidin conjugate. This antibody is

given 24-48 hours to accumulate in the tumour before a radionucleotide containing chelating agent is given. With bispecific antibodies, one chain recognises a tumour specific antigen whilst the other targets the chelating agent. For antibody-streptavidin conjugates the chelating agent is biotinylated. This process allows for the slow distribution of the antibody to be completed before administration of the small radionucleotide which is distributed much more rapidly before being trapped by its association with the antibody. Unbound radioactive reagents are quickly cleared via the urine reducing off-target toxicities[98,100,101].

Monoclonal antibodies conjugated to cytotoxic drugs are termed antibody-drug conjugates (ADCs). The antibody enables localisation of the drug to the tumour, reducing its off-target effects and allowing the delivery of more potent drugs that could not normally be used systemically without severe side effects [102,103]. The cytotoxic domain of the majority of ADCs approved and in development are anti-tubulins which prevent microtubule organisation and bring about cell death by mitotic arrest[104]. A whole range of ADCs utilising different cytotoxic payloads have been or are being developed [103,105]. The developmental predecessors to these ADCs are immunotoxins (ITs) where the mAb is instead conjugated to a protein toxin. These were first described in 1970 by Moolten and co-workers[106] and have undergone a great deal of development since then. Immunotoxins are part of a wider group of targeted anticancer therapies utilising protein toxins known as targeted toxins.

1.2 Targeted Toxins

Targeted Toxins open up the possibility of a highly tumour specific and potent cancer therapy. These are hybrid molecules comprised of two parts, a protein toxin molecule with enzymatic activity and a cell binding domain such as a cytokine, growth factor or an antibody (Immunotoxin) responsible for targeting the toxin to tumour associated or specific antigens. Targeted toxins offer several advantages over ADCs. They do not rely on disrupting mitosis and are therefore able to effectively kill slowly or non-dividing cells. Because their method of toxicity is different from other forms of chemotherapy they have little cross-resistance with other cytotoxic agents and could be combined with standard therapy for potential synergy.

Essential to the development of any targeted toxin is the identification of an appropriate target antigen. Unlike naked mAb therapies that in some instances partly rely on ADCC, antibodies used as a part of an IT need to bind to an antigen that is rapidly endocytosed into an appropriate intracellular compartment after ligand binding. To improve the specificity and therapeutic efficacy of the targeted toxin the target antigen should be one over-expressed by the cancer cell and expressed at low levels or not at all by normal life sustaining tissues.

The majority of developed targeted toxins incorporate either bacterial toxins such as pseudomonas exotoxin A (ETA) or diphtheria toxin (DT) , or plant derived ribosome inactivating protein (RIPs) toxins such as saporin or ricin A chain[107]. These toxins act to irreversibly arrest protein synthesis, though bacterial and plant derived toxins do so by different mechanisms. This review will focus mainly on targeted toxins incorporating the RIP saporin, though some brief consideration will be given to others.

1.2.1 Bacterial Toxins

The bacterial toxins ETA and DT enzymatically ADP-ribosylate the histidine-699 of elongation factor 2 (EF2) [108,109]. This inhibits its activity and thus halts protein synthesis at the elongation step. Bacterial toxins fall outside the scope of this work and will not be discussed further in this thesis, for a recent review on their use in targeted toxins see Zahaf et al[110].

1.2.2 Ribosome Inactivating Proteins

Ribosome inactivating proteins are a group of cytotoxic proteins initially identified in plants and thought to be involved in defence against viral attack. RIPs are produced by a large number of different plant species, both mono- and di-cotyledons. Prominent examples include abrin (*Abrus precatorius*), agrostin (*Agrostemma githago*), dianthin (*Dianthus caryophyllus*), gelonin (*Gelonium multiflorum*), saporin (*Saponaria officinalis*) and ricin (*Ricinus communis*)[111]. Other RIPs including Shiga toxins are produced by pathogenic bacteria as a virulence factor[112].

All RIPs possess an N-glycosidase activity (EC 3.2.2.22) which enzymatically cleaves a specific adenine (A^{4324}) from the highly conserved alpha-sarcin/ricin loop, a GAGA tetranucleotide loop, located in the 28S ribosomal RNA [113,114]. This depurinates the 60S ribosomal subunit and prevents its interaction with the elongation factor EF-2 [115]which is required for translocation of the tRNA between the A-site and the P-site of the ribosome. This permanently blocks translation and a single molecule of ricin is capable of inactivating over a thousand ribosomes per minute[116] leading to severe disruption of protein synthesis and subsequent cell death[117].

Whilst it is this inhibition of protein synthesis that is considered to be the principle mechanism behind the cytotoxicity of RIPs, many of these toxins have also demonstrated the ability to induce cell death by apoptosis[118-121]. This has been shown to occur via the intrinsic pathway [120,122] and involves activation of caspase 9 and caspase 3. Inhibition of caspase 3 in cells exposed to saporin inhibited apoptosis demonstrating the caspase-dependency of saporin induced cytotoxicity[123]. The same group also showed that the initiation of apoptosis in

response to an isoform of saporin occurs prior to detectable protein synthesis inhibition[123]. Upregulation of the mitochondrial anti-apoptotic protein Bcl-2 has been shown to have a protective effect against apoptotic cell death caused by abrin [119] and ricin [124].

A number of different pathways have been implicated in RIP induced apoptosis and these may not be mutually exclusive or involved in all cell types. Iordanov et al first showed that rRNA depurination of the 28s rRNA by ricin and α-sarcin activated Stress Activated Protein Kinases (SAPK) and JNK1[125]. This activation was independent of protein synthesis inhibition and the authors proposed that the 28s rRNA acts as a sensor for ribosomal stress and is responsible for activating the signalling pathway that activates SAPK/JNK1, although the mechanism by which this occurs is unknown. A ribotoxic stress response has also been shown to be triggered by Shiga toxin, resulting in activation of p38 MAPK and JNK1[126]. JNK has been shown to play a role in other forms of stress induced apoptosis triggered by mitochondria[127].

The involvement of mitochondria in RIP induced apoptosis has been demonstrated by a number of studies. Exposure of HeLa cells to Shiga toxin resulted in damage to mitochondrial membranes leading to a reduction in mitochondrial membrane potential and release of cytochrome c[128]. The RIP abrin has also been shown to trigger apoptosis via a mitochondrial pathway with loss of mitochondrial membrane potential, release of cytochrome c, activation of caspase 9 and an increase in reactive oxygen species (ROS) production. Shih et al proposed that this was due to an interaction between abrin and the mitochondrial anti-oxidant protein 1 (AOP1) which reduced its antioxidant activity[129]. It has also been reported that RIPs can activate the mitochondrial pathway of apoptosis via enhancement of poly(ADP-ribose) polymerase (PARP) activity resulting in depletion of NAD^+ and ATP[130]. Saporin and gelonin have been shown to directly depurinate auto-modified PARP and Barbieri et al proposed that this would result in inhibition of DNA repair and depletion of NAD^+[131].

There is some evidence to suggest that the N-glycosidase activity of Saporin is not the only route by which the toxin can lead to apoptosis. Some toxin mutants lacking RIP activity were still able to initiate apoptosis, although to a lesser degree than the native toxin, and it was proposed that this is due to internucleosomal DNA fragmentation[132]. However, this is a controversial issue and it has been suggested that the apparent DNase-like activity of some RIPs is in fact a consequence of contamination[133] as no such activity was observed with a recombinant saporin isoform[134].

RIPs can be divided into two groups, Type I and Type II. Type II RIPs, including ricin and abrin exist as holotoxins consisting of an enzymatically active A-chain and a B-chain containing a cell binding domain which is responsible for mediating endocytic cell entry[135]. Type I RIPs including saporin

and dianthin are comprised of only a single 30kDa [136,137] [138] enzymatic protein chain and therefore lack an efficient means of cell entry, making them significantly less cytotoxic than Type IIs.

For the N-glycosidase activity of a RIP to be exerted, the toxin must first gain access to the cell's cytoplasm. In the case of Type II RIPs such as Ricin, internalisation is initiated by binding of the toxin B chain, a lectin like peptide, to cellular surface galactose or N-acetylgalactosamine [139,140] which results in endocytosis of the holotoxin. Once within the endosomal compartment the ricin holotoxin undergoes retrograde transport to the golgi[141] and endoplasmic reticulum where the A and B chains dissociate due to the activity of protein disulphide isomerase[142] and thioredoxin reductase[143]. The released ricin A chain (RTA) is partially unfolded and is marked by the cell for degradation by the proteasome in the cytoplasm. The ER-associated protein degradation (ERAD) process[144] delivers the RTA into the cytoplasm [145,146] where the toxic A chain is refolded into its active form which can then act directly on the ribosome.

Type I RIPs such as Saporin do not possess a cell binding subunit and their exact mechanism of endocytosis is unknown. There is some evidence for an interaction between saporin and the alpha-2 macroglobulin receptor (a2MR), also known as low density lipoprotein receptor related protein (LRP)[147] and it was proposed that this may play a role in the toxin's endocytosis. This is supported by work showing that another type I RIP, trichosanthin, also binds to a2MR and that a competitive ligand inhibited entry of trichosanthin into the cell[148]. However, there does not appear to be any correlation between the expression of a2MR by a particular cell line and the toxicity of a saporin isoform for that cell line. This suggests that this receptor is not solely responsible for the internalisation of saporin-6 and that other endocytic mechanisms may be involved[149]. In the case of targeted toxins incorporating a Type I RIP, the targeting peptide or antibody is largely responsible for binding to the cell leading to subsequent endocytosis.

Post endocytosis the intracellular trafficking of saporin is incompletely understood but it appears that unlike RTA the toxin does not undergo retrograde transport through the golgi apparatus [150]. Confocal microscopy studies that followed fluorescently labelled saporin showed co-localisation with pHrodo Red dextran, a marker for acidic endosomes and lysosomes [151,152] and also with immunofluorescent staining for the lysosomal marker LAMP-1 and the late endosomal marker LBPA[152].

For the development of targeted toxins, the cell binding domains of Type II RIPs increase the risk of the targeted toxin binding non-specifically to and being endocytosed by off-target cells leading

to unwanted cytotoxicity. Type I RIPs or the isolated A-chain of Type II RIPs, which lack a cell binding domain, are therefore preferable in the development of a highly specific targeted therapy.

1.2.3 Saporin

Saporin is a Type I RIP produced by *Saponaria officinalis L.* (common soapwort) which belongs to the *Caryophyllaceae* family[153]. At least nine different isoforms of saporin proteins have been identified in soapwort leaves, roots and seeds [154] and these vary in their biological properties. Of the seed isoforms, Saporin 6 (Sap-SO6) is the commonest and makes up about 7% of the total seed protein[153]. Isoforms are named by the peak number from which they were obtained by HPLC of the crude extract, thus Sap-SO6 is from peak 6 of the seed preparation. Sequencing showed that this peak contains at least four different isoforms, with heterogeneity at position 48, either Asp or Glu, and at position 91, either Arg or Lys[136]. Sap-SO6 is highly active in both cell line and cell-free systems and this along with its abundance has led to it being the most well studied and utilised isoform of saporin.

Sap-SO6 is highly stable; it is resistant to denaturation by urea or guanidine, high temperatures and to proteolysis[155]. In addition to this, the chemical modifications used in the conjugation process do not significantly affect the catalytic activity of SO6[156]. These factors, in combination with its high enzymatic activity and its poor cell entry in its unconjugated form make it an excellent candidate for the development of targeted toxins.

1.2.4 Saporin Based Targeted Toxins

The first Sap-SO6 based IT was created in 1985 following its conjugation to a murine anti-Thy 1.1 mAb, OX7 and its F(ab')2 fragment by Thorpe and co-workers[157]. Since then Sap-SO6 has been incorporated into a number of different targeted toxins directed against a range of solid and haematological malignancies [158-160]. Conjugation of Sap-SO6 to mAbs or other ligands greatly increases its selective cytotoxicity towards target antigen expressing cells with in vitro IC50 values commonly at nanomolar concentrations or less[158]. In preclinical studies with xenotransplanted immunocompromised mice, saporin based immunotoxins have demonstrated significant therapeutic effects [157,161-163].

1.2.5 Clinical Trials with Targeted Toxins

The first clinical trial with a Sap-SO6 linked IT used an anti-CD30-saporin to treat four patients with advanced, refractory Hodgkin's lymphoma. A substantial (50-75%) but transient reduction in tumour mass was observed[164]. Subsequent small, pilot clinical trials involved anti-CD22 bispecific antibodies (BsAbs), whose second Fab was targeted to different epitopes on Sap-SO6. These antibodies were complexed with the toxin prior to administration to patients with low-grade, end-stage B-cell lymphomas. Short term, rapid and beneficial responses were observed in a number of these patients [165-167]. These trials had minimal toxic side effects including myalgia, pyrexia and weakness with a small number of patients showing signs of hepatotoxicity.

Two Phase I clinical trials have been undertaken with the anti-CD19 IT, BU12-Saporin. The first, conducted in patients with relapsed Non-Hodgkin Lymphoma showed minimal toxicity but only minor responses to treatment (Flavell et al. Unpublished results 1996). The second, in paediatric patients with relapsed pre-B-cell acute lymphoblastic leukaemia was closed prematurely due to the poor health of the patient population (Flavell et al. Unpublished results 2002).

Another Phase I trial with the anti-CD38 IT, OKT10-Saporin, in patients with myeloma was also closed prematurely due to concerns about off-target toxicities. Minor responses in some of the treated patients treated with OKT10-Saporin were observed (Flavell et al. Unpublished results 2001). In all of these trials the maximum tolerated dose was never reached.

More widely, a number of immunotoxins incorporating ETA, DT or deglycosylated ricin A chain (dgA) have undergone Phase I and II clinical trials against a range of malignancies with varying degrees of success. Responses in haematological malignancies have generally been significantly better than those achieved in solid tumours presumably because is easier for the IT to gain access to malignant haematological cells and patients are more immunosuppressed, reducing the chances for immunogenicity

The previous clinical development of targeted toxins has been hampered by a number of problems. The most major of these being immunogenicity and dose limiting toxicities particularly vascular leak syndrome (VLS). Antibodies against both the monoclonal antibody and against the toxin component of ITs occur in up to 40% of patients with haematological tumours and between 50% to 100% of those with solid tumours after a single cycle of IT therapy[168]. This difference in immune response is likely due to the immunocompromised state of patients with haematological tumours in comparison to those with solid tumours. Neutralising antibodies, that block the cytotoxicity of the IT either by blocking antibody binding to its target antigen or neutralising the RIPs active site, greatly reduce their efficacy and can prevent repeat treatment. Measures to

avoid immunotoxin immunogenicity[169] have included non-specific immunosuppression [170] and modification of the toxin by mutagenesis [171] or PEGylation [168,172].

The development of side-effects including VLS, hepatotoxicity and rhabdomyolysis has, in some trials, limited the maximum tolerated dose of IT that can be administered. It is believed that these toxicities are the result of nonspecific uptake into off-target cells[173-175]. In VLS, damage to vascular endothelial cells leads to interstitial oedema, hypoalbuminaemia and weight gain. In some of these trials severe and even fatal cases of VLS have occurred with hypotension and pulmonary oedema [176-178]. Identification of toxin motifs responsible for VLS has enabled the production of recombinant toxins including RTA[179] and ETA[180] which have reduced off-target toxicity.

Because of these hurdles only two targeted toxins have thus far been approved by the FDA for treatment of malignancy. The first of these, denileukin diftitox, which comprises a recombinant human interleukin-2 fused to diphtheria toxin [107,181] is indicated for the treatment of cutaneous T cell lymphoma and was approved in 1999. Purification and production issues led to its discontinuation in 2014. The second, moxetumomab pasudotox, is an anti-CD22ETA containing IT which showed a high degree of activity against hairy cell leukaemia (HCL) in Phase I/II trials and recently completed a Phase III trial (NCT01829711) before being approved by the FDA in September 2018[182]. Moxetumomab pasudotox demonstrated a 75% objective response rate and 41% complete response rate in patients with HCL[183].

There is therefore a need to widen the therapeutic window for targeted toxins so that a therapeutic effect can be achieved at lower dose levels that do not lead to significant off-target toxicity. Whilst coupling the toxin to a targeting domain confers specificity it does not guarantee clinical efficacy. Several obstacles to the efficient delivery of toxins into the cytosol have been identified. These include but are not exclusive to, poor internalisation of the immunotoxin[184], recycling of the immunotoxin back to the cell surface[185] and poor endosomal escape to the cytosol resulting in trafficking of the toxin component to the lysosome and subsequent degradation[151,152]

Several different approaches have been used in an effort to augment targeted toxin cytotoxicity, most of which act to improve the escape of the toxin from the endolysosomal pathway into the cytosol. This includes small molecule chemical enhancers such as the lysosomotropic amines[186] and carboxylic ionophores[187]. Both of these classes of chemicals act by raising the lysosomal pH and therefore inhibit the degradation of internalised targeted toxins by lysosomal enzymes that are active at low pH. Specific combinations of targeted toxins and various enhancer

molecules have demonstrated up to 50,000 fold increases in cytotoxicity *in vitro* [186,188]. Virally derived peptides[189] have also demonstrated limited enhancement of targeted toxin cytotoxicity with more significant enhancing effects seen with living adenovirus preparations[190]. The anti-CD20 antibody rituximab augments the cytotoxic effect of an anti-CD19 immunotoxin, suggesting that combination therapy of immunotoxins and certain antibody therapies may have a synergistic therapeutic effect[191]. *In vivo*, combinations of two or more different ITs targeting different antigens show superior therapeutic outcomes[161]. It is speculated that a cocktail of ITs overcomes heterogeneity of single antigen expression within a tumour population ensuring that a lethal dose of toxin is delivered to all tumour cells in the population.

The cytotoxicity of some ITs is proposed to involve synergistic action between the toxin following intracellular delivery and NK-cell mediated ADCC induced by antibodies bound to the target cell surface[192,193]. Activation of NK-cells and potentially macrophages by poly-inosinic-cytidylic acid, a synthetic dsRNA TLR3 agonist improved the therapeutic activity of the anti-CD7 IT HB2-Saporin in a SCID mouse model[194] suggesting the possibility of combining an immunotherapeutic approach with IT therapy to achieve a more robust outcome in the patient.

Arguably the most promising augmentative agents described to date are the saponins, constitutive secondary metabolites produced by plants. *In vitro* saponins derived from Gypsophila species have been shown to augment various targeted toxins with increases in cytotoxicity ranging from 3,000 fold to 31,000,000 fold[195-197].

1.3 Saponins

Saponins are a diverse group of structurally related molecules found in a large number and variety of plant species covering almost 100 families [198,199]. They are also produced by a number of marine animals [200,201]. They are so named from the Latin word '*sapo*' for soap because of their ability to produce stable soap-like foams in aqueous solution. Widely used for their haemolytic and membrane permeabilising properties, their biological role is thought to be part of the plant's defence system as many exhibit antimicrobial, fungicidal, insecticidal and molluscicidal abilities[202]. Saponins consist of a hydrophobic aglycone core, called a sapogenin, to which is attached one or more hydrophilic sugar chains (Figure 1). This structure makes them amphiphilic and gives rise to their detergent-like, surfactant properties.

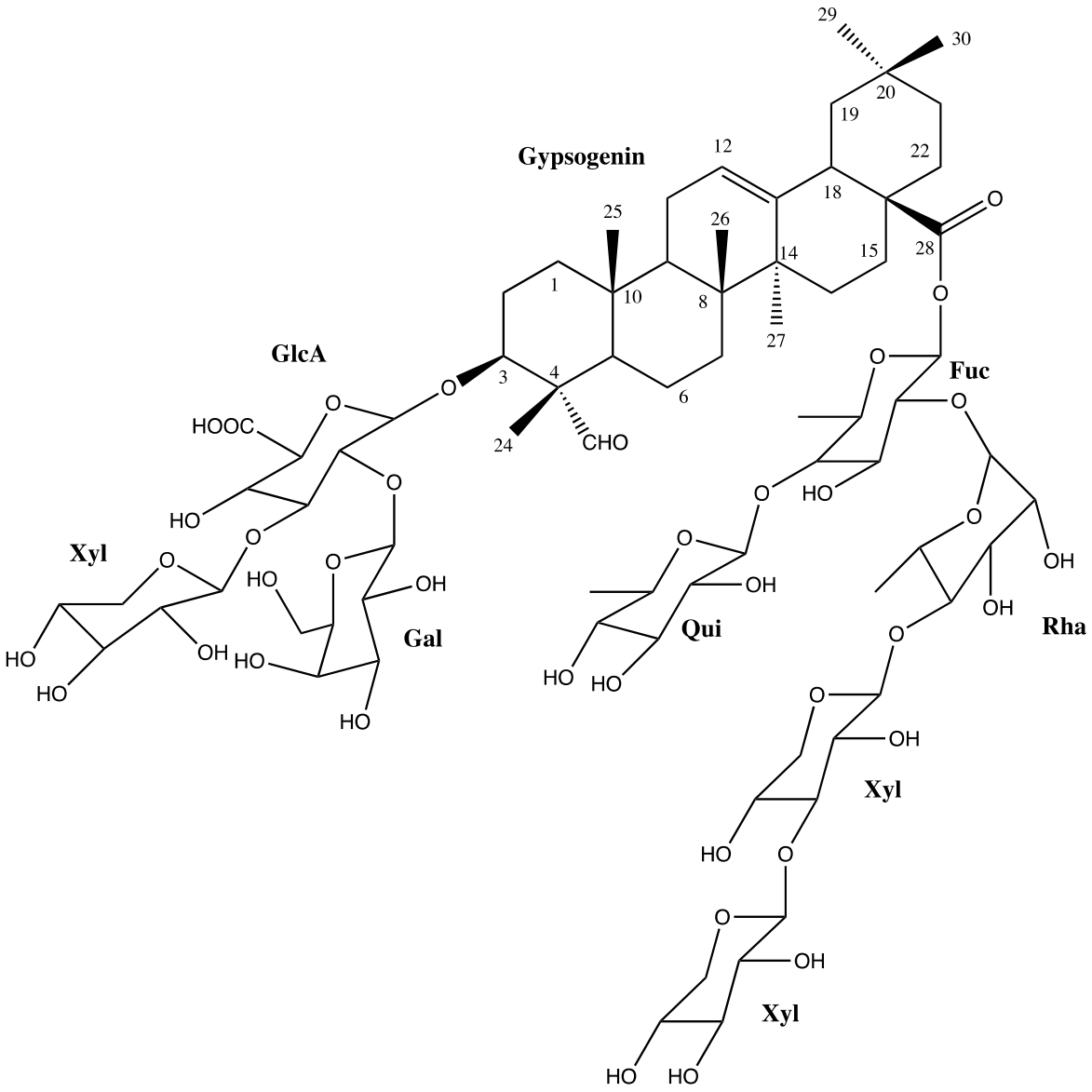

Figure 1. Structure of SA1641

An example of an oleanane type, bidesmosidic, triterpenoid saponin. This saponin possesses a gypsogenin aglycone core and has two carbohydrate side chains attached to C3 and C28. Fuc: Fucose (6-deoxy-galactose), Gal: galactose, GlcA: Glucuronic acid, Qui: Quinovose (6-deoxy-glucose), Rha: Rhamnose (6-deoxy-mannose), Xyl: Xylose.

The structural diversity of saponins arises from both the sapogenin core and the attached sugar chains. The primary classification divides saponins into two main classes, steroidal and triterpenoid saponins[203] based on the type of sapogenin core. Further sub-classification by the sapogenin leads to eleven major classes. This includes steroidal saponins, further subdivided into 5-ring furostane and 6-ring spirostane sapogenin skeletons and ten classes of pentacyclic and tetracyclic triterpenoid saponins[198]. All sapogenin cores are derived from the C30 precursor oxidosqualene[204] with steroidal saponins losing three methyl groups to become C27

compounds and triterpenoid saponins retaining all 30 carbon atoms. Over 100 different steroidal sapogenins and more than 360 triterpenoid sapogenins have been identified so far[205].

In addition to the number of different sapogenin cores, structural diversity is greatly increased by the differences in the number, composition and branching of attached sugar chains. The majority are monodesmosidic with one sugar chain, normally attached to the C3 hydroxyl group on the sapogenin. Those saponins with two sugar chains are defined as being bidesmosidic with the additional sugar usually attached to the C26 or C28 position. More rarely, tridesmosidic saponins possess three sugar chains attached to the sapogenin[206]. Individual sugar chains vary between 1 and 8 residues in length and can be linear or branched[198]. These chains generally contain common sugars such as glucose, fructose, galactose and fucose alongside others such as rhamnose and quinovose.

Thousands of different saponins have so far been isolated and characterised, each possessing a wide range of biological activities. These include a number of pharmacological activities that include anti-inflammatory, hypocholesterolemic, immunomodulatory, hypoglycaemic, expectorant, vasoprotective and anti tumour effects[202].

1.3.1 Activity of Saponins on Cell Membranes

The haemolytic and associated membrane permeabilising activity of saponins is generally attributed to their amphiphilic nature, which is hypothesised to allow their incorporation into the lipid bilayer. For the majority of saponins reported in the literature, the presence of membrane cholesterol is necessary for permeabilisation of liposomes or lipid monolayers [207-211] and the permeabilising activity of saponinum album (SA), a mixture of saponins from Gypsophila species, on living cells was recently demonstrated to be plasma membrane cholesterol dependent by Smith et al[212].

A similar cholesterol dependence has also been demonstrated for haemolysis[213] and for the cytotoxicity[207] exerted by hederagenin based saponins, with removal of membrane cholesterol conferring protection against lysis. However, for a small number of described bidesmosidic saponins membrane permeabilisation appears to be cholesterol independent [209,214].

Early electron microscopic imaging studies by Bangham et al[215] and Glauert et al[216] with cholesterol planar monolayers exposed to saponin, showed the formation of hexagonal ring like structures. These were proposed to be micellar-type complexes formed between saponins and cholesterol which, it was speculated, were responsible for the formation of membrane pores. Transmission electron microscopy and freeze etch microscopy revealed the presence of deep

invaginations and pit formation in the membranes of erythrocytes exposed to the saponin Holothurin A from the sea cucumber *Actinopyga assagizi*[217]. Since then several alternative mechanisms for saponin induced membrane permeabilisation have been proposed, including the formation of tubular aggregates similar to those observed with monodesmosidic glycoalkaloids[208] and pore formation via induction of a positive curvature strain on the external monolayer[207].

Liposomal models have been used to investigate the membrane permeabilising activity of triterpenoid, monodesmosidic saponins based on the hederagenin sapogenin and the cholesterol dependence of this activity[207]. In these models the saponin was found to produce a cholesterol-dependent permeabilisation which increased over time. Work by the same group using liposomes containing the fluorescent cholesterol analogue, dehydroergosterol (DHE), indicated that exposure to saponin caused the DHE to enter a more hydrophobic environment with the suggestion that the saponin was forming aggregates or micelles in the membrane[207].

1.3.2 Structure-Activity Relationships of Membrane Permeabilising Saponins

Haemolysis is the most described activity studied across the range of saponin species and consequently most of the structure-activity relationship (SAR) work has been performed in erythrocytes, with a smaller number of studies performed in liposomes. This makes it difficult to draw specific conclusions with regards to their membrane permeabilisation characteristics towards nucleated mammalian cells.

The haemolytic effects of saponins are primarily attributed to the aglycone structure as many sapogenins are themselves haemolytic[218] and early work suggested that post absorption into the membrane, deglycosylation and release of the aglycone is necessary for membrane permeabilisation. Differing aglycone cores have a large effect on the haemolytic activity of the saponins based upon them. A study by Gauthier et al showed that whilst pentameric triterpenoid oleanane type saponins tend to exhibit a strong haemolytic effect, lupane type saponins did not at the maximum concentration tested. This lack of haemolytic activity was irrespective of the number or type of attached sugar chains[219]. The same study also demonstrated a significant correlation between the haemolytic activity and membrane permeabilising activity of oleanane saponins. Esterification of the aglycone appears to be essential for haemolysis and hydrolysis to an un-esterified saponin removes all haemolytic activity[218,220]. It has been suggested that this esterification increases the lipophilicity of the saponin which may enable penetration of the cell membrane and pore formation[220].

The role of the attached sugar chains is less well characterised as the large variety of potential sugar chains can have greatly differing effects on the haemolytic activity of the sapogenin. This is further complicated because the effect on haemolytic activity of a specific sugar chain is not preserved between different aglycones[221]. Despite this, the number of sugar chains along with their length and structure can have large effects on the membrane permeabilising and haemolytic activities of saponins and some general conclusions can be drawn. Increasing the length of the C3 sugar chain increases the haemolytic effect with trisaccharides and disaccharides being more haemolytic than monosaccharides attached to the same aglycone core [211,222,223]. Increasing the length of the sugar chain also increases permeabilisation of liposomes[207]. For sugar chains that contain more than one sugar residue the linkages between the sugar residues may also be important. One study found that disaccharides with 1→ 4 linkages were more haemolytic than those with 1→ 6 linkages[224]. Saponins with branched chains seem to be more active than those with straight ones[223]. Evidence for the effect of additional sugar chains on haemolysis is inconsistent, some studies have reported that monodesmosidic saponins are generally more haemolytic than bidesmosidic ones [225,226], whilst others have reported the opposite [214]. It is likely that differences in the aglycone and the composition of the sugar chains is responsible for this variation.

Interestingly, it has been reported by some studies that there is little correlation between the haemolytic and cytotoxic activity. Saponins showing similar levels of haemolytic activity can greatly differ in their cytotoxic activity and those with similar cytotoxic activities can have disparate haemolytic activities. Similarly, high levels of either cytotoxic or haemolytic activity are not indicators of strong activity in the other [219,222].

1.4 Saponin Augmentation of Targeted Toxin Cytotoxicity

The interest in saponins as augmentative agents began when it was first noticed by Hebestreit and coworkers that the toxicity of the seeds of *Agrostemma githago* was due to a highly synergistic effect between the saponin agrostemmasaponin 1 and the Type I RIP agrostin[227]. Further work by Melzig et al revealed that the augmentation of agrostin cytotoxicity was not specific to agrostemmasaponin and was also observed with saponins from Gypsophila and Quillaja species[228]. Around the same time it was shown that Gypsophila saponins could also augment the cytotoxicity of the Type I RIP saporin both in its native form and coupled to epidermal growth factor (EGF) as part of a targeted toxin[229]. Investigation of a wider range of toxins revealed that the augmentative effects of saponins were highly toxin specific. The greatest levels of augmentation were seen in the type I RIPs agrostin and saporin, with a much lower degree of

augmentation seen with the type II RIPs, RTA and nigrin b, and the bacterial toxin microcystin LR. No augmentation was observed for DT or diphtheria toxin A chain (DTA)[230]. This toxin specificity was maintained when toxins were incorporated into range of EGF based targeted toxins. The application of the gypsophila saponin SA1641 augmented EGF-saporin and EGF-dianthin-30 (a type I RIP) cytotoxicity by over 4,000,000 fold, whilst for DT , ETA and for RTA the augmentation was effectively only up to 16 fold[195].

1.4.1 Structure-Activity Relationships of RIP Cytotoxicity Augmenting Saponins

There are only a limited number of studies investigating the SAR of saponins augmenting the cytotoxicity of RIPs. Melzig et al investigated the effect of nine saponins from a variety of Caryophyllaceae species on the cytotoxicity of agrostin. Bidesmosidic saponins showed greater levels of augmentation than a monodesmosidic saponin with the same aglycone core. Within the bidesmosidic saponins those with a trisaccharide at C3 exerted a greater effect than saponins with a monosaccharide at this position[228]. A larger study of 56 oleanane saponins by Böttger et al also concluded that bidesmosidic saponins augmented the cytotoxicity of saporin more than monodesmosidic saponins. They demonstrated the importance of carbohydrate side chain length with saponins containing six or more total sugars being the strongest augmenters especially those with branching side chains[231].

1.4.2 Mechanism of Augmentation

There is now a body of independent experimental evidence clearly demonstrating that some saponin molecular species significantly augment the cytotoxicity of some RIP-based targeted toxins (Table 1). However, the precise mechanism driving this augmentative process is not fully understood.

As described above, the cytotoxicity of RIPs is largely ascribed to their catalytic N-glycosidase activity against ribosomes. Saponins could bind to or otherwise influence the active site of saporin leading to a direct enhancement of this activity. In experiments using adenine release from herring sperm DNA by saporin or RTA as an indicator of N-glycosidase activity, no increase in activity was observed with the addition of saponin SA1641[232]. The inactivation of ribosomes by RIPs requires that the toxin reaches the cytosol. Augmentation of these toxins' activities by saponins might therefore involve an increased efficiency of cytosolic delivery. The most direct way for a saponin to achieve this would be through a limited, non-lethal permeabilisation of the plasma membrane that would allow direct access of soluble extracellular saporin into the cytosol. However several studies have shown that augmentation of toxin activity continues to be seen

even at saponin concentrations that are non-permeabilising, as assessed by influx of propidium iodide (PI) [195,212] or by cellular impedance[233].

These observations led to the proposal that saponins might exert their augmentative effect by increasing the endocytic uptake of the toxin or targeted toxin. Initially some very limited confocal evidence from Weng at al appeared to show that a mixture of Gypsophila saponins (SA) increase the uptake of a fluorescently labelled saporin[234]. However this finding is suspect as later studies from the same group using flow cytometry[152] or a radiolabeled saporin failed to confirm these earlier results[235].

Table 1. Augmentation of RIP Based Targeted Toxins by Saponins

Effect of different saporins on TT cytotoxicity in a range of cell lines. EC_{50} refers to half maximal viability compared to untreated cells. EGF: epidermal growth factor; EGFR: EGF receptor; NIH-3T3: embryonic mouse fibroblasts; HER14: NIH-3T3 cells stably transfected with human epidermal growth factor receptor; PHCC: human cervical carcinoma cells; SiHa: human cervical squamous carcinoma cells; HeLa: human cervical adenocarcinoma cells; CaSki: human cervical epidermoid carcinoma cells; MDA-MB-435S: human breast carcinoma cells; MCF-7: human breast adenocarcinoma cells; Ramos: human Burkitt's lymphoma cells; Daudi: human Burkitt's lymphoma cells; HSB-2: human lymphoblastic leukaemia cells.

Toxin	Targeting Domain	Target	Saponin	Cell Line	EC_{50} without Saponin (nM)	EC_{50} With Saponin (nM)	Enhancement Factor	Reference
RTA	EGF	EGFR	SA1641	HER14	>1000	61	>16.3	[195]
Dianthin	EGF		SA1641	HER 14	0.45	<0.0000001	>4000000	[195]
Saporin	EGF		SA1641	HER14	57	<0.0000001	>4000000	[195]
	EGF		SA	PHCC1	80	1.1	76000	[197]
				PHCC2	24.5	2.7	9000	
				SiHA	>300	0.12	2500000	
				CaSki	5	0.13	38000	
				NIH-3T3	30	0.6	50	
				HER14	2.5	0.9	2800	
				MDA-MB-435S	206	12	17100	
				HeLa	53	0.7	38000	
	Adapter-EGF		SA	HER14	2.5	0.0009	2800	[236]
				NIH-3T3	30	0.6	50	
				HER14	2.4	0.00067	3560	[229]
				MCF-7	1040	0.0027	385000	
				HER14	2.4	0.00018	13647	[237]
				NIH-3T3	27.7	0.014	1977	
			Quillaja Saponin	HER14	2.4	0.0017	1434	
				NIH-3T3	27.4	0.013	2113	
	Rituximab	CD20	SO1861	Ramos	7	0.01	700	[232]
	Anti-CD22	CD22			0.5	0.003	170	
	Anti-CD25	CD25			1	0.04	25	
	HB2	CD7	SA	Daudi	139	0.31	448	[196]
				Ramos	1000	0.89	1130	
				HSB-2	0.5	0.0036	146	
	BU12	CD19		Daudi	965	0.00003	31500000	
				Ramos	0.96	0.00095	1730	
				HSB-2	212	0.075	3140	
	4kB128	CD22		Daudi	0.0138	0.0000226	615	
				Ramos	0.127	0.00003	4521	
				HSB-2	1000	25.5	39	
	OKT10	CD38		Daudi	0.0532	0.000222	242	
				Ramos	1.11	0.00038	2890	
				HSB-2	0.177	0.00064	276	
	DF1513	CD71		Daudi	0.0143	0.0000413	346	
				Ramos	0.716	0.00035	2020	
				HSB-2	0.025	0.00015	174	

The ability of saponins to augment the cytotoxicity of both the native toxin and toxin incorporated in a wide range of different targeted toxins, including immunotoxins, suggests that the augmentative effect is not dependent on any single endocytic pathway for internalisation of the toxin. This contention is supported by experimental data obtained for an EGF based targeted toxin by Bachran et al[236]. The internalisation of EGF switches from a purely clathrin dependent mechanism at low concentrations of EGF to both clathrin dependent and independent mechanisms at higher concentrations[238]. This transition did not affect augmentation by SA although it should be kept in mind that at higher concentrations of EGF there is still clathrin dependent uptake of the growth factor confounding any meaningful interpretation of these results.

The current assumption, based on the above uncorroborated experimental evidence, is that saponins do not increase the rate of targeted toxin endocytosis. This correlates with evidence that, for a number of targeted toxins and immunotoxins the rate limiting step in the process of intoxication is not their internalisation into the cell but rather their escape from the endosomal lumen into the cytosol[239]. Instead the targeted toxin is trafficked to the endolysosomal compartment where it is degraded. Reducing lysosomal degradation and simultaneously improving endosomal escape of the toxin is the mechanism of action of many other classes of enhancer molecules[188].

Evidence for saponins causing the increased endosomal escape of saporin has been presented by Weng et al[152], using a fluorescent, Alexa Fluor coupled saporin to track the effect of saponin on the toxin's cellular location. The fluorescently labelled toxin was detected by live cell confocal microscopy in discrete perinuclear vesicles after a six-hour exposure period in ECV-304 cells. Subsequent addition of the saporin SA1641 and observation of the cells over a sixty minute period appeared to show a massive escape of the saporin from these vesicles into the cytoplasm[152]. However, caution should be used in the interpretation of these results as the internalisation and trafficking of the saporin may have been influenced by its conjugation to the fluorescent probe used. The endosomal escape of saporin seen by these workers was inhibited by preincubation with chloroquine which diffuses into the endosome and becomes protonated thus directly increasing luminal pH[240]. This suggests that this increased endosomal escape is dependent on the acidification of the endosome[152]. This finding is supported by evidence showing that the treatment of cells with chloroquine or with bafilomycin A1, an inhibitor of the vacuolar H^+ ATPase[241], greatly reduces the augmentation of EGF-Saporin toxicity by a saponin but does not affect the toxicity of the targeted toxin alone[236].

As previously discussed, the augmentative effect of these saponins is toxin specific. The reason for this is likely to be vital to ascertaining the precise mechanism of augmentation. This review will focus on the difference between the augmentable Type I RIPs saporin and dianthin and the non-augmentable Type II RIP RTA as these are amongst the mostly frequently used in targeted toxins and share a common N-glycosidase activity. Alignment of the amino acid sequences for these toxins revealed that there is a 72% sequence homology between saporin and dianthin-30, but only a 23% homology with RTA and it has been suggested that there may be a direct non-covalent interaction between saporin and saponin that is necessary to achieve the augmentative effect[195].

An interaction between saponin and saporin has been observed using surface plasmon resonance (SPR) measurements with a His-tagged saporin bound to a carboxymethylated gold surface and then exposed to SA1641[152]. Results from this study suggested that there was a pH dependent interaction between the two. Binding was greatly increased by reducing the pH from a neutral pH 7.5 to an acidic pH 5. Similar binding effects have also been observed with a soapwort (*Saponaria officinalis*) derived saponin, SO1861[152]. The nature of the association is unknown, but it has been suggested that it may involve an electrochemical interaction between the two. At pH 5-6 Saporin is positively charged because of its very high isoelectric point (IP) of ~9. Whilst both of the tested saponins contain a glucuronic acid which is negatively charged at the same pH, RTA (IP~5), which was shown not to be significantly augmented by saponins, did not interact with these saponins under the same acidic conditions. However, in the same paper by Weng et al it was also demonstrated that the type I RIP gelonin (IP ~9) did not associate with either SA1641 or SO1864 at pH5 suggesting that if there is an association it may not be entirely electrochemical[152]. It is unknown whether the toxic activity of gelonin is augmented by saponins. The pH dependency of the binding between saporin and certain saponins may be relevant to the mechanism of augmentation due to the acidification of the late endosome and lysosomal compartments into which the saporin is trafficked. Progression along the endolysosomal degradation pathway sees the endosomal contents exposed to increasingly acidic pH from the early endosome (pH 6.1-6.8) through the late endosome (pH 4.8-6) and ultimately to the lysosome (pH 4.5)[242]. The route of saponin internalisation is unknown but confocal imaging presented by Wang et al showed that a fluorescent conjugate of the spirostane saponin dioscin accumulated in the lysosomal compartment of HeLa cells[222].

It is therefore suggested that there is co-localisation of saporin and the saponin within the same endolysosomal compartment[196]. Here the saponin facilitates the endolysosomal escape of the saporin into the cytosol in a currently unknown way. It is possible that there is an accumulation of

saponin within the endolysosome so that a permeabilising concentration is achieved even when the extracellular concentration is sub-permeabilising. It may also be the case that the endosomal membrane is more susceptible to permeabilisation by saponins and does not possess the membrane repair mechanisms that operate to protect the plasma membrane. An alternative hypothesis suggests that a pH dependent association of saporin and saponin occurs within the endolysosomal compartment and that this association enables the endolysosomal escape of the saporin into the cytosol, possibly through a conformational change that renders the hypothetical saponin-saporin complex lytic on the endolysosomal membrane from the luminal side [196]. This hypothesis also concurs with the experimental evidence showing that inhibitors of endosomal acidification inhibit both augmentation and endosomal escape of saporin.

1.4.3 Endocytosis of Saponins

This co-localisation hypothesis requires that both saporin and saponin are trafficked to the same endolysosomal vesicle. The internalisation and trafficking of saponin species has not yet been determined and it is unknown whether saponins are internalised in the fluid phase or whilst integrated into portions of the plasma membrane that are subsequently endocytosed. It is also currently unknown whether saponins are internalised independent of the toxin or as part of the same process that leads to the toxin's endocytosis. Here I present the background to the potential endocytic routes that might be involved in delivering saponin into the endosomal pathway, together with the existing experimental evidence for their direct involvement in the augmentation of saporin by saponins.

1.4.3.1 Clathrin Mediated Endocytosis

Clathrin mediated endocytosis (CME) is the most well studied endocytic pathway. With well-defined molecular processes and cargo specificity it is ubiquitous in eukaryotic cells. Endocytosis is triggered by signals from a wide range of transmembrane receptors which can be stimulated by ligand binding or be constitutive. Binding of the cytosolic adaptor protein 2 (AP2) either directly to the cargo or to cargo specific adaptor proteins leads to recruitment of clathrin to the inner leaflet of the cell membrane and the formation of clathrin coated pits[243]. The subsequent polymerisation of dynamin-2 at the neck of the pit pinches off the pit into a clathrin coated vesicle [244,245]. Once detached from the cell membrane the clathrin coat is disassembled allowing the uncoated vesicle to be trafficked to and fuse with early endosomes[246].

There are several well described small molecule pharmacological agents that inhibit endocytic processes. One of these is chlorpromazine, a cationic amphipathic drug which causes clathrin and

AP2 complex assembly on endosomal membranes, thus depleting them from the plasma membrane and inhibiting CME[247]. Weng et al reported that along with other CME inhibitors, imipramine and cyclosporine A, chlorpromazine was able to reduce the cytotoxicity of saporin and saponin used in combination against ECV-304 cells[234]. The effect on the toxin alone was not investigated by these workers. Chlorpromazine also caused a significant decrease in the augmentation of the saporin-EGF targeted toxin (SE) by SA without affecting the cytotoxicity of SE used alone[236]. However, this drug has been demonstrated to have variable efficacy and toxicity when used against different cell lines and inhibition of clathrin independent endocytosis has been observed in some cell lines treated with chlorpromazine [248,249], making meaningful interpretation of these findings difficult.

1.4.3.2 Clathrin Independent Endocytosis

Clathrin independent endocytosis is less well understood and encompasses several different endocytic routes. These include small scale (<200nm) pathways as well as larger, micrometre scale pathways such as macropinocytosis[250].The small scale processes are commonly divided between those that are dynamin dependent and those that utilise other molecular machinery.

Of the dynamin dependent pathways, the best studied is the caveolar endocytic system. Caveolae are lipid raft domains that appear as 50-100nm flask shaped invaginations of the plasma membrane. Their formation involves a number of caveolin and cavin proteins. Caveolae have been implicated in lipid homeostasis, protection against mechanical stretching and endocytosis[251]. Caveolae have been shown to bud from the membrane but evidence for specific protein cargoes is incomplete [251,252]. Other small-scale endocytic processes including those involving, RhoA, Flotillin, cdc42 or Arf6 are less well understood[250]. Investigation of the role of dynamin in the augmentation of saporin-EGF by saponin was done by transfecting HeLa cervical carcinoma cells with a mutant, inactive copy of dynamin-2. This led to a considerable reduction in SE cytotoxicity in the presence and absence of saponin but interpretation of results was confounded as transfection was also shown to reduce the surface expression of the EGFR[236].

1.4.3.3 Macropinocytosis

Macropinocytosis is an actin-dependent, dynamin independent endocytic process which is responsible for the non-selective bulk internalisation of extracellular fluid. Here actin cytoskeleton rearrangement leads to the formation of membrane ruffles which can fold back on themselves and fuse with the base of the plasma membrane forming large macropinosomes[253].

Macropinocytosis can be induced by the stimulation of growth factor receptors or as a constitutive process in some cell types such as dendritic cells[254]. Once formed, macropinosomes are either recycled back to the plasma membrane or undergo maturation joining the late endocytic pathway to the lysosome[255], making this a potential candidate mechanism for saponin internalisation either in fluid phase or bound to the membrane.

Use of the actin polymerisation inhibitor latrunculin A has been shown to reduce the augmentation of SE cytotoxicity by saponin but similar to chlorpromazine had no effect on the cytotoxicity of the TT alone[236]. As a marker for endocytosis actin may not be very specific, being implicated as playing a role in both clathrin mediated endocytosis and the majority of clathrin independent pathways[256].

1.4.3.4 Membrane Repair Processes

The endocytosis of caveolae has been shown to play an important role in plasma membrane repair processes[257]. Damage to plasma membrane integrity is potentially lethal to the cell and must be repaired. In the case of damage caused by pore forming toxins such as streptolysin O (SLO); the protein toxin lines the outer edge of the pore and membrane repair requires more than the addition of new phospholipids and a subsequent reduction in membrane tension. Instead repair can only be achieved by removal of the pore from the membrane. The influx of calcium ions into the cell down a concentration gradient through the pore initiates this repair process[258] by triggering lysosomal exocytosis [259,260] and thus reducing membrane tension. It also releases the lysosomal enzyme, acid sphingomyelinase onto the outer leaflet of the membrane[261]. This converts sphingomyelin in the plasma membrane into ceramide, a lipid with a smaller, less hydrated head group. This in turn leads to a condensation of the outer leaflet and segregation of the ceramide molecules into a domain. Spontaneous negative curvature of this domain, along with the area difference between the two leaflets, induces membrane invagination[262]. These invaginations strongly resemble caveolae and are rapidly endocytosed. Internalised SLO pores are subsequently found in vesicles containing caveolin[257]. Interestingly, the caveolar endocytosis implicated in membrane repair appears to be dynamin independent[257]. In B-cells, which do not express caveolin-1 constitutively and appear to lack caveolae[263], repair is proposed to occur via lipid raft mediated endocytosis[264].

Such endocytic processes have been termed MEND (massive endocytosis [265] and have been shown to internalise SLO pores and traffic the toxin to multivesicular bodies (MVBs), late endosomes and ultimately lysosomes [266] for degradation. It is also theorised to be a route of

entry for some non-enveloped viruses such as human adenovirus[267] and for *Clostridium botulinum* C2 toxin[268].

As discussed earlier, saponins possess a membrane disrupting activity. Whilst augmentation of saporin or IT cytotoxicity by saponins occurs at a concentration below that required for detectable membrane permeabilisation it is possible that a low level of limited membrane damage occurs and that this is subsequently repaired by the cell through a MEND-like mechanism that results in the endocytosis of portions of damaged membrane containing saponin. This process may be partially or wholly responsible for the intracellular delivery of saponins into vesicles that later fuse with endocytic vesicles containing targeted toxin, thus bringing both into a common endocytic vesicle.

1.5 Objectives

Saporin-based immunotoxins hold the potential to offer a highly specific and potent cancer therapy, but their clinical development has been hindered by dose-limiting off-target toxicities. Triterpenoid saponins have been shown to augment the cytotoxicity of saporin and saporin based immunotoxins. The mechanism behind this augmentation is not fully understood but is hypothesised to involve the internalisation of both the toxin/IT and the saponin to the lumen of the same endolysosomal compartment. Here the saponin in some way enables the endolysosomal escape of the toxin/IT into the cytosol where it's ribotoxic effect can be exerted. This thesis aimed to investigate the mechanism(s) involved in the saponin-mediated augmentation of the cytotoxicity of saporin and saporin-based ITs. To achieve this a number of sub goals were defined.

1. To investigate whether or not exposure of cells to a sub-toxic, but augmentative concentration of saponin results in a low level permeabilisation of the plasma membrane and, if so, whether subsequent membrane repair processes are involved in the internalisation of the saponin and its augmentative activity on the cytotoxicity of the saporin based IT, OKT10-SAP.
2. To investigate the role of different endocytic processes and endosomal acidification in the saponin-mediated augmentation of saporin and OKT10-SAP cytotoxicity.
3. The development of a reporter assay to study the endolysosomal escape of saporin and OKT10-SAP into the cytosol. This assay will be used to confirm the action of saponin as an endolysosomal escape enhancer and to investigate the role played by different endocytic processes and endosomal acidification in this activity.

Chapter 2 Materials and Methods

2.1 Materials

2.1.1 Chemicals

2.1.1.1 Ribosome Inactivating Toxins

- Saporin S06 previously extracted and purified by members of this research group [160] from the seeds of *Saponaria officinalis L*. (Soapwort) (Chiltern Seeds, Ulverston, Cumbria, United Kingdom) as described elsewhere [153].
- Gelonin from *Gelonium multiflorum* (kindly provided by Professor Andrei Bolognesi, University of Bologna)

2.1.1.2 Immunotoxins

An IgG_1 murine monoclonal antibody (OKT10) against human CD38 had been previously produced from cultures of the OKT10 hybridoma cell line by Flavell et al and purified by standard ion exchange and gel filtration chromatography.

OKT10 was covalently coupled to the SO6 isoform of saporin using the cross-linking reagent SPDP[162] to produce the OKT10-SAP IT. The purity and molecular weight was determined by SDS-PAGE and the immunospecific cytotoxic activity on Daudi cells determined as described [162]. OKT10-SAP was filter sterilised through a 0.2µm filter and stored at -80^{o}C in 1ml aliquots at 0.5mg/ml.

2.1.1.3 Saponinum Album

Saponinum Album (SA), a root extract containing saponins from *Gypsophila paniculata* L. and *Gypsophila arrostii* Guss., was obtained from Merck (Darmstadt, Germany). SA contains a mixture of saponin species with the same aglycone core but varying carbohydrate side chains [269]. The most abundant of these are SA1641 and SA1657, whose structures are shown in Figure 3.

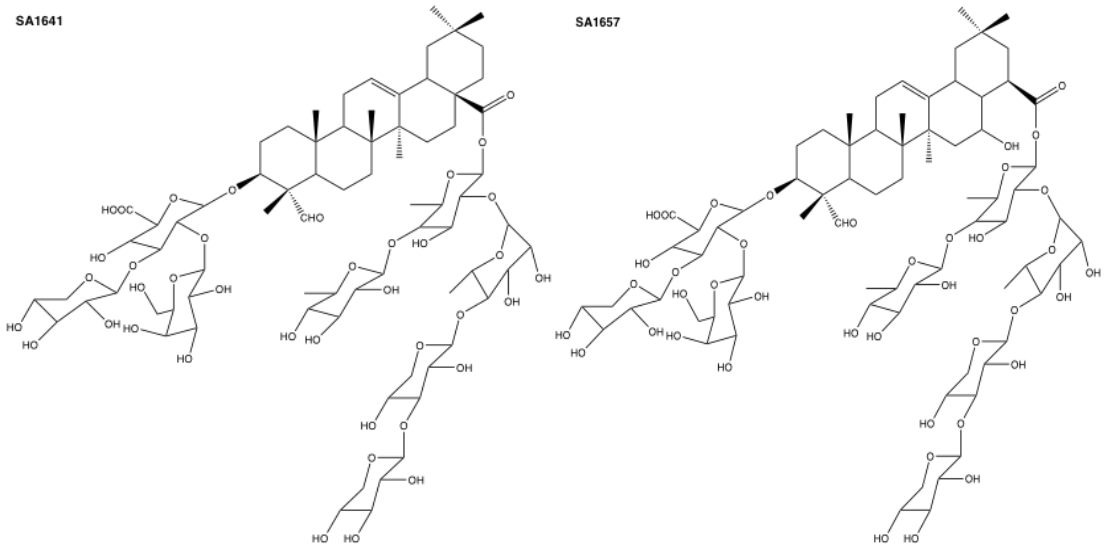

Figure 2. Molecular Structures of SA1641 and SA1657

Two major saponin species from saponinum album.

2.1.1.4 Pharmacological Inhibitors

- Amitriptyline hydrochloride (Sigma, MO, USA)
- Bafilomycin A (Cayman Chemical Company, MI, USA)
- Chloroquine (Sigma, MO, USA)
- Chlorpromazine (Sigma, MO, USA)
- Cytochalasin D (Invitrogen, CA, USA)
- Ethylisopropylamiloride (EIPA) (Sigma, MO, USA)
- Nocadazole (Acros Organics, NJ, USA)

2.1.1.5 Antibodies

- Anti-human LAMP-1/CD107a antibody. Monoclonal Mouse IgG2B Clone 508921 (R+D Systems, MN, USA)
- Anti-ceramide antibody. Monoclonal Mouse IgM Clone MIB 15B4 (Sigma, MO, USA)
- Anti-EEA1 Polyclonal Chicken IgY (Sigma-Aldrich Company Ltd., Gillingham, UK)
- IgM Isotype Control Clone 1E11 (Invitrogen, CA, USA)
- IgG2b Isotype Control Clone eBMG2b (Invitrogen, CA, USA)
- Goat anti-mouse IgM:FITC (102002)(Bio-Rad, CA, USA)
- Rabbit F(ab')2 Anti-mouse IgG:FITC (STAR9B) (Bio-Rad, CA, USA)
- Goat anti-mouse IgG Alexa Fluor 568 (ab175473) (Abcam, Cambridge, UK)

- Goat anti-chicken IgY (H+L) Alexa Fluor 555 (A21437) (Thermofisher Scientific, Loughborough, UK).
- Rabbit anti-mouse IgG:HRP (Dako, Glostrup, Denmark)
- Rabbit anti-cyclophilin B polyclonal IgG (Bio-Rad, CA, USA)
- Goat anti-rabbit IgG (H/L):HRP (Bio-Rad, CA, USA)

2.1.1.6 siRNA Transfection

- INTERFERin (Polyplus Transfection, Illkirch, France)
- ON-TARGETplus Control siRNA (Dharmacon, CO, USA)
- siGLO Cyclophilin B siRNA (Dharmacon, CO, USA)
- siGLO Green Transfection Indicator (Dharmacon, CO, USA)

2.1.1.7 Gel Electrophoresis

- Precision Plus Protein All Blue Standards (Bio-Rad, CA, USA)
- RunBlue 20x SDS Run Buffer TEO-Tricine-SDS (Expedeon, Cambridge, UK)
- RunBlue LDS Sample Buffer 4x (Expedeon, Cambridge, UK)
- RunBlue SDS Gel 12% (Expedeon, Cambridge, UK)

2.1.1.8 Western Blot

- Pierce ECL Western Blotting Substrate (Thermofisher Scientific, Loughborough, UK).
- Protran 0.45 µl Nitrocellulose transfer membrane (GE Healthcare, IL, USA).

2.1.1.9 Cell Culture

- Calcium free Dulbecco's modified Eagle's Media (Gibco, NY, USA)
- Dulbecco's modified Eagle's Media (DMEM), high glucose (Sigma, MO, USA)
- Foetal Calf Serum (Sigma, MO, USA)
- Glutamine (Sigma, MO, USA)
- RPMI-1640 medium (Sigma, MO, USA)
- RPMI-1640 medium without phenol red (Sigma, MO, USA)
- Sodium Pyruvate (Sigma, MO, USA)

2.1.1.10 Fluorescent Dyes

- Alexa-Fluor 488- tetrafluorophenyl ester (TFP) (Life Technologies, OR, USA)
- bisBenzimide Hoechst 33342 trihydrochloride (Sigma, MO, USA)

- Propidium Iodide (PI) (Life Technologies, OR, USA)

2.1.1.11 Other Chemicals

- Adenine (Sigma, MO, USA)
- Agarose, Low Gelling Temperature (Sigma, MO, USA)
- 2,3-Bis-(2-Methoxy-4-Nitro-5-Sulfophenyl)-2H-Tetrazolium-5-Carboxanilide (XTT) (Sigma, MO, USA)
- Calcium Chloride (Fisher Chemical, Loughborough, UK)
- Chelex-100 resin (Bio-Rad, CA, USA)
- DER 736 Diglycidylether of Polypropylene glycol (Agar Scientific, Stansted, UK)
- 1,4-Dithiothreitol (DTT) (Roche Diagnostics, Mannheim Germany)
- ERL 4221(Agar Scientific, Stansted, UK)
- Ethanol (Fisher Brand, Loughborough, UK)
- Glutaraldehyde (TAAB Laboratories Equipment, Aldermaston, UK)
- Glycerol (VWR, PA, USA)
- Herring sperm DNA (Promega, WI, USA)
- Hydrogen Peroxide (Sigma, MO, USA)
- Lead Nitrate (Agar Scientific, Stansted, UK)
- Nonidet P40 (VWR, PA, USA)
- NSA (Nonenyl Succinic Anhydride) redistilled (Agar Scientific, Stansted, UK)
- Osmium tetroxide (Oxkem, Reading, UK)
- Phenazine-methosulphate (PMS) (Sigma, MO, USA)
- Protease Inhibitor Cocktail 100x (Thermofisher Scientific, Loughborough, UK)
- S-1 (Dimethylaminoethanol) (Agar Scientific, Stansted, UK)
- Sodium Acetate (VWR, PA, USA)
- Sodium Alginate (Thermofisher Scientific, Loughborough, UK)
- Sodium azide (Acros Organics, Geel, Belgium)
- Sodium Cacodylate (Agar Scientific, Stansted, UK)
- Sodium Carbonate (Fisher Chemical, Loughborough, UK)
- Sodium Chloride (Fisher Chemical, Loughborough, UK)
- Sodium Deoxycholate (Sigma, MO, USA)
- Sodium hydrogen carbonate (VWR, PA, USA)
- Streptolysin O from *Streptococcus pyogenes* (Sigma, MO, USA)
- Tris(hydroxymethyl)methylamine (VWR, PA, USA)
- Triton X-100 (Merck, NJ, USA)

- Tween-20 (VWR, PA, USA)
- Uranyl Acetate (Agar Scientific, Stansted, UK)

2.1.1.12 Kits

- Amplite Colorimetric Calcium Quantitation Kit (AAT Bioquest, CA, USA)
- Pierce BCA Protein Assay Kit (Thermofisher Scientific, Loughborough, UK)
- Screen Quest Fluo-8 No Wash Calcium Assay Kit (AAT Bioquest, CA, USA)

2.1.2 Consumables

- Amicon Ultra-0.5 Centrifugal Filter Devices 3000 nominal molecular weight limit (NMWL) (Merck Millipore, Carrigtwohill, Ireland)
- EM grids (Cu/Pd) (EM Resolutions, Sheffield, UK)
- Eppendorf tubes 1.5 ml (Fisher Brand, Loughborough, UK)
- Glass (for glass knives) (Agar Scientific, Stansted, UK)
- Minisart 0.2 µm filter units (Sartorius Stedim, Göttingen, Germany)
- Nunclon Delta Surface 96 well plates (Thermo Scientific Nunc, Roskilde, Denmark)
- Nunclon Delta Surface cell culture flasks (Thermo Scientific Nunc, Roskilde, Denmark)
- Nunclon MaxiSorp 96 well plates (Thermo Scientific Nunc, Roskilde, Denmark)
- Razorblades (Fisher Brand, Loughborough, UK)
- SEM stubs (EM Resolutions, Sheffield, UK)
- Slide-a-lyzer G2 Dialysis Cassettes. 10000 MWCO (Thermo Scientific, IL, USA)
- µ-Slide 8 well Glass Bottom (Ibidi GmbH, Martinsried, Gemany)

2.1.3 Instruments and Devices

- Centrifuge 5702 (Eppendorf, Hamburg, Germany)
- Chemidoc XRS chemiluminescence detection system (Bio-Rad, CA, USA)
- Cytoflex flow cytometer (Beckman Coulter, Brea, CA, USA)
- FEI Quanta 250 Scanning Electron Microscope (Thermofisher Scientific, Loughborough, UK)
- FluoStar Omega microplate reader (BMG Labtech, Offenburg, Germany)
- Hera cell 150 Incubator (Thermo electron corporation, MA USA)
- Hera Safe Cell Culture Hood (Thermo electron corporation, MA USA)
- Hitachi U1100 Spectrophotometer (Hitachi, Tokyo, Japan)

- Leica TCS SP5 (Leica Microsystems, Wetzlar, Germany)
- Leica TCS SP8 (Leica Microsystems, Wetzlar, Germany)
- Megafuge 1.0 (Heraeus, Hanau, Germany)
- Microcentaur (Sanyo, Osaka, Japan)
- Nanodrop ND-1000 (Thermofisher Scientific, Loughborough, UK)
- Neubauer Chamber (Marienfield, Lauda-Königshofen, Germany)
- Q150T ES Turbomolecular pumped coater (Quorum, Laughton, UK)
- Reichert Om3-U3 Ultramicrotome (Leica Reichert, Germany)
- Technai T12 Transmission Electron Microscope (Thermofisher Scientific, Loughborough, UK)

2.1.4 Software

- CytExpert (Version 2.1.0.92, Beckman Coulter Life Sciences, Indianapolis, IN, USA)
- GraphPad Prism 7 (GraphPad Software, La Jolla, CA, USA)
- LAS AF Lite (Leica Microsystems, Wetzlar, Germany)
- MARS Data Analysis Software (BMG Labtech, Offenburg, Germany)
- SigmaPlot 13.0 (Systat software Inc, San Jose, CA, USA)

2.2 Chemistry Methods

2.2.1 Calcium Ion Depletion of Foetal Calf Serum

In order to perform cell-based assays in the absence of extracellular Ca^{2+} it was necessary to remove Ca^{2+} from the FCS used to supplement culture medium. In brief, 20 g Chelex-100 chelating resin (Biorad) was resuspended in 500 ml of water and the pH adjusted to 7.4 with concentrated HCl. The resin was then filtered and added to 50 ml FCS. The mixture was stirred for 3h at room temperature before filtering to remove the resin. The filtered FCS was then sterilized via a 0.2 µm filter. 10 ml Ca^{2+} free FCS was added to 100 ml Ca^{2+} free Dulbecco's Modified Eagle's Media (DMEM) (Gibco) containing 2 mM glutamine and 2 mM sodium pyruvate. Supplemented Ca^{2+} depleted media hereafter known as CFD10.

2.2.2 Ca^{2+} Quantitation

Ca^{2+} concentration of FCS and media was determined using a chromogenic Ca^{2+} indicator (Amplite Colorimetric Calcium Quantitation Kit, AAT Bioquest). The assay was run following the manufacturer's instructions and a standard curve was prepared from the provided Ca^{2+} standard

solution by measuring the absorbance at 450 nm for the concentrations of 0.047, 0.094, 0.1875, 0.375, 0.75, 1.5 and 3 mM Ca^{2+}. The absorbance was measured on a FLUOstar Omega microplate reader. This standard curve was used to determine the Ca^{2+} concentration of FCS, RPMI 1640 medium containing 10% FCS, supplemented with 2 mM glutamine and 2 mM sodium pyruvate (referred to hereafter as R10) and DMEM containing 10% foetal calf serum (FCS), supplemented with 2 mM glutamine and 2 mM sodium pyruvate (referred to hereafter as D10. It was also used to measure the effect of Ca^{2+} depletion on FCS and the Ca^{2+} concentration of CFD10. All samples were run in duplicate and the assay was repeated three times using separate standard curves.

2.2.3 Fluorescent Labelling of Saporin and OKT10-SAP

To observe the trafficking of internalised saporin and OKT10-SAP and their proposed endosomal escape in the presence of SA, fluorescent conjugates were constructed with an Alexa Fluor 488 5-TFP (Life Technologies).

To do this 800 µl of 9.3 mg/ml saporin SO6 or 3.5 mg/ml OKT10-SAPORIN were added to 100 µl carbonate buffer (1 M $NaHCO_3$, pH 9.0) and 100 µl of Alexa-Fluor 488 5-TFP (10 mg/ml in DMSO). Following stirring for 1 h at room temperature to effect conjugation, unconjugated fluorophore was removed by exhaustive dialysis for two hours at 4°C against 2 L PBS followed by a further 2 L of PBS overnight at 4°C. The concentrations of the resultant fluorescent conjugates were calculated using the Beer-Lambert law from their absorbance at 280 nm and 495 nm as measured on a Hitachi U1100 Spectrophotometer.

2.2.4 Determination of N-glycosidase activity

The N-glycosidase activity of RIPs and RIP conjugates was determined by measurement of adenine release from herring sperm DNA[195]. A standard curve was prepared with adenine at concentrations of 2, 5, 10, 20, 30, 40, 50 and 60 µg/ml in acetate buffer (50 mM CH_3COONa, 100 mM KCl, pH 5.0). Absorbance for each concentration at 260 nm was measured with a Nanodrop 1000 spectrophotometer (Thermofisher Scientific). To determine the N-glycosidase activity of a toxin, 10 µl of 3 µM toxin was added to 10 µl of herring sperm DNA (10 mg/ml, Promega) and 30 µl of acetate buffer. Enzymatic activity occurred over 1 hour at 50°C with continuous shaking. Samples were diluted with 200 µl of acetate buffer before being filtered with an Amicon Ultra 0.5 centrifuge filters (3000 MWCO for 20 min at 13000 g). The adenine concentration in the filtrate was determined by measuring absorbance at 260 nm and comparing to the standard curve. All experiments were performed in duplicate and the mean calculated

2.3 Cell Biology Methods

2.3.1 Cell Culture

Cell culture experiments were performed using the Daudi human Burkitt lymphoma cell line[270] and the T-cell acute lymphoblastic leukaemia cell line HSB-2[271]. These were obtained from the European Collection of Cell Cultures (ECACC, Porton Down, Salisbury, UK). Cell lines were authenticated using the Identifier Plus DNA profiling system (Applied Biosciences, Carlsbad, CA, USA). Working cell banks were produced and frozen in liquid nitrogen. Cultures were maintained in the logarithmic growth phase at a concentration of no more than $1x10^6$ cells per ml by regular passage in R10. Cells were incubated at 37°C in 7% CO_2 in a humidified environment for no longer than four weeks following which a fresh vial of cells were resurrected from the working cell bank. Cell counts were performed using a haemocytometer in the presence of 0.2% trypan blue.

Reagent availability meant that for experiments requiring cells in a low extracellular Ca^{2+} media, a Ca^{2+} free variant of DMEM was used. This was supplemented with Ca^{2+} depleted FCS as described above (2.2.1). Cells used in these experiments were resurrected and maintained in D10.

2.3.2 Cytotoxicity Determination by XTT Assay

The cytotoxicity of toxins and immunotoxins for Daudi and HSB-2 cells were determined by a metabolic cell viability assay using the tetrazolium salt 2,3-Bis-(2-Methoxy-4-Nitro-5-Sulfophenyl)-2H-Tetrazolium-5-Carboxanilide (XTT). In the presence of an electron coupling reagent, XTT is reduced to a water-soluble orange coloured formazan compound by electron transport across the plasma membrane of living cells [272] [273]. The amount of XTT reduced is relative to the cellular metabolic activity. By measuring the absorbance of the formazan compound and comparing to untreated control cells the cytotoxicity of different toxins can be assessed.

For evaluation of the cytotoxicity of Saporin, Gelonin or OKT10-SAP and their augmentation by SA, Daudi or HSB-2 cells were plated in clear 96 well plates (Nunc) at a density of 50000 cells per well in phenol free R10. Toxin or immunotoxin at varying concentrations was added to the wells in the presence or absence of 1 or 5 µg/ml SA. Each concentration of IT was tested in quadruplicate. Plates were incubated for 48 h at 37°C before cytotoxicity was measured by XTT assay.

To perform the assay, 50 µl of 1 mg/ml XTT solution with 125 µM phenazine-methosulphate (PMS) was added to each well and plates were incubated for 4.5 h at 37°C. Absorbance at 470 nm and 650 nm were measured on a microplate reader (FLUOstar Omega, BMG Labtech). The 470 nm readings were corrected against blank wells containing no cells and against the 650 nm reading

for non-specific absorbance. Results were expressed as a percentage of control cells cultured in medium or SA alone and are the mean of four separate wells. The EC_{50} was determined from the intercept of the dose-response curve with the 50% level on the y-axis and the fold increase in cytotoxicity due to SA then calculated as the ratio of the EC_{50} of the toxin alone and the EC_{50} of the toxin with SA as described in the following formula:

$$\frac{EC_{50}\text{ Value for IT without SA}}{EC_{50}\text{ Value for IT with SA}} = \text{Fold Increase}$$

2.3.2.1 Investigation of the Effect of Ca^{2+} Depletion on the Augmentation of OKT10-SAP Cytotoxicity by SA

To investigate the Ca^{2+} dependency of SA-mediated augmentation of OKT10-SAP cytotoxicity, Daudi cells were plated in 96 well plates at a density of 50000 cells per well in D10 or CFD10 and experiments using the XTT assay carried out as described above for OKT10-SAP or Saporin. The Ca^{2+} free DMEM used in the production of CFD10 contained phenol red, therefore phenol red containing DMEM was also used to produce the D10 used in these experiments. The presence of phenol red in the media increased the absorbance measurements above the level readable by the microplate reader. To compensate for this the path length was reduced by removing 150 µl from each well after incubation with XTT and transferring this to a new 96-well plate for measurement.

CFD10 was supplemented with $CaCl_2$ to 0.02, 0.2, 1.2 and 2.0 mM to perform add-back experiments. Cytotoxicity assays were performed as above in supplemented CFD10 at each concentration of $CaCl_2$.The difference in fold increase between cells in D10 and CFD10 and between cells in CFD10 and CFD10 supplemented with each concentration of $CaCl_2$ was analysed by Mann-Whitney U-Test.

2.3.2.2 Investigation of the Effects of Pharmacological Inhibitors on the Augmentation of Saporin and OKT10-SAP Cytotoxicity by SA

Small molecule pharmacological inhibitors were used to investigate the role of different endocytic pathways and endosomal acidification on SA-mediated augmentation of cytotoxicity. To identify an optimum concentration of each inhibitor toxicity titrations were performed against Daudi cells by XTT assay alone and in the presence of a fixed concentration of OKT10-SAP or OKT10-SAP and SA. The results of these titrations were used as a guide to select the highest sub toxic concentration for use in subsequent experiments.

Using the XTT assay, a dose-response titration with Saporin ($1x10^{-14}$ M to $1x10^{-5}$ M) or OKT10-SAP ($1x10^{-16}$ M to $1x10^{-7}$ M) was conducted in the presence or absence of 1 or 5 µg/ml of SA in cultures

of Daudi or HSB-2 cells. Daudi cells were exposed continuously to 0.01 µM nocodazole, 0.005 µM bafilomycin A1, 25 µM EIPA, 100 µM chloroquine, 7.5 µM chlorpromazine, 0.75 µM cytochalasin D or $1x10^{-5}$ M amitriptyline and HSB-2 cells to 0.01 µM nocodazole, 0.005 µM bafilomycin A1, 20 µM EIPA, 10 µM chloroquine, 7.5 µM chlorpromazine or 0.75 µM cytochalasin D. The difference in fold increase between uninhibited control cells and cells treated with each inhibitor was analysed by Mann-Whitney U-Test.

2.3.3 Investigation of the Effect of Ca^{2+} Depletion on Daudi Cell Growth and the Augmentation of OKT10-SAP Cytotoxicity by SA

To determine the effect of calcium depletion on Daudi cell growth 25ml cell culture flasks (Corning) were seeded with 15 ml of cells at 25000 cells per ml in D10 or CFD10. Cells were incubated at 37°C with 7% CO_2. After 24, 48, 72 and 96 hours 1ml of cells were taken from each flask and the cell count number was determined with a Neubauer chamber using trypan blue to assess cell viability.

2.3.4 Fluorescent Measurement of Ca^{2+} Influx

To measure any influx of Ca^{2+} from the media into the cytoplasm of the cell upon exposure to various concentrations of SA, Daudi cells were loaded with the fluorescent Ca^{2+} binding dye Fluo-8 (AAT Bioquest, California). For measurement by microplate reader, cells were plated into 96 well clear bottomed black plates at 25000 cells per well as described in the manufacturers protocol with the modification that Ca^{2+} free HHBS was used and that cells were resuspended in D10 or CFD10. Plates were centrifuged at 135 g for 2min to settle out the cell suspension and then incubated in the dark at 37°C for 30min followed by 30min at room temperature. In the microplate reader (FLUOstar Omega, BMG Labtech) 10µl of SA in Ca^{2+} free HHBS or buffer alone was injected into each well at a final concentration of 1, 10, 20 and 40 µg/ml and fluorescence with 485 nm excitation/520 nm emission was recorded every 0.2 s for 50 s. To investigate longer term fluctuations measurements were made every 3.6 s for 15 min.

2.3.5 Propidium Iodide Cell Permeabilisation Assay

The membrane impermeant fluorescent DNA/RNA binding stain propidium iodide (PI) was used to measure the permeabilisation of membranes by SA. To measure the effect of a low extracellular Ca^{2+} level on the permeabilisation of Daudi cells by SA. Cells were washed three times in DMEM or DMEM containing 10 mM EGTA before being pulse exposed to a variety of SA concentrations for 1 min, washed and resuspended in DMEM or DMEM with 10 mM EGTA. Cells were incubated at

37°C for 5 min. Samples were centrifuged at 470 g for 5 min, the supernatant was aspirated off and 200 µl 5 µg/ml PI in DMEM or DMEM with 10 mM EGTA was added. Samples were read on a Cytoflex flow cytometer (Beckman Coulter) and results analysed with CytExpert software. Cells with a fluorescence on the phycoerythrin (PE) filter (585/42 band pass) 2 logs greater than the mean fluorescence of control cells were considered permeabilised. The number of permeabilised cells was expressed as a percentage of total cells.

2.3.6 Investigation of the Effect of SA on Surface LAMP-1 and Ceramide by Flow Cytometry and Confocal Microscopy

The effect of SA on the surface expression of LAMP-1 and ceramide was investigated by flow cytometry and confocal microscopy. Daudi cells were counted and resuspended in RPMI-1640 supplemented with 1 mM $CaCl_2$ before being added to flow cytometry tubes at $2.5x10^5$ cells per tube. Cells were then exposed to SA at 1, 10, 20 or 40 µg/ml. Tubes were incubated at 4°C for 5 min followed by 37°C for 15 min. After incubation cells were washed with RPMI, then tubes were centrifuged and aspirated. Cells were stained with murine anti-ceramide IgM or anti-LAMP-1 IgG2b mAbs or with IgM or IgG2b Isotype control mAbs at 10 µg/ml in a blocking buffer of PBS and 1% BSA for 30 min at 4°C. This was followed by washing and then exposure to a relevant, FITC labelled secondary antibody for a further 30 min at 4°C. For measurement by flow cytometry cells were resuspended in 200 µl of RPMI and read on a Cytoflex flow cytometer. The difference in mean fluorescence intensity between untreated cells and those treated with each concentration of SA was analysed by unpaired t-test for significance.

For confocal microscopy, cells were fixed in 1 ml of 4% PFA for 90 min at 4°C. After fixing cells were washed twice in RPMI and resuspended in 10 µl of RPMI before being embedded in agarose. Moulds were made by gluing two no. 1.5 glass coverslips to either end of a microscope slide. A second slide was placed on top so that the coverslips create a gap of approximately 0.35 mm between the slides. The two slides were then taped together and kept on a hotplate set at 37°C to keep warm. Aliquots of 2% low melting point agarose were melted in a beaker of hot water and 10 µl of melted agarose was added to the cells. The mixture was then quickly pipetted between the two slides to form small discs. Prepared slides were kept at 4°C for 1 h to allow the gel to set. Once set gels were transferred to 24 well plates and stained for 30 min with 10 µg/ml Hoechst 33342 nuclear stain. Gels were then mounted on glass microscope slides under a coverslip with mowiol. Slides were left overnight at 4°C to set before being read on a Leica SP8 confocal microscope.

2.3.7 Transmission Electron Microscopy

Transmission electron microscopy was used to investigate ultra-structural changes induced in Daudi cells by SA that might be indicative of membrane damage and subsequent MEND characterised by excessive caveolae, endosomes and multivesicular body formation. Daudi cells were incubated in varying concentrations of SA (1-20 µg/ml) for 30 s, 5 min, 15 min and 30 min at 37°C in order to observe any MEND-like activity. Additionally, cultures of Daudi cells were treated with SA at 1 µg/ml SA for 48h to observe any longer-term effects. The bacterial pore forming toxin streptolysin O (SLO)(Sigma) from *Streptococcus pyogenes* was used as a positive control for membrane permeabilisation and repair via MEND[266]. To activate the oxygen sensitive toxin, stock SLO (Sigma) at 300 U/µl was added to an equal volume of the reducing agent DTT at 0.2 mM and incubated at 37°C for 15 min prior to being diluted to working concentrations. Daudi cells were incubated with 100 U/ml of SLO for 30 s, 5 min, 15 min and 30 min.

Following treatment, cells were washed and then fixed in 1 ml of 3% glutaraldehyde in 0.1M cacodylate buffer with 2 mM $CaCl_2$ (pH 7.4). Cells were fixed at room temperature for 1 h followed by 4°C overnight. After fixation cells were resuspended and pipetted on top of 2 drops of 5% sodium alginate in an Eppendorf and centrifuged at 4500 g. Excess fixative was removed, and the tube filled with 0.1 M $CaCl_2$ before being stored at 4°C overnight for the alginate to set. Set alginate pieces were stained for 2 h with 2% osmium tetroxide in 0.1 M cacodylate buffer followed by staining for 30 min with 2% uranyl acetate (aq). Samples were dehydrated stepwise in increasing concentrations of ethanol and then embedded in Spurr resin. Resin was polymerised at 60°C for 24 h. Once set, resin embedded cells were sectioned on an ultra-microtome (Leica Reichert), mounted on Cu/Pd grids and stained with Reynolds lead stain [274] before being observed with a Tecnai T12 transmission electron microscope.

2.3.8 Scanning Electron Microscopy

Daudi cells were exposed to 20 µg/ml SA or R10 for 15 min at 37°C before being washed with RPMI-1640 and then fixed in 3% glutaraldehyde in 0.1 M cacodylate buffer. Cells were settled onto APES coated coverslips and post fixed with 1% osmium tetroxide in cacodylate buffer for 1 h. Cells were then dehydrated with ethanol before undergoing critical point drying and sputter coating with platinum. Samples were observed with a FEI Quanta 250 scanning electron microscope.

2.3.9 Investigation of the Internalisation of SAP-AF and OKSAP-AF

Daudi and HSB-2 cells were incubated in 24-well plate wells with $1x10^{-6}$ M SAP-AF or $5x10^{-8}$ M OKSAP-AF in R10 at 37°C, 7 % CO_2 with a separate well per timepoint. At 0, 2, 8, 16, and 24 hours after the start of the incubation, cells were removed from the appropriate wells and washed by centrifugation in RPMI-1640. For confocal microscopy, Hoechst 33342 was added to a final concentration of 5 µg/ml thirty minutes prior to the end of each incubation time.

Cells were resuspended in 200 µl of R10 and added to Ibidi 8 well glass bottomed plates. Images were acquired using a Leica TCs-SP8 laser scanning confocal microscope on a DMi8 inverted microscope stand with a HC PL APO CS2 63x /1.30 glycerol immersion objective zoom 2.25 and Leica LAS-X acquisition software at 37°C. Excitation lengths of 405 nm and 488 nm were used for Hoechst 33342 and the Alexa Fluor 488 conjugates respectively.

For flow cytometry, cells were resuspended in 100 µl of RPMI-1640 in flow tubes and analysed at 10 µl/min on a Cytoflex flow cytometer (Beckman Coulter) equipped with 488 nm 50 mW laser. Approximately 10000 events were recorded per sample. Alexa Fluor 488 data was collected with a 525/40 nm bandpass filter with height (FITC-H), width (FITC-W) and area parameters recorded. Data was recorded and analysed using CytExpert software.

2.3.10 Co-localisation Studies

Daudi and HSB-2 cells were incubated with $1x10^{-6}$ M SAP-AF for 24 hours in R10 at 37°C, 7 % CO_2. Cells were washed in RPMI-1640 and fixed in 4 % PFA before being set in 2 % low melting point agarose. Cells were permeabilised with 0.2 % Triton X-100 and incubated with either chicken anti EEA1 or mouse anti LAMP-1, washed, incubated with goat anti-chicken Alexa Fluor 555 or goat anti-mouse Alexa Fluor 568, washed and mounted. Images were acquired using a Leica TCs-SP8 laser scanning confocal microscope on a DMi8 inverted microscope stand with a HC PL APO CS2 63x /1.30 glycerol immersion objective zoom 2.25 and Leica LAS-X acquisition software at 37°C. Excitation lengths of 405 nm and 488 nm were used for Hoechst 33342 and the Alexa Fluor 488 conjugates respectively. An analysis of co-localisation between SAP-AF and EEA1 or LAMP-1 was performed on the slice at the midline of cells relative to the coverslip for each Z-stack. The Coloc2 plugin for ImageJ was used to calculate the Pearson correlation coefficient as a measure of colocalisation.

2.3.11 Investigation of Endolysosomal Escape of SAP-AF and OKSAP-AF by Confocal Live Cell Imaging

Daudi and HSB-2 cells were incubated with $1x10^{-6}$ M SAP-AF or $5x10^{-6}$ M OKSAP-AF in R10 at 37°C, 7 % CO_2 for 24 hours. Hoechst 33342 was added to a final concentration of 5 µg/ml thirty minutes prior to the end of each incubation time. Cells were washed, resuspended in 200 µl of R10 with or without SA at 1 µg/ml or 5 µg/ml, added to Ibidi 8 well glass bottomed plates and incubated at 37°C, 7 % CO_2. Images were acquired using a Leica TCs-SP8 laser scanning confocal microscope at 37°C after 0, 8, 16 and 24 hours of incubation. The gain on the FITC channel was set at t = 0 h and not modified for the duration of the experiment. In order to maximise the sensitivity of the microscope to detect low levels of cytosolic fluorescence, the gain was set so that the fluorescent intensity of endosomal compartments at this time point were saturating. For inhibitor experiments, 100 µM chloroquine, 25 µM EIPA or 7.5 µM chlorpromazine were added to Daudi cells prior to the addition of SA.

2.3.12 Investigation of Endolysosomal Escape of SAP-AF and OKSAP-AF by Flow Cytometry

Daudi cells were incubated with $1x10^{-6}$ M SAP-AF or $5x10^{-9}$ M OKSAP-AF in R10 at 37°C, 7 % CO_2 for 24 hours. This was repeated with HSB-2 cells with $1x10^{-6}$ M SAP-AF or $5x10^{-9}$ M OKSAP-AF. Cells were washed and resuspended in R10 before being plated in 96 well plates at $1.25x10^5$ cells per well with or without SA at 5 µg/ml, 1 µg/ml or 0.1 µg/ml in a final volume of 250 µl. Plates were incubated at 37°C, 7 % CO_2 and duplicated samples of cells were removed from appropriate wells at 0 and 24 hours after the addition of SA. Cells were washed, resuspended in 100 µl of RPMI-1640 in flow tubes and the FITC-H and FITC-W of 10000 events were measured on a Cytoflex Flow Cytometer (Beckman Coulter) using CytExpert software (Version 2.1.0.92, Beckman Coulter Life Sciences, Indianapolis, IN, USA).

For inhibitor experiments, Daudi cells were exposed to 0.01 µM nocodazole, 0.005 µM bafilomycin A1, 25 µM EIPA, 100 µM chloroquine, 7.5 µM chlorpromazine or 0.75 µM cytochalasin D and HSB-2 cells to 0.01 µM nocodazole, 0.005 µM bafilomycin A1, 20 µM EIPA, 10 µM chloroquine, 7.5 µM chlorpromazine or 0.75 µM cytochalasin D prior to the addition of SA. Cells were recorded at 0, 6, 24 and 48 hours after the addition of SA.

2.4 Biochemistry Methods

2.4.1 Investigation of CD38 Binding by OKT10-SAP and OKSAP-AF by Enzyme Linked Immunosorbent assay

Nunclon MaxiSorp 96 well plates were coated with 100 µl of 400 µg/ml recombinant CD38 in ELISA coating buffer (15 mM Na_2CO_3, 35 mM $NaHCO_3$, 15 mM NaN_3) for 1 h at 37°C and then overnight at 4°C. Plates were blocked with 1% BSA in PBS for 1 h at 37°C before being washed with PBS-Tween. OKT10-SAP or OKSAP-AF at a range of concentrations between 0.01 and 100 µg/ml were added to the plate and incubated at 37°C for 1 h. Plates were then washed three times in PBS-Tween before the addition of 100 µl rabbit anti-mouse IgG:Horseradish Peroxidase (HRP) at 1:1000 to each well. After incubation for 1 h at 37°C, plates were washed five times with PBS-Tween. 100 µl of TMB substrate was added to each well. After 10 min the reaction was stopped with 25 µl of 2.5 M H_2SO_4 and the absorbance at 450 nm was read using a FluoStar Omega microplate reader with 655 nm used as a reference value.

2.4.2 Investigation of Secondary Antibody Binding to OKT10-SAP and OKSAP-AF

Nunclon MaxiSorp 96 well plates were coated with OKSAP-AF or OKT10-SAP at a range of concentrations between 0.01 and 100 µg/ml in ELISA coating buffer. Plates were incubated for 1 h at 37°C and then overnight at 4°C before being blocked with 1% BSA in PBS for 1 h at 37°C. Following washing three times in PBS-Tween, 100 µl rabbit anti-mouse IgG HRP at 1:1000 was added to each well. After incubation for 1 h at 37°C, plates were washed five times with PBS-Tween. 100 µl of TMB substrate was added to each well. After 10 min the reaction was stopped with 25 µl of 2.5 M H_2SO_4 and the absorbance at 450 nm was read using a FluoStar Omega microplate reader with 655 nm used as a reference value.

Chapter 3 Role of Membrane Repair Processes in the Augmentation of OKT10-SAP Cytotoxicity by SA

3.1 Introduction

Plasma membrane repair processes are activated by membrane damage and result in the internalisation of damaged membrane sections via MEND. The aim of the work performed in this chapter was to investigate the hypothesis that membrane repair processes may be involved in the internalisation of saponins and their ability to augment the cytotoxicity of saporin based ITs. Such augmentation occurs at saponin concentrations that do not appear to permeabilise the plasma membrane as measured by PI influx[195,212] or cellular impedance[233]. However there remains the possibility that lower concentrations of SA cause plasma membrane damage that is quickly repaired and thus is not detected by these methods. Previous work in our laboratory with the Daudi cell line has identified an optimal, non-permeabilising and sub-toxic yet augmentative concentration of the saponin mixture saponinum album (SA) as 1 µg/ml [196]. To this end, experiments were performed to look for evidence of membrane repair in Daudi cells exposed to SA, particularly at 1 µg/ml.

Membrane repair involves a complex, multi-stage process as described in 1.4.3.4. The triggering step of which is the influx of Ca^{2+} into the cell from the extracellular milieu through the permeabilised plasma membrane. Therefore, it was investigated whether Ca^{2+} influx could be detected in Daudi cells in response to SA exposure over a broad range of concentrations from permeabilising to non-permeabilising. Depletion of Ca^{2+} from the extracellular environment has been shown to inhibit the resealing of damaged plasma membrane[260]. Chelation of Ca^{2+} by EGTA was used to study whether the level of cell membrane permeabilisation caused by SA was increased in the absence of extracellular Ca^{2+} due to a reduction in membrane repair. To investigate whether membrane repair processes are involved in augmentation of cytotoxicity, the cytotoxicity of the IT OKT10-SAP was measured with and without SA in Ca^{2+} depleted media. Influx of Ca^{2+} caused by membrane damage leads to lysosomal exocytosis and the release of ASM onto the surface of the cell. This leads to the generation of ceramide on the external leaflet of the plasma membrane. To look for evidence of lysosomal exocytosis in response to exposure to SA, plasma membrane expression of the abundant, lysosome luminal membrane associated glycoprotein, LAMP-1 was investigated. LAMP-1 is not normally present on the plasma membrane but becomes exposed on the cell surface following lysosomal exocytosis[260]. The activity of ASM released from the lysosomal lumen onto the plasma membrane was also looked for by measuring

any changes in plasma membrane ceramide levels. The ASM dependency of augmentation was determined through the use of the pharmacological inhibitor amitriptyline. Finally, evidence of the ultrastructural changes associated with MEND, including the generation of large numbers of endocytic vesicles or caveolae and the formation of MVBs, were looked for using electron microscopy.

3.2 Results

3.2.1 Production and Testing of a Ca^{2+} Depleted Growth Media

In order to investigate the potential role of Ca^{2+} influx in the augmentation of OKT10-SAP cytotoxicity by SA it was necessary to produce a Ca^{2+} depleted growth media. In experiments performed in this media there would be a reduced Ca^{2+} influx in response to plasma membrane permeabilisation and therefore an inhibition of membrane repair processes. In these experiments DMEM was used as an alternative to RPMI-1640 due to the easier availability of a Ca^{2+} free version of the media. Ca^{2+} free DMEM was supplemented with FCS that had been treated with Chelex-100 Ca^{2+} chelating resin (2.2.1). The Ca^{2+} concentration of the Chelex-100 treated FCS was confirmed using an Amplite Colorimetric Calcium Quantitation Kit (2.2.2). Calcium chelation successfully reduced the Ca^{2+} concentration of FCS from 2.9 mM to approximately 0.1 mM. When used to supplement Ca^{2+} free DMEM the resulting CFD10 had a Ca^{2+} concentration of < 0.05 mM. Standard DMEM supplemented with untreated FCS (D10) has a Ca^{2+} content of 1.25 mM (Table 2).

Table 2 Ca^{2+} Concentration of Media

Ca^{2+} concentration of FCS and media used in Ca^{2+} deprivation experiments as measured by Amplite Colorimetric Calcium Quantitation Kit. D10 and CFD10 are described in 2.3.1 and 2.2.1 respectively. Concentrations represent the mean of three independent experiments and the standard deviation either side of this mean.

	Ca^{2+} Concentration (mM)
Foetal Calf Serum	2.93 ± 0.04
Chelex-100 Treated FCS	< 0.1
D10 Media	1.25 ± 0.02
CFD10 Media	< 0.05

The effect of Ca^{2+} depletion on Daudi cell growth and viability was assessed by cell counts and trypan blue exclusion. Daudi cells grown in CFD10 showed extensive clumping on visual inspection and greatly reduced growth rates over 72 hours compared to those grown in D10 (Figure 3). However, no significant decrease in cell viability by trypan blue exclusion was observed (>90% in all cultures).

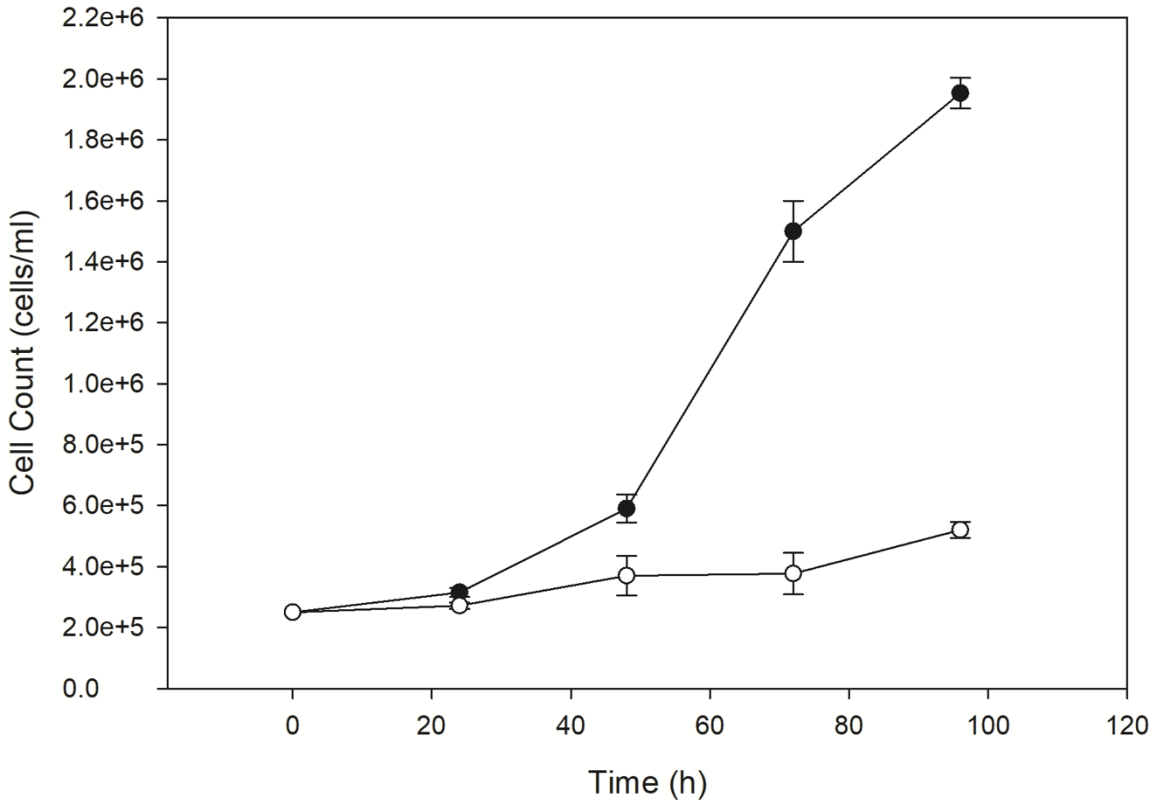

Figure 3 Daudi Cell Growth in Ca^{2+} Depleted Media

Growth of Daudi cells in D10 medium (●) and Ca^{2+} depleted D10 (CFD10) media (○). Cells were resuspended at $2.5x10^5$ cells per ml at t = 0 and counted every 24 hours. Each data point represents the mean of 3 independent cell cultures and the error bars the standard deviation either side of this mean.

3.2.2 Fluorescent Measurement of Ca^{2+} Influx into Daudi Cells Treated with SA

Fluo-8 is a cell permeable fluorescent dye consisting of a Ca^{2+} chelator conjugated to a fluorescein molecule. In the absence of Ca^{2+} the chelator acts to quench the fluorescence of the fluorophore. An increase in Ca^{2+} concentration and binding of Ca^{2+} to the chelator inhibits this quenching activity. The fluorescence intensity Fluo-8 therefore increases when it binds to Ca^{2+} allowing it to be used as a detector for Ca^{2+} influx into the low Ca^{2+} intracellular environment following membrane permeabilisation[275]. Studies were conducted in which Fluo-8 was pre-loaded into

Daudi cells followed by treatment with a range of SA concentrations and the fluorescence measured over a period of time using a BMG microplate reader.

Initial fluorescence readings were performed over a 50 s period with measurements taken every 0.2 s. SA, or D10 in control cells, was added after 12 s. Ca^{2+} influx was observed in Daudi cells within approximately 15 s of exposure to both 40 µg/ml and 20 µg/ml of SA and within 35 s of exposure to 10 µg/ml (Figure 4A). The rate of increase in fluorescence was concentration dependent, with SA at 40 µg/ml inducing the most rapid change. To compare the effect of different concentrations of SA on Ca^{2+} influx the percentage change between the fluorescence at 12.2 s and that at 50 s was calculated. A significant increase in fluorescent signal was recorded in cells treated with 10, 20 and 40 µg/ml of SA compared to control cells mock treated with D10. No significant increase in fluorescence was measured in cells treated with 1 µg/ml of SA as determined by Mann-Whitney U test(Figure 4B).

To confirm whether the increase in fluorescence was due to Ca^{2+} influx into cells the experiment was performed in a reduced Ca^{2+} environment. D10 was replaced with CFD10 and Ca^{2+} free HBSS was used. It was not possible to run the experiment in a completely Ca^{2+} free environment due to the presence of Ca^{2+} in the assay kit reagents. Daudi cells were treated with both 1 µg/ml and 20 µg/ml of SA. In the reduced Ca^{2+} media the increase in fluorescence seen in cells treated with 20 µg/ml of SA was slower and fluorescence intensities were lower for the duration of the experiment (Figure 4C). No calcium influx was observed in control cells or in those cells exposed to 1 µg/ml SA.

To investigate whether a slower influx of Ca^{2+} would be observed with the lower concentration of 1 µg/ml over a longer period of time the experiment was repeated recording fluorescence every 3.6 s for 15 min (Figure 4D). In cells treated with 10, 20 and 40 µg/ml of SA an initial rapid increase in fluorescence was observed followed by a concentration dependent gradual increase over time. This change is likely due to leakage of Fluo-8 out of permeabilised cells into the high Ca^{2+} extracellular media where it fluoresces. Over this time period no difference was observed in cells treated with 1 µg/ml of SA when compared to control cells. This observation provides further evidence that 1 µg/ml of SA does not permeabilise the plasma membrane.

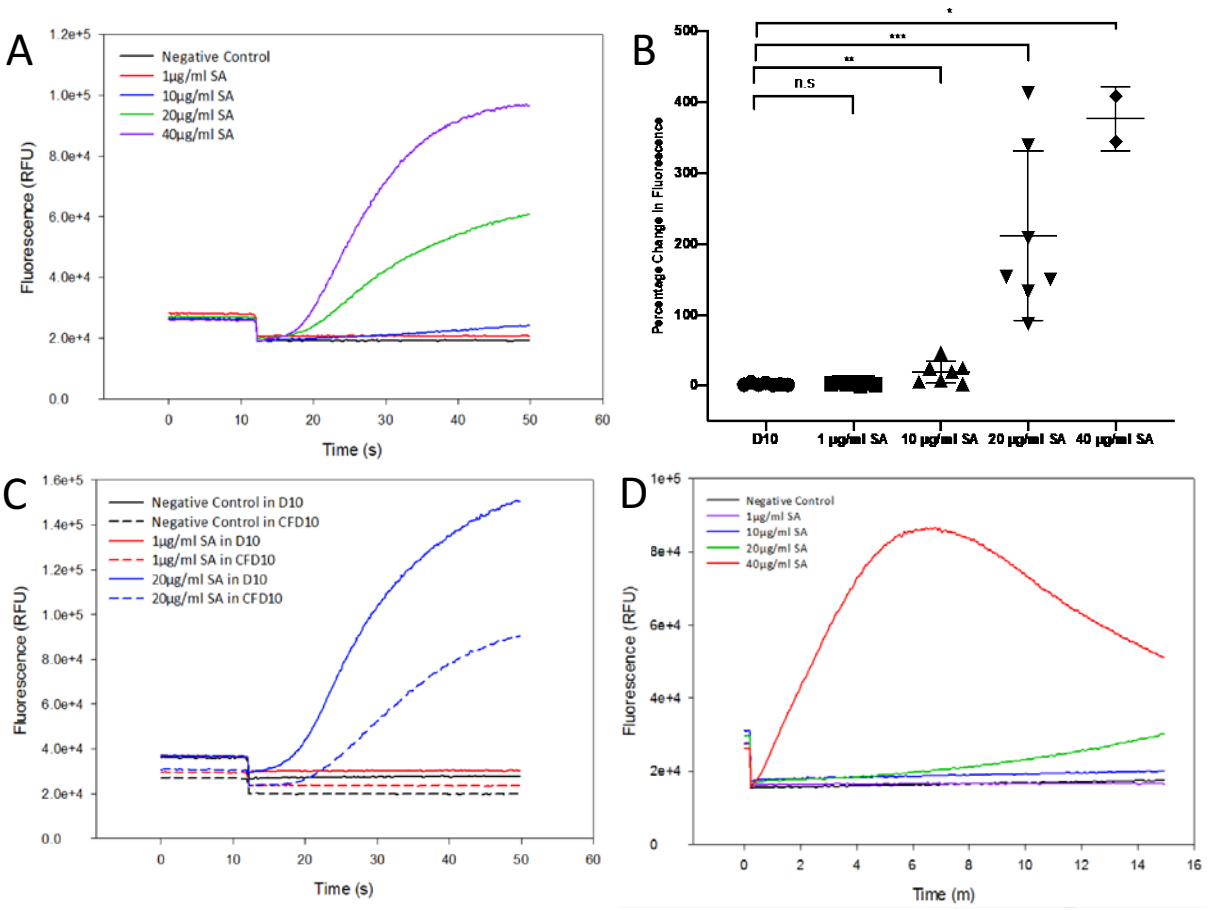

Figure 4 **Fluorescent Measurement of Ca^{2+} Influx in Daudi Cells Following Treatment with SA**

Daudi cells seeded in 96 well plates were pre-loaded with the fluorescent Ca^{2+} sensor Fluo-8. Fluorescence in each well was measured by BMG microplate reader as cells were treated with a range of SA concentrations. A: Each line represents the change in fluorescence over time of a single, representative well of Daudi cells treated with 1, 10, 20 or 40 µg/ml of SA at t = 12 s (indicated by the arrow) with fluorescence measured every 0.2s for 50 s. B: Percentage change in fluorescence between 12.2 s and 50 s in Daudi cells treated with D10 (●), 1 (■), 10 (▲), 20 (▼) and 40 (◆) µg/ml of SA. A significant increase in fluorescence was measured in cells treated with 10 µg/ml (p = 0.0023), 20 µg/ml (p 0.006) and 40 µg/ml (p = 0.0444). Dots represent percentage change in individual experiments with the lines showing the mean and one standard deviation either side of this mean (n_{D10} = 7, $n_{1\ \mu g/ml}$ = 7, $n_{10\ \mu g/ml}$ = 7, $n_{20\ \mu g/ml}$ = 7, $n_{40\ \mu g/ml}$ = 2) A smaller number of experiments were performed with 40 µg/ml of SA due to limitations in the availability of high concentration stock. C: Fluo-8 loaded Daudi cells in D10 medium or Ca^{2+} depleted CFD10 medium treated with 1 µg/ml or 20 µg/ml of SA after 12 s with fluorescence measured every 0.2 s for 50 s. D: Fluo-8 loaded Daudi cells in D10 medium treated with 1, 10, 20 or 40 µg/ml of SA after 12 s with fluorescence measured every 3.6 s for 15 min.

3.2.3 Ca^{2+} Depletion Reduces the Augmentation of OKT10-SAP Cytotoxicity by SA

The cytotoxicity of the IT OKT10-SAP was evaluated in Daudi cells grown in D10 using the XTT assay and the dose-response curves obtained are shown in Figure 5A. A clear cytotoxic effect from OKT10-SAP was observed at concentrations greater than $1x10^{-12}$ M. The concentration of OKT10-SAP alone that caused a 50% reduction in viability (EC_{50}) of OKT10-SAP on Daudi cells was estimated to be $1x10^{-10}$ M. To investigate the augmentation of OKT10-SAP cytotoxicity by SA Daudi cells were treated with a combination of OKT10-SAP and SA at the non-lytic concentration of 1 µg/ml. This combination showed increased cytotoxicity and the EC_{50} value for OKT10-SAP and 1 µg/ml SA used in combination was $2x10^{-13}$ M. A 500-fold increase in the EC_{50} was calculated as the ratio of the EC_{50} of OKT10-SAP and the EC_{50} of OKT10-SAP with SA.

When this assay was performed in CFD10 the cytotoxicity of the OKT10-SAP was slightly increased and an EC_{50} of $5x10^{-11}$ M was observed (Figure 5B). However, the cytotoxic effect of the combination of OKT10-SAP and SA was greatly reduced and the EC_{50} for the combination was estimated as being $9x10^{-11}$ M with a fold increase of just 5.5 over OKT10-SAP alone. This observation shows that the augmentation of OKT10-SAP by SA in Daudi cells was largely abrogated following growth in CFD10 and is therefore Ca^{2+} dependent.

To confirm that the observed abrogation was caused by the depletion of Ca^{2+}, and not by the depletion of other metal ions by the chelating resin, $CaCl_2$ was used to restore the Ca^{2+} concentration of CFD10 in add-back experiments. CFD10 was supplemented with 0.2 mM, 0.6 mM or 1.2 mM $CaCl_2$ and the effect of this Ca^{2+} add-back on the augmentation of OKT10-SAP cytotoxicity was measured using the XTT assay (Figure 5C-E). Augmentation of OKT10-SAP by SA was restored in a Ca^{2+} concentration dependent manner with fold gains in cytotoxicity of 70, 220 and 300-fold at 0.2 mM, 0.6 mM and 1.2 mM of $CaCl_2$ respectively (Figure 5F). This observation further demonstrates that the SA augmentation of OKT10-SAP cytotoxicity is Ca^{2+} dependent.

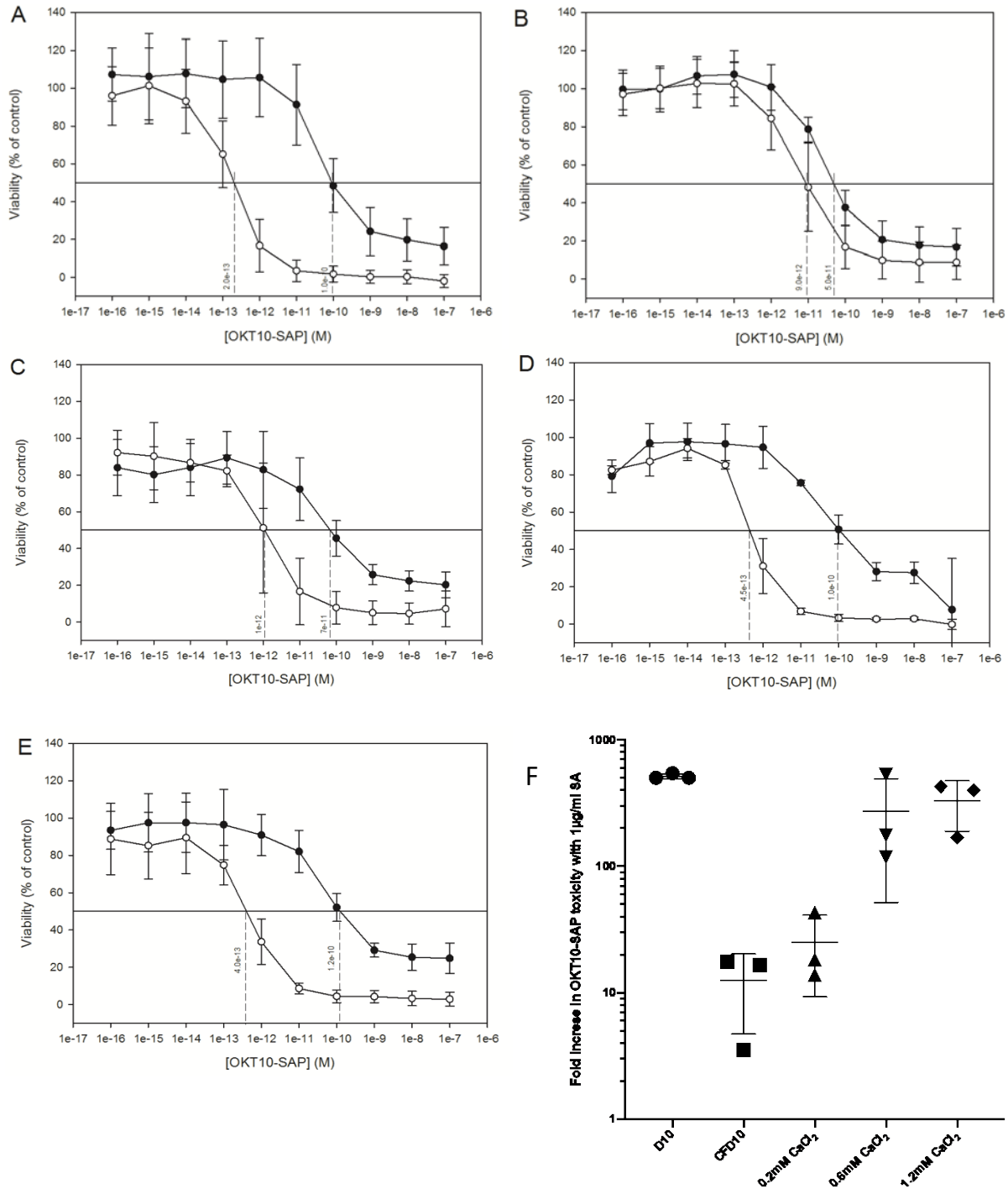

Figure 5 **Effect of Ca^{2+} Deprivation and Add-back on the Augmentation of OKT10-SAP Cytotoxicity by SA**

A-E: Dose-response curves determined by XTT assay for Daudi lymphoma cells in D10 (A), CFD10 (B) and CFD10 supplemented with 0.2 mM (C), 0.6 mM (D) or 1.2 mM (E) CaCl2 in the absence (●) or presence (○) of SA at 1 µg/ml. Each datum point represents the calculated mean of three independent experiments performed in quadruplicate and the error bars one standard deviation either side of this mean. The EC_{50} obtained from each curve is shown against the perpendicular dotted line. F: Fold increases in OKT10-SAP cytotoxicity with 1 µg/ml in D10 (●), CFD10 (■) and CFD10

supplemented with 0.2 mM (▲), 0.6 mM (▼) and 1.2 mM (◆) $CaCl_2$. Dots represent fold increase in individual experiments with the lines showing the mean and one standard deviation either side of this mean. (SA: Saponinum album, D10: DMEM containing 10% FCS, CFD10: Ca^{2+} free DMEM with 10% Ca^{2+} depleted FCS)

3.2.4 Ca^{2+} Deprivation by EGTA Increased the Rates of Permeabilisation in Cells Exposed to SA

Following membrane damage, repair processes are initiated by lysosomal exocytosis triggered by the influx of Ca^{2+} down a 10,000-fold concentration gradient into the cell. Removal of this concentration gradient has been shown to prevent membrane repair[260]. The purpose of this part of the study was to investigate whether the permeabilisation of cell membranes by SA is repaired in a calcium dependent fashion using the fluorescent DNA intercalating agent PI as a reporter. Daudi cells exposed to a range of SA concentrations for 1 min were allowed 5 min to repair in DMEM or DMEM containing the Ca^{2+} chelator EGTA. Figure 6 shows that cells incubated in the presence of EGTA showed an increase in the number of permeabilised cells when compared with those incubated in Ca^{2+} containing DMEM. A significant increase, as determined by unpaired, two-tailed t-test, was seen with all concentrations of SA (Figure 6D). This result suggests that extracellular Ca^{2+} is necessary for the repair of cellular plasma membrane damage caused by SA and that depletion of Ca^{2+} in the extracellular medium reduces the effectiveness of membrane repair mechanisms.

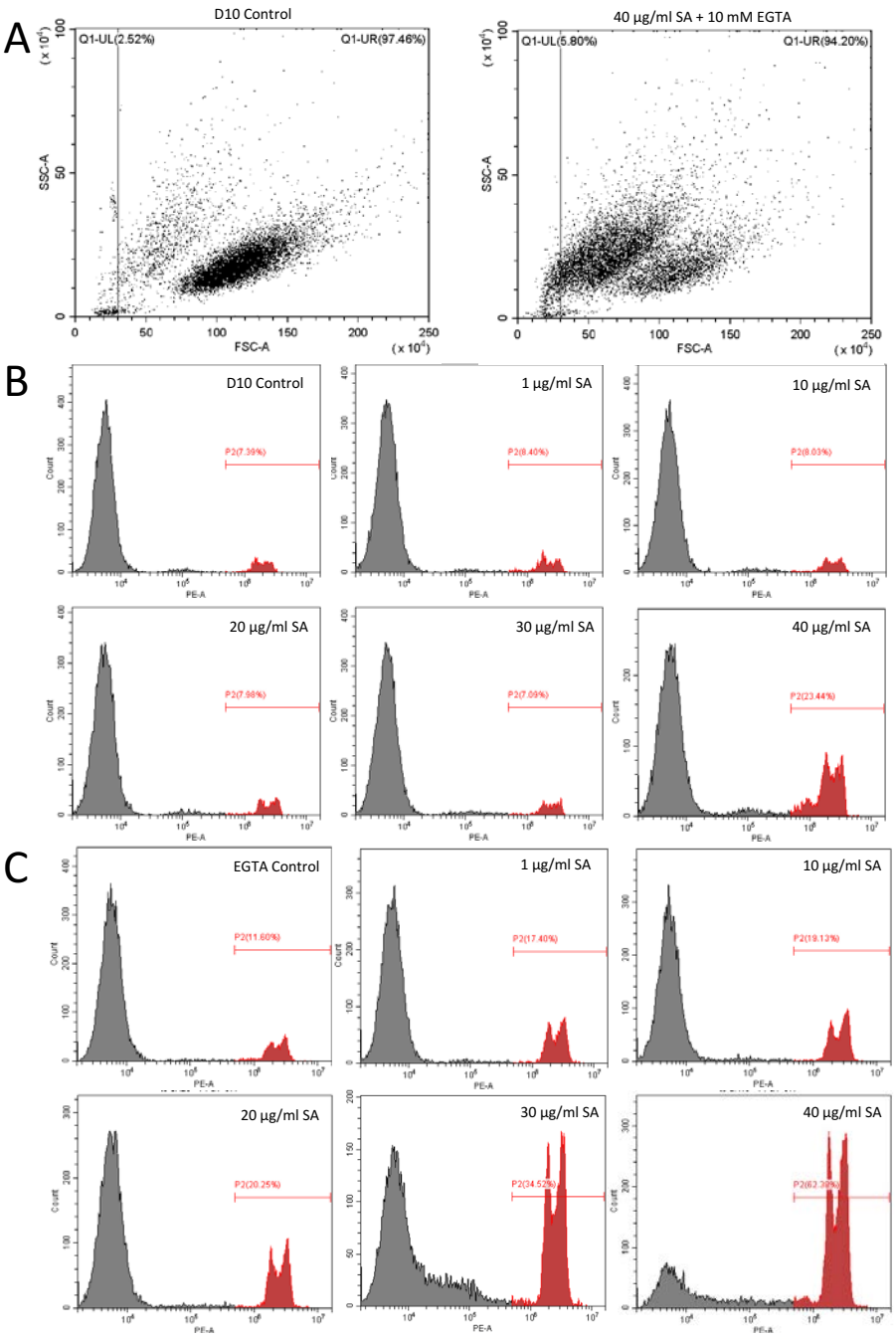
A
D10 Control
40 µg/ml SA + 10 mM EGTA
Q1-UL(2.52%)
Q1-UR(97.46%)
Q1-UL(5.80%)
Q1-UR(94.20%)
SSC-A
FSC-A
B
D10 Control
1 µg/ml SA
10 µg/ml SA
20 µg/ml SA
30 µg/ml SA
40 µg/ml SA
C
EGTA Control
1 µg/ml SA
10 µg/ml SA
20 µg/ml SA
30 µg/ml SA
40 µg/ml SA
D
DMEM
DMEM + 10 mM EGTA
Percentage of Cells Permeabilised
[SA] (µg/ml)
n.s
*
**
**
**
***

Figure 6 The Effect of Extracellular Ca^{2+} Concentration on Daudi Plasma Membrane Permeabilisation by SA

(A) Example dot plots showing the change in forward and side scatter between Daudi cells in DMEM and those treated with 40 µg/ml of SA in 10 mM EGTA. Cells were gated as shown to exclude cell debris and the upper right quadrant gate (Q1-UR) was analysed for PI influx. (B) Histograms showing PE filter fluorescence in Daudi cells treated with different concentrations of SA in DMEM as shown. Gating for permeabilised cells was set at 2 logs above control cells. (C) Histograms showing PE filter fluorescence in Daudi cells treated with different concentrations of SA in DMEM with 10 mM EGTA as shown. Gating for permeabilised cells was set at 2 logs above control cells. (D) Graph showing the percentage of permeabilised Daudi cells in DMEM or DMEM with 10 mM EGTA following treatment with 1, 10, 20, 30 or 40 µg/ml of SA or mock treated with DMEM. Each bar is the mean of 5 independent experiments and the error bars one standard deviation either side of this mean. A significant increase in the percentage of permeabilised cells in the presence of EGTA was seen with 1 ($p = 0.0162$), 10 ($p = 0.0043$), 20 ($p = 0.001$), 30 ($p = 0.0057$) and 40 µg/ml ($p = 0.0003$) of SA when compared to the same concentrations of SA in the absence of EGTA.

3.2.5 Cell Surface Expression of LAMP-1 and Ceramide in Daudi Cells Exposed to SA

Ca^{2+} influx into the cell through permeabilised sections of the plasma membrane triggers lysosomal exocytosis. This releases ASM from the lysosomal lumen onto the outer leaflet of the plasma membrane which then acts to convert sphingomyelin in this leaflet into ceramide leading to the initiation of MEND. To look for evidence that lysosomal exocytosis is occurring in Daudi cells exposed to a range of SA concentrations, the surface expression of the lysosomal protein LAMP-1 and of ceramide were investigated using flow cytometry and confocal microscopy.

With both anti-LAMP-1 and anti-ceramide antibodies the mean fluorescence of untreated cells was higher with the specific primary antibody and secondary than with the equivalent non-specific isotype control and secondary antibodies. No significant increase in fluorescence was observed by flow cytometry for Daudi cells treated with 1, 10 or 20 µg/ml of SA ($p > 0.05$, unpaired t-test) and then stained with anti-LAMP-1 antibody (Figure 7A). A significant increase in fluorescence for LAMP-1 was only seen in cells treated with 40 µg/ml of SA ($p = 0.0002$). Consistently between different experiments, there was a small but non-significant reduction in LAMP-1 signal observed with both 10 µg/ml and 20 µg/ml of SA. Confocal microscopy was used to image what was taking place at the intracellular level. In a small number of untreated control cells

LAMP-1 was observed in discrete sections of the plasma membrane in a small number of cells (Figure 7C-F). No observable increase in surface LAMP-1 expression was seen in cells exposed to 1 μg/ml of SA. In Daudi cells treated with 40 μg/ml of SA, vesicular intracellular LAMP-1 was detected. This indicates that the increase in fluorescence seen by flow cytometry with this concentration of SA was due to permeabilisation of the plasma membrane allowing access of the primary and secondary antibodies into the cytosol that then interacted with intracellular antigen. The likelihood therefore is that the increase in fluorescence see with 40 μg/ml of SA by flow cytometry was probably not due to an increase in surface LAMP-1 expression following membrane repair.

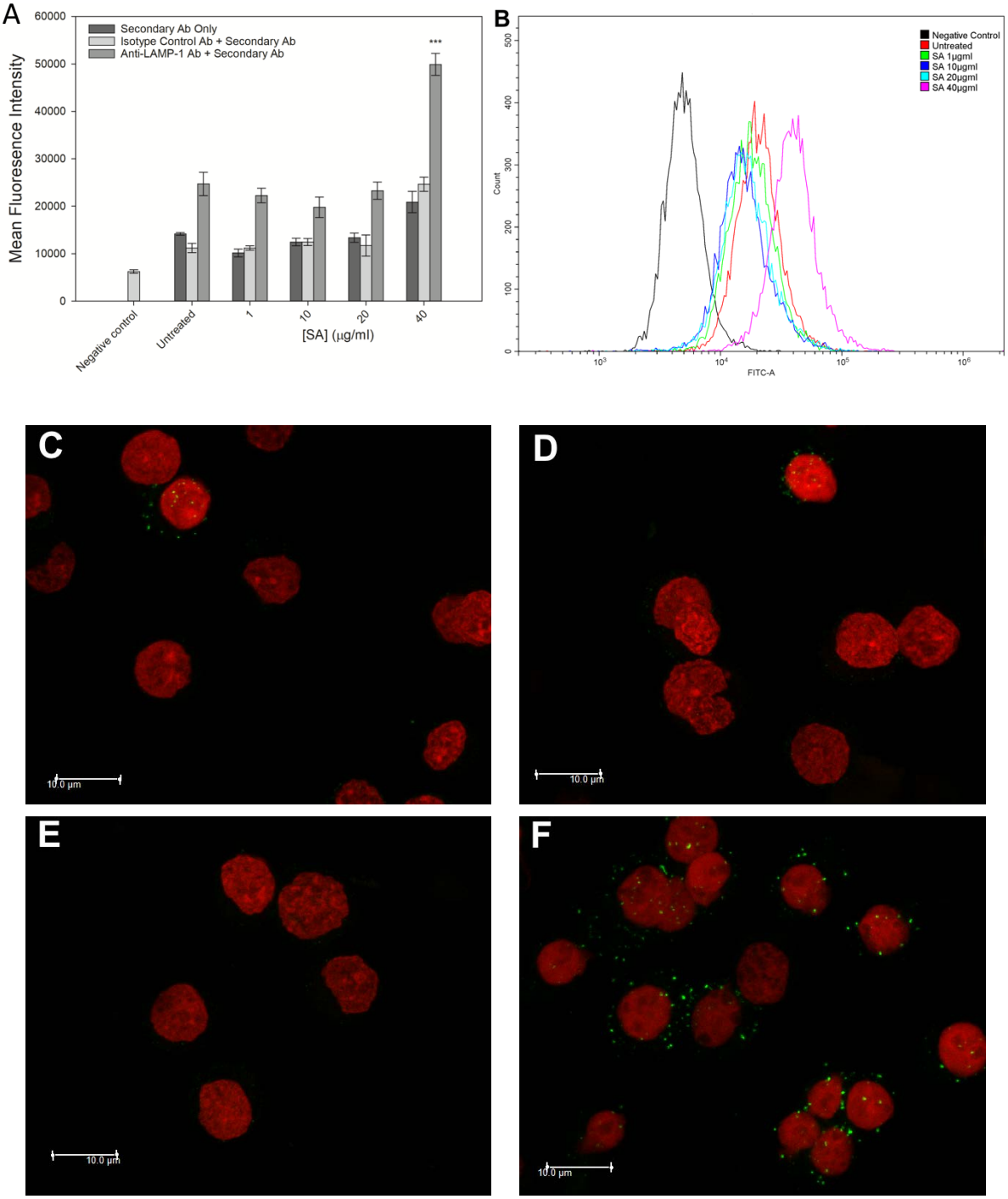

Figure 7 **LAMP-1 Surface Expression in Daudi Cells Treated with SA**

(A) Mean fluorescence intensity of Daudi cells treated with 1, 10, 20 or 40 µg/ml of SA. Columns in each group represent cells stained, from left to right, with FITC labelled secondary antibody only, isotype control and secondary and anti-LAMP-1 and secondary antibodies. Treatment with 40 µg/ml of SA significantly increased LAMP-1 MFI (p=0.0002 ***) over untreated cells, no other treatment was significant. (B) Flow cytometry histogram showing fluorescence for Daudi cells treated with 1, 10, 20 or 40 µg/ml of SA and stained with anti-LAMP-1 and FITC labelled secondary

antibodies. Confocal microscopy of untreated Daudi cells (C) or those treated with 1 µg/ml (D), 20 µg/ml (E) and 40 µg/ml (F) and stained with anti-LAMP-1 and FITC labelled secondary antibodies and Hoechst 33342 nuclear stain. Images presented are maximum projections of 13 x 1 µm z-stacks.

Similar results were observed in Daudi cells stained with anti-ceramide antibodies; there were no significant changes in mean fluorescence intensity with concentrations of SA below 40 µg/ml whilst treating cells with 40 µg/ml of SA resulted in a significant increase in fluorescence ($p < 0.0001$) (Figure 8A). Using confocal microscopy, it was demonstrated that the fluorescence seen with 40 µg/ml of SA was due to staining of intracellular membranes once again probably due to ingress of primary and secondary antibodies into the cytosol through the permeabilised plasma membrane. In control cells, ceramide was detected in the plasma membrane of a majority of cells observed and there was no increase in the amount of plasma membrane ceramide detected when cells were treated with 1 µg/ml SA, supporting the flow cytometry data (Figure 8C-F).

These combined data suggest that no lysosomal exocytosis is occurring in cells exposed to SA including at the augmentative but non-permeabilising concentration of 1 µg/ml of SA and by inference that no obvious membrane repair processes are activate when Daudi cells are treated with this concentration.

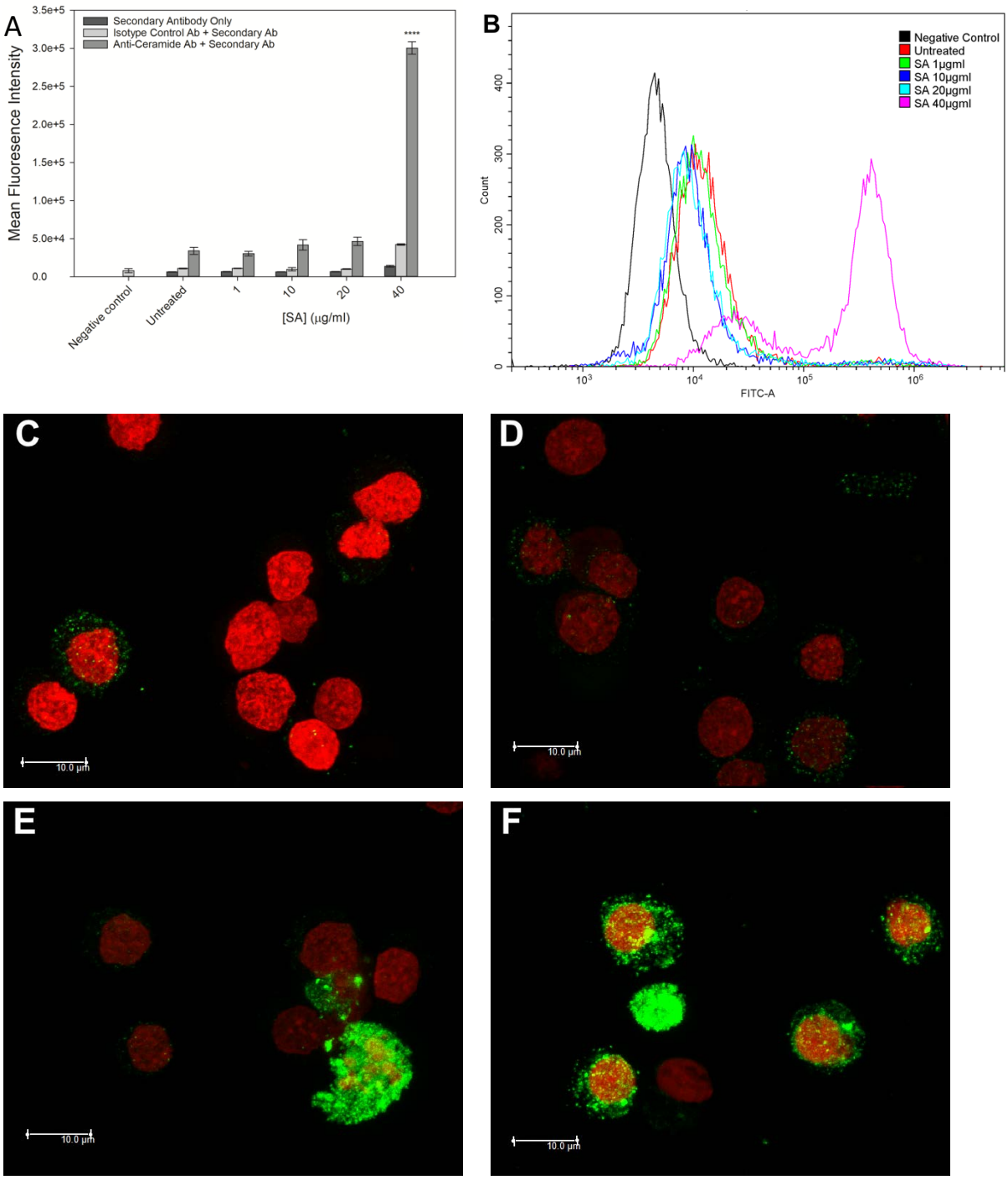

Figure 8 **Plasma Membrane Ceramide Levels in Daudi Cells Treated with SA**

Mean fluorescence intensity of Daudi cells treated with 1, 10, 20 or 40 µg/ml of SA. Columns in each group represent cells stained, from left to right, with FITC labelled secondary antibody only, isotype control and secondary and anti-ceramide and secondary antibodies. Treatment with 40 µg/ml of SA significantly increased Ceramide MFI ($p < 0.0001$ ***) over untreated cells, no other treatment was significant. (B) Histogram showing fluorescence for Daudi cells treated with 1, 10, 20 or 40 µg/ml of SA and stained with anti-ceramide and FITC labelled secondary antibodies. Confocal microscopy of untreated Daudi cells (C) or those treated with 1

µg/ml (D), 20 µg/ml (E) and 40 µg/ml (F) and stained with anti-ceramide and FITC labelled secondary antibodies and Hoechst 33342 nuclear stain. (The bright cell in the bottom right corner of (E) is anomalous) Images presented are maximum projections of 13 x 1µm z-stacks. The high Hoechst staining seen in (C) was anomalous and not representative of other imaging.

3.2.6 Augmentation of OKT10-SAP Cytotoxicity by SA is Inhibited by the ASM Inhibitor Amitriptyline

Acid sphingomyelinase implicated in MEND resides in the lysosome, electrostatically bound to the inner lysosomal membrane[276,277]. The tricyclic antidepressant amitriptyline is a functional inhibitor of ASM[278]. Amitriptyline has weak basicity and high lipophilicity allowing it to diffuse across the lysosomal membrane. Inside the acidic lysosomal compartment the drug is protonated and becomes trapped, leading to its accumulation in the lysosome[279]. This disrupts the binding of ASM to the inner membrane and leads to its proteolytic degradation within the lysosomal lumen[280]. Amitriptyline was therefore selected for experiments whose aim was to explore whether or not inhibition of ASM activity also abrogated the augmentative effect of SA on IT cytotoxicity.

The cytotoxicity of amitriptyline for Daudi cells was evaluated using the XTT assay in the absence and presence of SA. The cytotoxicity of amitriptyline was not affected by SA (Figure 9A). To find a balance between amitriptyline cytotoxicity and any inhibitory effect it might have on the SA augmentation of OKT10-SAP Daudi cells were treated with increasing concentrations of amitriptyline in the presence of a fixed concentration of OKT10-SAP with or without SA (Figure 9B). From these experiments an optimal sub-toxic concentration of $1x10^{-5}$ M amitriptyline was chosen.

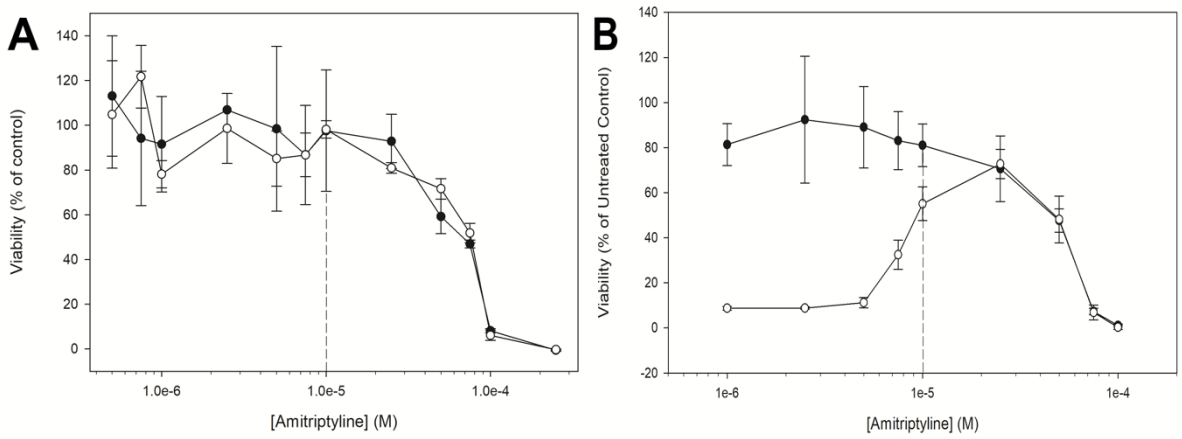

Figure 9 Optimisation of Amitriptyline Cytotoxicity in Daudi Cells

Dose-response curves determined by XTT assay for Daudi cells treated with amitriptyline. (A) shows the cytotoxicity of amitriptyline in the presence (○) and absence (●) of 1µg/ml SA. (B) shows the effect of an increasing concentration of amitriptyline on Daudi cells treated with $1x10^{-11}$M OKT10-SAP in the presence (○) and absence (●) of 1µg/ml SA. Each data point is the mean ± SD, n = 3.

Treatment of Daudi cells with $1x10^{-5}$ M amitriptyline did not affect the cytotoxicity of OKT10-SAP for these cells. In contrast, the cytotoxicity of OKT10-SAP in combination with 1µg/ml SA was significantly reduced (p = 0.0004, 2-way ANOVA), with an almost complete abrogation of augmentation (Figure 10). The fold increase in EC_{50} with SA was reduced from 200-fold in control cells to 7.5-fold with amitriptyline suggesting that ASM may play a role in the augmentation process.

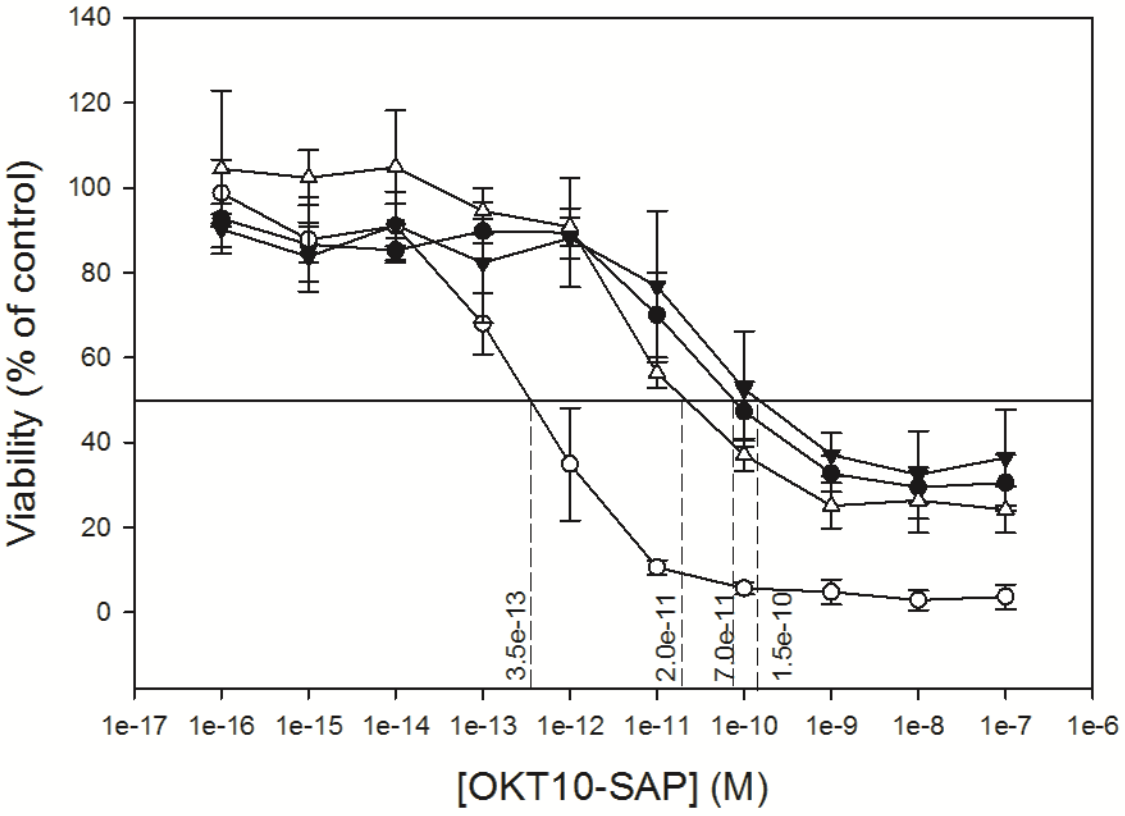

Figure 10 Amitriptyline Abrogates the Augmentation of OKT10-SAP Cytotoxicity by SA

Dose-response curves determined by XTT assay for OKT10-SAP on Daudi lymphoma cells with $1x10^{-5}$ M amitriptyline in the absence (▼) and presence (▽) of 1 µg/ml SA, the data for OKT10-SAP without inhibitor in the absence (●) and presence (○) of SA is also presented for comparison. Each datum point represents the calculated mean of three independent experiments and the error bars one standard deviation either side of this mean. The EC_{50} value obtained from each curve is shown against the perpendicular dotted line.

3.2.7 Ultrastructural Changes in Daudi Cells Treated with SA

3.2.7.1 Transmission Electron Microscopy

Transmission electron microscopy (TEM) was used to investigate any ultrastructural changes taking place in Daudi cells treated with lytic or sublytic concentrations of SA. Cells undergoing membrane repair after treatment with SLO typically show evidence of large numbers of caveolae or endocytic vesicles via TEM[257,258] within a few minutes of exposure. Over time these vesicles have been observed to mature, acquire features of early and late endosomes and treated cells are seen to contain increased numbers of MVBs[266]. In B-cells, treatment with SLO has been shown to result in a significant increase in tubular invaginations of the plasma membrane and small endocytic vesicles[264]. In the current study described here TEM was therefore used to look for evidence of MEND in Daudi cells in the form of caveolae, invaginations of the plasma membrane, increased numbers of endocytic vesicles and the presence of MVBs.

As a positive control for the ultrastructural changes found in Daudi cells following plasma membrane permeabilisation with SA, cells were also treated with SLO. Daudi cells treated with 100 U/ml of SLO demonstrated ultrastructural changes suggestive of MEND. In cells exposed to SLO for 5 min increased numbers of vesicles were observed. These structures varied in size between 100-400 nm and likely represent early endosomes formed from the merging of initial endocytic vesicles (Figure 11A+B). By 15 min after initial exposure these endosomes matured and MVB formation was observed in a number of cells (Figure 11C-E).

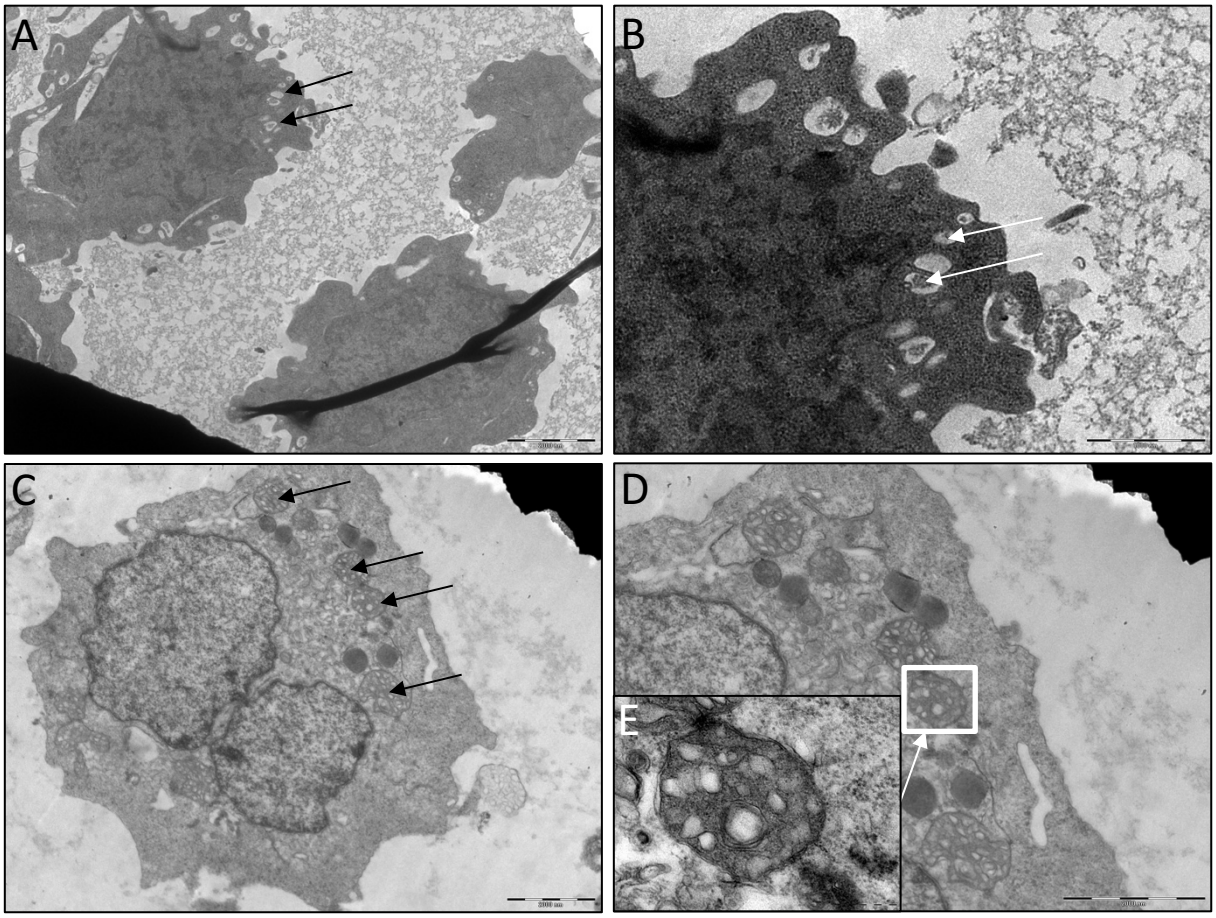

Figure 11 Transmission Electron Microscopy Showing Daudi Cells Exposed to SLO

Daudi cells treated with SLO for 5 min and then imaged by transmission electron microscopy showed increased numbers of endosomal vesicles as indicated by arrows in A and B. After 15 min of treatment with SLO, the formation of MVBs was observed as indicated by black arrows in C. Image D shows an increased magnification of the cell shown in C. A high magnification image of the MVB indicated by the arrow in D is shown in the insert E. Scale bars are shown in the bottom right of each image and represent 2 µm in A, C and D; 1 µm in B and 200 nm in E.

TEM did not reveal any obvious ultrastructural evidence of membrane damage or repair in Daudi cells that were exposed to 1 µg/ml of SA at any time point up to 48 hours. The representative images in Figure 12 show no clear evidence of caveolae, increased levels of endocytosis or MVBs. In cells exposed to 10 µg/ml of SA an increased number of endosomal vesicles were observed after 30 s (Figure 13). These vesicles closely resembled those observed in cells treated with SLO and suggest that membrane repair processes are active in cells treated with this concentration of SA. Unlike cells treated with SLO, no formation of MVBs was observed in these cells at later time points. There was no obvious evidence of membrane disruption or pore formation at any concentration of SA tested.

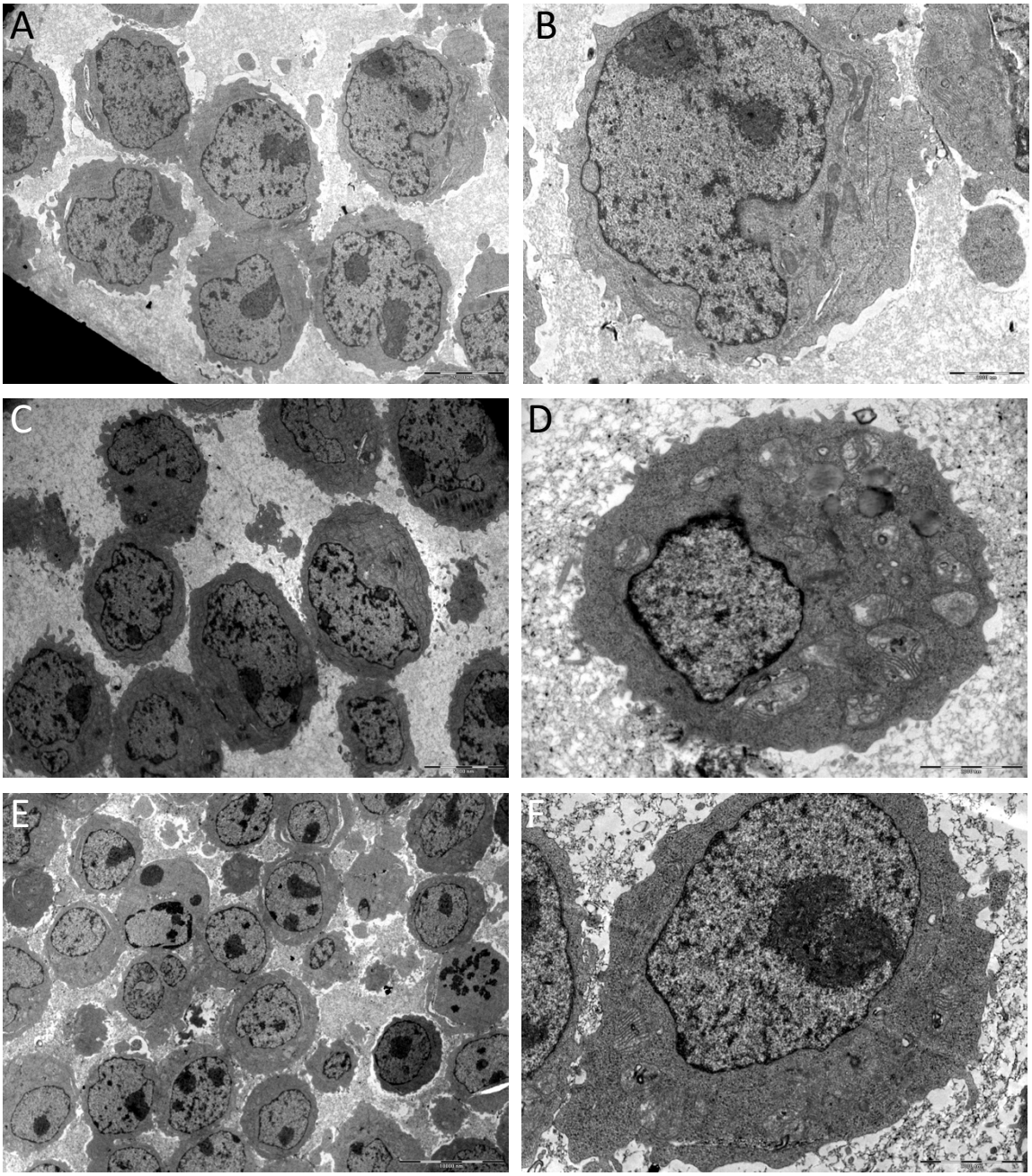

Figure 12 Transmission Electron Microscopy of Daudi Cells Treated with 1µg/ml of SA

Daudi cells treated with 1 µg/ml of SA for varying lengths of time showed no ultrastructural changes associated with MEND at any of the timepoints tested. Representative images of cells exposed to SA for 30 s (C+D) and 48 h (E+F) are shown here. Representative images of untreated control cells are shown in A and B. Scale bars are shown in the bottom right of each image and represent 5 µm in A and C; 2 µm in B, D and F and 10 µm in E.

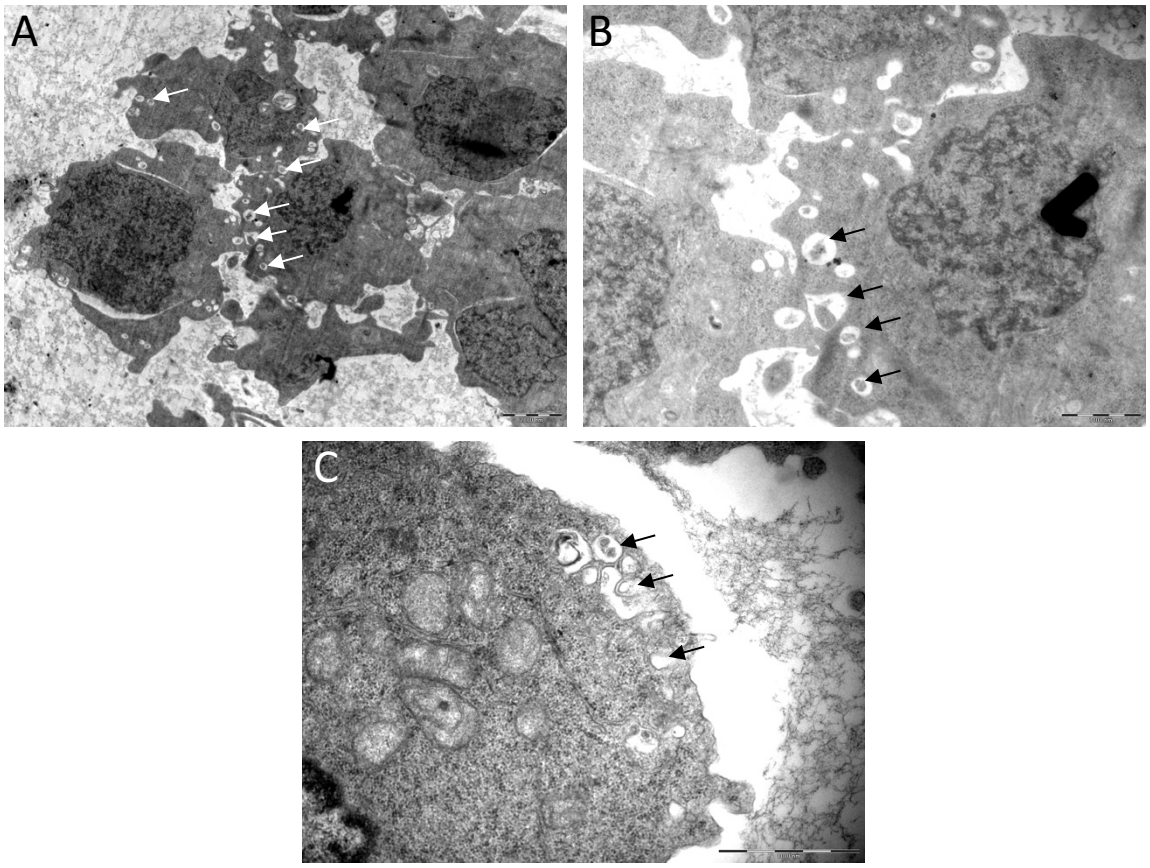

Figure 13 Transmission Electron Microscopy of Daudi Cells Treated with 10 µg/ml of SA

Daudi cells treated with 10 µg/ml of SA showed increased numbers of endosomal vesicles after 30 s of treatment as indicated by arrows in the representative images above. Scale bars are shown in the bottom right of each image and represent 2 µm in A and 1 µm in B and C.

3.2.7.2 Scanning Electron Microscopy

Scanning electron microscopy (SEM) has previously been used to show the presence of membrane holes [281] and plasma membrane blebbing[282] in cells exposed to saponins. Initial TEM work suggested that there might be an increase in membrane ruffling and/or blebbing in SA treated cells. To examine this possibility, SEM was performed to investigate this and to additionally look for any evidence of pore formation. Figure 14 shows representative fields of Daudi cells exposed to 20 µg/ml of SA for 15 min where there was no apparent increase in membrane ruffling activity. Furthermore, no obvious pores were discernible at the plasma membrane surface by SEM.

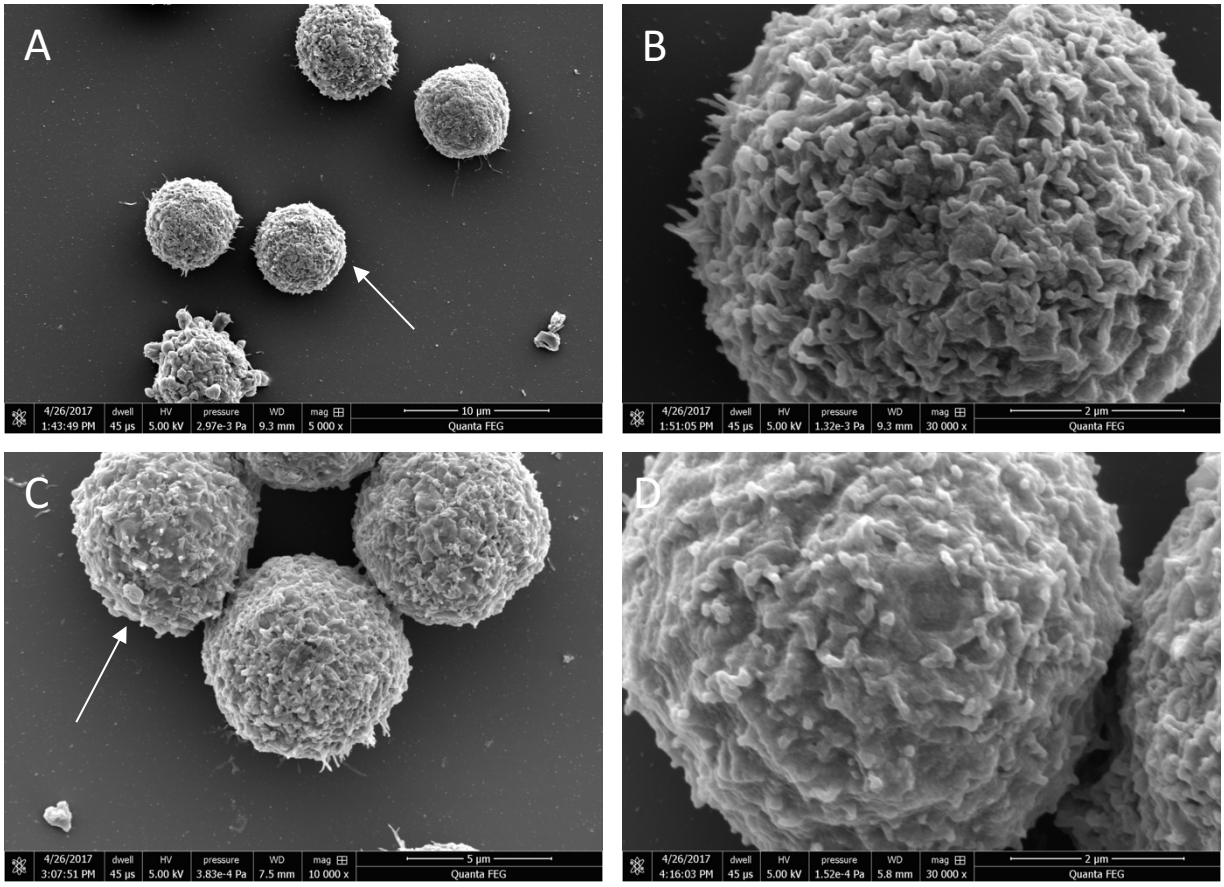

Figure 14 Scanning Electron Microscopy Images of Daudi Cells Treated with SA

Representative SEM images of Daudi cells incubated for 15 min in the absence (A + B) or presence (C + D) of 20 µg/ml of SA. B shows a higher magnification of the cell indicated by an arrow in A, and D a higher magnification of the cell indicated by arrow in C.

3.3 Discussion

The mechanism by which saponins are internalised and their subsequent trafficking to the endolysosomal compartment, where they are theorised to enhance the endolysosomal escape of saporin, is not fully understood. The purpose of the work performed in this chapter was to investigate the hypothesis that sub-lytic concentrations of SA inflict low levels of cell membrane damage leading to the activation of membrane repair processes including MEND that may then internalise membrane associated SA.

Initial experiments focused on the role of Ca^{2+} influx in the repair of cell membranes permeabilised by SA. The use of the Ca^{2+} sensitive dye Fluo-8 clearly detected Ca^{2+} influx into Daudi cells after 35 s of exposure to 10 µg/ml of SA. This concentration of SA was previously considered non-permeabilising as determined by PI assay after 5 min of exposure, suggesting that for investigating transient membrane permeabilisation, a higher level of sensitivity can be achieved by measuring at Ca^{2+} influx. The rate of Ca^{2+} influx was increased by exposing cells to increasing concentrations of SA a result that almost certainly reflects an increasing amount of membrane damage. Critically, no Ca^{2+} influx was detectable even after 15 min of treatment with the augmentative concentration of 1 µg/ml of SA. It is not known whether this was because no membrane damage occurred at this concentration or alternatively whether any resulting Ca^{2+} influx due to low levels of membrane damage was below the sensitivity limit of the assay to detect. These results confirm that SA transiently permeabilises the cell membrane at sub-toxic concentrations, suggesting that this damage must be repaired by the cell. In addition, it confirms that Ca^{2+} influx takes place through the SA-mediated membrane damage.

To confirm whether SA induced plasma membrane damage was repaired in a Ca^{2+} dependent manner, PI permeabilisation assays were performed in the presence of the extracellular Ca^{2+} chelator EGTA. These demonstrated that reduced extracellular Ca^{2+} significantly increased the number of cells permeabilised by PI at all concentrations of SA tested. This suggests that the repair of SA induced membrane damage is dependent on the influx of Ca^{2+} into the cell. It also shows that the use of PI as an indicator of membrane damage is inadequate to investigate low levels of membrane permeabilisation as membrane repair mechanisms are activated before a sufficiently high concentration of PI can enter the cell for detection. The observation in the present study that Ca^{2+} chelation by EGTA increased the permeabilisation of cells exposed to 1 µg/ml of SA hints that this ostensibly sub-lytic concentration of SA does cause a low level of membrane permeabilisation despite the inability to detect any Ca^{2+} influx due to the sensitivity limit of this method.

In the work described in the current chapter the role of Ca^{2+} influx on the augmentation of cytotoxicity was investigated by removing extracellular Ca^{2+} to reduce its influx into damaged cells. Cytotoxicity assays in Ca^{2+} depleted media showed that the augmentation of OKT10-SAP cytotoxicity by SA is abrogated in a low Ca^{2+} extracellular milieu. Augmentation was restored by adding Ca^{2+} back into the media confirming the Ca^{2+} dependency of augmentation. However, it is not possible to conclude from this that membrane repair processes are directly involved due to the vital role Ca^{2+} plays in a wide range of other cellular process. Cytosolic Ca^{2+} concentrations are tightly regulated and localised fluctuations in Ca^{2+} concentration play an important role in intracellular signalling[283]. Ca^{2+} binding activates the adaptor protein calmodulin (CaM) which in turn interacts with hundreds of different proteins resulting in structural changes that remove auto-inhibition, initiate protein dimerisation reactions and/or modify enzyme active sites[284]. Activated CaM enables Ca^{2+} signalling by removing the auto-inhibition of calmodulin kinase enzymes thus activating phosphorylation cascade pathways. Of particular relevance to these observations is the pivotal role that Ca^{2+} plays in cell cycle control[285] and in apoptosis.

Ca^{2+} signals are involved in a number of stages in the cell cycle and Ca^{2+} is required for cell proliferation in non-neoplastic cells [286,287]. Ca^{2+} transients are involved in nuclear envelope breakdown and CaM and Ca^{2+}-CaM dependent protein kinase II are required for progression through mitosis[285]. In the present study, Daudi cells grown in CFD10 were shown to have a greatly reduced growth rate and this may have affected the relative survival rates of these cells whether they were treated with SA or not.

Ca^{2+} plays a major role in many apoptotic pathways with increases in cytosolic Ca^{2+} concentration occurring at both early and late stages in the apoptotic process[288-290]. Under normal conditions cytosolic Ca^{2+} is normally maintained at ~100 nM[283] but can be increased by sustained release from intracellular stores such as the endoplasmic reticulum or alternatively by influx from the extracellular environment[291]. Increased cytosolic Ca^{2+} leads to uptake of Ca^{2+} into the mitochondria and subsequent mitochondrial overload with production of reactive oxygen species (ROS)[292] and mitochondrial permeabilisation leading to cytochrome C release and subsequent caspase activation via the apoptosome[293]. Voccoli and co-workers have demonstrated that extracellular Ca^{2+} depletion reduced mitochondrial ROS production and increased cell survival in cells exposed to a known apoptotic stimulus[289]. It is therefore possible that the reduction in augmentation of OKT10-SAP cytotoxicity by SA in Ca^{2+} depleted media maybe a consequence of a generalised protective effect against apoptotic programmes.

This study examined for evidence of the subsequent stages of membrane repair processes that are activated following Ca^{2+} influx through plasma membrane permeabilisation, including lysosomal exocytosis and MEND. No evidence of an increase in extracellular LAMP-1, which occurs following lysosomal exocytosis[260], was measured with immunocytochemical methods in Daudi cells treated with any concentration of SA. There was also no evidence of an increased level of ceramide on the outer membrane of the cell membrane in SA treated cells which would show the activity of ASM released onto the cell surface by lysosomal exocytosis and is necessary for the membrane invagination that initiates endocytosis of damaged membrane sections. Despite this apparent lack of repair activity, inhibition of ASM by amitriptyline significantly abrogated augmentation by SA. This may show that ASM is involved in augmentation through its role in MEND. However, interpretation of these results is confounded because amitriptyline is not a direct inhibitor of ASM. Instead it acts by increasing lysosomal pH which then causes ASM to disassociate from the inner leaflet of the lysosomal membrane into the lumen where it is degraded by proteases[294]. The mechanism behind the increase in lysosomal pH brought about by amitriptyline is similar to that of chloroquine[240,277]. Therefore, the abrogation of SA augmentation of OKT10-SAP cytotoxicity seen with amitriptyline may instead be due to a reduction in the endolysosomal escape of the toxin resulting from this increase in endosomal pH. This may be due to prevention of the proposed pH dependent association between saponins and saporin, rather than the drug's effect on the degradation of ASM. The question of a mechanistic involvement of ASM in the augmentation of saporin based IT by SA therefore remains unanswered by the present work. Knockdown of the ASM gene using siRNA would be a direct way of disentangling the other effects of a pharmacological agent such as amitriptyline and may represent the best way forward to answer this question.

Lysosomal exocytosis and the activity of ASM at the plasma membrane initiates MEND[295]. In this study TEM was used to look for evidence of this process in the form of caveolae or increased numbers of endocytic vesicles just below the surface of the plasma membrane. Increased numbers of vesicles were seen in Daudi cells exposed to 10 µg/ml of SA, but critically no evidence of MEND was observed at the augmentative concentration of 1 µg/ml of SA.

In conclusion, the evidence presented in this chapter gives a mixed picture about the involvement of membrane damage and membrane repair processes in the augmentation of OKT10-SAP cytotoxicity by SA. There is certainly evidence for membrane damage caused by higher concentrations of SA and for the activation of membrane repair processes in response to this damage. However, augmentation occurs in Daudi cells with concentrations of SA as low as 1 µg/ml and at this concentration there was little evidence for plasma membrane damage and repair using the techniques described. The effects of Ca^{2+} depletion and amitriptyline treatment

on cytotoxicity augmentation are interesting but come with many confounding factors, especially in light of the lack of any apparent lysosomal exocytosis or MEND. Further investigation into the potential role of membrane repair processes would require confirmation that SA at 1 µg/ml causes transient damage to the plasma membrane. A flow cytometric assay to continuously monitor intracellular Ca^{2+} as described by Vines et al may offer a more sensitive method than the microplate reader-based assay used in this study[296]. Any future TEM investigating the internalisation of SA by MEND would be greatly enhanced by the development of antibodies targeting its component saponins. This would allow for the location of any internalised saponins to be identified by immunogold staining which would be crucial for confirming whether MEND is involved in their uptake.

Chapter 4 Role of Major Endocytic Processes in the Augmentation of IT Cytotoxicity and Endolysosomal Escape

4.1 Introduction

As previously discussed, the current hypothesis explaining the mechanism by which saponins augment the cytotoxic activity of saporin and saporin based TTs involves the internalisation and trafficking of both saporin and saponin into same endolysosomal compartment in the target cell. Here the endolysosomal membrane is permeabilised resulting in the escape of the toxin into the cytosol. This permeabilisation occurs at external concentrations of SA which appear to be non-permeabilising for the plasma membrane. A number of possible mechanisms to explain this discrepancy have been suggested. The simplest of these is that the internalisation of SA leads to its accumulation and concentration within the lumen of endolysosomal vesicles, to a level above the lytic threshold. It is also possible that the membrane repair system for endosomal membranes is less robust than that involved in plasma membrane repair and this makes them more susceptible to permeabilisation by SA. Finally, there is some limited experimental evidence showing that saporin and saponins associate non-covalently at the acidic pH levels found in the lumen of endolysosomal vesicles. This has led to the proposal that the endolysosomal escape of saporin to the cytosol is facilitated in some way by such an association in the endolysosomal compartment.

The work detailed in this chapter was therefore aimed at testing a number of aspects of this hypothesis. The first of these was to investigate the role of several endosomal processes in the SA-mediated augmentation of the cytotoxicity of saporin and the saporin based IT, OKT10-SAP. For this purpose, a number of small molecule pharmacological agents with defined activities were employed (Table 3). These experiments aimed to determine the role played in the augmentation of cytotoxicity by endocytic processes such as CME and macropinocytosis and by the polymerisation of actin and microtubules which are involved in the endocytosis and the trafficking of endocytic vesicles respectively. It was anticipated that the use of such pharmacological agents would provide insights into the mechanism of saponin internalisation. The process of endosomal acidification was also inhibited by two separate pharmacological inhibitors in order to investigate the requirement for an acidic intravesicular pH on the augmentation of cytotoxicity. In addition, to further study the requirement for a pH dependent association between augmentable RIPs and

saponin, the potential for the cytotoxicity of the type I RIP gelonin to be augmented by SA was investigated. Gelonin has previously been shown to not associate with saponins at acidic pH[152] but its capacity for augmentation is unknown.

The activity of SA as an endolysosomal escape enhancer was then investigated alongside the role that any SA induced increase in endolysosomal escape might play in the process of the augmentation of cytotoxicity. In order to compare the effects of the pharmacological inhibitors on cytotoxicity with their effects on endolysosomal escape it was necessary to develop an assay to investigate endolysosomal escape. Fluorescent conjugates of saporin and OKT10-SAP were therefore constructed. Initially confocal microscopy was used to determine the effect of SA on the endolysosomal escape of these conjugates. However, limitations in the sensitivity and difficulties in the accurate quantification of results obtained using this methodology together with other technical difficulties prevented the use of confocal microscopy to determine the effect of the tested pharmacological agents on endolysosomal escape. The shortcomings of confocal microscopy as applied to this research question led to the development of an alternative flow cytometric assay. This allowed for a straightforward method to quantify the results and obtain reliable and meaningful data describing the effects of pharmacological agents on endolysosomal escape.

Table 3 Summary of Pharmacological Agents

Summary of the pharmacological agents used in this study to inhibit endocytic processes and endosomal acidification. Listing the process targeted by each agent and a summary of their mechanism of action.

Agent	Process Targeted	Mechanism of Action	References
Chlorpromazine	Clathrin mediated endocytosis	Depletion of clathrin and AP2 from the plasma membrane	[247]
EIPA	Macropinocytosis	Inhibits plasma membrane Na^+/H^+ exchanger leading to sub-membranous acidification and inhibition of Rac1 and Cdc42	[297] [298]
Nocadazole	Microtubule polymerisation	Binds to β-tubulin and disrupts microtubule polymerisation	[299]
Cytochalasin D	Actin polymerisation	Inhibits polymerisation of actin filaments	[300]
Chloroquine	Endosomal acidification	Lysosomotropic, protonated in the endolysosome	[240]
Bafilomycin A1	Endosomal acidification	Inhibits vacuolar H^+ ATPase	[241]

4.2 Results

4.2.1 Effects of Small Molecule Pharmacological Agents on the Augmentation of OKT10-SAP and Saporin Cytotoxicity by SA

The role of different endocytic processes and endosomal acidification on the augmentation of saporin cytotoxicity by SA were investigated with the use of a range of pharmacological agents with known inhibitory activities. These included: chlorpromazine, ethylisopropylamiloride (EIPA), chloroquine, bafilomycin A1, cytochalasin D and nocadazole. Details on the pharmacological activity of each inhibitor are described in the sections below and a summary is presented in Table 3.

To select the optimum concentration of each pharmacological agent the toxicity of each inhibitor in Daudi cells was first investigated via XTT assay (Figure 15). Cells were then exposed to increasing concentrations of inhibitor in the presence of a fixed concentration of $1x10^{-11}$ M OKT10-SAP with and without SA at 1 µg/ml. Results of these optimisation experiments are shown in Figure 16. From these studies optimal concentrations of 7.5 µM chlorpromazine, 25 µM (EIPA), 0.01 µM nocadazole, 0.005 µM bafilomycin A1, 100 µM chloroquine and 0.75 µM cytochalasin D were selected based on minimal toxicity with maximal effect. These optimisation experiments were conducted as validation of work being performed by other members of the research team in this laboratory. As such, only a single representative assay is presented here and experiments determining the optimum concentrations of the listed agents on the T cell acute lymphoblastic leukaemia cell line HSB-2 are not presented here. The relevant studies on HSB-2 cells were subsequently published by Smith et al[301]. From these, the optimal concentrations of 7.5 µM chlorpromazine, 20 µM (EIPA), 0.01 µM nocadazole, 0.005 µM bafilomycin A1, 10 µM chloroquine and 0.75 µM cytochalasin D were selected for use on the HSB-2 cell line.

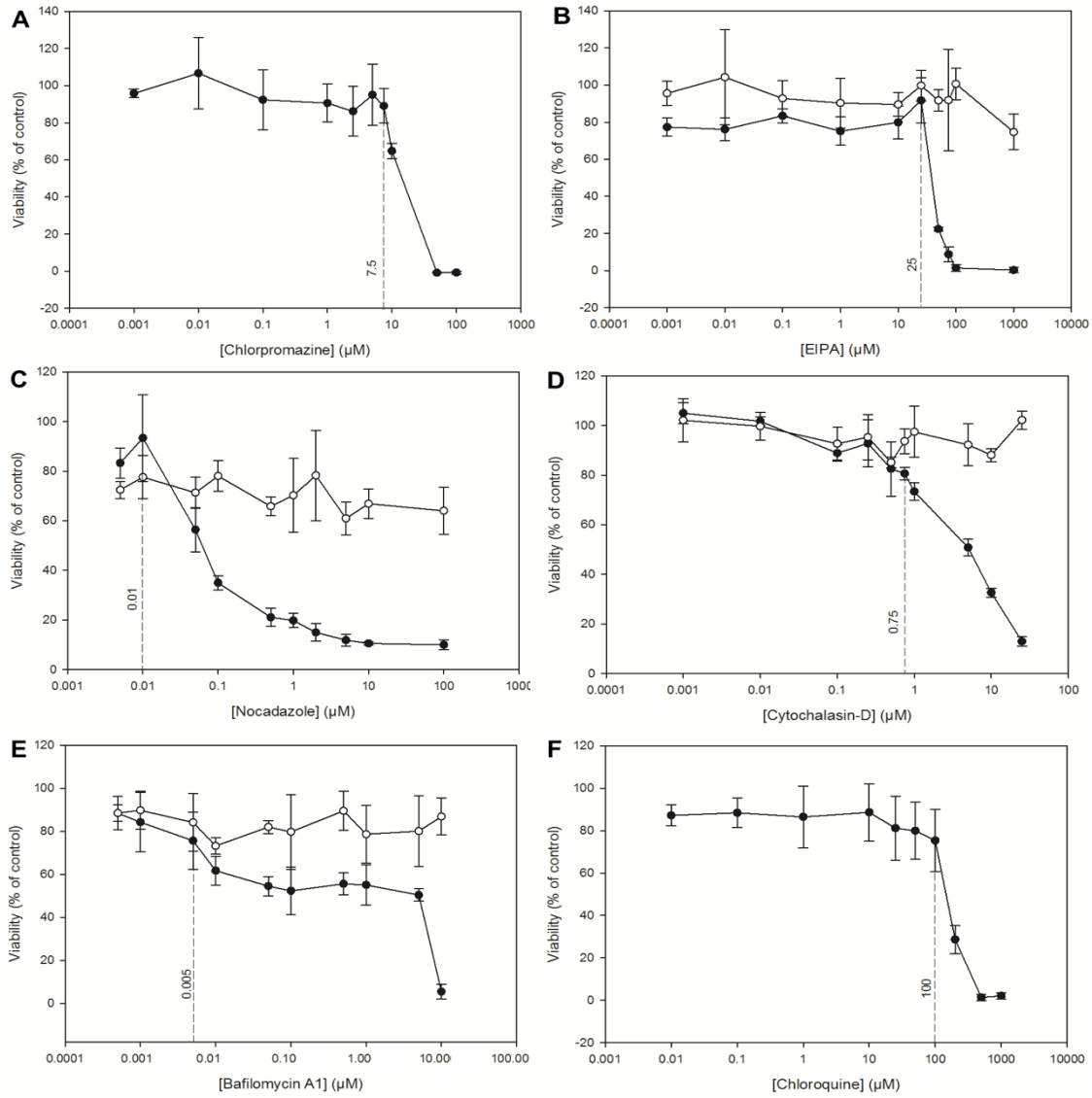

Figure 15 Dose-response Curves Determined by XTT Assay for Daudi cells Treated with Varying Concentrations of Each Pharmacological Agent

Dose-response curves determined by XTT assay for Daudi cells treated with varying concentrations of (A) chlorpromazine, (B) EIPA, (C) nocadazole, (D) cytochalasin-D, (E) bafilomycin A1 and (F) chloroquine. In those instances where the stock solution of inhibitor was made up in DMSO, the inhibitor (●) is shown alongside an equivalent concentration range of DMSO (○) for comparison. A single representative experiment is presented here. Datum points represents the calculated mean of four wells and the error bars one standard deviation either side of this mean. The concentration selected for inhibition of augmentation experiments is shown against the perpendicular dotted line.

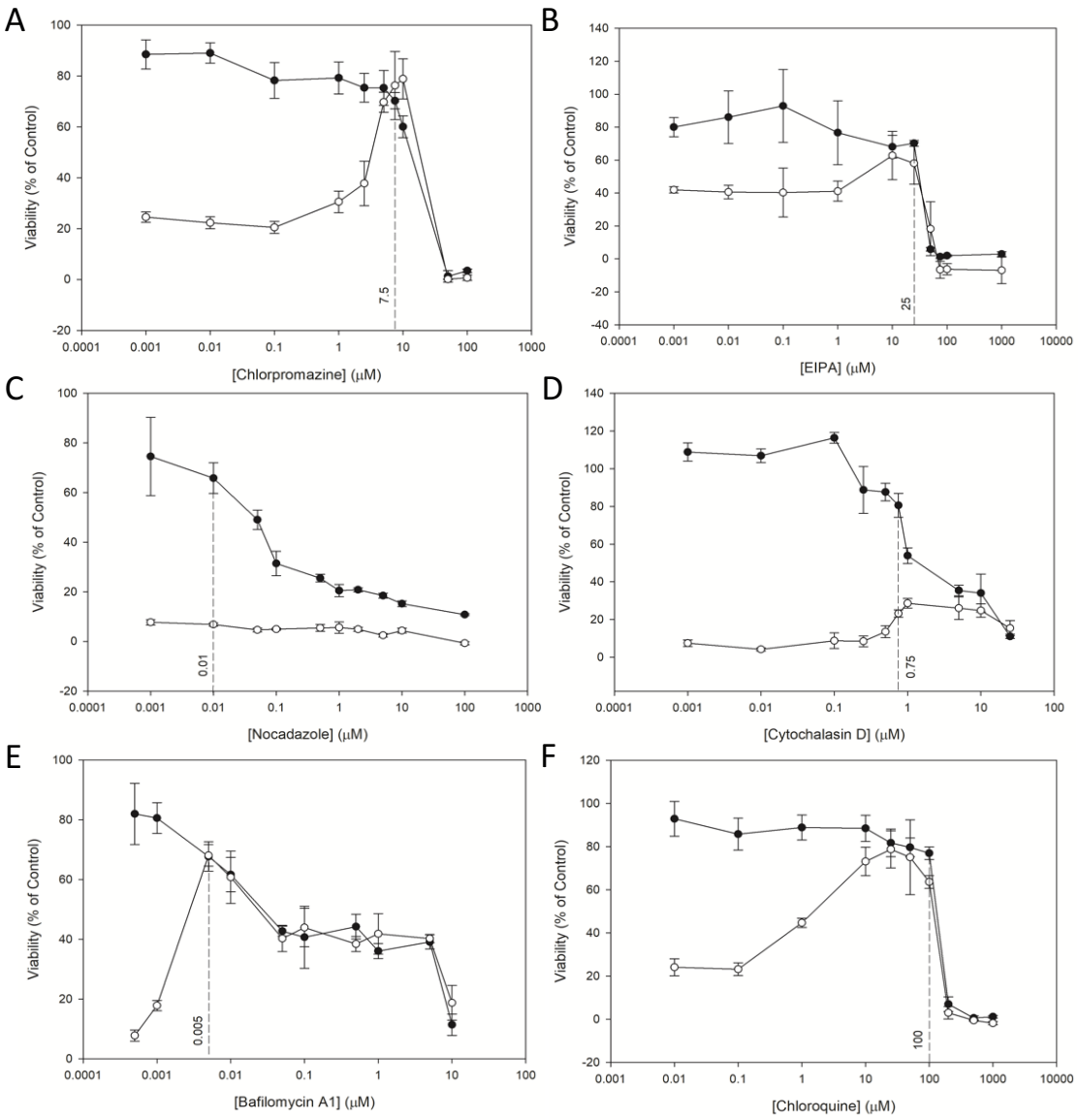

Figure 16 Optimisation of Pharmacological Agent Concentrations

Dose-response curves determined by XTT assay for Daudi cells treated with varying concentrations of (A) chlorpromazine, (B) EIPA, (C) nocadazole, (D) cytochalasin-D, (E) bafilomycin A1 and (F) chloroquine with $1x10^{-11}$ M OKT10-SAP in the presence (○) or absence (●) of 1 μg/ml SA. A single representative experiment is presented here. Datum points represents the calculated mean of four wells and the error bars one standard deviation either side of this mean. The concentration selected for inhibition of augmentation experiments is shown against the perpendicular dotted line.

The effect of each of these inhibitors at the selected optimal concentration on the augmentation of OKT10-SAP and saporin by 1 µg/ml of SA was then investigated in Daudi and HSB-2 cells. In each experiment the EC_{50} was determined from the intercept of the dose-response curve with the 50% level on the y-axis and the fold increase in cytotoxicity due to SA was then calculated as the ratio of the EC_{50} of the toxin alone and the EC_{50} of the toxin with SA. A statistical analysis of the change in fold increase made by each pharmacological agent was made by Mann-Whitney U-Test. The results of this analysis for OKT10-SAP and saporin in the presence of 1 µg/ml of SA on Daudi cells are presented in Figure 17G and Figure 18G respectively. In HSB-2 cells the results for saporin and SA are presented in Figure 20G. It was not possible to perform this statistical analysis with OKT10-SAP and SA on HSB-2 cells as the IT alone or in the presence of the varying agents investigated often did not achieve 50% toxicity at the concentrations of OKT10-SAP tested. It was not possible to test higher concentrations due to the concentration of the IT stock available.

4.2.1.1 Inhibition of Clathrin Mediated Endocytosis

The effect of the CME inhibitor chlorpromazine on the augmentation of OKT10-SAP and Saporin cytotoxicity by SA in Daudi and HSB-2 cells was investigated by XTT assay. Chlorpromazine causes the assembly of clathrin and AP2 complexes on endosomal membranes, thus depleting them from the plasma membrane and preventing formation of clathrin coated pits. It is widely used as an inhibitor of CME[247]. Treatment of both Daudi and HSB-2 cells with chlorpromazine did not affect their sensitivity to the cytotoxicity of OKT10-SAP or saporin suggesting that the cytotoxic activity of OKT10-SAP or saporin is not clathrin dependent. In contrast the augmentation of both OKT10-SAP and saporin by SA was almost completely abrogated in both cell lines. In Daudi cells treated with OKT10-SAP and SA the fold increase in cytotoxicity was reduced to 1.24-fold with chlorpromazine from 209-fold in control cells without chlorpromazine (Figure 17A). Similarly, the fold increase in saporin with SA cytotoxicity was reduced from four thousand to two in this cell line (Figure18A). In HSB-2 cells the fold increase of two hundred-fold that was observed with both OKT10-SAP and saporin in the presence of 1 µg/ml SA in control cells was completely abrogated by the addition of chlorpromazine (Figure 19A & Figure 20A)

4.2.1.2 Inhibition of Macropinocytosis

The role of macropinocytosis in the augmentation of OKT10-SAP and Saporin cytotoxicity by SA was analysed on Daudi cells with EIPA, an analogue of amiloride. EIPA inhibits the Na^+/H^+ exchanger isoform 1 at the plasma membrane. This prevents the exchange of protons generated metabolically by actin polymerisation and leads to sub-membranous acidification which inhibits the functions of the proteins Rac1 and Cdc42 resulting in the suppression of ruffle formation in the cell membrane and the inhibition of macropinocytosis [297,298]. Incubation with 25µM EIPA

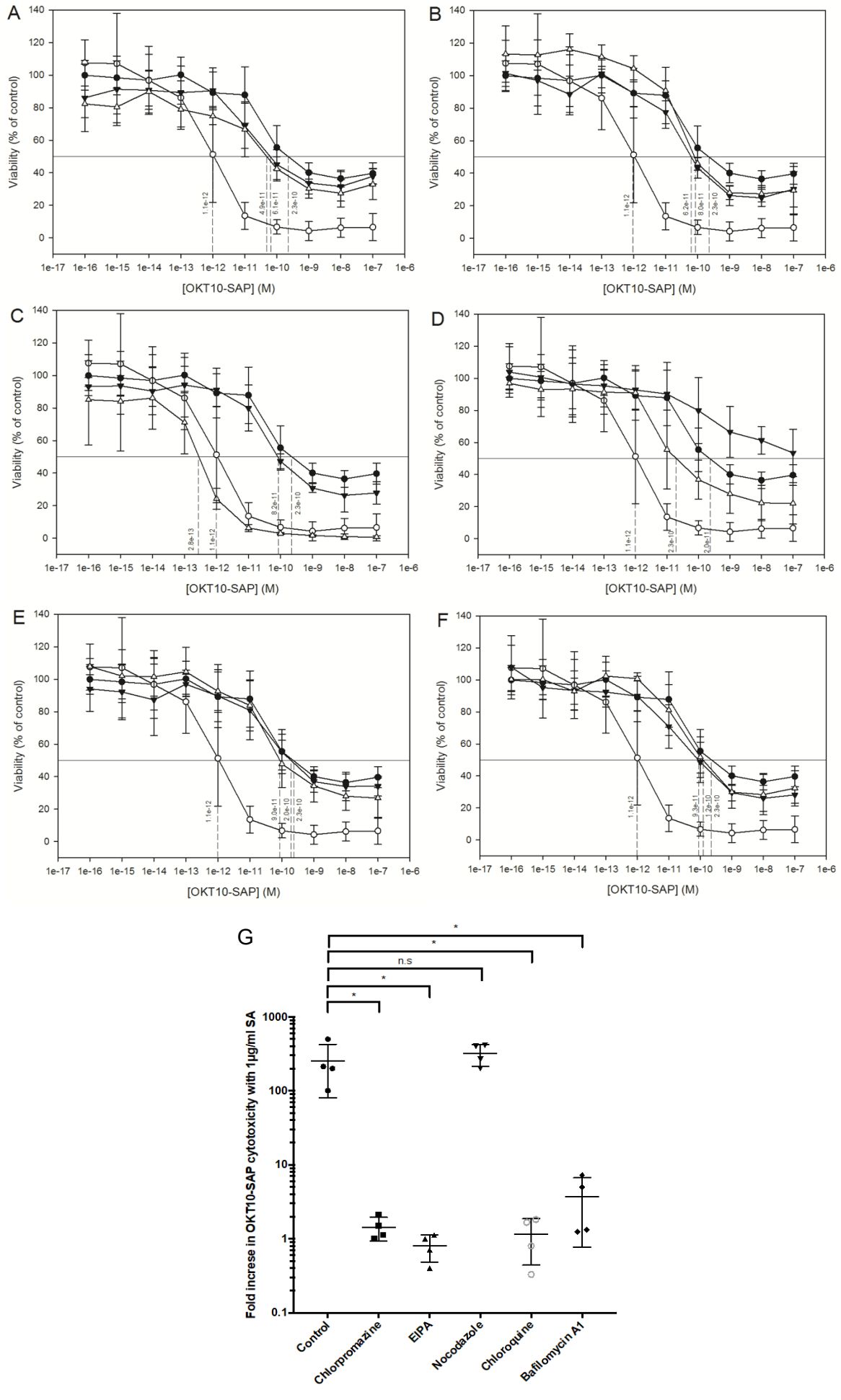
A
B
C
D
E
F
G
Viability (% of control)
[OKT10-SAP] (M)
1e-17 1e-16 1e-15 1e-14 1e-13 1e-12 1e-11 1e-10 1e-9 1e-8 1e-7 1e-6
0 20 40 60 80 100 120 140
1.1e-12
4.9e-11
6.1e-11
2.3e-10
8.2e-11
8.0e-11
2.8e-13
9.2e-11
9.0e-11
2.0e-10
1.2e-10
n.s
Fold increse in OKT10-SAP cytotoxicity with 1µg/ml SA
0.1 1 10 100 1000
Control
Chlorpromazine
EIPA
Nocodazole
Chloroquine
Bafilomycin A1

Figure 17 Inhibition of SA-Mediated Augmentation of OKT10-SAP Cytotoxicity in Daudi Cells by the Various Pharmacological Agents Studied

Effect of chlorpromazine (A), EIPA (B), nocodazole (C), cytochalasin D (D), bafilomycin A1 (E) and chloroquine (F) on the cytotoxicity of OKT10-SAP and OKT10-SAP used in combination with 1 µg/ml of SA. A-F: Dose-response curves determined by XTT assay for OKT10-SAP on Daudi lymphoma cells with each agent in the absence (▼) and presence (▽) of SA. In each chart the data for OKT10-SAP without inhibitor in the absence (●) and presence (○) of SA is also presented for comparison. Each datum point represents the calculated mean of four separate experiments each performed in quadruplicate cell cultures. Error bars represent one standard deviation either side of this mean. The EC50 obtained from each curve is shown against the perpendicular dotted line. G: Fold increases in OKT10-SAP cytotoxicity with 1µg/ml SA in control (●), chlorpromazine (■), EIPA (▲), nocodazole (▼), chloroquine (○) and bafilomycin A (◆). Dots represent fold increase in individual experiments with the lines showing the mean and one standard deviation either side of this mean. Augmentation was significantly abrogated by chlorpromazine ($p = 0.0286$ *), EIPA ($p = 0.0286$ *), chloroquine ($p = 0.0286$ *) and bafilomycin A1 ($p = 0.0286$ *) as determined by Mann-Whitney U-Test.

in Daudi cells did not affect the toxicity of OKT10-SAP or saporin alone but completely abrogated augmentation of OKT10-SAP (Figure 17B) and almost completely abrogated augmentation of saporin by 1 µg/ml SA (Figure 18B). In HSB-2 cells complete abrogation of the augmentation of OKT10-SAP by SA was recorded in cells treated with 20 µM EIPA (Figure 19B). In the same cell line the fold increase for saporin and 1 µg/ml of SA was reduced from two hundred to two by the addition of EIPA (Figure 20B)

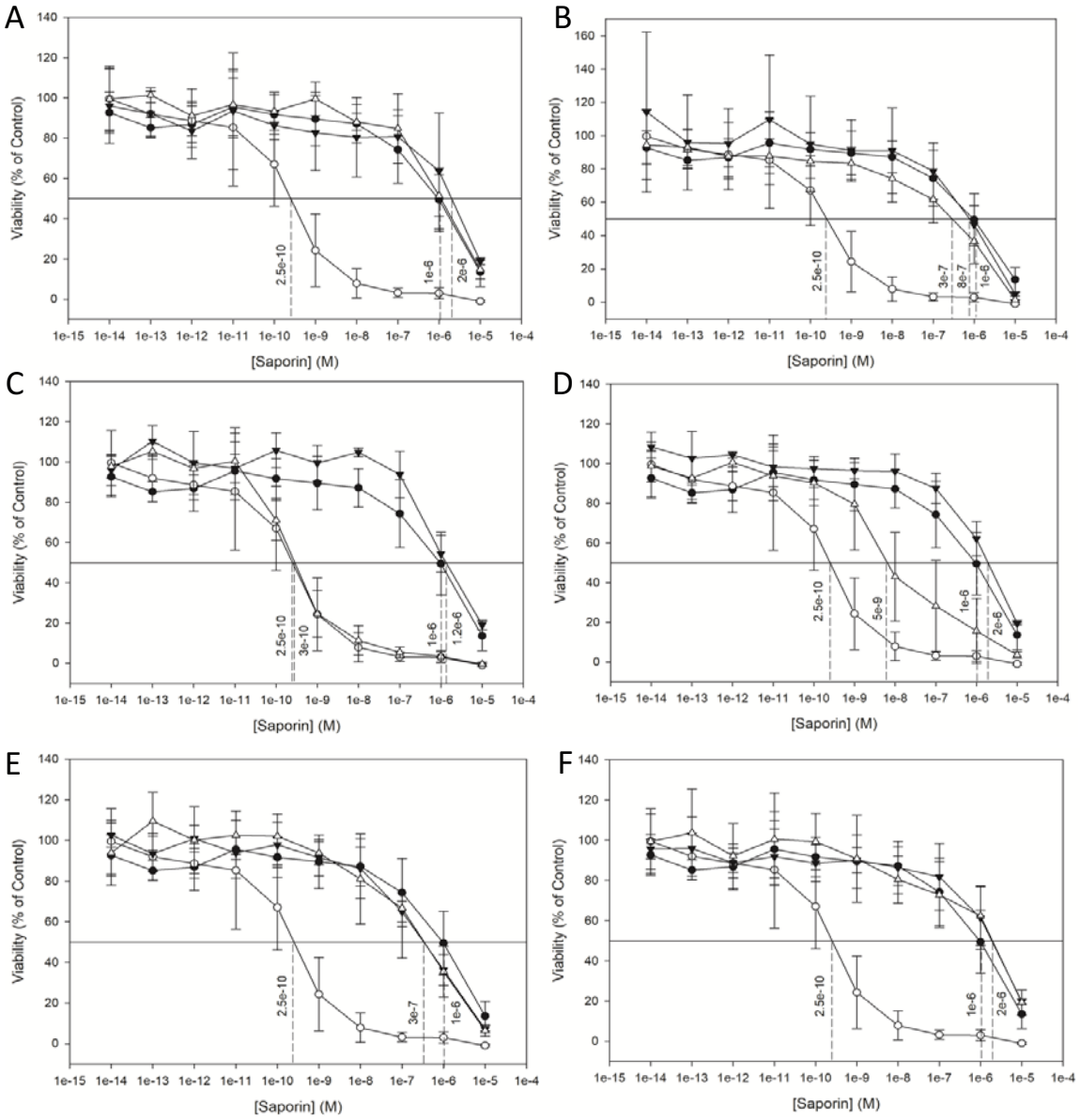
A
B
C
D
E
F
Viability (% of Control)
[Saporin] (M)
2.5e-10
1e-6
2e-6
8e-7
3e-7
3e-10
1.2e-6
5e-9

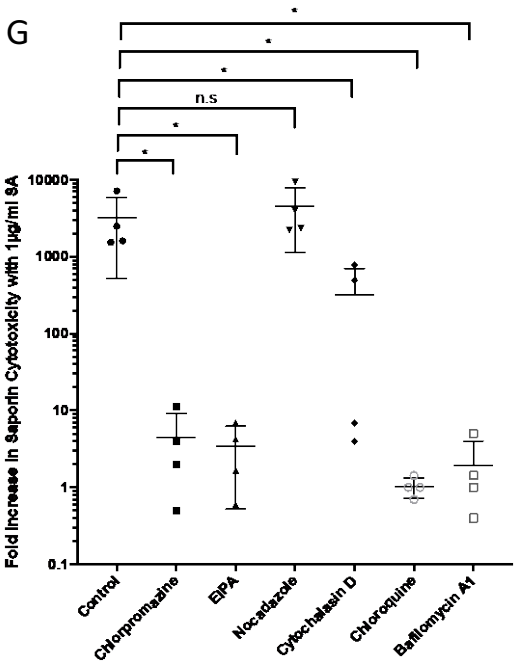
G
n.s
Fold Increase in Saporin Cytotoxicity with 1µg/ml SA
Control
Chlorpromazine
EIPA
Nocadazole
Cytochalasin D
Chloroquine
Bafilomycin A1

Figure 18 Inhibition of SA-Mediated Augmentation of Saporin Cytotoxicity in Daudi Cells by the Various Pharmacological Agents Studied

Effect of chlorpromazine (A), EIPA (B), nocodazole (C), cytochalasin D (D), bafilomycin A1 (E) and chloroquine (F) on the cytotoxicity of saporin and saporin used in combination with 1 µg/ml of SA. A-F: Dose-response curves determined by XTT assay for saporin on Daudi lymphoma cells with each agent in the absence (▼) and presence (▽) of SA. In each chart the data for saporin without each agent in the absence (●) and presence (○) of SA is also presented for comparison. Each datum point represents the calculated mean of four experiments each performed in quadruplicate cell cultures and the error bars one standard deviation either side of this mean. The EC_{50} obtained from each curve is shown against the perpendicular dotted line. G: Fold increases in saporin cytotoxicity with 1µg/ml SA in control (●), chlorpromazine (■), EIPA (▲), nocodazole (▼), cytochalasin D (◆), chloroquine (○) and bafilomycin A (□). Dots represent fold increase for individual experiments with the lines showing the mean and one standard deviation either side of this mean. Augmentation was significantly abrogated by chlorpromazine (p = 0.0286 *), EIPA (p = 0.0286 *), cytochalasin D (p = 0.0286 *), chloroquine (p = 0.0286 *) and bafilomycin A1 (p = 0.0286 *) as determined by Mann-Whitney U-Test.

4.2.1.3 Inhibition of Microtubule Polymerisation

Newly formed endocytic vesicles are transported away from the cortical region along microtubules. The inward trafficking and localisation of endosomes as they mature from early to late endosomal compartments and finally to the endolysosomal system requires their active motility along microtubules[302]. Treatment with the microtubule disrupting drug nocodazole has been shown to prevent transport to the endolysosomal compartment[303]. Microtubules are also involved in the lysosomal exocytosis observed with plasma membrane permeabilisation[304], and nocodazole disrupts the repair process[260].Nocodazole was used here with the aim of preventing the trafficking of the toxin or SA to an acidic endolysosomal compartment where endosomal escape has been reported to occur[152]. Nocadazole had no effect on the cytotoxicity of OKT10-SAP or saporin either alone or in combination with SA in either Daudi cells (Figure 17C & Figure 18C) or HSB-2 cells (Figure 19C & Figure 20C).

4.2.1.4 Inhibition of Actin Polymerisation

Actin polymerisation is involved in a wide range of endocytic processes including macropinocytosis[253], phagocytosis[305], clathrin independent endocytosis [250,298] and has been implicated in CME in some circumstances depending on the size of the cargo and the location of endocytosis [306,307]. The fungal alkaloid, cytochalasin D which blocks the polymerisation and elongation of actin microfilaments[300] was used to investigate the involvement of actin in the augmentation of OKT10-SAP and saporin cytotoxicity by SA. In Daudi cells cytochalasin D significantly reduced the toxicity of OKT10-SAP alone ($p = 0.0038$, 2-way ANOVA) and when used in combination with SA ($p = 0.0002$, 2-way ANOVA) (Figure17D). A similar reduction in the cytotoxicity of OKT10-SAP alone was observed in HSB-2 cells ($p < 0.0001$, 2-way ANOVA) and IT in combination with 1 µg/ml of SA ($p < 0.0001$, 2-way ANOVA) (Figure 19). It was not possible to calculate a mean fold increase for the effect of SA on OKT10-SAP EC_{50} in the presence of cytochalasin D in Daudi cells as the EC_{50} was not reached over the concentration range tested ($1x10^{-16}$ M– $1x10^{-7}$ M) (Figure17D). In comparison to its effect on OKT10-SAP, cytochalasin D did not reduce the cytotoxicity of the native toxin in the absence of SA. In the presence of SA, treatment with cytochalasin D partially abrogated the augmentation of saporin cytotoxicity in Daudi cells (Figure 18D). The fold increase in cytotoxicity was significantly reduced from four thousand to four hundred-fold (Figure18G). In HSB-2 cells a greater level of abrogation of the cytotoxicity of saporin in the presence of SA was observed, with a reduction in the fold increase in cytotoxicity from two hundred-fold to 3.33-fold (Figure 20D & G).

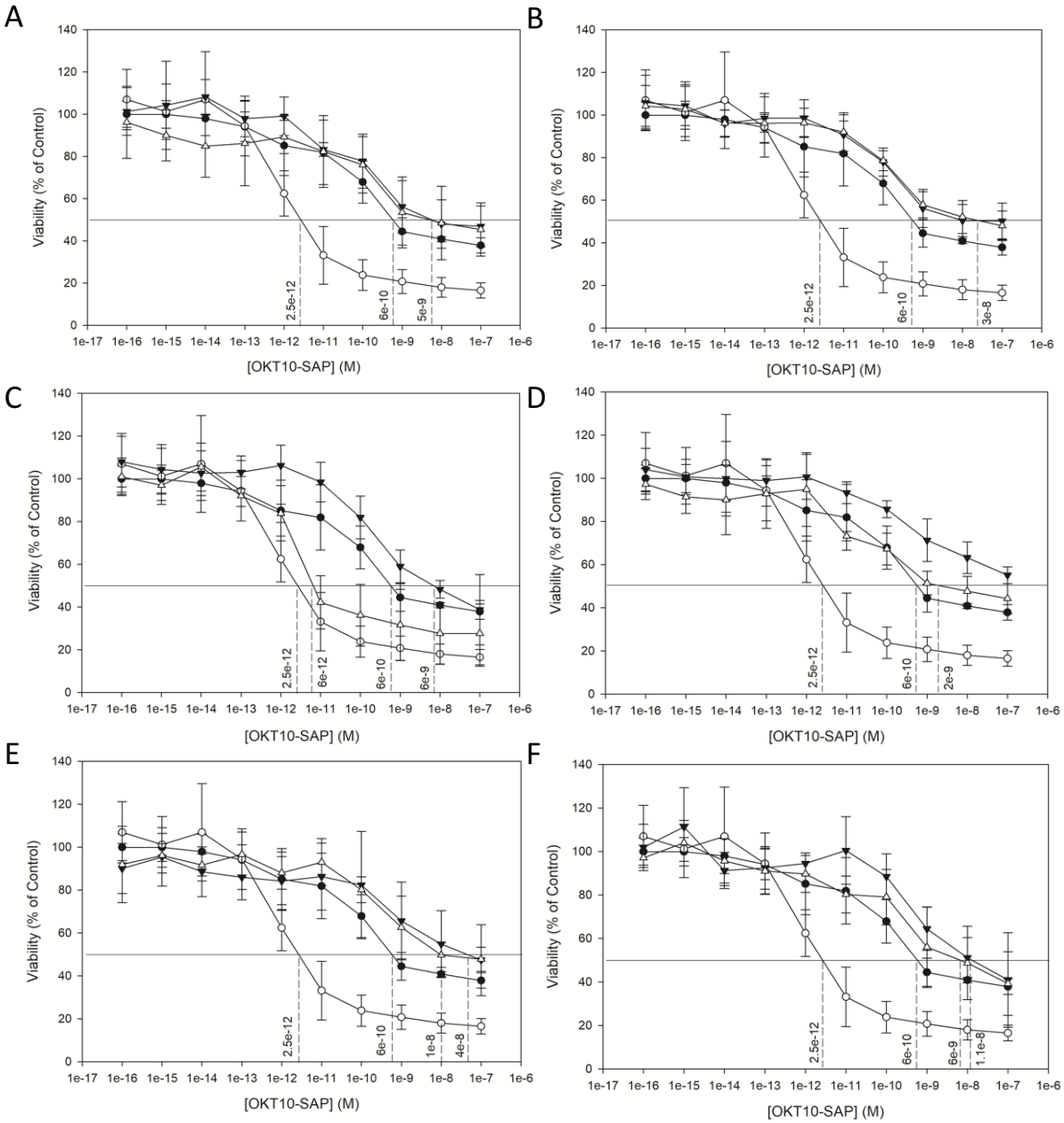

Figure 19 Inhibition of SA-Mediated Augmentation of OKT10-SAP Cytotoxicity in HSB-2 Cells by the Various Pharmacological Agents Studied

Effect of chlorpromazine (A), EIPA (B), nocodazole (C), cytochalasin D (D), chloroquine (E) and bafilomycin A1 (F) on the cytotoxicity of OKT10-SAP and OKT10-SAP used in combination with 1µg/ml of SA. A-F: Dose-response curves determined by XTT assay for OKT10-SAP on HSB-2 cells with each agent in the absence (▼) and presence (▽) of SA. In each chart the data for OKT10-SAP without inhibitor in the absence (●) and presence (○) of SA is also presented for comparison. Each datum point represents the calculated mean of four separate experiments each performed in quadruplicate cell cultures. Error bars represent one standard deviation either side of this mean. The EC_{50} obtained from each curve is shown against the perpendicular dotted line.

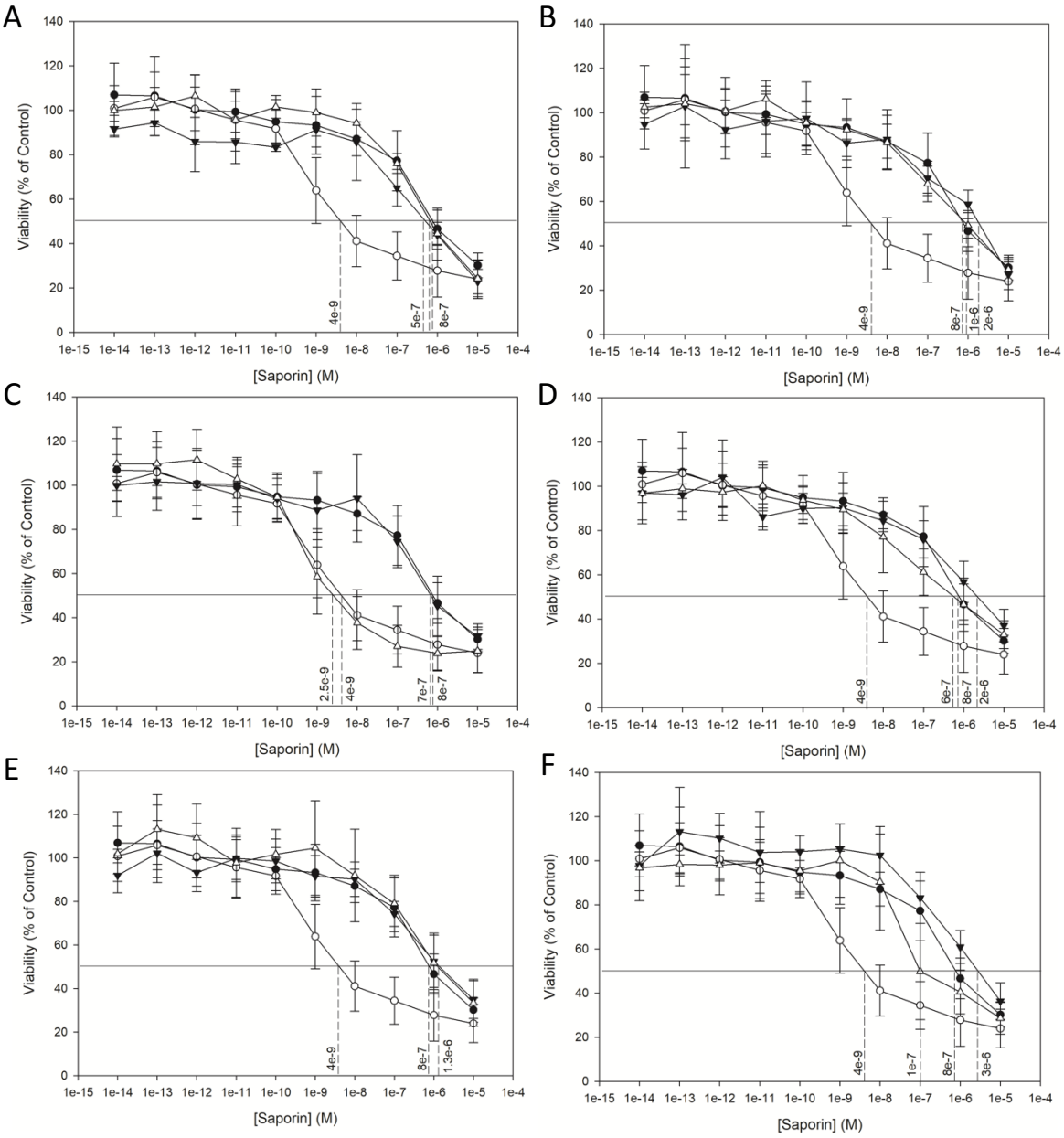
A
B
C
D
E
F
Viability (% of Control)
[Saporin] (M)
4e-9
5e-7
8e-7
1e-6
2e-6
2.5e-9
7e-7
6e-7
1.3e-6
3e-6
1e-7

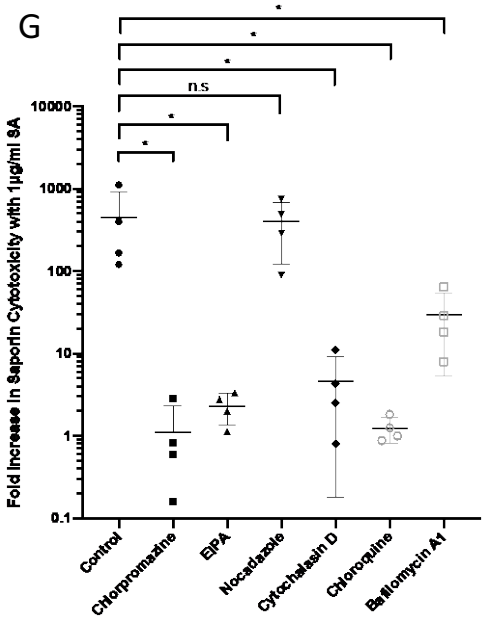
G
ns
*
Fold Increase in Saporin Cytotoxicity with 1µg/ml SA
Control
Chlorpromazine
EIPA
Nocadazole
Cytochalasin D
Chloroquine
Bafilomycin A1

Figure 20 Inhibition of SA-Mediated Augmentation of Saporin Cytotoxicity in HSB-2 Cells by the Various Pharmacological Agents Studied

Effect of chlorpromazine (A), EIPA (B), nocodazole (C), cytochalasin D (D), chloroquine A1 (E) and bafilomycin A1 (F) on the cytotoxicity of saporin and saporin used in combination with 1 µg/ml of SA. A-F: Dose-response curves determined by XTT assay for saporin on HSB-2 cells with each agent in the absence (▼) and presence (▽) of SA. In each chart the data for saporin without each agent in the absence (●) and presence (○) of SA is also presented for comparison. Each datum point represents the calculated mean of four experiments each performed in quadruplicate cell cultures and the error bars one standard deviation either side of this mean. The EC_{50} obtained from each curve is shown against the perpendicular dotted line. G: Fold increases in saporin cytotoxicity with 1µg/ml SA in control (●), chlorpromazine (■), EIPA (▲), nocodazole (▼), cytochalasin D (◆), chloroquine (○) and bafilomycin A (□). Dots represent fold increase for individual experiments with the lines showing the mean and one standard deviation either side of this mean. Augmentation was significantly abrogated by chlorpromazine (p = 0.0286 *), EIPA (p = 0.0286 *), cytochalasin D (p = 0.0286 *), chloroquine (p = 0.0286 *) and bafilomycin A1 (p = 0.0286 *) as determined by Mann-Whitney U-Test.

4.2.1.5 Inhibition of Endosomal Acidification

To investigate the role of a low endolysosomal pH on the augmentation of OKT10-SAP and saporin cytotoxicity by SA, two pharmacological inhibitors of endolysosomal acidification were used. Daudi cells were incubated with either bafilomycin A1, a specific inhibitor of the vacuolar H^+ ATPase[241] or with the lysosomotropic drug chloroquine, which diffuses into the endolysosomal compartment where it becomes protonated thereby directly increasing endolysosomal pH[240]. In the presence of these inhibitors the cytotoxicity of OKT10-SAP and saporin alone or used in combination with 1 µg/ml SA were evaluated by XTT assay. Neither bafilomycin A1 or chloroquine affected the cytotoxicity of either OKT10-SAP or saporin alone in Daudi or HSB-2 cells. However, both reagents greatly reduced the SA-mediated augmentation of OKT10-SAP in Daudi (Figure 17E & F) and HSB-2 cells (Figure 19E & F). In Daudi cells the augmentation of saporin cytotoxicity by SA was almost completely abrogated by both agents (Figure 18E & F). In HSB-2 cells complete abrogation the augmentation of saporin cytotoxicity was seen with chloroquine (Figure 20E), whilst a partial abrogation was seen with bafilomycin A1 which reduced the fold increase in cytotoxicity from two hundred-fold to thirty-fold (Figure 20F). This result confirms previously

published data that lysosomal acidification plays an important role in the augmentation of saporin based targeted toxin cytotoxicity by SA[236].

4.2.2 Augmentation of Gelonin Cytotoxicity in Daudi Cells by SA

Gelonin is a type I RIP produced by *Gelonium multiflorum.* This toxin is relevant to the investigation of the hypothesis that augmentable RIPs form a non-covalent, pH dependent association with saponins in the endolysosomal compartment and that this is in some way responsible for their endolysosomal escape. This hypothesis was the result of several previously published experimental observations. The first being that the inhibitors of endosomal acidification, chloroquine and bafilomycin A1, inhibited the augmentation of EGF-saporin cytotoxicity by saponin[236]. The saponin induced endolysosomal escape of a fluorescent saporin conjugate was also shown to be inhibited by chloroquine[152]. In addition to this a pH dependent association between the saponin SA1641 and saporin was observed by surface plasmon resonance[152]. It was suggested that this was due to an electrochemical interaction, as the high isoelectric point (IP~9) of saporin means that it is positively charged at pH 5-6, whilst the saponins tested contained a glucuronic acid which is negatively charged at the same pH. RTA (IP~5) is not significantly augmented by SA1641 and did not associate with the saponin at this pH. At the same time Weng et al also demonstrated that gelonin (IP ~9) did not associate with SA1641 as measured by surface plasmon resonance but they failed to report whether the cytotoxicity of gelonin was augmented by SA1641. Therefore, it is important to know whether the cytotoxic activity of gelonin is augmented by saponins to determine whether or not an electrochemical association between the saponin and the RIP is necessary for augmentation.

Gelonin was kindly provided by Professor Andrei Bolognesi at the University of Bologna and its enzymatic activity was tested by adenine release assay (2.2.4). Gelonin demonstrated N-glycosidase enzymatic activity lower than that of saporin, with an adenine release rate of 252.8 pmol/pmol of toxin/h. The ability of SA to augment gelonin cytotoxicity was then investigated with the XTT assay and the results are shown in Figure 21. The presence of 1 µg/ml SA enhanced gelonin cytotoxicity by 1720-Fold.

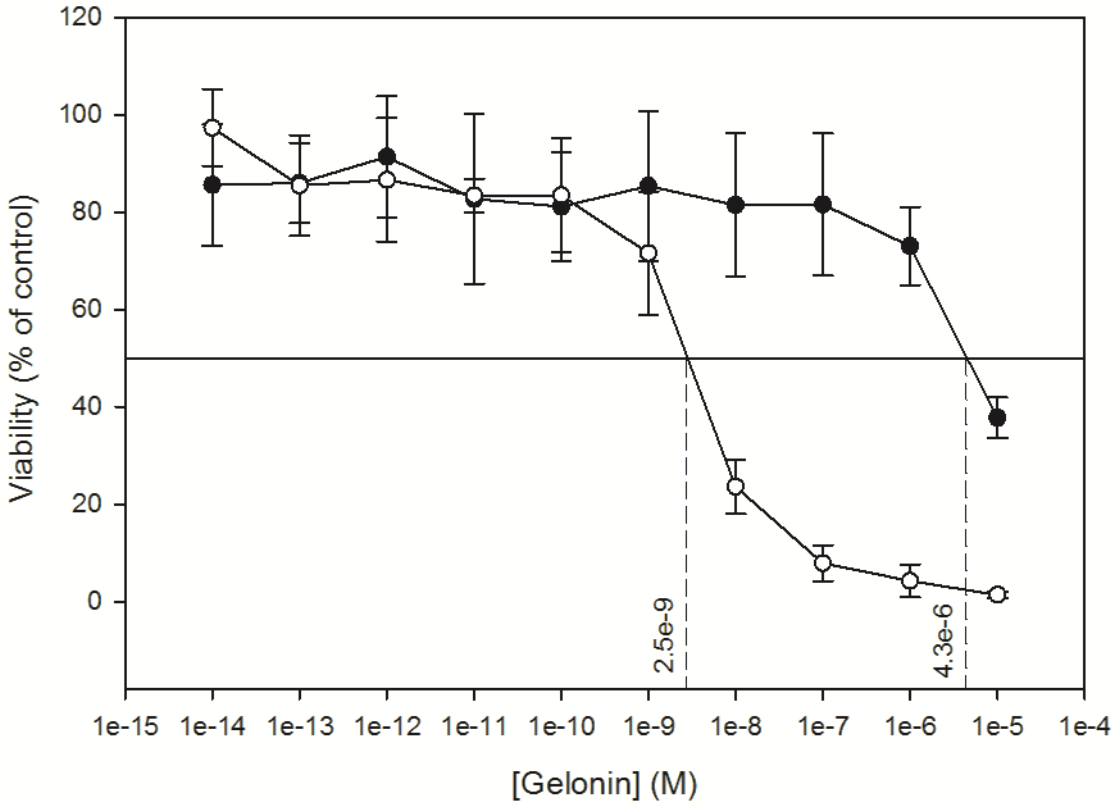

Figure 21 Augmentation of Gelonin Cytotoxicity in Daudi Cells by SA

Dose-response curves determined by XTT assay for Daudi lymphoma cells exposed to increasing concentrations of gelonin in the absence (●) and presence (○) of 1 µg/ml SA. Each datum point represents the calculated mean of three independent experiments performed in quadruplicate wells and the error bars one standard deviation either side of this mean. The EC_{50} value obtained from each curve is shown against the perpendicular dotted line.

This demonstration of gelonin augmentation by SA suggests that the augmentation of selected RIPs by SA may not be wholly dependent on a pH dependent association between the SA and the RIP and by inference that this may not be necessary for the endolysosomal escape of the RIP.

4.2.3 Construction of Fluorescently Labelled Saporin and OKT10-SAP Conjugates

Investigation of the internalisation and trafficking of saporin along with its proposed endolysosomal escape route in cells exposed to SA requires an assay that is capable of tracking the intracellular location of the saporin. Previously published work [152,308] described the use of saporin conjugated to the fluorescent dye Alexa Fluor 488 to demonstrate endolysosomal escape of this RIP in carcinoma cells using live cell imaging. Development of a similar experimental system for use in Daudi lymphoma cells would allow us to confirm these previously reported results thereby providing us with an assay that could be used to further investigate the effects of the

pharmacological inhibitors of endocytosis and endosomal acidification (4.2.1) on endolysosomal escape. Comparing the effect of the various pharmacological inhibitors on any observed endolysosomal escape together with the cytotoxicity data described under section 4.2.1 will confirm whether abrogation SA augmentation of saporin/IT cytotoxicity is due to their effects on the endolysosomal escape of the toxin/IT. It will also provide additional evidence that increased endolysosomal escape is indeed the mechanism by which SA augments saporin cytotoxicity. To test this, fluorescent conjugates of saporin and OKT10-SAP were constructed with Alexa Fluor 488 and termed SAP-AF and OKSAP-AF respectively for the subsequent experimental studies described in the following sections.

4.2.3.1 Cytotoxicity of SAP-AF and OKSAP-AF

In order to draw meaningful conclusions about the connection between endolysosomal escape of toxin and IT and SA augmentation of cytotoxicity, it was necessary to confirm that the fluorescent conjugate constructs continued to exhibit cytotoxic activity and that this activity remained augmentable by SA. The cytotoxicity of the fluorescent conjugates was therefore measured by XTT assay and compared to the unlabelled toxin and IT both alone and in the presence of 1 μg/ml of SA. The cytotoxicity of both saporin and OKT10-SAP were reduced following conjugation to Alexa Fluor 488 (Figure 22). This was especially apparent with OKSAP-AF which showed no cytotoxic activity in the absence of SA within the concentration range tested. It was no longer possible to determine an EC_{50} for either fluorescent conjugate due to the limited quantities of material available. The cytotoxicity of both SAP-AF and OKSAP-AF was augmented by cotreatment with 1 μg/ml of SA. In the presence of SA, the EC_{50} of saporin was reduced from $2.4x10^{-10}$ M to $1.8x10^{-9}$ M with SAP-AF. A reduction from $1x10^{-12}$ M to $3x10^{-9}$ M was observed after conjugation of OKT10-SAP (Figure 22).

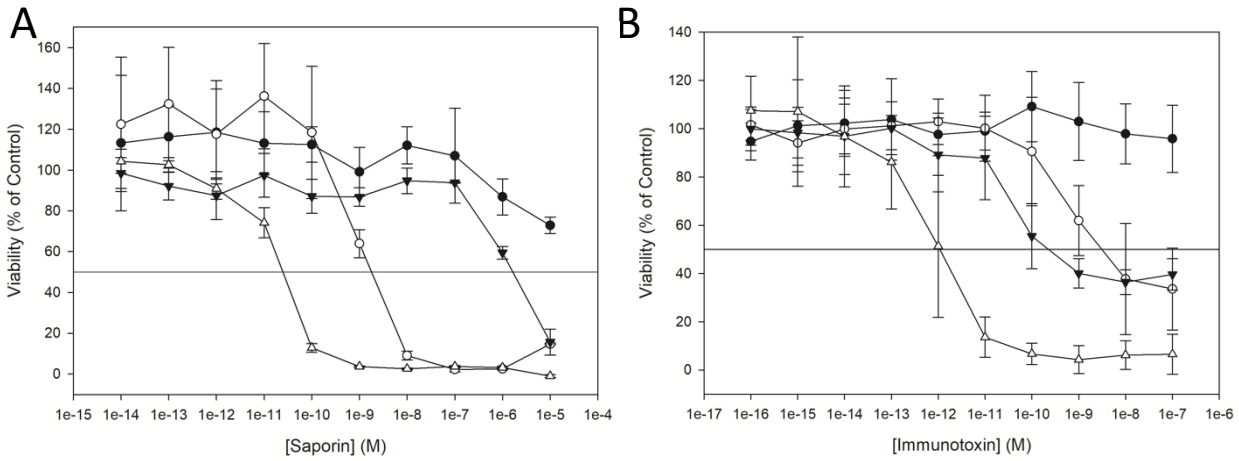

Figure 22 Cytotoxicity of SAP-AF and OKSAP-AF for Daudi Lymphoma Cells Determined by XTT Assay

Dose-response curves determined by XTT assay comparing the cytotoxicity of SAP-AF (A) and OKSAPAF (B) in Daudi cells with the unconjugated saporin and OKT10-SAP respectively. Each chart shows the conjugated toxin or IT in the absence (●) and presence (○) of 1 µg/ml of SA alongside the unconjugated toxin or IT in the absence (▼) and presence (▽) of SA. Each datum point represents the calculated mean of three experiments each performed in quadruplicate cell cultures and the error bars one standard deviation either side of this mean.

4.2.3.2 N-glycosidase Activity of SAP-AF

To investigate whether the enzymatic N-glycosidase activity of saporin was affected by its conjugation to Alexa Fluor 488 an adenine release assay was performed as described under section 2.2.4. The N-glycosidase activity of SAP-AF was compared to that of the native toxin. Saporin caused an adenine release of 616.7 pmol/pmol of toxin/h when incubated with herring sperm DNA. In comparison SAP-AF exhibited an adenine release rate of 382.3 pmol/pmol of toxin/h representing a reduction in enzymatic activity of 38%. This reduction suggests that the enzymatic activity of the toxin has been negatively affected by its conjugation to the fluorescent dye. This is most likely due to the labelling procedure blocking or damaging the N-glycosidase active site in a proportion of the saporin molecules labelled.

4.2.3.3 Binding of OKSAP-AF to CD38

The effect of Alexa Fluor 488 conjugation on the binding of OKT10-SAP to its target antigen, CD38, was investigated by indirect ELISA. 96 well plates were coated with a recombinant extracellular portion of CD38 and treated with OKT10-SAP or OKSAP-AF at varying concentrations between 0.01 and 10 µg/ml. Bound IT was detected by a rabbit anti-mouse IgG HRP conjugate. OKSAP-AF

showed greatly reduced binding to CD38 compared to the unconjugated IT. At the highest concentration of each IT investigated OKSAP-AF showed an 82% reduction in binding compared to OKT10-SAP. To investigate whether or not this result was due to reduced binding of the secondary antibody to the IT, a direct ELISA was performed against each IT adsorbed onto a 96 well plate. No difference in the binding of the rabbit anti-mouse IgG HRP secondary antibody was seen between OKT10-SAP and OKSAP-AF. These results suggest that the conjugation of Alexa Fluor 488 to OKT10-SAP has negatively affected its binding to CD38. This, in combination with the reduced N-glycosidase activity of Alexa Fluor 488 conjugated saporin, would account for the reduction in the cytotoxicity of OKSAP-AF when compared to OKT10-SAP. However, this assay did not confirm whether the measured OKSAP-AF binding was CD38 specific. Evidence of cell surface binding with OKSAP-AF but not SAP-AF was observed by confocal microscopy and is reported in 4.2.4.1.

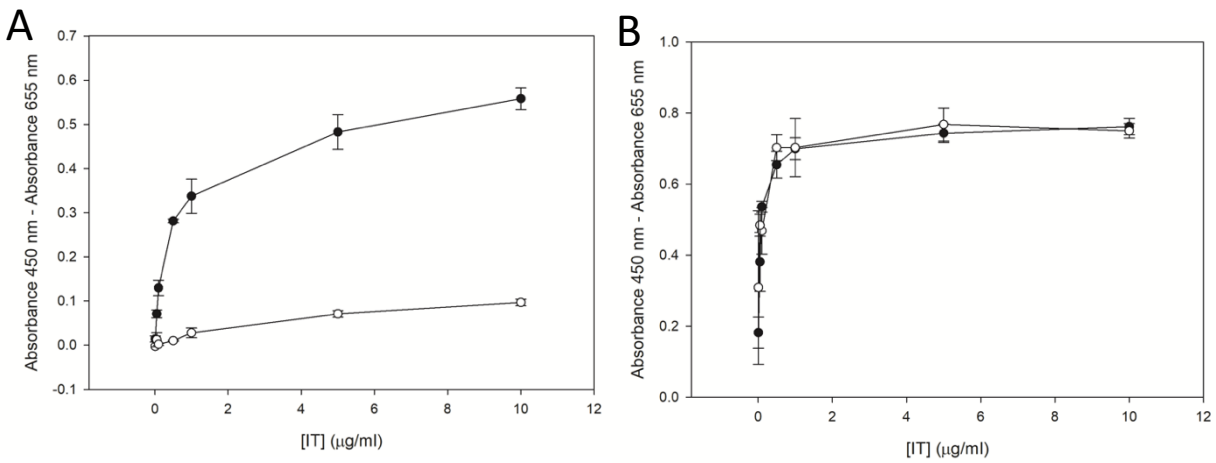

Figure 23 ELISA Analysis of the Effect of Alexa Fluor 488 Conjugation on the Binding Characteristics of OKT10-SAP

(A) Indirect ELISA showing binding of varying concentrations of OKT10-SAP (●) and OKSAP-AF (○) to plate bound recombinant CD38. (B) Direct ELISA showing binding of rabbit anti-mouse IgG HRP to a range of concentrations of plate bound OKT10-SAP (●) and OKSAP-AF (○).

4.2.4 Investigation of the Endolysosomal Escape of Saporin and OKT10-SAP by Confocal Microscopy

4.2.4.1 Uptake and Localisation of SAP-AF and OKSAP-AF

In order to investigate the endolysosomal escape of saporin and OKT10-SAP with the fluorescently labelled conjugates, SAP-AF and OKSAP-AF, it was necessary to confirm their internalisation and trafficking to the endolysosomal compartment. Daudi and HSB-2 cells were incubated with $1x10^{-6}$

M SAP-AF or $5x10^{-8}$ M OKSAP-AF and confocal imaging was performed at intervals to track the uptake of the conjugate into the cell (Figure 24). In order to maximise any potential differences in endolysosomal escape these concentrations were selected from the toxicity data presented in section 4.2.3.1 that exhibit low levels of toxicity when used alone but a high level of toxicity when used in combination with SA.

In Daudi cells but not HSB-2 cells OKSAP-AF was observed bound to the plasma membrane immediately after initial exposure. SAP-AF was not observed to bind to the plasma membrane of either cell line at any time point studied. Endocytosis of OKSAP-AF was observed as intracellular, punctate fluorescence in both cell lines after two hours. Imaging at later time points showed a reduction in surface fluorescence in Daudi cells with an increasing intracellular fluorescence (Figure 24). Internalised SAP-AF was observed in a similar fashion after two hours incubation in HSB-2 cells and after eight hours for Daudi cells (Figure 24). After 24 h both OKSAP-AF and SAP-AF had accumulated in discrete vesicular compartments. In Daudi cells these vesicles were found to be tightly packed in a single perinuclear region but in HSB-2 cells, vesicles were more widely distributed throughout the cytosol (Figure 24). There was little visual evidence of escape of SAP-AF or OKSAP-AF into the cytosol of either cell line over the entire time course of the experiment except in a very small number of isolated cells

The identity of the vesicles containing SAP-AF was investigated by co-localisation studies. Daudi and HSB-2 cells were incubated with SAP-AF for 24 h before staining with mAb targeting the lysosomal marker LAMP-1 and the early endosomal marker EEA1 (Figure 25). SAP-AF co-localised with LAMP-1 in both cell lines. The calculated Pearson correlation coefficient between SAP-AF and LAMP-1 was 0.7067 in Daudi cells and 0.6845 in HSB-2 cells. A much-reduced correlation was observed between SAP-AF and EEA1 with Pearson coefficients of 0.55 in Daudi cells and 0.34 in HSB-2 cells. This observation indicates that after 24 h of exposure the toxin has mostly been trafficked through early endosomes and has accumulated in the late endosomal/lysosomal compartment

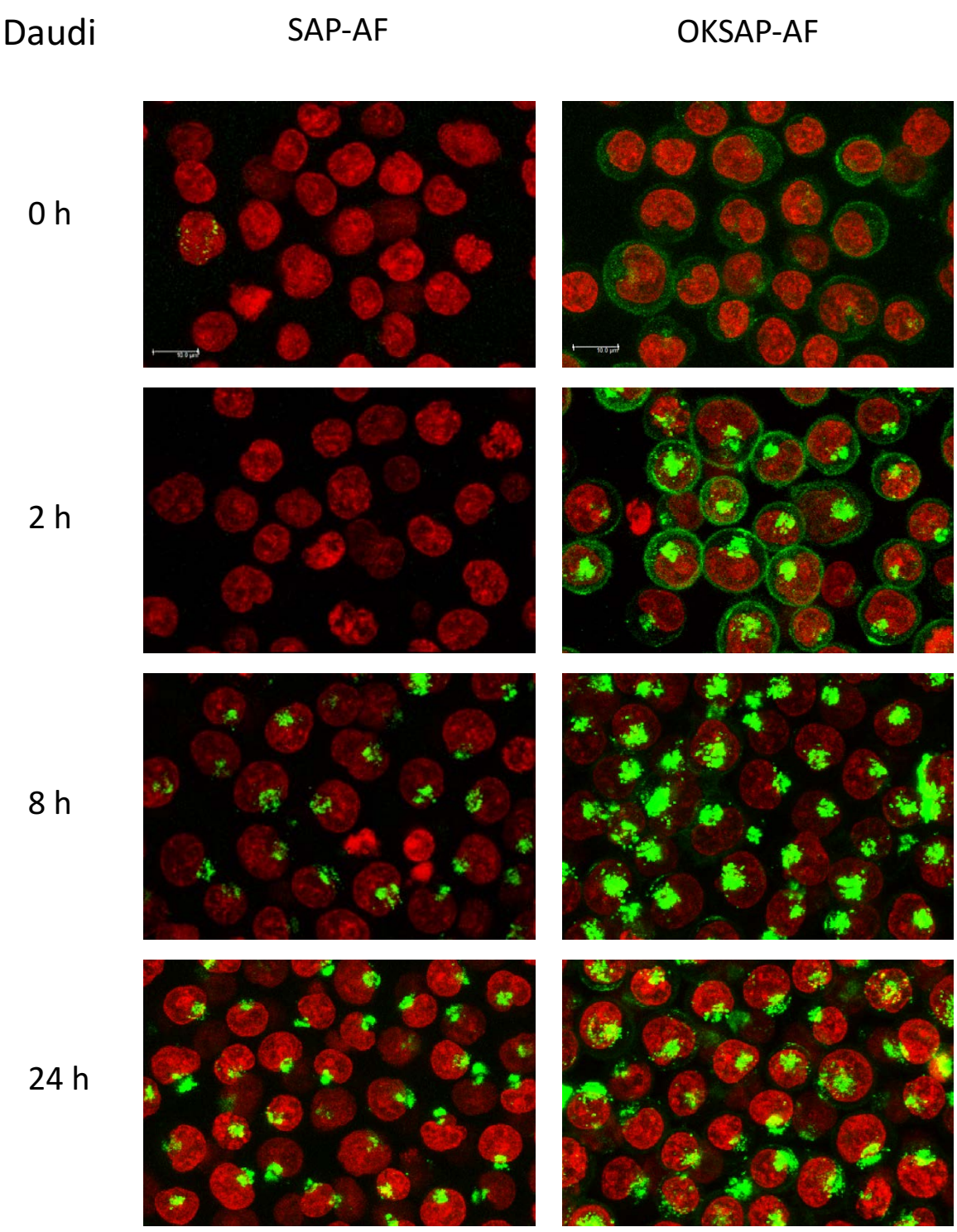
Daudi
SAP-AF
OKSAP-AF
0 h
2 h
8 h
24 h

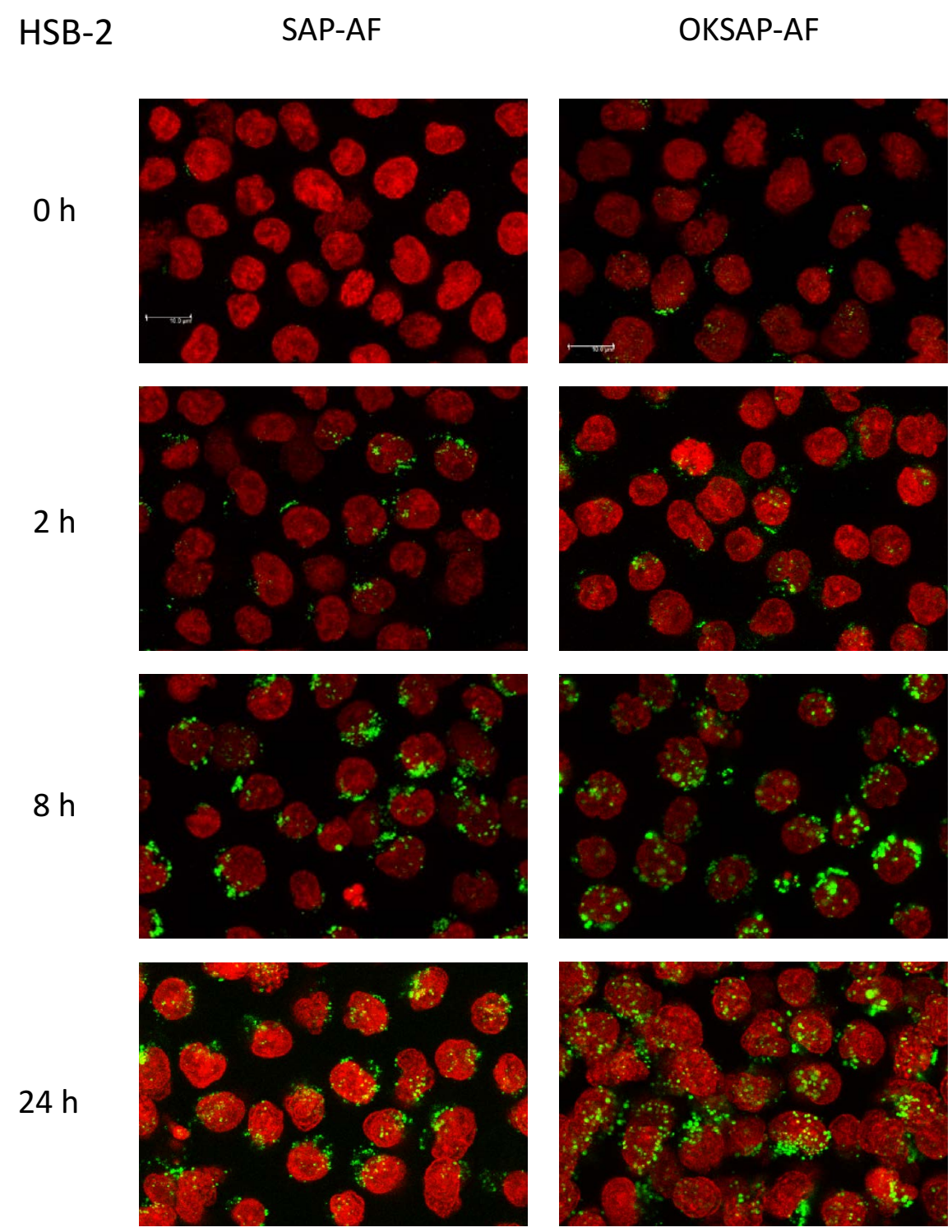

Figure 24 Confocal Microscopy Imaging Showing the Internalisation of OKSAP-AF and SAP-AF in Daudi and HSB-2 Cells

The uptake of SAP-AF and OKSAP-AF by Daudi and HSB-2 cells. Cells were incubated with SAP-AF or OKSAP-AF (green) and live cell confocal images taken after 0, 2, 8 and 24 hours. The nucleus (red) was stained with Hoechst 33342. Images presented are maximum projections of 21 x 1 µm Z-stacks. Scale bar represents 10 µm.

.

Daudi

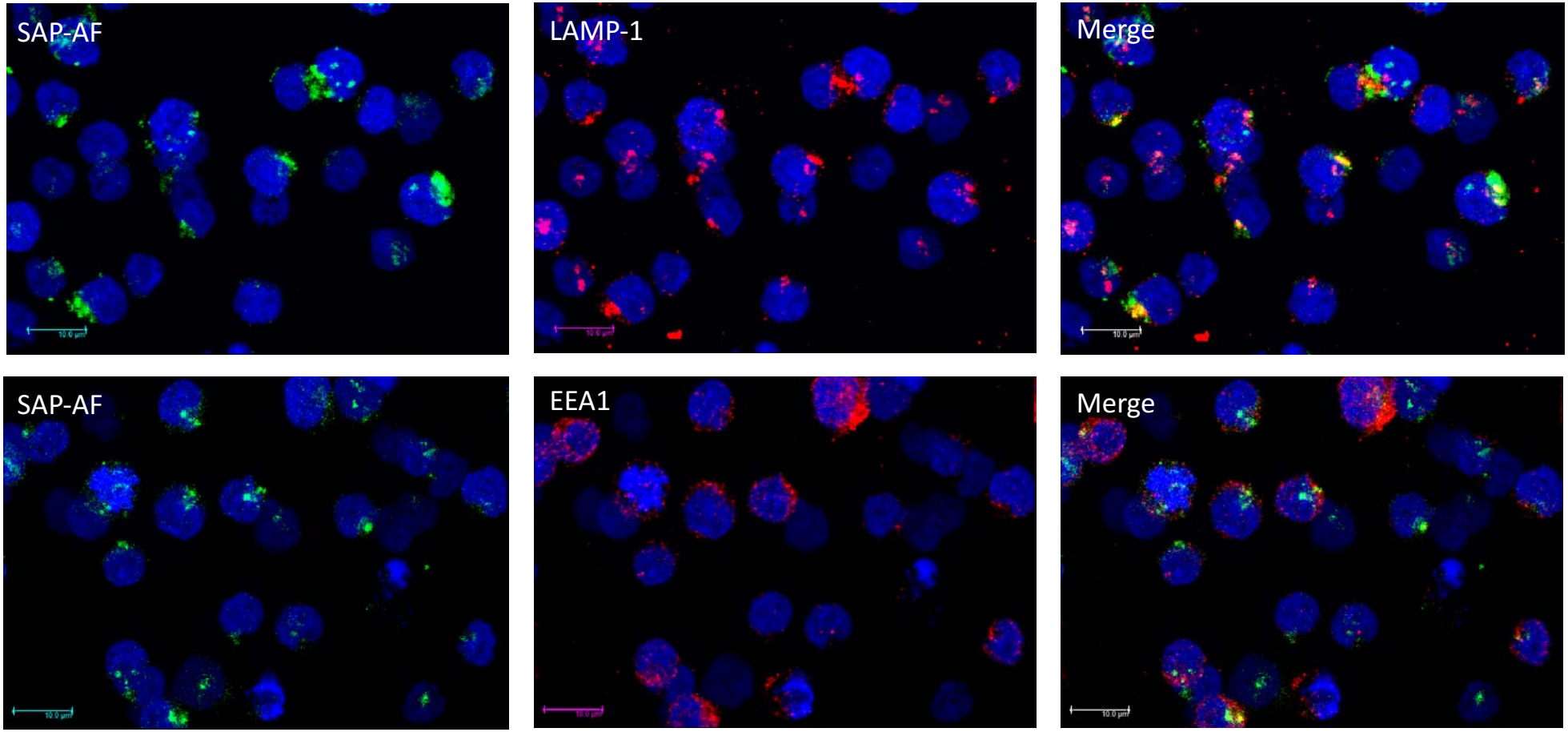

HSB2

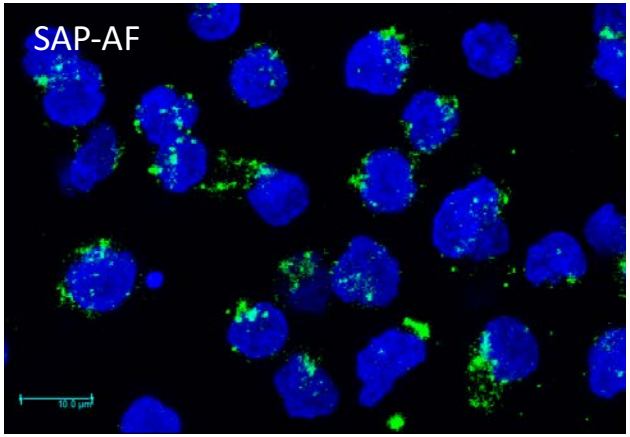

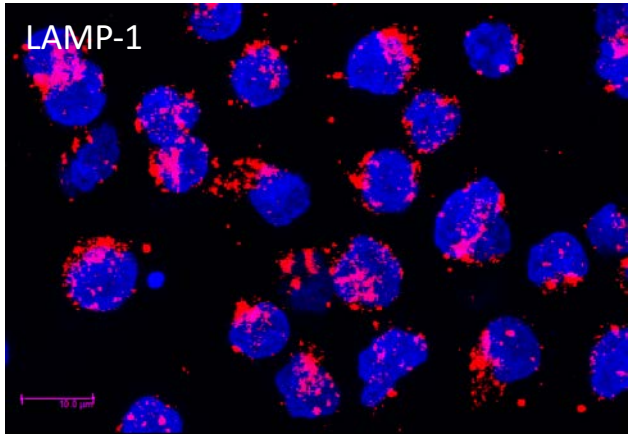

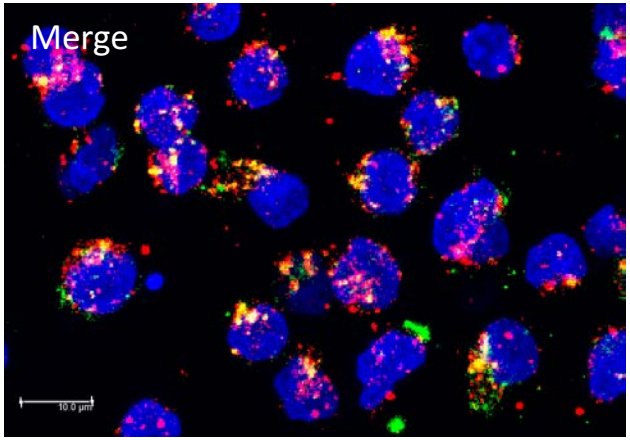

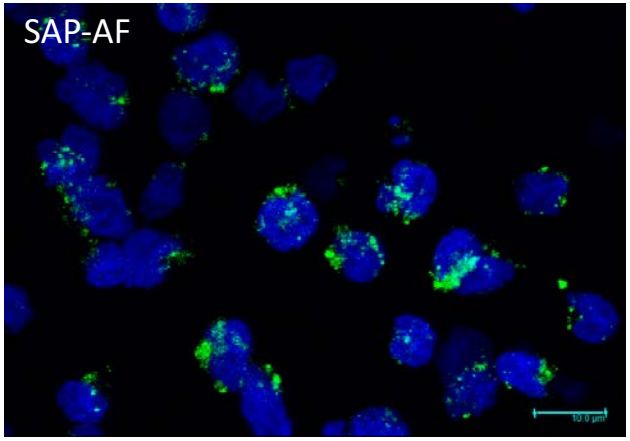

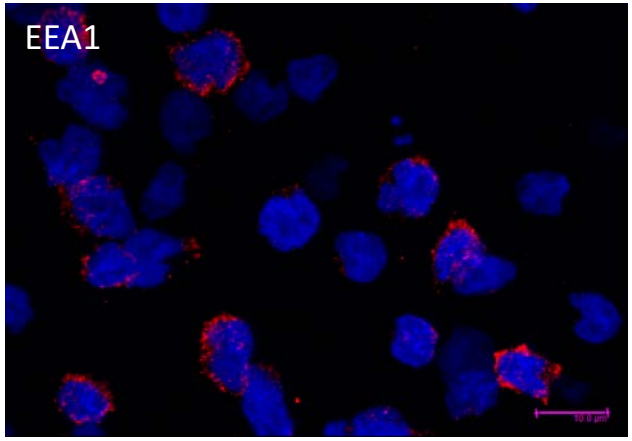

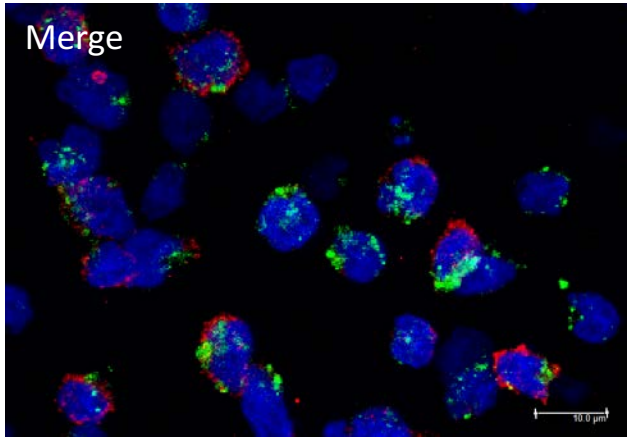

Figure 25 Confocal Microscopy Studies Showing Co-localisation of SAP-AF with LAMP-1 and EEA1

Co-localisation studies were performed in Daudi and HSB-2 cells between SAP-AF (green) and the lysosomal marker LAMP-1 (red) or the early endosomal marker EEA1 (red). In merged images, sites of co-localisation appear in yellow. The nucleus (blue) was stained with Hoechst 33342. Images presented are maximum projections of 21 x 1 µm Z-stacks. Scale bar represents 10 µm.

4.2.4.2 SA Increases the Endolysosomal Escape of OKSAP-AF and SAP-AF

The effect of SA on the endolysosomal escape of saporin (SAP-AF) and IT (OKSAP-AF) was investigated by confocal microscopy. Daudi and HSB-2 cells were incubated with SAP-AF or OKSAP-AF for 24 h. Loaded cells were recorded by live cell confocal microscopy at time intervals ranging from 0 h to 24 h after the addition of SA at 1 µg/ml or 5 µg/ml. Control cells treated with R10 were also observed over the same time period to act as a comparator.

Endolysosomal escape of both SAP-AF and OKSAP-AF was observed in a small proportion of Daudi cells eight hours after the addition of 5 µg/ml of SA (Figure 26). This could be seen as a reduction in vesicular fluorescence and the diffusion of the fluorescently labelled toxin throughout the cytosol. At later timepoints the proportion of cells showing cytosolic fluorescence increased, with almost all cells showing escape by 24 hours (Figure 26). The intensity of cytosolic fluorescence increased over time demonstrating the continuing endolysosomal escape of SAP-AF and OKSAP-AF.

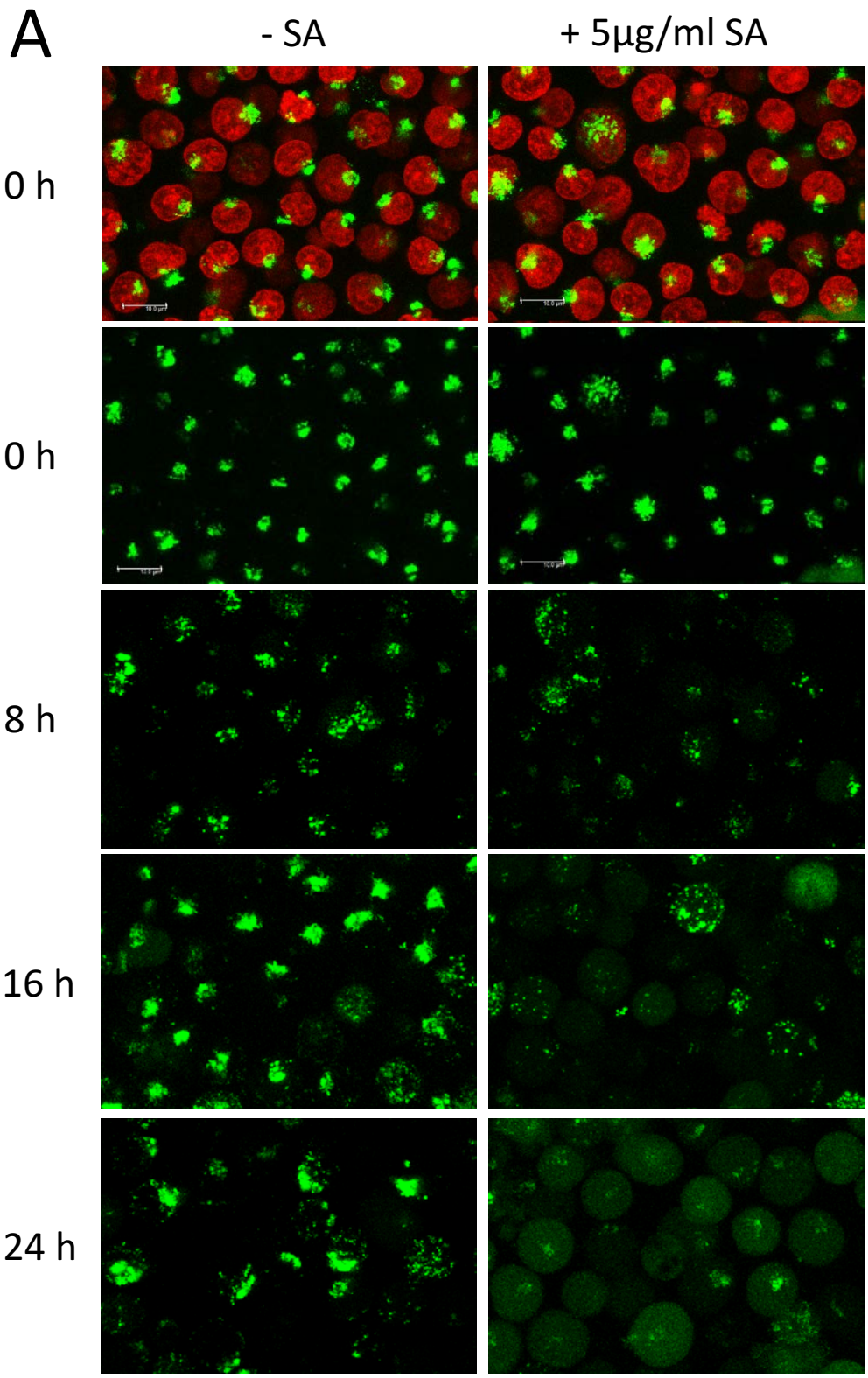
A
- SA
+ 5µg/ml SA
0 h
0 h
8 h
16 h
24 h

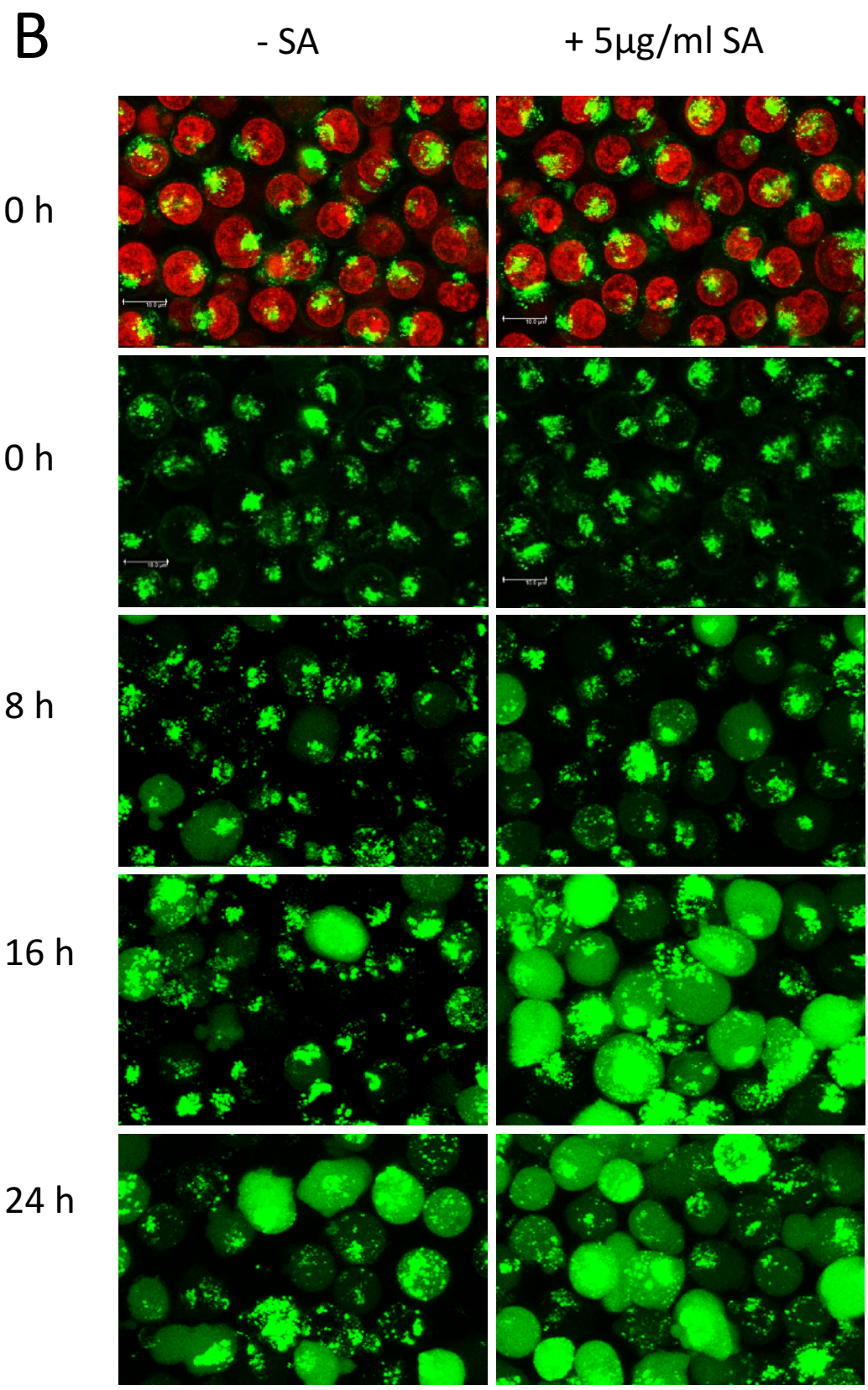

Figure 26 Endolysosomal Escape of SAP-AF and OKSAP-AF in Daudi Cells

Daudi cells incubated with (A) SAP-AF or (B) OKSAP-AF for 24 hours were treated with 5µg/ml of SA and live cell confocal images taken after 0, 8, 16 and 24 hours. Untreated cells are shown for comparison. Endolysosomal escape is seen as a change

from punctate vesicular fluorescence to a diffuse staining pattern throughout the cytoplasm. Images for the initial timepoint at zero hours are shown with and without Hoechst 33342 nuclear stain (red). The increased brightness of cells incubated with OKSAP-AF and treated with SA at the 16 and 24 h timepoints is due to the way the fluorescence gain was set to maximise assay sensitivity. See 2.3.11 for details. Images presented are maximum projections of 21 x 1 µm Z-stacks. Scale bar represents 10 µm.

Similar results were obtained for both SAP-AF and OKSAP-AF in HSB-2 cells (Figure 27) with endolysosomal escape of SAP-AF observed after 8 h and OKSAP-AF after 16 h. In comparison, in untreated control cells, endolysosomal escape was only observed in a small number of cells imaged, even after 24 hours. These results demonstrate that it is possible to observe the release of SAP-AF and OKSAP-AF using confocal microscopy when SA is used at a concentration of 5 µg/ml. This indicates that SA at this concentration is acting as an endolysosomal escape enhancer for saporin and saporin based ITs in both of these cell lines.

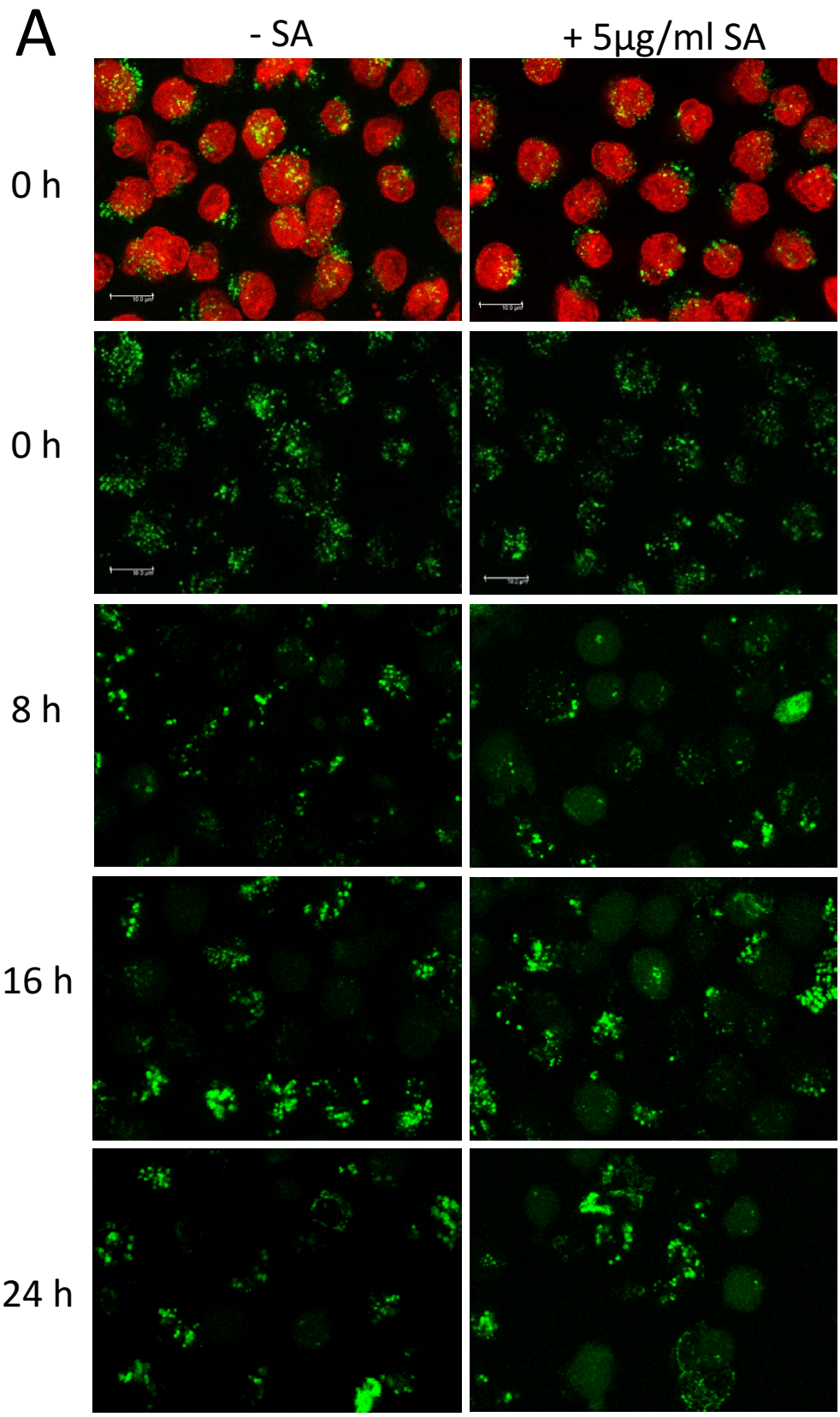
A
- SA
+ 5µg/ml SA
0 h
0 h
8 h
16 h
24 h

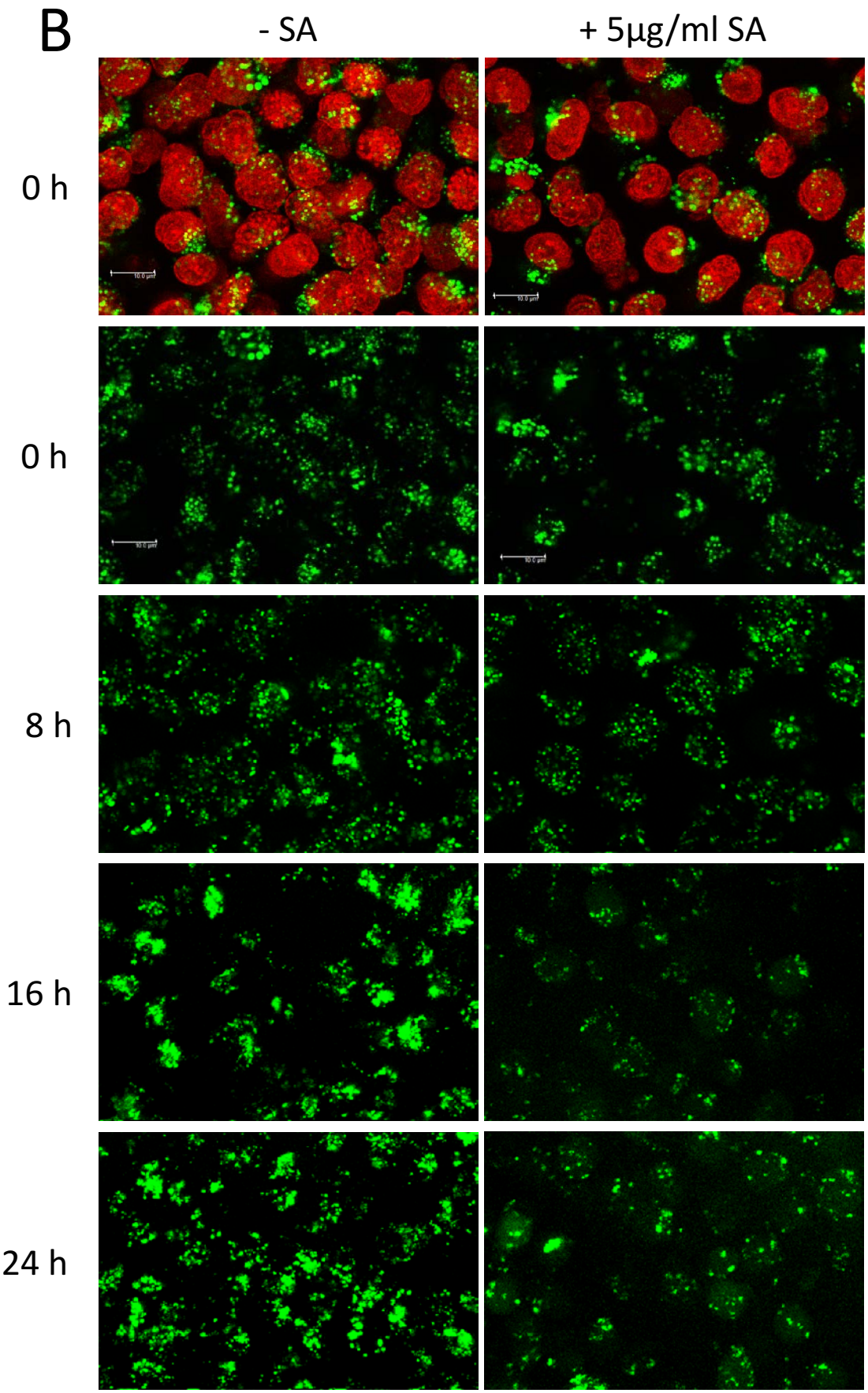

Figure 27 Endolysosomal Escape of SAP-AF and OKSAP-AF in HSB-2 Cells

HSB-2 cells incubated with (A) SAP-AF or (B) OKSAP-AF for 24 hours were treated with 5 µg/ml of SA and live cell confocal images taken after 0, 8, 16 and 24 hours. Untreated cells are shown for comparison. Endolysosomal escape is seen as a change from punctate vesicular fluorescence to a diffuse staining pattern throughout the cytoplasm. Images for the initial timepoint at zero hours are shown with and without Hoechst 33342 nuclear stain (red). Images presented are maximum projections of 21 x 1 µm Z-stacks. Scale bar represents 10 µm.

The concentration of 5 µg/ml of SA is partially cytotoxic in both Daudi and HSB-2 cells as measured by XTT assay after 48 hours of exposure [196]. At the subtoxic, but augmentative of saporin cytotoxicity, concentration of 1 µg/ml of SA, no increase in endolysosomal escape of either saporin or IT was apparent on confocal microscopy over that seen in untreated control cells (Figure 28).

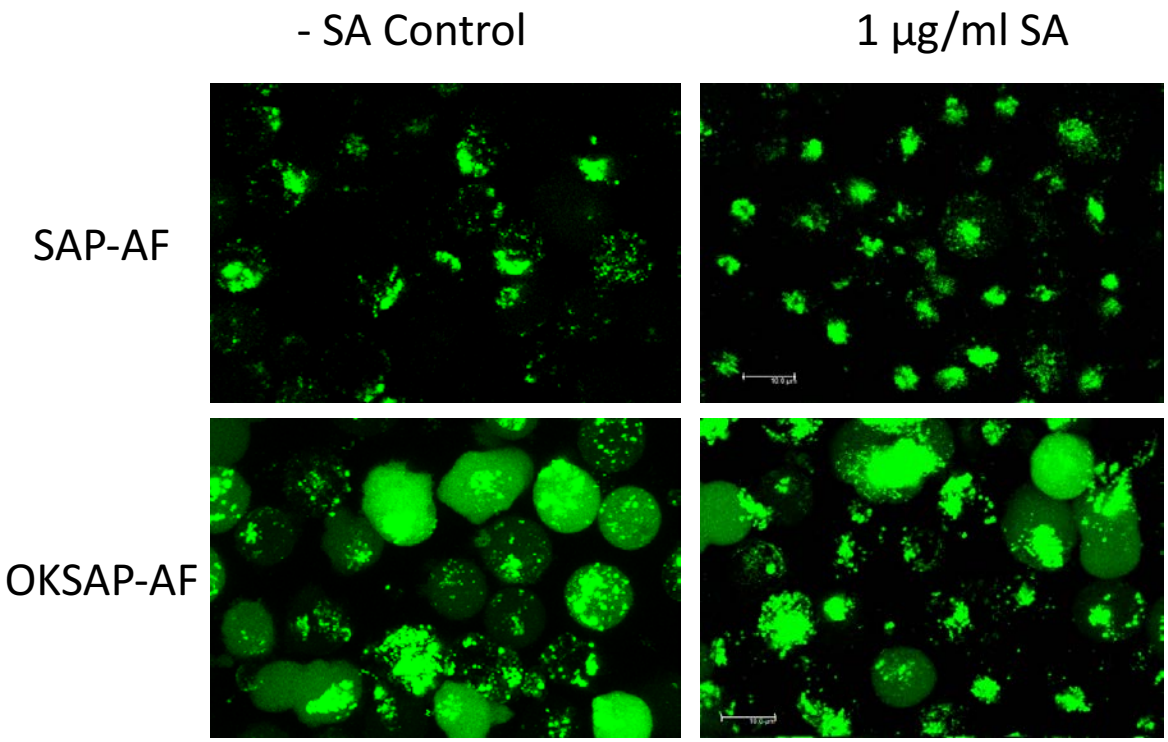

Figure 28 Confocal Imaging Showing the Effect of 1µg/ml of SA on Endolysosomal Escape in Daudi Cells

Daudi cells incubated with SAP-AF or OKSAP-AF for 24 hours were treated with 1 µg/ml of SA and live cell confocal images taken after 24 hours. Untreated cells are shown for comparison. Images presented are maximum projections of 21 x 1 µm Z-stacks. Scale bar represents 10 µm.

It was not possible to determine whether this result was due to a reduced rate of endolysosomal escape with 1 µg/ml of SA which resulted in cytosolic fluorescence below the sensitivity level of the microscopic assay or whether the augmentation of cytotoxicity by 1 µg/ml of SA is not due to increased endolysosomal escape.

An attempt was made to perform a semi-quantitative analysis of these confocal microscopic images. The aim of this quantification was to determine whether or not 1 µg/ml of SA had any effect on the endolysosomal escape of SAP-AF or OKSAP-AF that could not otherwise be easily determined. It would also be necessary to investigate the effects of inhibitors of endocytosis and endosomal acidification on SA induced endolysosomal escape. This method was ultimately unsuccessful due to difficulties in removing subjective user bias and inter-experimental variations in cytosolic fluorescence intensity compared to background levels. More details are provided in Appendix B.

4.2.4.3 Effects of Small Molecule Pharmacological Inhibitors on the Endolysosomal Escape of SAP-AF

An increase in the endolysosomal escape of SAP-AF and OKSAP-AF was successfully demonstrated in cells treated with 5 µg/ml of SA. An attempt was therefore made to inhibit this increase in endolysosomal escape with pharmacological inhibitors of CME, macropinocytosis and endosomal acidification. Daudi cells loaded with SAP-AF for 24 h were treated with 5 µg/ml of SA in the presence of chlorpromazine, EIPA or chloroquine. Live cell confocal images were taken 24 h after addition of SA.

In cells treated with chloroquine a dispersal of the SAP-AF containing vesicles throughout the cytosol from their initial perinuclear location was observed. The endolysosomal escape of SAP-AF into the cytosol was prevented by treatment with chloroquine. This data corresponds with the abrogatory effect of chloroquine on the augmentation of saporin cytotoxicity by SA. No reduction in the endolysosomal escape of SAP-AF was observed in cells treated with either chlorpromazine or EIPA (Figure 29). This is contrast to cytotoxicity experiments where the augmentation of saporin by SA was completely abrogated by chlorpromazine and greatly reduced by EIPA (4.2.1).

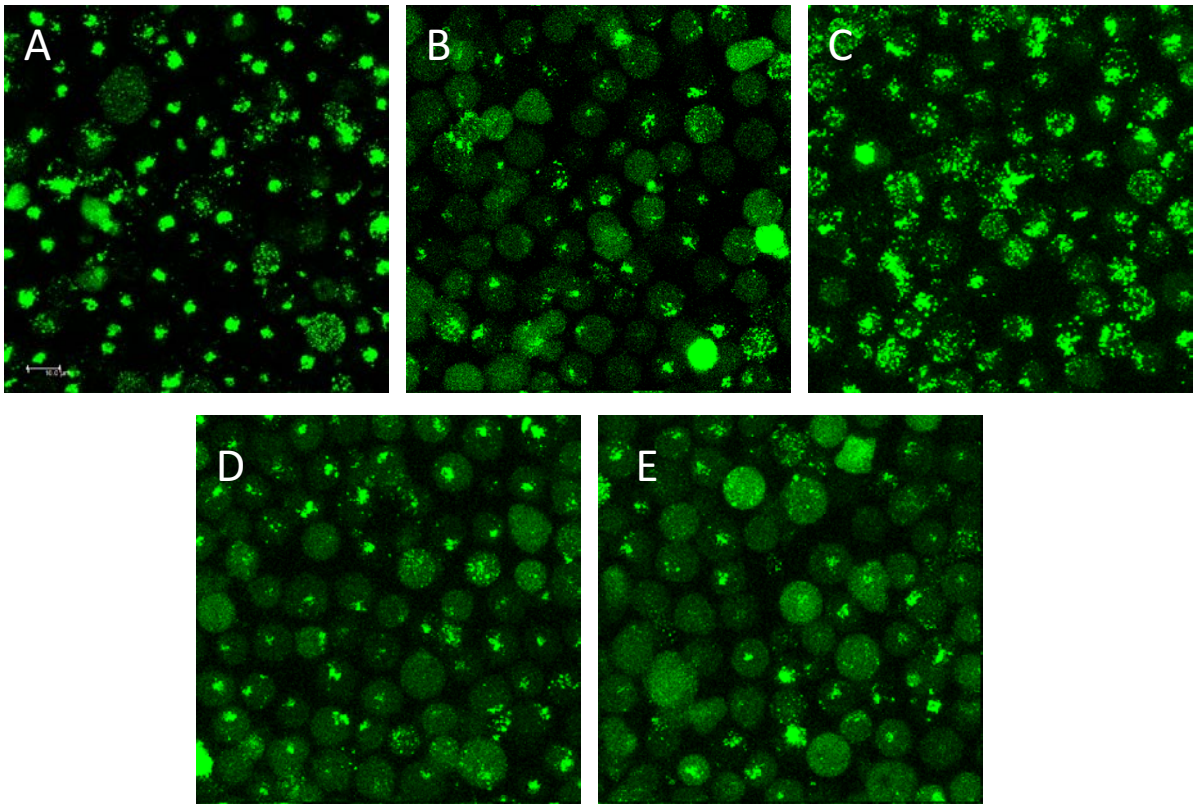

Figure 29 Effect of Inhibitors on the Endolysosomal Escape of SAP-AF in Daudi Cells

Confocal microscopy showing the effect of pharmacological inhibitors on the endolysosomal escape of SAP-AF. Daudi cells were loaded with SAP-AF (green) for 24 h before being treated with 5 µg/ml of SA in the presence or absence of inhibitors. Confocal images were taken after a further 24 h. Images show untreated control cells (A), cells treated with SA only (B) and cells treated with SA and the inhibitors chloroquine (C), chlorpromazine (D) and EIPA (E). Scale bar represents 10 µm.

4.2.5 Investigation of the Effect of an Increased Concentration of SA on the Inhibition of Augmentation

The confocal microscopy images presented above demonstrated that it was not possible to inhibit the endolysosomal escape of SAP-AF induced by 5 µg/ml of SA with EIPA or chlorpromazine. However, both of these inhibitors had been shown to significantly abrogate the augmentation of saporin cytotoxicity by SA at 1 µg/ml. It was necessary to determine whether or not this was due to a disconnection between the augmentation of cytotoxicity and the effect of SA on the endolysosomal escape of the toxin. Alternatively, these results may be due to the higher concentration of SA that had to be used to observe an increase in endolysosomal escape by confocal microscopy compared to that used in the previous cytotoxicity assays. It was not possible to increase the concentrations of the inhibitors further due to the effects of toxicity. In order to inform further experiments looking at endolysosomal escape, cytotoxicity assays were performed

in Daudi and HSB-2 cells investigating the effect of these inhibitors on the effect of 5 μg/ml of SA on the augmentation of saporin and OKT10-SAP. The results presented below are the average of three independent experiments and time limitations prevented further repeat experiments, no statistical analysis is presented due to their being insufficient power to determine statistical significance.

4.2.5.1 Inhibition of Clathrin mediated Endocytosis

The CME inhibitor chlorpromazine has been shown to completely abrogate the augmentation of saporin and OKT10-SAP in Daudi (4.2.1.1) and HSB-2 cells[301] by 1 μg/ml of SA. However, the maximum sub-toxic concentration of chlorpromazine showed no abrogatory effect on the augmentation of OKT10-SAP cytotoxicity by 5 μg/ml of SA in either Daudi or HSB-2 cells and only a partial abrogation of the augmentation of saporin toxicity. The fold increase in toxicity for saporin and SA was reduced from approximately 71,000 to 37,000-fold in Daudi cells and from 13,000 to 1,700-fold in HSB-2 cells. The incomplete abrogation of the augmentation of saporin cytotoxicity by 5 μg/ml of SA suggests that the failure of chlorpromazine to inhibit the endolysosomal escape of SAP-AF in cells treated with 5 μg/ml of SA is due to the higher concentration of SA used. This result is consistent with increased endolysosomal escape being the mechanism for augmentation of cytotoxicity.

4.2.5.2 Inhibition of Macropinocytosis

The augmentation of both saporin and OKT10-SAP by 1 μg/ml of SA was completely abrogated by the macropinocytosis inhibitor EIPA in Daudi (4.2.1.2) and HSB-2 cells[301]. In Daudi cells treated with 5 μg/ml of SA, the abrogatory effect on saporin and OKT10-SAP cytotoxicity was reduced but an incomplete reduction in augmentation was still apparent. With saporin the fold increase in cytotoxicity was reduced from 71,000 to 161-fold and with OKT10-SAP a near complete reduction from 2500 to 20-fold was observed. The incomplete reduction in the augmentation of saporin cytotoxicity with EIPA is consistent with the inability of EIPA to inhibit the endolysosomal escape of SAP-AF seen with confocal microscopy. However, no apparent reduction in escape was observed that would be in line with the partial reduction in augmentation. The difficulties with quantifying escape with confocal microscopy make it difficult to draw a conclusion from these results.

In HSB-2 cells a much greater reduction in abrogation was measured. The augmentation of saporin was reduced from 13,000 to 680-fold whilst the augmentation of OKT10-SAP was almost completely intact, with a reduction in the fold increase from 4,300-fold to 1,500-fold.

A

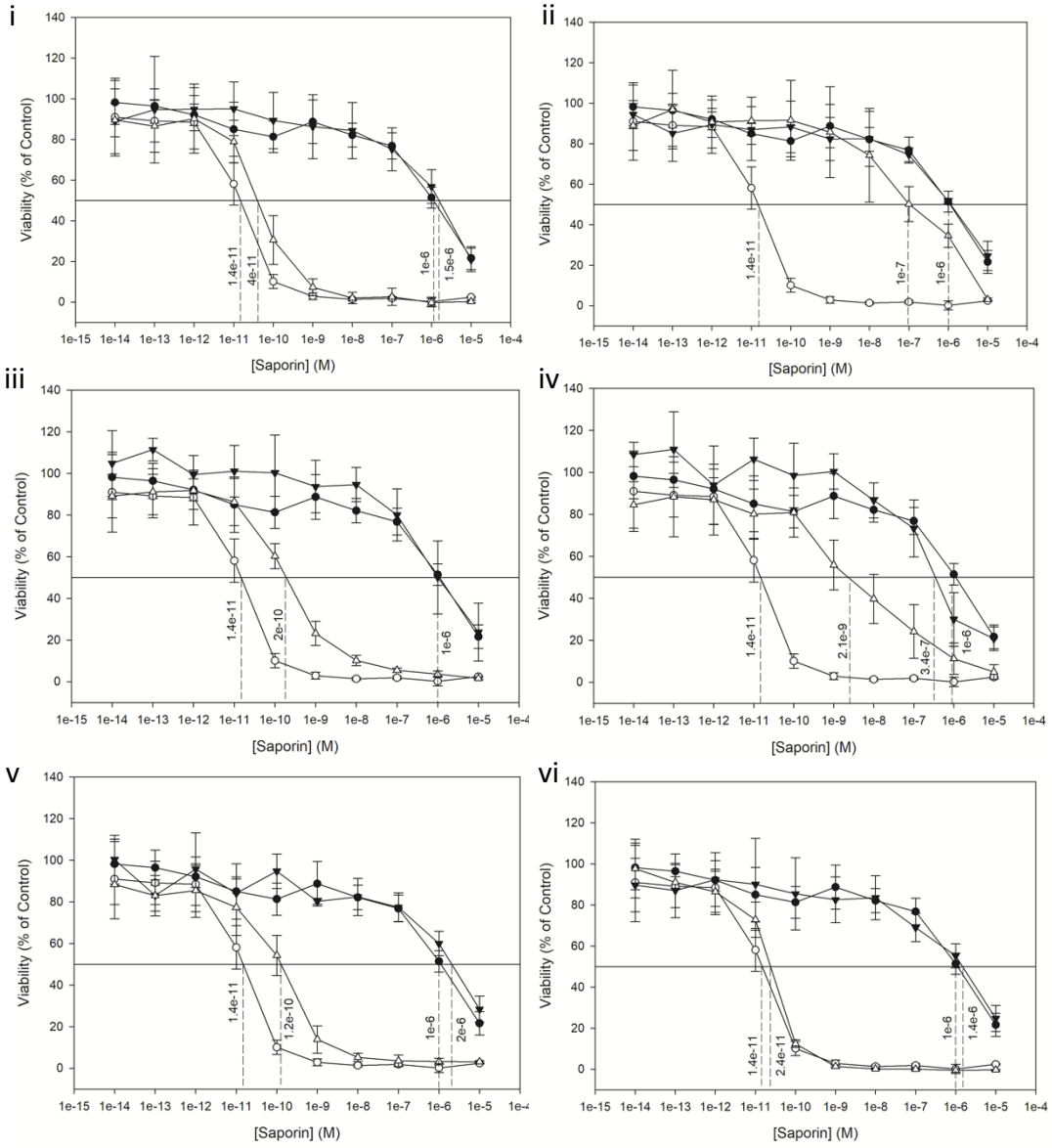
i
ii
iii
iv
v
vi
Viability (% of Control)
[Saporin] (M)
1e-15 1e-14 1e-13 1e-12 1e-11 1e-10 1e-9 1e-8 1e-7 1e-6 1e-5 1e-4
0 20 40 60 80 100 120 140
1.4e-11
4e-11
1e-6
1.5e-6
1.4e-11
1e-7
1e-6
1.4e-11
2e-10
1e-6
1.4e-11
2.1e-9
3.4e-7
1e-6
1.4e-11
1.2e-10
1e-6
2e-6
1.4e-11
2.4e-11
1e-6
1.4e-6

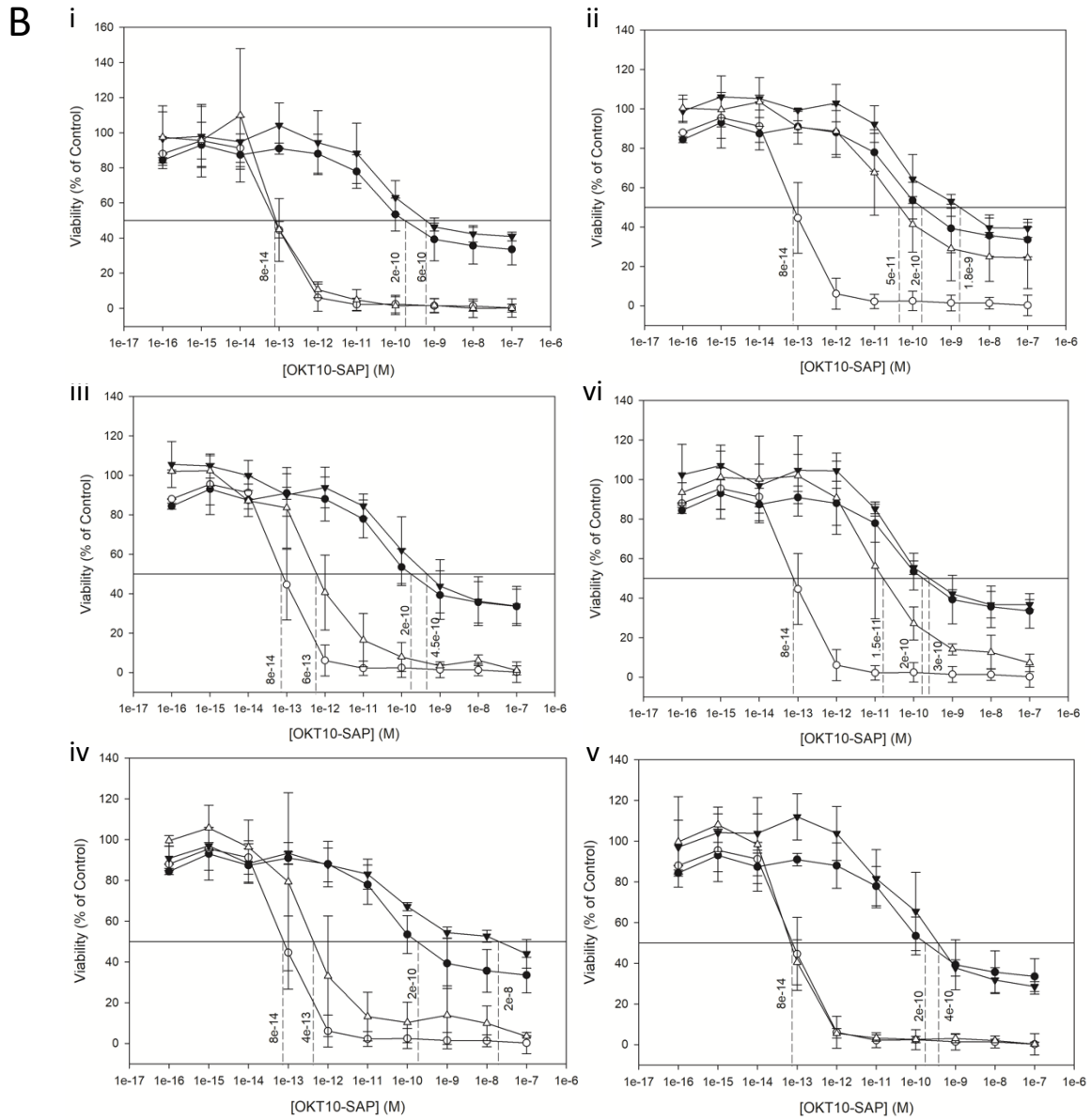

Figure 30 Effect of Pharmacological Inhibitors on the Augmentation of Saporin and OKT10-SAP Cytotoxicity by 5 µg/ml of SA in Daudi Cells

Dose-response curves determined by XTT assay showing the effect of (i) chlorpromazine, (ii) chloroquine, (iii) bafilomycin A1, (iv) EIPA, (v) cytochalasin D and (vi) nocadazole on the augmentation of (A) saporin or (B) OKT10-SAP by 5 µg/ml of SA in Daudi cells. Each chart shows the effect of a fixed concentration of the inhibitor in the absence (▼) and presence (▽) of SA. In each chart the data for saporin or OKT10-SAP without inhibitor in the absence (●) and presence (○) of SA is also presented for comparison. Each datum point represents the calculated mean of three experiments each performed in quadruplicate cell cultures and the error bars one standard deviation either side of this mean. The EC_{50} obtained from each curve is shown against the perpendicular dotted line.

A

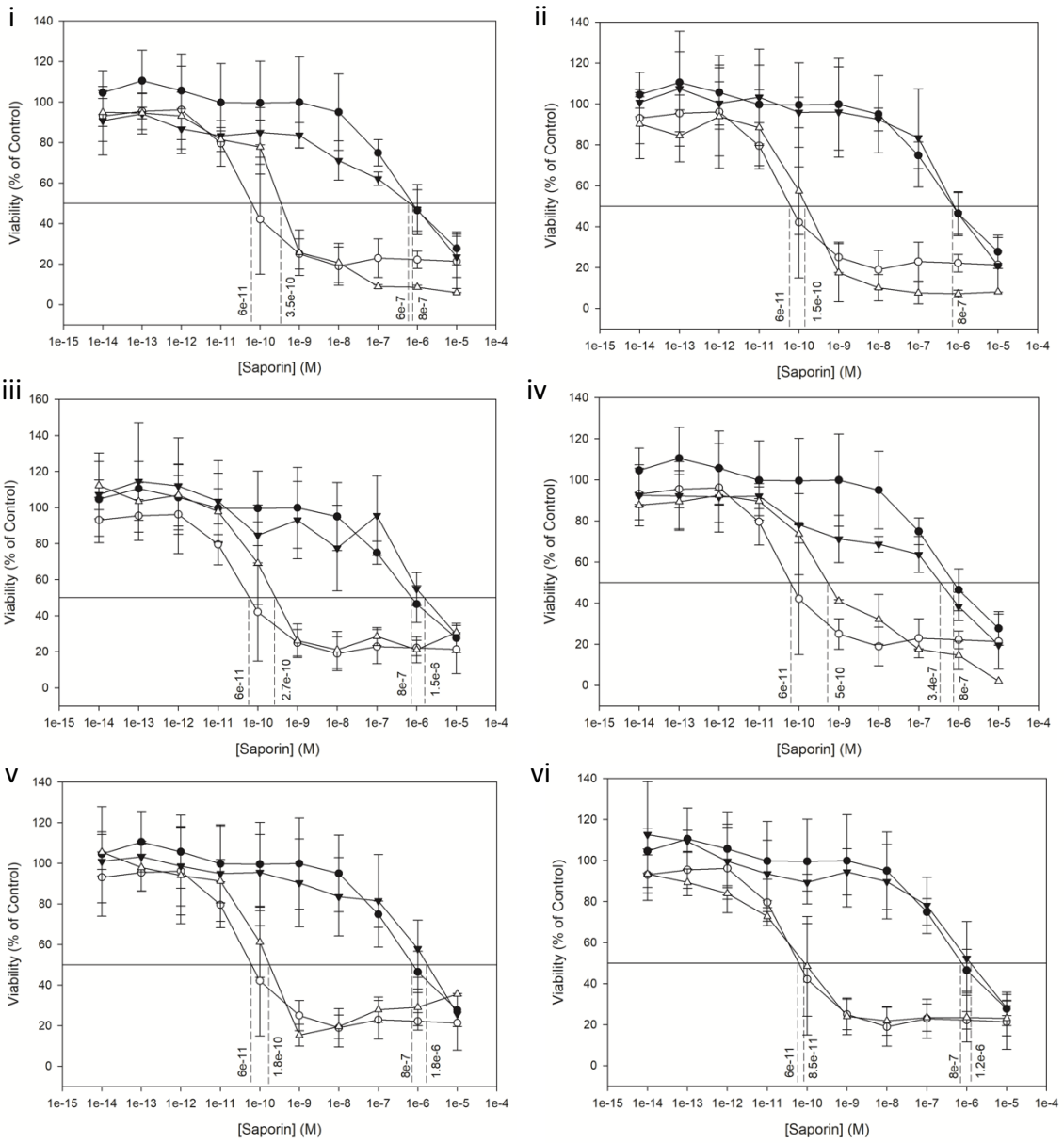
i
ii
iii
iv
v
vi
Viability (% of Control)
[Saporin] (M)
6e-11
3.5e-10
6e-7
8e-7
1.5e-10
2.7e-10
1.5e-6
5e-10
3.4e-7
1.8e-10
1.8e-6
8.5e-11
1.2e-6

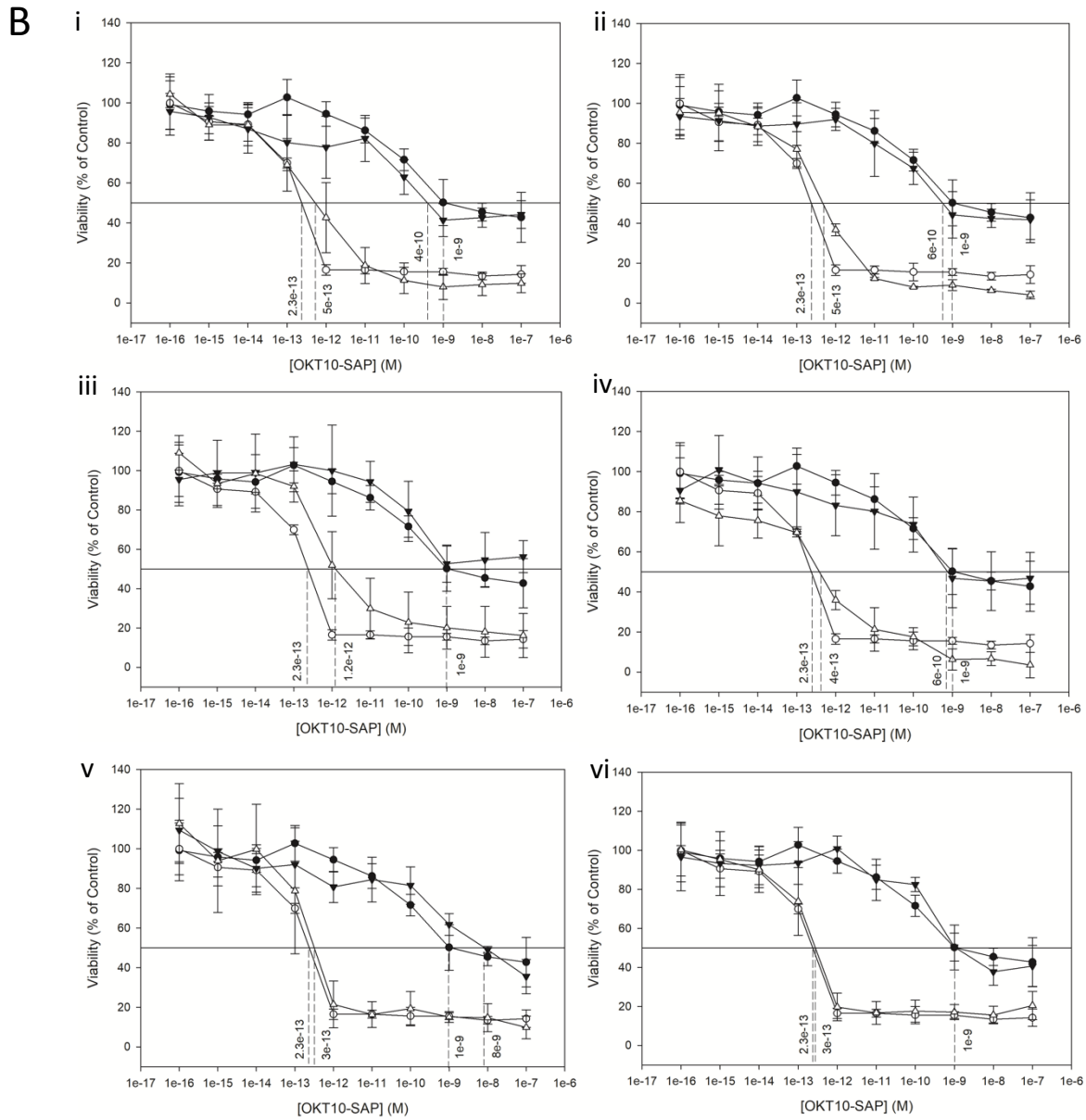

Figure 31 Effect of Pharmacological Inhibitors on the Augmentation of Saporin and OKT10-SAP Cytotoxicity by 5 µg/ml of SA in HSB-2 Cells

Dose-response curves determined by XTT assay showing the effect of (i) chlorpromazine, (ii) chloroquine, (iii) bafilomycin A1, (iv) EIPA, (v) cytochalasin D and (vi) nocadazole on the augmentation of (A) saporin or (B) OKT10-SAP by 5 µg/ml of SA in HSB-2 cells. Each chart shows the effect of a fixed concentration of the inhibitor in the absence (▼) and presence (▽) of SA. In each chart the data for saporin or OKT10-SAP without inhibitor in the absence (●) and presence (○) of SA is also presented for comparison. Each datum point represents the calculated mean of three experiments each performed in quadruplicate cell cultures and the error bars one standard deviation either side of this mean. The EC_{50} obtained from each curve is shown against the perpendicular dotted line.

4.2.5.3 Inhibition of Microtubule Polymerisation

The microtubule polymerisation inhibitor nocadazole was shown to have no effect on the augmentation of both saporin and OKT10-SAP in Daudi and HSB-2 cells by 1 μg/ml of SA. As expected, this result was not changed by increasing the concentration of SA.

4.2.5.4 Inhibition of Actin Polymerisation

The effect of the actin polymerisation inhibitor cytochalasin D on augmentation of cytotoxicity by 1 μg/ml varied between cell lines. In Daudi cells, a partial abrogation of the augmentation of both saporin and OKT10-SAP was observed (4.2.1.4). In HSB-2 cells, complete abrogation of both compounds was seen [301]. In Daudi cells the abrogation of augmentation of both saporin and OKT10-SAP was reduced but not completely prevented in cells treated with 5 μg/ml of SA. Whilst in HSB-2 cells, no abrogation of augmentation was observed at this concentration of SA with either saporin or OKT10-SAP.

4.2.5.5 Inhibition of Endosomal Acidification

The two inhibitors of endosomal acidification used in this project, chloroquine and bafilomycin A1 both completely abrogated the augmentation of saporin and OKT10-SAP cytotoxicity by 1 μg/ml of SA in both cell lines (4.2.1.5) [301]. In Daudi cells treated with 5 μg/ml of SA, the abrogatory effect of chloroquine was on the augmentation of saporin and OKT10-SAP was unchanged with near complete abrogation achieved. This agrees with the observed prevention of SAP-AF endolysosomal escape by chloroquine seen by confocal microscopy. In HSB-2 cells however, the abrogatory effect of chloroquine was greatly reduced. In these cells the fold increase in saporin cytotoxicity was only reduced from 13,000-fold to 5,300-fold and from 4,300 to 1,200-fold with OKT10-SAP. In the case of bafilomycin A1, the abrogation of both saporin and OKT10-SAP was greatly reduced at this concentration of SA in both Daudi and HSB-2 cells.

4.2.6 Development of a Flow Cytometric Assay to Investigate the Endolysosomal Escape of Fluorescently Labelled Toxin

The use of confocal microscopy to investigate the effect of inhibitors of endosomal processes on the SA-mediated endolysosomal escape of SAP-AF and OKSAP-AF was limited by a number of factors. The low throughput of confocal microscopy means that information is provided on only a small number of cells at a time. Additionally, the analysis of microscopic images was time consuming and presented the risk of potential operator bias in the selection of analysed cells. Attempts to automate analysis and extend it to all imaged cells were complicated by the

requirement for a subjective determination of fluorescence thresholds. Together these factors made even semi-quantitative analysis of these images complicated and unreliable. Alongside these problems, there was also a requirement for the use of SA at 5 μg/ml to observe an increase in endolysosomal escape. The inability of the majority of tested pharmacological inhibitors to abrogate the effects of SA at this concentration on toxin cytotoxicity and endolysosomal escape thus prevented further investigations. However, discrepancies between the effect of SA at different concentrations on cytotoxicity and on endolysosomal escape strongly suggested that confocal microscopy probably had insufficient sensitivity to measure any escape of the fluorescently labelled toxin that occurs in cells treated with SA at the augmentative but sub-toxic concentration of 1 μg/ml. Therefore, an attempt was made to develop a more sensitive and more reliably quantifiable assay to determine whether or not endolysosomal escape of the toxin had occurred within a cell.

Flow cytometry measures the fluorescent and optical characteristics of suspended single cells as they pass through a laser. Capable of recording information from thousands of cells per second, flow cytometry is ideal for quantitative analysis of samples. As a cell containing a fluorophore passes through the laser, the fluorophore is excited and emits photons which are then detected and measured. The information for an entire cell is recorded as a signal pulse of voltage over time from which several parameters can be quantified. Typically, the most commonly reported parameter is the area under the pulse or 'pulse area' which is proportional to the total fluorescence emitted from the cell.

The major disadvantage of flow cytometry is that it offers no means of localising intracellular fluorescence. However, by analysing two other important parameters that define the signal pulse, the pulse height and the pulse width, information about the general distribution of a fluorescent compound within a cell can be determined. This method has been termed pulse shape analysis. The pulse height represents the point of maximum fluorescence intensity within the cell, whilst the pulse width provides information on the duration for which a fluorescent signal is detected as the cell passes through the laser beam. Pulse width can therefore be used to characterise the distribution of a fluorescent marker within the cell. Analysis of pulse width has been used to investigate nuclear enlargement[309], the aggregation states of cytoplasmic proteins[310] and to differentiate between surface bound and golgi located fluorescent markers[311]. In the context of measuring the efficacy of endolysosomal escape enhancers, pulse width analysis may provide a method of differentiating cells where escape of a fluorescently labelled toxin has occurred. In cells where the toxin has accumulated purely within the endolysosomal compartment, the corresponding voltage pulse will be tall and narrow representative of its punctate distribution. Endosomal escape of the toxin and its subsequent diffusion throughout the cytoplasm would lead

to an increase in the pulse width as the length of time taken for the area of fluorescent label to pass through the laser increases (Figure 32). Measurement of this change across a large number of cells would allow for the quantification of endolysosomal escape enhancer efficacy.

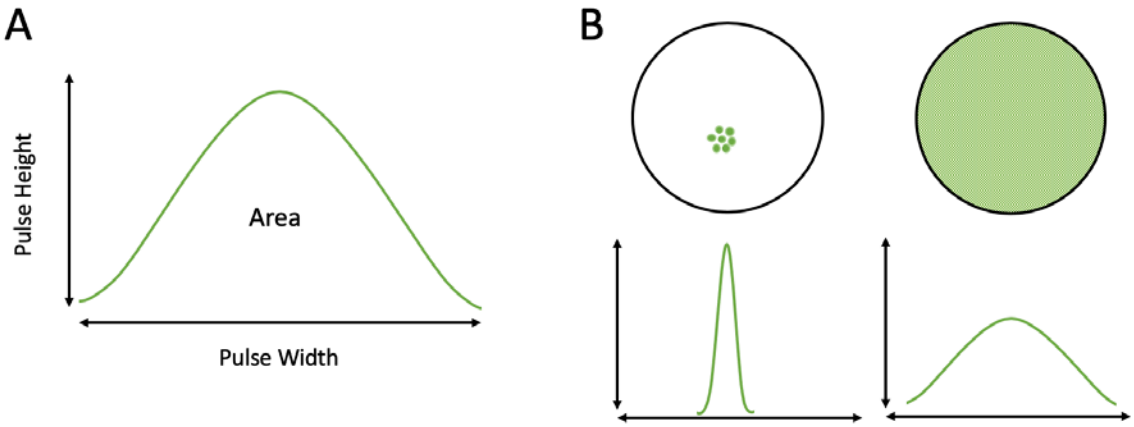

Figure 32 Pulse Shape Analysis

(A) Idealised cartoon illustrating the flow cytometry signal pulse for a fluorescent particle. The pulse height is the maximum fluorescence intensity. Pulse width represents the amount of time taken for the particle to pass through the laser. (B) The distribution of a fluorescent label within the cell changes the fluorescent pulse width. A localised, vesicular distribution will result in a narrow pulse width. In contrast, a fluorescent label with a diffuse, cytosolic distribution will be recorded as a wide pulse width.

Flow cytometry is considered to be more sensitive than fluorescent imaging and its high throughput allows for an unbiased quantitative analysis of results. Pulse width analysis was therefore investigated and developed as an assay to measure the endolysosomal escape of SAP-AF and OKSAP-AF.

4.2.7 Analysis of SAP-AF and OKSAP-AF Internalisation and Trafficking by Flow Cytometry

In order to confirm that a change in pulse width could be observed with changes in the intracellular distribution of the fluorescently labelled toxin, pulse shape analysis was used to investigate the uptake of the toxin over time. Daudi and HSB-2 cells were incubated with SAP-AF or OKSAP-AF for 2, 8, or 24 hours. At each time point cells were analysed by flow cytometry and the height (FITC-H) and width (FITC-W) of the signal pulse from the 525/40 filter FITC channel was recorded. In both cell lines, with both SAP-AF and OKSAP-AF, a gradual, time dependent reduction in FITC-W was recorded (Figure 33 & Figure 34). This corresponds with the internalisation

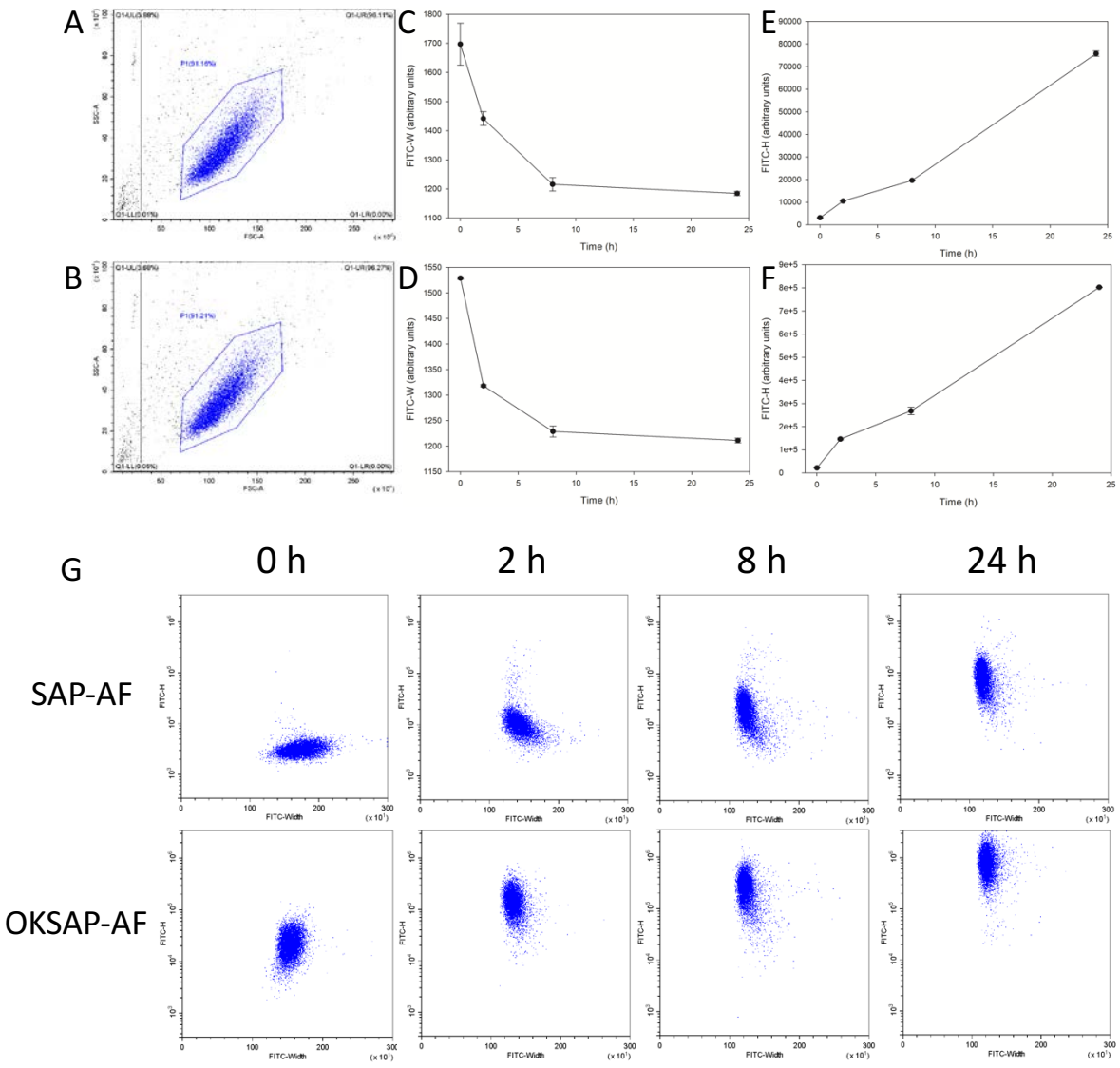

Figure 33 Pulse shape analysis of the uptake of SAP-AF and OKSAP-AF into Daudi cells

Forward and side scatter dot plots for Daudi cells incubated with SAP-AF (A) and OKSAP-AF (B) showing gating used for further analysis. The changes in FITC-W and FITC-H over time for Daudi cells treated with SAP-AF (C & E) or OKSAP-AF (D & F) (n = 2, ±SD). (G) Example dot plots showing FITC-W against FITC-H parameters for cells incubated with SAP-AF or OKSAP-AF for 0, 2, 8 and 24 h.

observed by confocal microscopy. The initial, diffuse, surface bound location is recorded as a wide FITC-W. The subsequent trafficking of the toxin along the endolysosomal pathway into vesicles progressively further from the plasma membrane results in a smaller area of fluorescent signal indicated by a reduction in FITC-W. This also leads to the concentration of the labelled toxin within a single location and a consequent increase in the maximum fluorescent intensity, resulting in a higher FITC-H.

After 24 hours FITC-H levels demonstrated that almost all recorded cells had internalised the toxin. From the dot plots shown in Figure 33G, the range of FITC-W for SAP-AF and OKSAP-AF positive Daudi cells was narrow suggesting that the intracellular distribution was similar in the majority of cells (Figure 33G). In HSB-2 cells the range of FITC-W was increased with a larger number of cells showing a higher FITC-W than those seen in Daudi cells (Figure 34G). This agrees with confocal imaging showing that in Daudi cells SAP-AF and OKSAP-AF occupied vesicles that were tightly packed in a single peri-nuclear region but in HSB-2 cells, vesicles were more widely distributed throughout the cytoplasm (Figure 25).

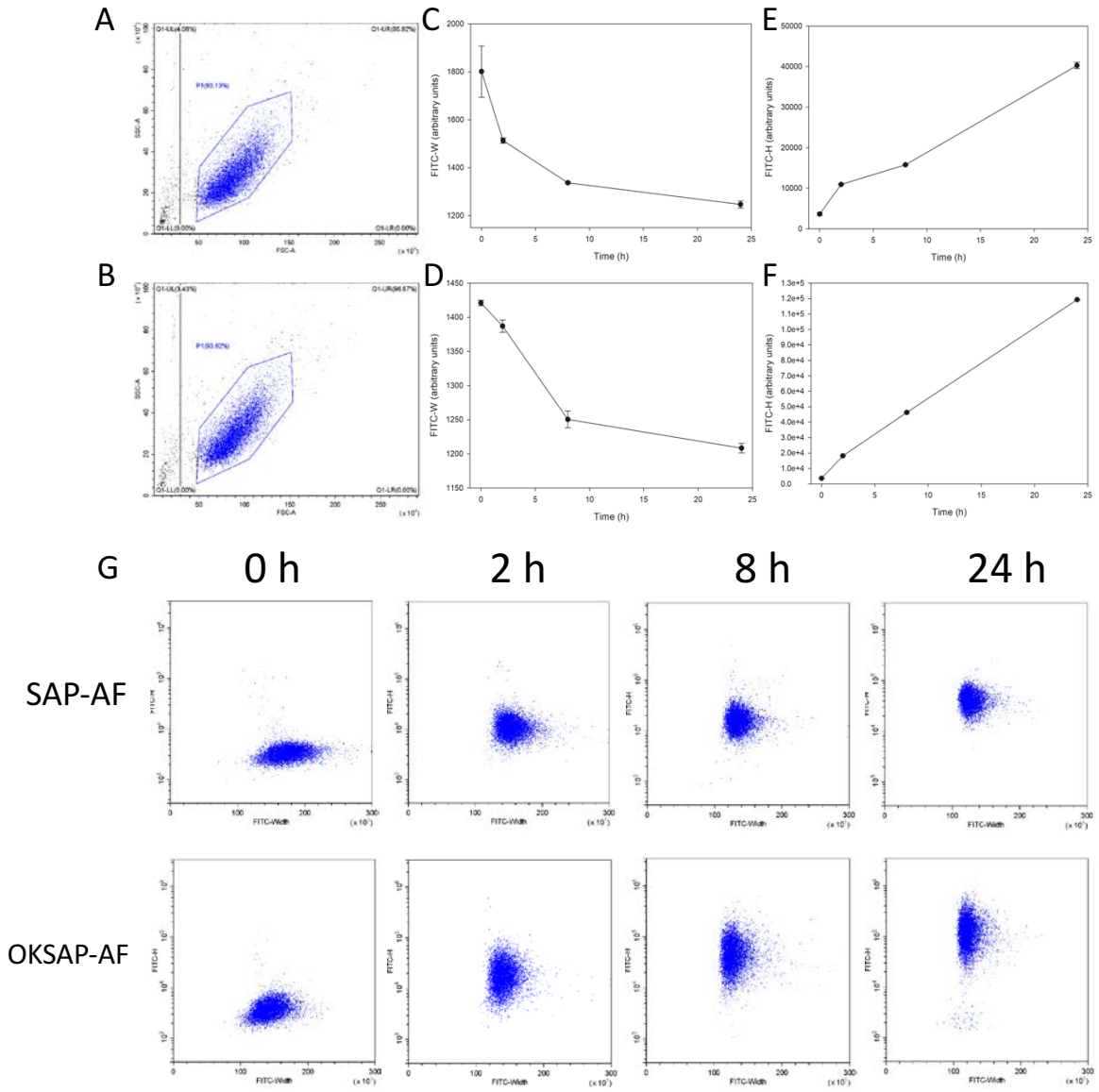

Figure 34 Pulse shape analysis of the uptake of SAP-AF and OKSAP-AF into HSB-2 cells

Forward and side scatter dot plots for HSB-2 cells incubated with SAP-AF (A) and OKSAP-AF (B) showing gating used for further analysis. The changes in FITC-W and FITC-H over time for HSB-2 cells treated with SAP-AF (C & E) or OKSAP-AF (D & F) (n = 2, ±SD). (G) Example dot plots showing FITC-W against FITC-H parameters for cells incubated with SAP-AF or OKSAP-AF for 0, 2, 8 and 24 h.

4.2.8 Evaluation of Endolysosomal Escape by Pulse Shape Analysis

Experiments were conducted with the aim of developing an assay that was capable of quantifying the increase in the number of cells in which the endolysosomal escape of saporin to the cytosol occurs when the cells are treated with SA. In order to confirm that analysis that analysis of FITC-W was capable of differentiating between SAP-AF or OKSAP-AF located in the endolysosomal compartment and that located in the cytosol, SAP-AF and OKSAP-AF loaded Daudi and HSB-2 cells

were treated with SA at a range of concentrations and analysed by flow cytometry at 0 and 24 hours following the addition of SA.

Control cells, mock treated with R10, showed a significant increase in median FITC-W after 24 hours. This agrees with the confocal microscopic imaging that showed endolysosomal escape in a small number of control cells (Figure 26 & Figure 27). SA treated cells were therefore compared to control cells at 24 hours post treatment. A significant increase in median FITC-W was seen in SAP-AF and OKSAP-AF loaded Daudi cells treated with SA at 5 µg/ml when compared to control cells (Figure 35). These results confirmed that the increased levels of endolysosomal escape observed by confocal microscopy could reliably be measured by pulse shape analysis and that they corresponded with an increased FITC-W as predicted.

A smaller but still significant increase in FITC-W was seen in Daudi cells treated with 1 µg/ml of SA with both SAP-AF and OKSAP-AF (Figure 35). As previously reported in section 4.2.4.2, no increase in endolysosomal escape was seen at this concentration of SA by confocal imaging. This suggests that 1 µg/ml of SA induces a lower level of escape of the labelled toxin from the endolysosomal compartment possibly due to a lower level of endolysosomal membrane permeabilisation. This would result in a lower concentration in the cytosol measurable by flow cytometry but could not be observed by confocal microscopy due to the lower level of sensitivity of this method. In Daudi cells treated with 0.1 µg/ml SA, a non-augmentative concentration, no increase in FITC-W was observed indicating that there was no increase in endolysosomal escape beyond that seen in control cells (Figure 35).

In the HSB-2 cell-line there was a significant increase in FITC-W in cells loaded with SAP-AF or OKSAP-AF treated with 5 µg/ml of SA after 24 hours suggesting that this concentration of SA has increased the amount of endolysosomal escape (Figure 36). This increase was also observed previously by confocal microscopy (Figure 27). However, in cells treated with 1 µg/ml of SA no significant increase was seen after this time. Increasing the length of exposure of these cells to 1 µg/ml SA to 48 hours, the duration used in the cytotoxicity assays, resulted in a significant increase in FITC-W with both saporin and the IT over untreated controls (Figure 36). This difference between HSB-2 and Daudi cells in these experiments may be due to the different distribution of endolysosomal vesicles within the two cell lines. In HSB-2 cells the endolysosomal vesicles are widely distributed throughout the cell in comparison to the much more clustered pattern observed in Daudi cells (Figure 25). This wider spread of vesicles in HSB-2 cells resulted in a broader range of FITC-W within the untreated cell population which may have had the consequence of reducing the sensitivity of the assay because of the smaller difference in FITC-W between untreated control cells and cells in which endolysosomal escape has occurred. No

increase in FITC-W over control was observed in cells treated with 0.1 µg/ml, even after 48 h (Figure 36).

A

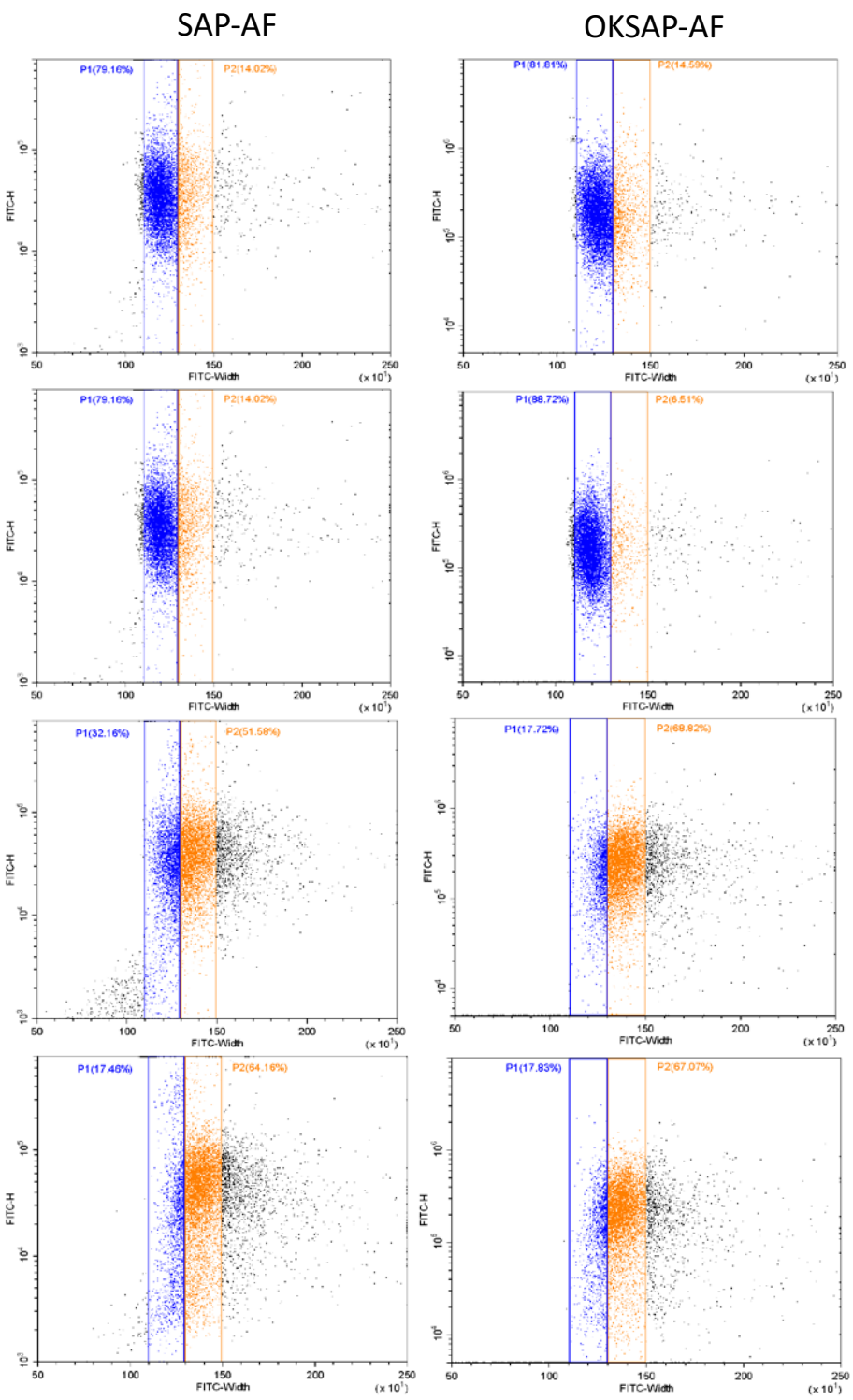
SAP-AF
OKSAP-AF
Untreated
0.1 µg/ml SA
1 µg/ml SA
5 µg/ml SA
P1(79.16%)
P2(14.02%)
P1(81.81%)
P2(14.59%)
P1(79.16%)
P2(14.02%)
P1(88.72%)
P2(6.51%)
P1(32.16%)
P2(51.58%)
P1(17.72%)
P2(68.82%)
P1(17.46%)
P2(64.16%)
P1(17.83%)
P2(67.07%)
FITC-H
FITC-Width
(x 10¹)

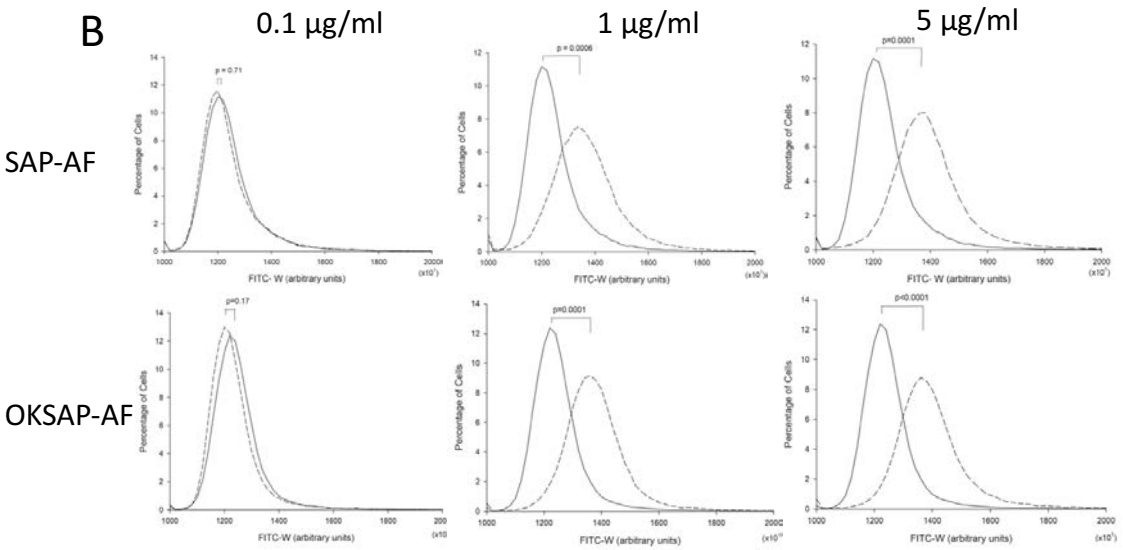

Figure 35 Investigation of Endolysosomal Escape in Daudi Cells by Pulse Shape Analysis

(A) Dot plots showing FITC-W against FITC-H for Daudi cells incubated with SAP-AF or OKSAP-AF for 24 hours before being treated with 0.1 µg/ml, 1 µg/ml or 5 µg/ml of SA or mock treated with R10 for a further 24 hours before cells were analysed by flow cytometry. Each displayed dot plot represents approximately 10,000 events. (B) Pulse width histograms show the distribution in FITC-W for Daudi cells from three combined experiments preincubated with SAP-AF or OKSAP-AF for 24 hours before being treated with 0.1 µg/ml, 1 µg/ml or 5 µg/ml of SA for a further 24 hours. Cells treated with SA are shown with a dashed line, each chart also shows the histogram for untreated cells measured at the same time point and is shown as a solid line. P values for the difference in median FITC-W between treated and untreated cells are shown on each chart (n=3 independent experiments).

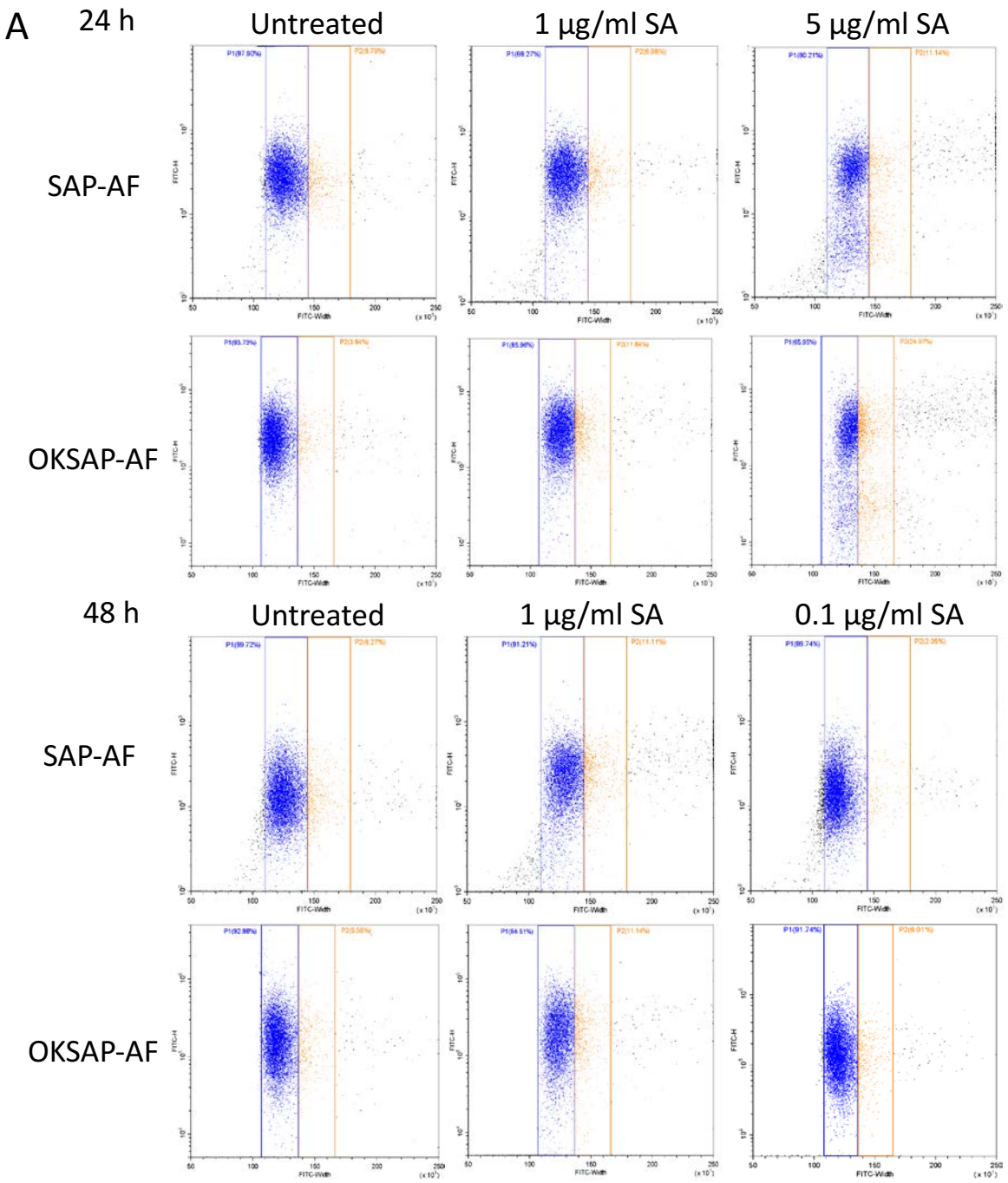
A
24 h
Untreated
1 µg/ml SA
5 µg/ml SA
SAP-AF
OKSAP-AF
48 h
Untreated
1 µg/ml SA
0.1 µg/ml SA
SAP-AF
OKSAP-AF

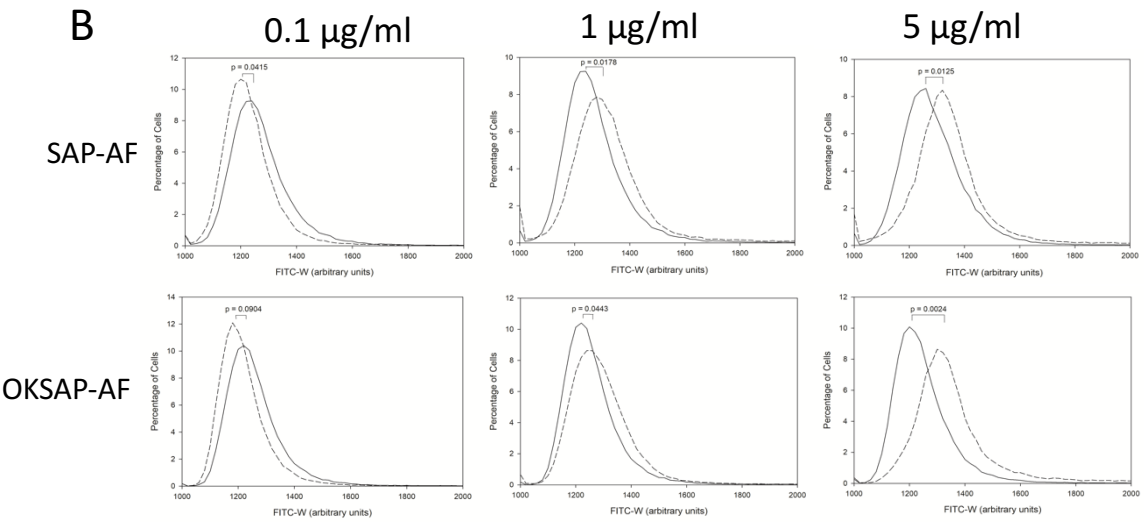

Figure 36 Investigation of Endolysosomal Escape in HSB-2 Cells by Pulse Shape Analysis

(A) Dot plots showing FITC-W against FITC-H for HSB-2 cells incubated with SAP-AF or OKSAP-AF for 24 hours before being treated with 0.1 µg/ml, 1 µg/ml or 5 µg/ml of SA or mock treated with R10 for a further 24 or 48 hours before cells were analysed by flow cytometry. Each displayed dot plot represents approximately 10,000 events. (B) Pulse width histograms show the distribution in FITC-W for Daudi cells from three combined experiments preincubated with SAP-AF or OKSAP-AF for 24 hours before being treated with 5 µg/ml of SA for 24 hours or for 48 hours with 0.1 µg/ml or 1 µg/ml of SA. Cells treated with SA are shown with a dashed line, each chart also shows the histogram for untreated cells measured at the same time point, shown with a solid line. P values for the difference in median FITC-W between treated and untreated cells are shown on each chart (n=3 independent experiments).

4.2.9 Investigation of the Effects of Inhibitors of Endocytosis on the Endolysosomal Escape of SAP-AF and OKSAP-AF Measured by Pulse Shape Analysis

The higher level of sensitivity and ease of quantification of flow cytometric pulse shape analysis makes this methodology more suitable than confocal microscopy to determine the effects of inhibitors of endocytic processes on endolysosomal escape. Daudi and HSB-2 cells were incubated with SAP-AF or OKSAP-AF for 24 hours before treatment with 1 or 5 µg/ml of SA or mock treated with R10 in the presence of absence of a range of endosomal inhibitors. The changes in FITC-W corresponding with endolysosomal escape were recorded immediately after the addition of SA and then after 6, 24 and 48 hours. The results of these experiments are presented below (Figure 37, Figure 39, Figure 40 and Figure 42). To compare the effects of each inhibitor on endolysosomal escape, two-way repeated measures ANOVA was used to look for significant differences between cells treated with each concentration of SA alone and those treated with SA in the presence of an inhibitor. The p values for the variation caused by the addition of inhibitor, but not the effect of increasing lengths of time are presented with each of the figures below (Figure 37, Figure 39, Figure 40 and Figure 42). Analysis by ANOVA does not determine the nature of any significant differences, therefore any significant variation that does not arise from a reduction in FITC-W at all time points is further detailed in the descriptions of results that follow.

4.2.9.1 Inhibition of Clathrin Mediated Endocytosis

Chlorpromazine completely prevented the increase in FITC-W caused by 1 µg/ml SA observed in Daudi cells loaded with SAP-AF or OKSAP-AF (Figure 37B & Figure 39B). There was no significant inhibitory effect on the increase observed with 5 µg/ml of SA. This result corresponds with the inability of chlorpromazine to prevent the endolysosomal escape observed by confocal microscopy when using SA at a concentration of 5 µg/ml (Figure 29).

In HSB-2 cells a significant reduction in the increase in FITC-W was observed with both OKSAP-AF and SAP-AF at both concentrations of SA (Figure 40B & Figure 42B). In HSB-2 cells treated with 5 µg/ml this was seen as both a reduction in the rate of median FITC-W increase and a lower median FITC-W measured after 48 hours when compared to cells treated with SA alone.

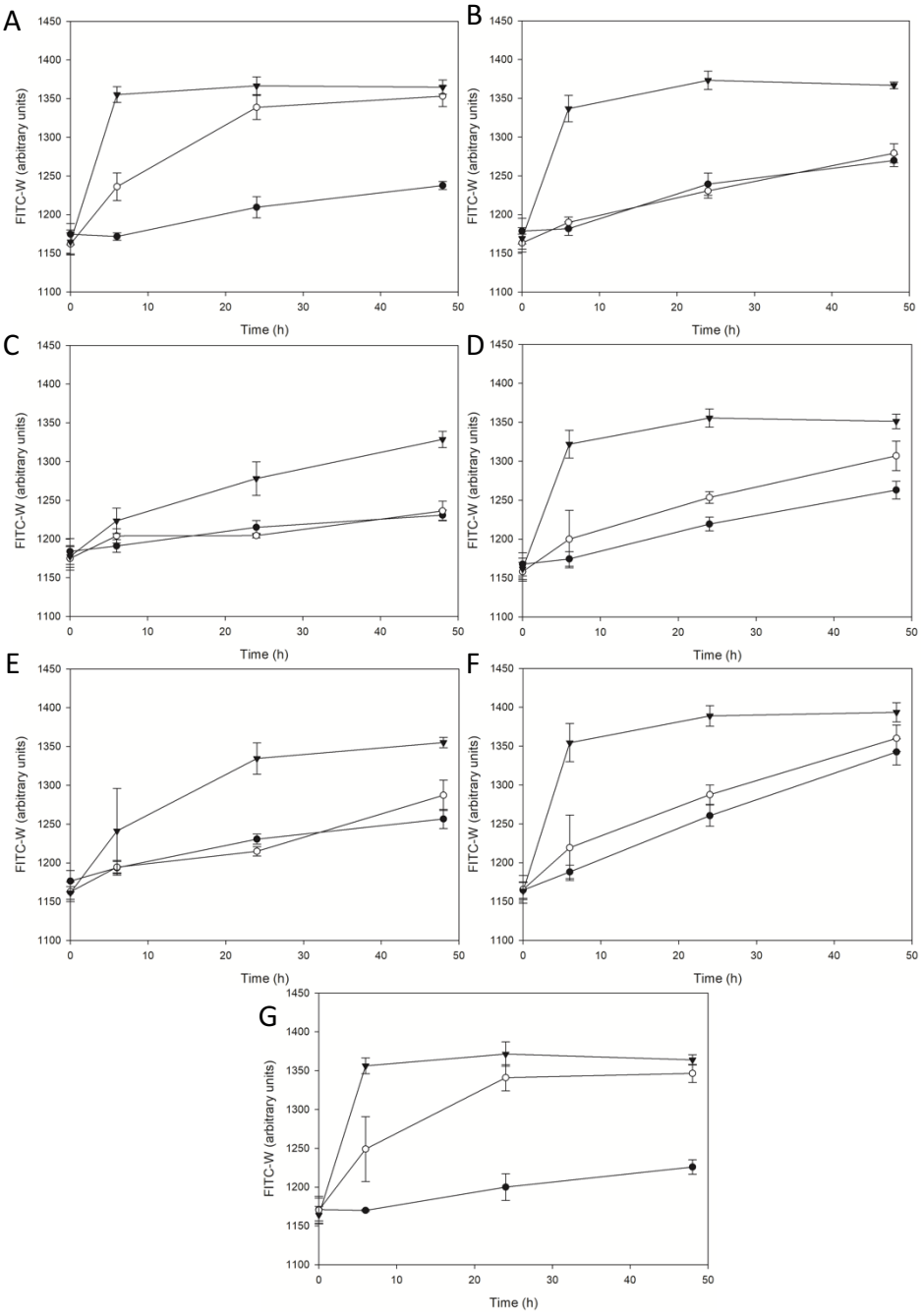

H	CPZ	CQN	BAF	EIPA	CYT-D	NOC
1µg/ml SA	< 0.0001	<0.0001	0.0018	0.0001	0.1048	0.5146
	****	****	**	***	ns	ns
5µg/ml SA	0.8310	0.001	0.0981	0.0022	0.1145	0.8597
	ns	**	ns	**	ns	ns

Figure 37 Investigation of the Inhibition of SAP-AF Endolysosomal Escape in Daudi Cells by Pulse Width Analysis

Effect of chlorpromazine (B), chloroquine (C), bafilomycin A1 (D), EIPA (E), cytochalasin D (F) and nocadazole (G) on the endolysosomal escape of SAP-AF in Daudi cells compared to control (A). Charts show the changes in FITC-W over time in

untreated control cells (●), cells treated with 1 μg/ml of SA (○) and with 5 μg/ml of SA (▼). Each datum point represents the calculated mean of three experiments each performed in duplicate and error bars one standard deviation either side of this mean. The significance of variation between results for each concentration of SA based on the presence or absence of each inhibitor was calculated by 2-way repeated measures ANOVA. The P values obtained in this way are reported in the table (H). CPZ: Chlorpromazine; CQN: Chloroquine; BAF: Bafilomycin A1; CYT-D: Cytochalasin D; NOC: Nocadazole

4.2.9.2 Inhibition of Endolysosomal Acidification

Treatment of OKSAP-AF loaded Daudi cells with bafilomycin A1 in the absence of SA resulted in an increase in FITC-W ($p = 0.015$, 2-way ANOVA) (Figure 39). Confocal microscopy of these cells revealed that bafilomycin A1 caused OKSAP-AF loaded vesicles to become distributed throughout the cytosol, in comparison to their more localised, peri-nuclear distribution observed in control cells (Figure 38). In these Daudi cells the presence of bafilomycin A1 prevented any further increase in FITC-W from SA 1 μg/ml compared to control cells and there was also a significant reduction in FITC-W compared to cells treated with SA alone (Figure 39D). This suggests that bafilomycin A1 prevents endolysosomal escape of OKSAP-AF at this concentration of SA. In cells treated with 5 μg/ml of SA a reduced rate of increase in FITC-W was observed compared to control cells without bafilomycin A1. No increase was seen after six hours but parity with control cells was reached after 24 hours of treatment with 5 μg/ml of SA (Figure 39D). Bafilomycin A1 did not significantly increase FITC-W in the absence of SA in Daudi cells loaded with SAP-AF (Figure 37D). The inhibitor significantly reduced the increase due to 1 μg/ml SA but was unable to reduce the increase seen with 5 μg/ml of SA.

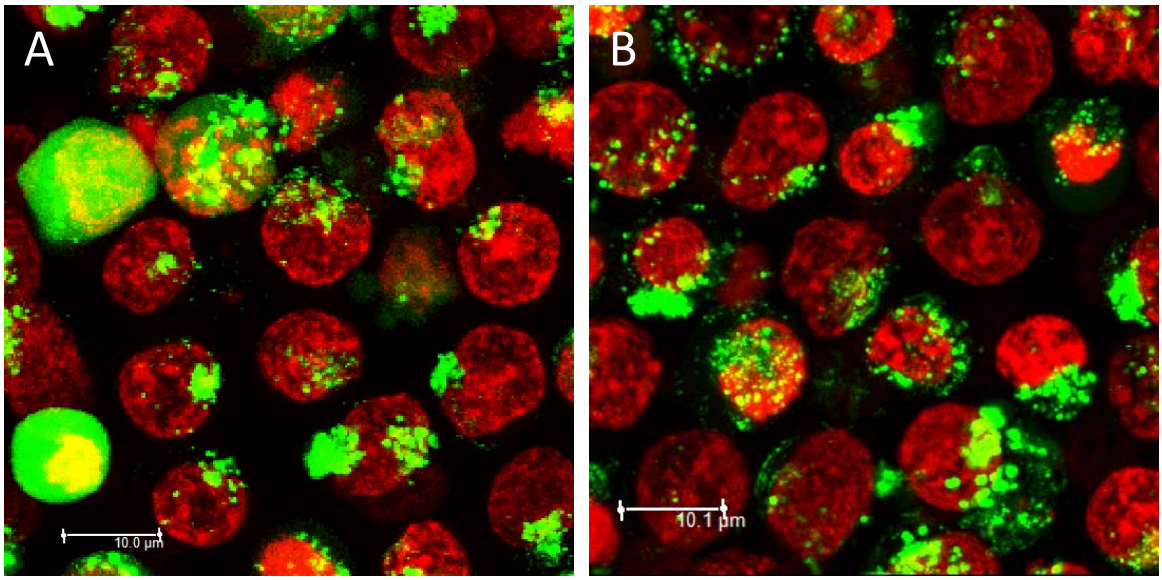

Figure 38 Effect of Bafilomycin A1 on Daudi Cells with OKSAP-AF

Confocal microscopy showing Daudi Cells preloaded with OKSAP-AF (Green) for 24 hours followed by incubation in the absence (A) and presence (B) of bafilomycin A1. The nucleus (red) was stained with Hoechst 33342. Images presented are maximum projections of 21 x 1 µm Z-stacks. Scale bar represents 10 µm.

Bafilomycin A1 alone did not increase FITC-W in HSB-2 cells pre-loaded with SAP-AF or OKSAP-AF. In cells pre-incubated with SAP-AF bafilomycin A1 did not significantly reduce the increase in FITC-W caused by treatment with 1 µg/ml or 5 µg/ml of SA. In contrast, in cells loaded with OKSAP-AF, bafilomycin A1 significantly reduced the increase in FITC-W caused by both concentrations of SA (Figure 40D & Figure 42D).

In both Daudi and HSB-2 cells, chloroquine completely abrogated the increase in FITC-W seen for both SAP-AF and OKSAP-AF with 1 µg/ml SA (Figure 37C, Figure 39C, Figure 40C and Figure 42C). In cells treated with 5 µg/ml of SA, chloroquine significantly reduced but was unable to completely prevent the increase in median FITC-W as measured for both conjugates in Daudi cells and with SAP-AF in HSB-2 cells.

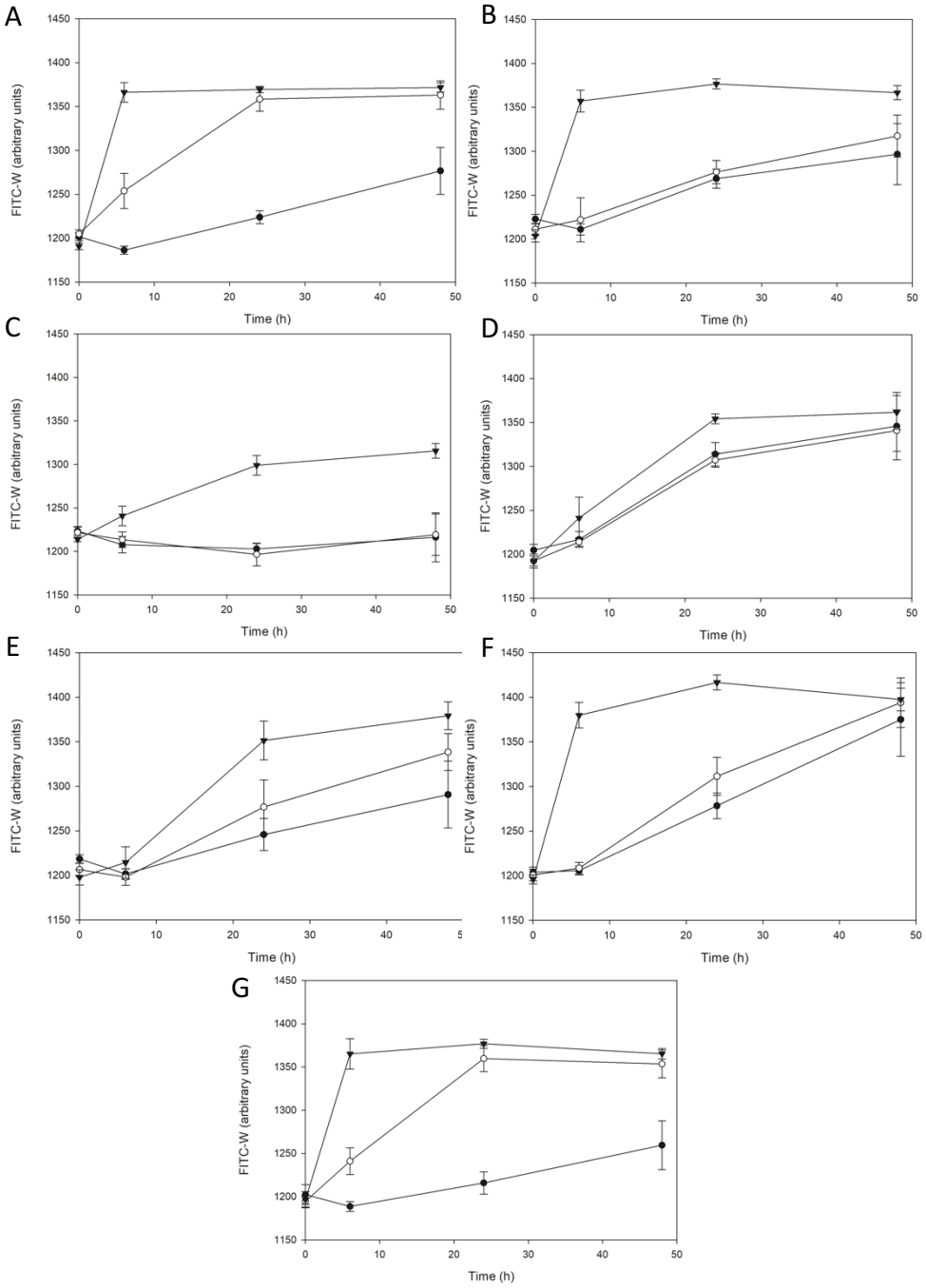

H	CPZ	CQN	BAF	EIPA	CYT-D	NOC
1µg/ml SA	0.0218	0.0013	0.0265	0.0113	0.7582	0.6682
	*	**	*	*	ns	ns
5µg/ml SA	0.6620	0.0001	0.0015	0.0011	0.0015	0.6654
	ns	***	**	**	**	ns

Figure 39 Investigation of the Inhibition of OKSAP-AF Endolysosomal Escape in Daudi Cells Measured by Pulse Width Analysis

Effect of chlorpromazine (B), chloroquine (C), bafilomycin A1 (D), EIPA (E), cytochalasin D (F) and nocadazole (G) on the endolysosomal escape of OKSAP-AF in Daudi cells compared to control (A). Charts show the changes in FITC-W over time in

untreated control cells (●), cells treated with 1 µg/ml of SA (○) and with 5 µg/ml of SA (▼). Each datum point represents the calculated mean of three experiments each performed in duplicate and error bars one standard deviation either side of this mean. The significance of variation between results for each concentration of SA based on the presence or absence of each inhibitor was calculated by 2-way repeated measures ANOVA. The P values obtained in this way are reported in the table (H). CPZ: Chlorpromazine; CQN: Chloroquine; BAF: Bafilomycin A1; CYT-D: Cytochalasin D; NOC: Nocadazole

4.2.9.3 Inhibition of Macropinocytosis

In Daudi cells, the macropinocytosis inhibitor EIPA completely abrogated the increase in FITC-W in SAP-AF loaded cells treated with 1 µg/ml of SA and significantly reduced the increase observed with 5 µg/ml (Figure 37E). For cells incubated with OKSAP-AF, a significant reduction in the increase in FITC-W was observed at both concentrations of SA (Figure 39E). In both cases in cells treated with 5 µg/ml of SA, EIPA reduced the rate at which FITC-W increased in such a way that no increase was observed at 6 hours. This is in comparison to control cells where the majority of the increase in FITC-W occurs within the first 6 hours. However, by the 48-hour time point the median FITC-W of these EIPA treated cells reached the same level as that seen in control cells.

In HSB-2 cells pre-loaded with SAP-AF, EIPA completely inhibited the increase in FITC-W caused by both concentrations of SA (Figure 40E). With OKSAP-AF a significant reduction in the increase in FITC-W caused by 5 µg/ml of SA was seen (Figure 42E), this was especially apparent as a reduction in the rate of increase although unlike in Daudi cells parity with control cells treated with 5 µg/ml of SA alone was not reached by 48 hours. In cells treated with 1 µg/ml of SA the increase in FITC-W was inhibited for the first 24 hours but reached control levels by 48 hours.

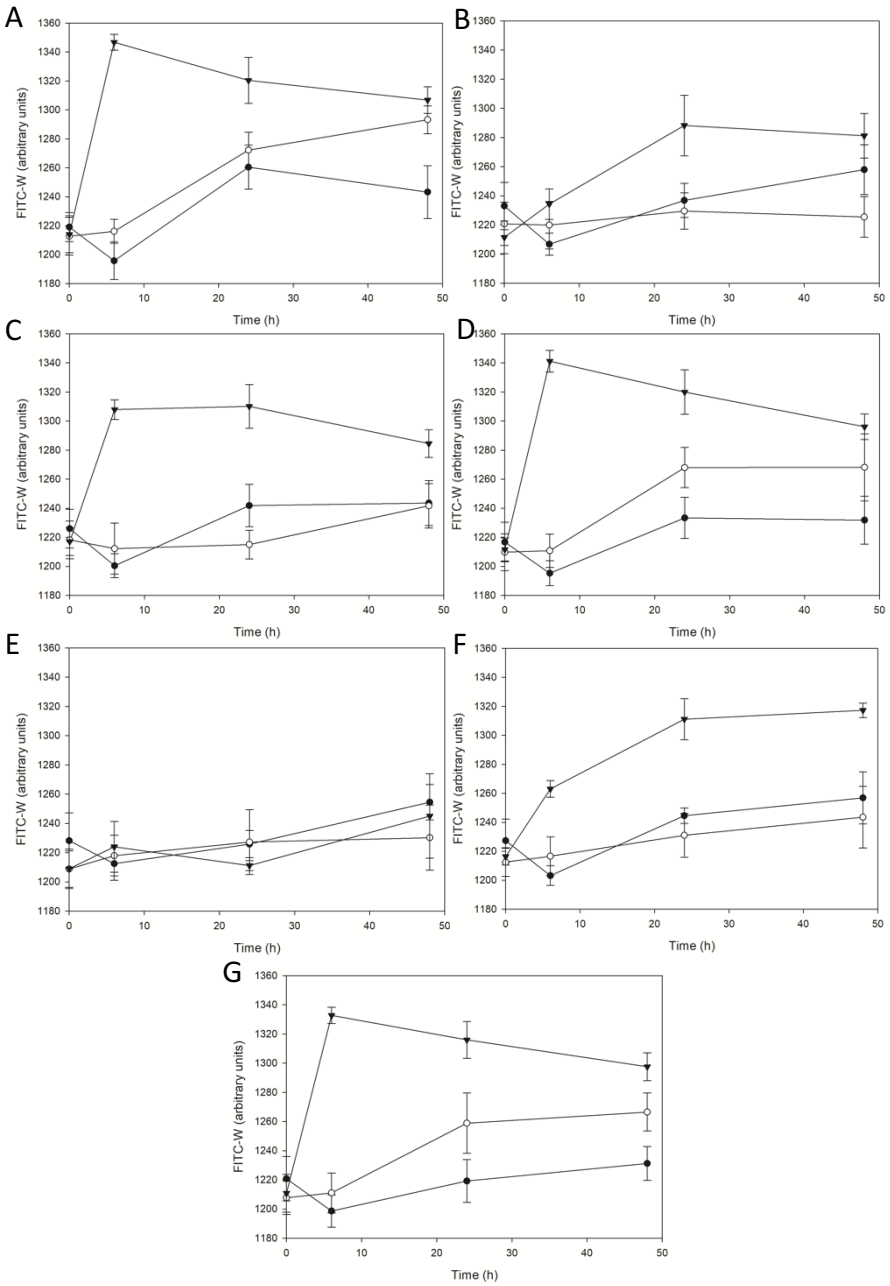

H	CPZ	CQN	BAF	EIPA	CYT-D	NOC
1 µg/ml SA	0.0002	0.0026	0.0597	0.0078	0.0017	0.0246
	***	**	ns	**	**	*
5 µg/ml SA	0.0004	0.0186	0.3682	0.0002	0.0036	0.0957
	***	*	ns	***	**	ns

Figure 40 Investigation of the Inhibition of SAP-AF Endolysosomal Escape in HSB-2 Cells Measured by Pulse Width Analysis

Effect of chlorpromazine (B), chloroquine (C), bafilomycin A1 (D), EIPA (E), cytochalasin D (F) and nocadazole (G) on the endolysosomal escape of SAP-AF in HSB-2 cells compared to control (A). Charts show the changes in FITC-W over time in untreated control cells (●), cells treated with 1 µg/ml of SA (○) and with 5 µg/ml of SA

(▼). Each datum point represents the calculated mean of three experiments each performed in duplicate and error bars one standard deviation either side of this mean. The significance of variation between results for each concentration of SA based on the presence or absence of each inhibitor was calculated by 2-way repeated measures ANOVA. The P values obtained in this way are reported in the table (H). CPZ: Chlorpromazine; CQN: Chloroquine; BAF: Bafilomycin A1; CYT-D: Cytochalasin D; NOC: Nocadazole

4.2.9.4 Inhibition of Actin Polymerisation

In Daudi cells pre-loaded with SAP-AF or OKSAP-AF and treated with cytochalasin D in the absence of SA, there was a time dependent increase in FITC-W (Figure 37F & Figure 39F). This increase in FITC-W was due to cell swelling caused by cytochalasin D and was measured as an increased forward scatter by flow cytometry (Figure 41). In the presence of 1 µg/ml of SA there was no significant abrogation of the increase in FITC-W. In cells treated with 5 µg/ml of SA the FITC-W after 48 h was greater than that in control cells.

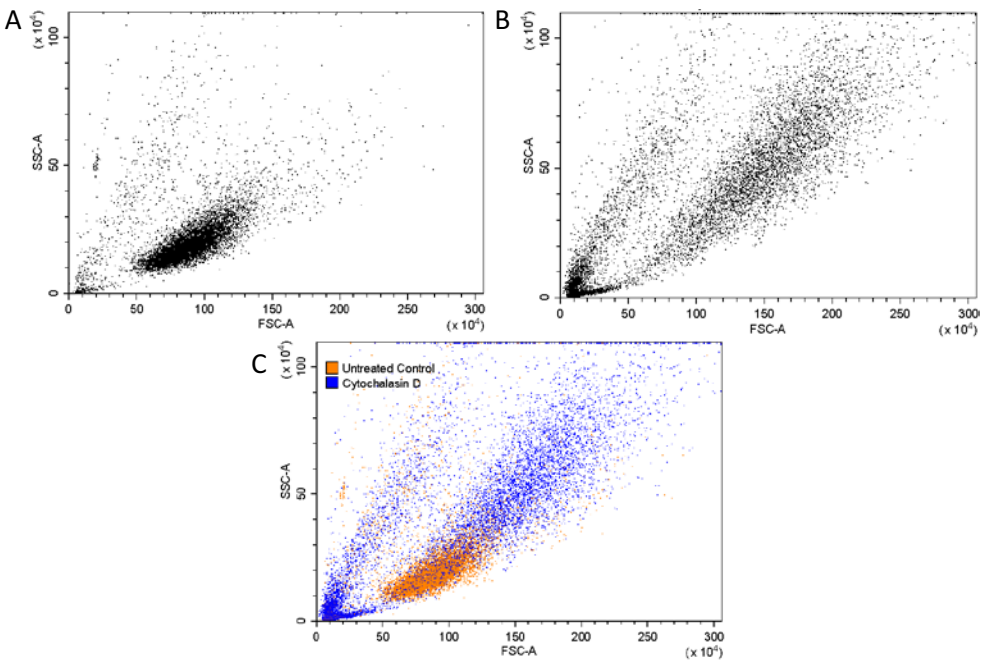

Figure 41 Effect of Cytochalasin D on Daudi Cell Morphology

Dot plots showing the forward (FSC) and side scatter (SSC) of Daudi cells, both untreated controls (A) and cells treated with 0.75 µM cytochalasin D for 48 hours (B) as recorded by flow cytometry. An overlay of these plots is presented in (C).

In HSB-2 cells cytochalasin D did not increase FITC-W in the absence of SA. In the presence of 1 µg/ml of SA, cytochalasin D abrogated the increase on FITC-W seen with both SAP-AF and OKSAP-AF (Figure 40F & Figure 42F). In cells treated with 5 µg/ml of SA, cytochalasin D reduced the increase in FITC-W observed after 6 hours but did not affect the increase recorded after 48 hours with both conjugates.

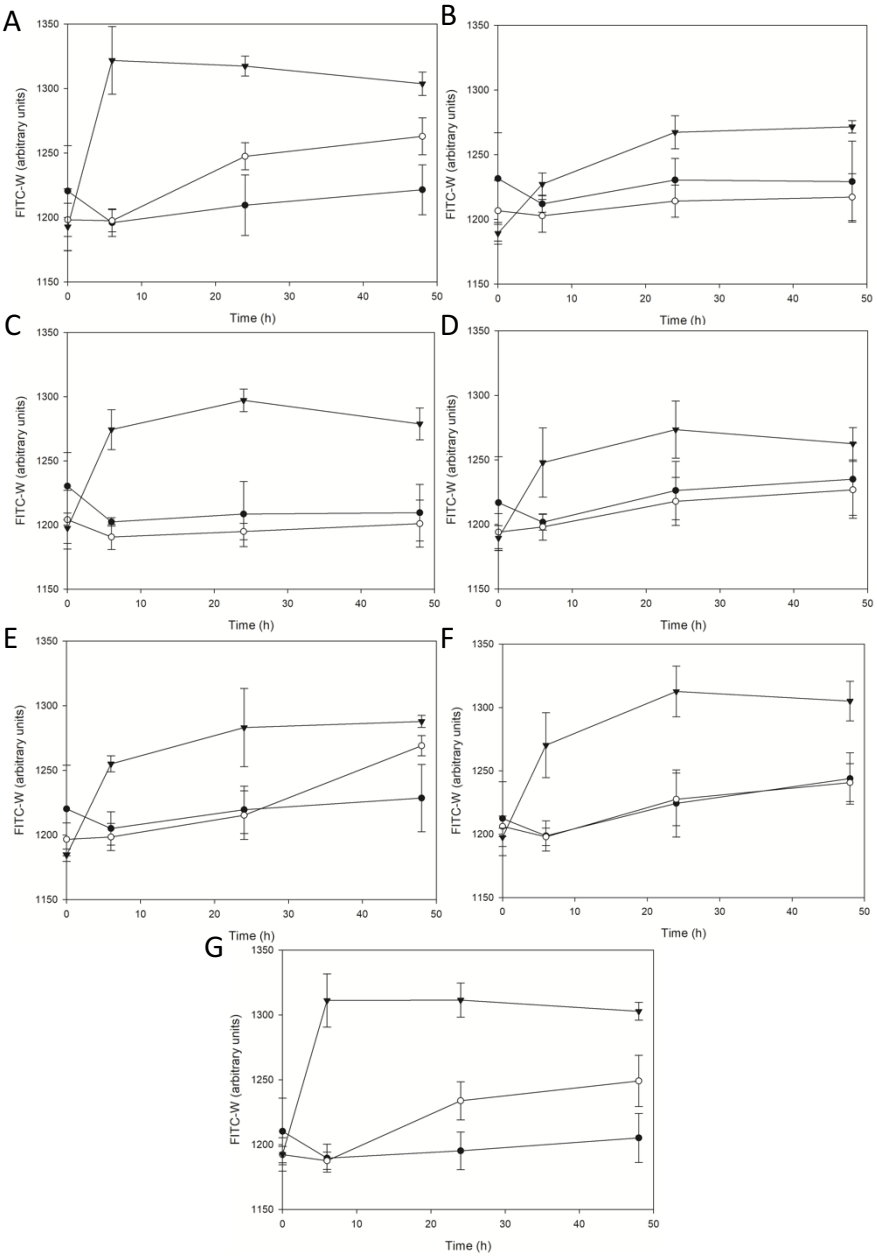

H	CPZ	CQN	BAF	EIPA	CYT-D	NOC
1 µg/ml SA	0.0225	0.025	0.0486	0.3281	0.0487	0.1912
	*	*	*	ns	*	ns
5 µg/ml SA	0.01	0.117	0.0461	0.0264	0.3805	0.7042
	**	ns	*	*	ns	ns

Figure 42 Investigation of the Inhibition of OKSAP-AF Endolysosomal Escape in HSB-2 Cells Measured by Pulse Width Analysis

Effect of chlorpromazine (B), chloroquine (C), bafilomycin A1 (D), EIPA (E), cytochalasin D (F) and nocadazole (G) on the endolysosomal escape of OKSAP-AF in HSB-2 cells compared to control (A). Charts show the changes in FITC-W over time in untreated control cells (●), cells treated with 1 µg/ml of SA (○) and with 5 µg/ml of SA (▼). Each datum point represents the calculated mean of three experiments performed in duplicate and error bars one standard deviation either side of this mean. The significance of variation between results for each concentration of SA based on the presence or absence of each inhibitor was calculated by 2-way repeated measures ANOVA. The P values obtained in this way are reported in the table (H). CPZ: Chlorpromazine; CQN: Chloroquine; BAF: Bafilomycin A1; CYT-D: Cytochalasin D; NOC: Nocadazole

4.2.9.5 Inhibition of Microtubule Polymerisation

In Daudi cells nocadazole had no significant effect on the increased FITC-W observed with either concentration of SA in cells loaded with either SAP-AF or OKSAP-AF (Figure 37G & Figure 39G). In HSB-2 cells a significant change in the increase in FITC-W was only seen in cells pre-incubated with SAP-AF and treated with 1 µg/ml of SA (Figure 40G & Figure 42G).

4.2.10 Comparison of the Effect of Pharmacological Agents on the SA-Mediated Augmentation of Cytotoxicity and its Correlation with the Observed Endolysosomal Escape of Saporin and OKT10-SAP

A comparison was made between the effects of each of the pharmacological agents used in the present study on the augmentation of saporin and OKT10-SAP cytotoxicity by SA and their effect on the SA-mediated increase in FITC-W as a marker for endolysosomal escape. The accompaniment of an inhibition of cytotoxicity augmentation by a corresponding inhibition of endolysosomal escape would provide further evidence that enhancement of endolysosomal escape is the mechanism at least partially responsible for the SA-mediated augmentation of saporin cytotoxicity.

To compare the changes in these variables, the fold increase in EC_{50} in cells treated with saporin or OKT10-SAP in the presence of 1 µg/ml of SA as described in section 2.3.2 was used as a marker for the augmentation of cytotoxicity. These were calculated from XTT assays conducted in section 4.2.1. As a marker for the effect of SA on endolysosomal escape, the difference in the FITC-W between cells loaded with SAP-AF or OKSAP-AF and treated with SA for 48 h and the FITC-W of

cells mock treated with R10 for the same time period, in the presence of each inhibitor, was calculated from the flow cytometric assays performed in section 4.2.9.

From these comparisons a clear trend can be observed. Pharmacological agents which abrogated the SA-mediated augmentation of saporin and OKT10-SAP cytotoxicity also reduced the SA-mediated increase in FITC-W corresponding with the increased endolysosomal escape of SAP-AF and OKSAP-AF (Figure 43). Similarly, for both cell lines, nocadazole, which had no effect on the augmentation of the cytotoxicity of saporin and OKT10-SAP also had no effect on their SA-mediated endolysosomal escape.

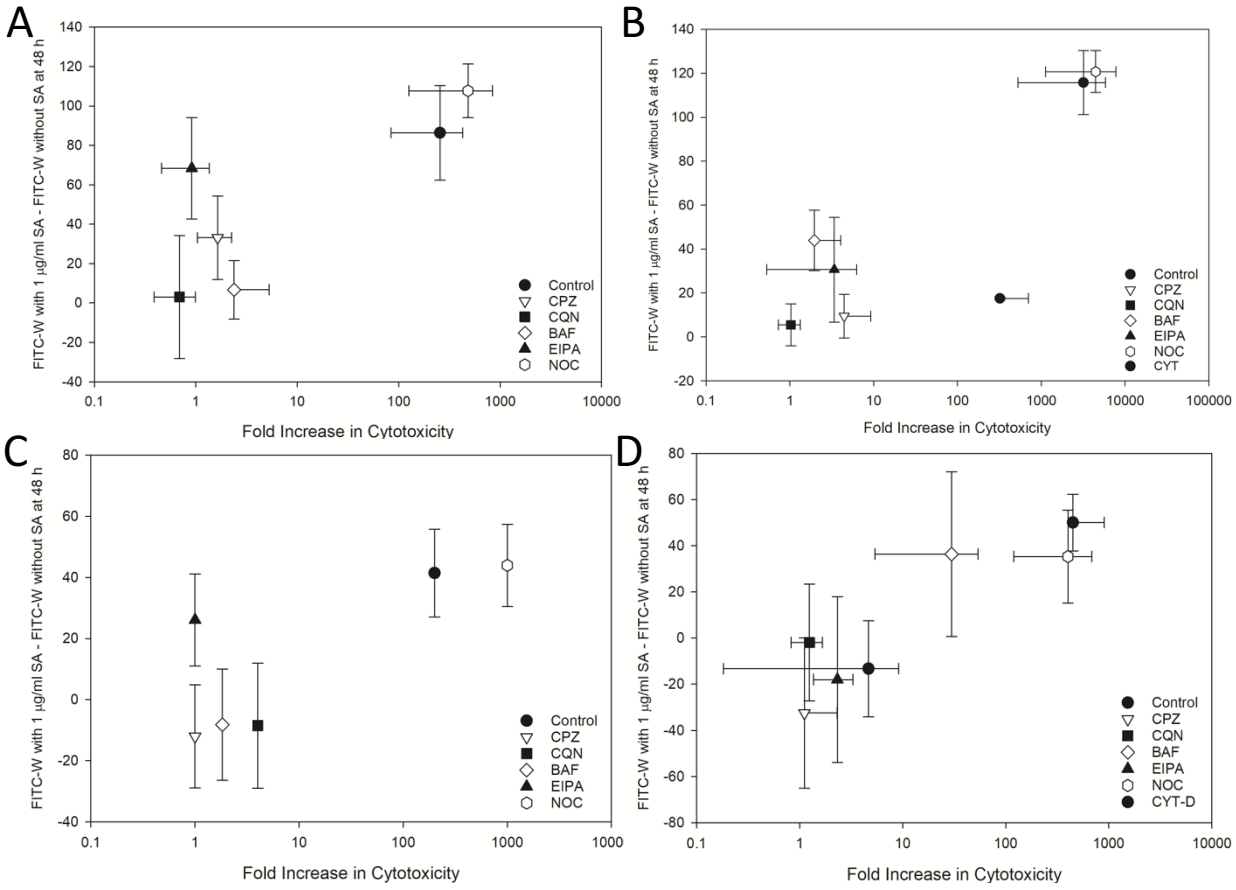

Figure 43 Correlation Between the Effect of Pharmacological Agents on the SA-Mediated Augmentation of Saporin and OKT10-SAP Cytotoxicity and on the SA-mediated Increase in Endolysosomal Escape of SAP-AF and OKSAP-AF

Scatter graphs comparing the SA-mediated fold increase in cytoxicity against the SA-mediated difference in FITC-W after 48 hours of exposure to 1 µg/ml. A and B show the data for Daudi cells with OKT10-SAP/OKSAP-AF and saporin/SAP-AF respectively with C and D showing the data for HSB-2 cells with OKT10-SAP/OKSAP-AF and saporin/SAP-AF respectively. Each data point shows the mean fold increase in cytotoxicity from four independent XTT assays and the mean difference in FITC-W

from three independent flow cytometry studies with each inhibitor and untreated controls included for comparison. These experiments were not paired. Error bars represent the standard deviation from the mean. No error bars are presented for the fold increase in cytotoxicity for OKT10-SAP on HSB-2 cells (C) as an EC_{50} was achieved in only some of the experiments performed. CPZ: Chlorpromazine; CQN: Chloroquine; BAF: Bafilomycin A1; CYT-D: Cytochalasin D; NOC: Nocadazole.

Several exceptions to this trend were observed. In both Daudi and HSB-2 cells, EIPA abrogated the SA-mediated augmentation of OKT10-SAP cytotoxicity but did not significantly reduce the endolysosomal escape of OKSAP-AF after 48 hours (Figure 43A & C). EIPA reduced the SA-mediated increase in FITC-W for OKT10-SAP at earlier time points suggesting that this agent reduced the rate of endolysosomal escape of the IT in these cells. This would delay the cytotoxic effect of the toxin and this may therefore explain the discrepancy between the effect of EIPA on endolysosomal escape and on the augmentation of cytotoxicity. In HSB-2 cells, bafilomycin A1 only partially though still significantly abrogated the cytotoxicity of saporin but failed to reduce the SA-mediated increase in FITC-W for SAP-AF (Figure 43D). Another exception to the observed trend was the effect of cytochalasin D on saporin in Daudi cells (Figure 43B). This agent slightly reduced the augmentation of saporin cytotoxicity by SA but appeared to almost completely abrogate the SA-mediated increase in FITC-W. Cytochalasin D also increased the FITC-W of cells untreated with SA and this would have reduced the difference in FITC-W between SA treated and untreated cells.

4.3 Discussion

The current hypothesis for the mechanism by which saponins augment the cytotoxicity of saporin and saporin based ITs states that both saporin and saponin are internalised by cells and trafficked through sequential endosomal compartments to the endolysosome. Here saponin augments the endolysosomal escape of saporin into the cytosol by a currently unknown mechanism which may involve a pH dependent association between saponin and the toxin. The experiments performed in this chapter aimed to make use of a number of pharmacological inhibitors to investigate the roles of different endocytic processes and of endosomal acidification in this augmentative process.

Cytotoxicity experiments were first performed to investigate the effect of these inhibitors on the augmentation of saporin and OKT10-SAP cytotoxicity by SA. It was shown that the CME inhibitor chlorpromazine reduced the augmentative effect of SA on both saporin and OKT10-SAP.

Chlorpromazine did not reduce the toxicity of the toxin or IT alone indicating that the internalisation of these was not clathrin dependent. This agrees with the work of Bachran et al, who demonstrated that chlorpromazine significantly reduced the augmentation of saporin-EGF by SA[236] in HER14 cells. Work by other members of our laboratory has shown that chlorpromazine does not affect the expression levels of CD38[301]. These results suggest a role for CME in the internalisation of saponins and their augmentation of saporin cytotoxicity.

In the present study, a firm conclusion about the role of CME in augmentation is confounded by the results that were obtained when inhibiting macropinocytosis, an alternative major endocytic process. Holmes et al[196] have suggested that macropinocytosis could be a potential route for the non-specific internalisation of saponin, either in fluid phase or in association with the internalised membrane. In the present study the amiloride analogue EIPA was used as an inhibitor of macropinocytosis. Treatment of cells with EIPA abrogated the augmentation of saporin and OKT10-SAP cytotoxicity by SA but did not reduce the cytotoxicity of the toxin alone. This finding provides some evidence that macropinocytosis is in some way involved in the augmentation of saporin cytotoxicity by SA.

That neither chlorpromazine or EIPA inhibited the cytotoxicity of saporin or OKT10-SAP in the absence of SA raises questions about the internalisation of these agents in light of their lysosomal destination. As discussed in 1.2.2, the mechanism of saporin internalisation is unknown and these results suggest that it is not endocytosed by either of the inhibited pathways. Whist the mechanism of internalisation of saporin may be partially responsible for the internalisation of OKT10-SAP, it is likely that the binding of the IT to CD38 followed by subsequent endocytosis of the CD38-IT complex is the main route of internalisation. More than one endocytic pathway has been implicated in the internalisation of CD38 and the mechanism may be ligand dependent. CD38 has been shown to internalise by CME when bound by anti-CD38 nanobodies [312] but its internalisation is also induced by nicotinamide adenine dinucleotide via a clathrin independent mechanism [313]. The mechanism by which OKT10-SAP induces the internalisation of CD38 is not known but the results presented here suggest that a clathrin independent mechanism is responsible.

It is entirely possible that both CME and macropinocytosis are involved in the internalisation of SA. However, the near complete abrogation of cytotoxicity augmentation by both chlorpromazine and EIPA would make this seen unlikely thus making it difficult to draw any firm conclusion as to whether one or both processes are involved in augmentation. One possible explanation for these results is that either or both of chlorpromazine and EIPA are exerting an off-target inhibition of the other endocytic pathway or that both inhibitors may be affecting an unidentified, separate

process involved in augmentation. Whilst both chlorpromazine and EIPA are often used as specific inhibitors of CME [247,248] and macropinocytosis[249,314] respectively, they have both been shown to exert effects elsewhere in the cell[249]. Chlorpromazine is amphipathic and incorporates into lipid bilayers resulting in increased lipid fluidity of the plasma membrane[315,316]. Changes to lipid fluidity have been shown to affect fluid phase endocytosis and exocytic processes[317]. Chlorpromazine is also a known inhibitor of calmodulin[318] and is known to inhibit phospholipase C (PLC)[319]. PLC is involved in activation of actin modifying proteins[320] and is necessary for the actin cytoskeletal reorganisation in membrane ruffling and macropinocytosis in fibroblasts[321]. It is also of interest that chlorpromazine has been shown to inhibit exogenous cholesterol esterification and sphingomyelinase activity[322] along with depleting cells of un-esterified cholesterol by increasing the net transfer of cholesterol from cells to the serum[323]. This is particularly relevant as the augmentation of saporin based IT's cytotoxicity by SA has recently been demonstrated to be dependent on plasma membrane cholesterol[212]. EIPA cannot be considered to directly or specifically inhibit macropinocytosis, as it acts by inhibiting the Na^+/H^+ exchanger (NHE1) at the plasma membrane causing sub-membranous acidification, leading to the inhibition of ruffle formation in the cell membrane and macropinocytosis[297]. Inhibition of the NHE1 by EIPA has been shown to affect the actin cytoskeleton[324] which may therefore lead to a non-specific inhibition of endocytosis.

Actin polymerisation is known to be involved in a number of endocytic processes, in particular macropinocytosis[253,325,326] and clathrin independent endocytosis [250,298]. The actin disrupting agent cytochalasin D is widely used as an inhibitor of both macropinocytosis and phagocytosis[327]. In the present study cytochalasin-D inhibited the cytotoxicity of OKT10-SAP in both Daudi and HSB-2 cells suggesting that actin is involved in the internalisation of this IT. The effects of cytochalasin-D on the SA-mediated augmentation of cytotoxicity was observed to vary between cell lines. In Daudi cells, only a partial abrogation of the augmentation of both saporin and OKT10-SAP cytotoxicity was achieved. By comparison in HSB-2 cells, complete inhibition of augmentation of cytotoxicity was observed with cytochalasin-D. These results provide some evidence that saponin may be internalised via an actin dependent endocytic pathway but cannot provide any further discrimination between pathways. This is further confounded by the fact that actin is known to be involved in the formation of clathrin coated pits and treatment of cells with actin disrupting agents can also reduce the efficiency of CME and has been shown to inhibit the uptake of transferrin by this endocytic pathway[328]. Furthermore, the effect of cytochalasin D on CME has been shown be variable between cell lines suggesting that the role of actin in CME is not obligatory[329].

As newly formed endocytic vesicles are internalised and transported away from the actin cortex on the inner leaflet of the cell membrane their movement is switched from being actin dependent to being microtubule dependent. Microtubules formed by the polymerisation of α and β-tubulin subunits act as a platform for the transport of endosomes by molecular motors; dynein and the kinesins[302]. In the studies described in this chapter the role of endosomal trafficking along microtubules in the augmentation of saporin cytotoxicity by SA was investigated in cells treated with nocadazole. Nocadazole binds to β-tubulin and disrupts microtubule assembly[299]. In both Daudi and HSB-2 cells nocadazole did not affect the cytotoxicity of either OKT10-SAP or saporin. In addition, nocadazole had no abrogatory effect on the augmentation of OKT10-SAP or saporin cytotoxicity by SA. These results suggest that microtubule dependent trafficking is not required for saporin cytotoxicity or for the augmentation of cytotoxicity by SA. It has been reported that nocadazole inhibits the trafficking of endosomal cargo from the early endosomal compartment to the late endosome but not transport of cargo from the plasma membrane to the early endosome[330]. Additionally, Weng et al reported that the preincubation of ECV-304 cells with nocadazole prior to their exposure to an Alexa Fluor labelled, histidine tagged saporin resulted in its accumulation in larger vesicles than in cells not treated with nocadazole[234]. No co-localisation studies were performed by this group, so it is not possible to say definitively whether these vesicles represented early endosomes but if so then this might suggest that nocadazole prevents the transfer of saporin between the early and late endosomal compartments. The lack of any inhibitory effect of nocadazole on the augmentation of saporin or OKT10-SAP by SA suggests that the trafficking of the toxin and SA to the late endosome or lysosome is not be required for augmentation. This finding may indicate that SA-mediated escape of saporin occurs from the early endosomal compartment and that further trafficking of the toxin to the late endosome or endolysosomal compartment may not be necessary for any SA-mediated increase in endosomal escape to occur. This would run contrary to the hypothesis that trafficking of the saporin and SA to the more acidic endolysosomal compartment is a prerequisite for SA-mediated cytotoxicity augmentation. It is important to note here that nocadazole does not directly affect the pH of endosomes, but by preventing the trafficking of cargo to the late endosome it does prevent further acidification of this cargo [330]. Future work to confirm the effects of nocadazole on the intracellular trafficking of saporin and OKT10-SAP should include internalisation studies of SAP-AF or OKSAP-AF in cells pre-treated with nocadazole. This would allow for fluorescent microscopy studies to investigate the co-localisation of these fluorescent conjugates with markers for early endosomes such as EEA-1 to determine if nocadazole prevents further trafficking beyond the early endosomal compartment. In addition, treatment of cells loaded with SAP-AF or OKSAP-AF in

the presence of nocadazole with SA could be used to investigate the possible endosomal escape of the toxin from the early endosomal compartment.

To investigate the role of endosomal acidification on the augmentation of saporin and OKT10-SAP cytotoxicity by SA, cells were treated with the pharmacological inhibitors; chloroquine and bafilomycin A1 both of which prevent late endosomal acidification but via different mechanisms. Neither of these inhibitors affected the cytotoxicity of saporin or OKT10-SAP alone. Conversely, both chloroquine and bafilomycin A1 significantly abrogated the augmentation of saporin and OKT10-SAP cytotoxicity by SA. These experiments offer independent confirmation, with a different cell line and targeted toxin, of work performed by Bachran and co-workers who showed that the augmentation of SE cytotoxicity by saponins was inhibited by both chloroquine and bafilomycin A1[236]. Taken together these results suggest that a low endosomal pH is a requirement for the augmentation of cytotoxicity by SA. However, it should be noted that this does not inform us as to whether it is a direct, pH dependent effect on saporin or saponin that is responsible for the augmentation effect. The pH of endosomal contents and the pH differential between different vesicular compartments is important for a wide range of processes including enzyme activity and co-ordination of recycling between endosomes and the extracellular milieu[331]. Disruption of the normal endosomal pH by these inhibitors could therefore affect a number of different processes that might be responsible for the SA-mediated augmentation of saporin cytotoxicity. Furthermore, both bafilomycin A1 and chloroquine have been demonstrated to inhibit autophagy via their effects on lysosomal pH[332,333] and this may be relevant considering the potential for saporin to cause cell death by multiple death pathways[159]. In addition, Bafilomycin A1 has previously been shown to inhibit the transfer of endosomal contents from the early endosome to endosomal carrier vesicles thus preventing their trafficking to the late endosomal compartment[330]. A similar effect has been demonstrated with chloroquine, which blocks the transfer of endocytosed material from early to late endosomal compartments resulting in their accumulation in the early endosome[334,335]. Therefore, these inhibitors of endosomal acidification might prevent the trafficking of saporin and/or saponin to later endosomal compartments and thereby prevent saponin achieving a concentration in the endosomal lumen that is sufficiently high enough to permeabilise the endosomal membrane.

Weng et al has previously demonstrated by SPR that saporin associates with SA1641 at an acidic pH. This result, taken together with their observations on the effects of chloroquine and bafilomycin A1 lead this group to propose that a pH dependent electrostatic association between RIPs that are augmentable and saponins is required for the endolysosomal escape of the toxin to the cytosol[152]. In the same publication they showed that gelonin does not associate with

SA1641 at an acidic pH but did not demonstrate whether the cytotoxicity of gelonin was augmented by SA1641. In this present study it was shown that the cytotoxicity of gelonin for Daudi cells is indeed augmentable by SA, suggesting that a pH-dependent association between the saponin and the RIP is not a requirement for endolysosomal escape and subsequent augmentation of cytotoxicity. However, the observation of a lack of association between gelonin and SA1641 made by Weng and co-workers has not yet been independently confirmed and this must be done before any firm conclusions can be drawn. As discussed above, the role of endolysosomal pH as an important factor underlying the mechanism of saponin driven augmentation may not be as simple as a direct effect on either the saporin or saponin within the endolysosome.

Whilst all of the pharmacological agents used in this study are widely used as inhibitors of their respective processes, further work involving the use of these agents should include confirmation of their inhibitory activity in the cell lines used here. For chlorpromazine, a transferrin uptake assay can be used as a reporter the inhibitor's effect on CME activity [336]. Likewise, the internalisation of fluorescent dextran conjugates can be used to investigate macropinocytosis[337] and the effect of EIPA on this process. Work performed prior to the start of this degree by the author demonstrated that the macropinocytic uptake of fluorescent dextran conjugates into Daudi cells was low (Unpublished Data). To investigate the activity of nocodazole on microtubules, staining of the cytoskeleton with anti-tubulin mAb[338] or a fluorescent tubulin stain[339] would enable evaluation of the abundance of polymerised tubulin by fluorescence microscopy or flow cytometry. Similarly, the use of a fluorescent F-actin probe such as rhodamine phalloidin with fluorescence microscopy could be used to investigate the effect of cytochalasin-D on actin[338]. Finally, the effect of chloroquine and bafilomycin A1 on the pH of the endolysosomal compartment could be investigated with the use of ratiometric pH probes to measure the pH of acidic organelles[340]. It was not possible to perform these confirmatory experiments due to time constraints within this project.

Further work investigating the augmentation of saporin and IT cytotoxicity by SA should also ideally incorporate the use of other assays for determining cell viability. The XTT assay used in this study measures cellular metabolic activity as a widely accepted proxy for cell viability[272,273]. This measurement does not however confirm that the bulk cells under measurement are dead or irreparably damaged. The concurrent use of assays measuring other indicators of cell viability such as mitochondrial membrane potential[341] or plasma membrane permeability would reinforce and confirm results obtained by XTT assay. During the course of this study, preliminary experiments were carried out to compare the XTT cytotoxicity assay with PI staining by flow

cytometry. The results of these are presented in Appendix C and showed that changes in metabolic activity occurred after exposure to lower concentrations of OKT10-SAP than those causing cell death as determined by PI influx. It is therefore possible that a population of treated cells were more resistant to the cytotoxic effect of the IT and that a proportion of cells may recover from the effects of the toxin once removed from further exposure.

Taken overall these results do provide useful insights into the potential mechanisms that might be involved in the augmentation of saporin and OKT10-SAP cytotoxicity by SA but should be interpreted with caution for all the reasons stated earlier. They confirm that there is a requirement for SA internalisation and trafficking in the augmentative process but due to the limitations of the pharmacological agents used it was not possible to determine the precise pathways and/or mechanisms involved. To overcome these limitations, the use of siRNA to knockdown specific genes involved in these processes would present a much more selective way to investigate the role of specific components of the endocytic machinery in IT augmentation by SA. During the course of this work plans were made to undertake some siRNA knockdown studies to further investigate the role of different endocytic pathways in both the augmentation of cytotoxicity by SA and the effect of SA on the endolysosomal escape of SAP-AF and OKSAP-AF. It was determined that electroporation would likely not produce sufficient healthy cells to perform the necessary experiments and that viral transduction methods would take too long to develop within the time limit of this project. Therefore, an attempt was made at using lipofection reagents to transfect the monocytic cell line U937 with siRNA. This cell line was determined to be more susceptible to lipofection, based on published work and manufacturer's guidelines, than the lymphocytic cell lines otherwise used in this study. This work was ultimately unsuccessful for technical reasons, and a description of the preliminary work that was performed is presented in Appendix A. For future work looking at the involvement of the various endocytic pathways in the augmentation of cytotoxicity, a viral transduction method with shRNA would likely provide the best form of knockdown in these cell lines.

The next stage of this project aimed to correlate the effects of each pharmacological inhibitor on the SA-mediated augmentation of cytotoxicity with the effect that they might have on the endolysosomal escape of saporin or OKT10-SAP into the cytosol of target cells. The objective of this comparison was to provide confirmatory evidence of the hypothesis that increased endolysosomal escape of toxin is the mechanism by which SA augments saporin cytotoxicity. Confocal microscopy performed at time points in cells exposed to fluorescently labelled conjugates of saporin and OKT10-SAP was capable of tracking their internalisation into the cell and their accumulation after 24 hours in vesicular structures. Co-localisation studies with the lysosomal protein LAMP-1 confirmed that these structures were endolysosomes.

Daudi and HSB-2 cells loaded with SAP-AF or OKSAP-AF were then treated with 1 or 5 μg/ml of SA and live cell imaging performed at a number of time points. In both cell lines escape of both SAP-AF and OKSAP-AF into the cytosol was observed after 8 hours of exposure to 5 μg/ml of SA. By 24 hours after initial treatment with SA 5 μg/ml, almost all cells showed evidence of endolysosomal escape. This was in contrast to untreated control cells where cytosolic fluorescence was only observed in a small number of cells. However, no obvious increase in endolysosomal escape was observed in cells treated with SA at the augmentative concentration of 1 μg/ml.

These results offer independent confirmation of live cell imaging previously presented by Weng et al which showed the endolysosomal escape of a fluorescently labelled saporin in ECV-304 cells treated with 10 μg/ml of SA1641[152]. In addition, the results from this present study include observations of control cells, not treated with SA, over the same time course. Similar controls were not included in the work described by Weng and co-workers to unequivocally demonstrate that endolysosomal escape of SAP-AF and OKSAP-AF does not occur in a lower percentage of cells in the absence of SA. In their assay Weng et al showed initial evidence of endolysosomal escape within just 5 minutes of adding SA1641. This is notably different from the 8 hours required to observe endolysosomal escape in this current study. It is feasible that this discrepancy in results is due to the differences between the cell lines being used. It is likely that ECV-304 cells are more endocytically active as they were shown to internalise fluorescently labelled saporin to the endolysosomal compartment within 6 hours compared to the 24 hours required for Daudi and HSB-2 cells to internalise sufficient SAP-AF to perform the assay reliably.

Conjugation of both SAP-AF and OKSAP-AF to Alexa Fluor 488 reduced the cytotoxicity of both agents compared to their unlabelled forms. An adenine release assay demonstrated that the N-glycosidase activity of saporin was reduced by its conjugation which is likely the cause of the reduction in cytotoxicity of the toxin. Furthermore, the binding of OKSAP-AF to CD38 was shown to be greatly reduced and this would have also affected the cytotoxic effect of the IT. In the case of OKSAP-AF it was not possible to determine the identity of the labelled component within this conjugate. However, the negative effects of conjugation on the adenine release assay and on the binding of the IT to CD38 suggest that the AF488 label can be associated with either the saporin toxin or the mAb component of the IT. It was not possible to determine in what proportion of IT molecules each or both of these components were bound by the fluorescent label.

Despite the effect of the labelling on the biological activity of these molecules, the observable binding of OKSAP-AF to the cell membrane of Daudi cells by confocal microscopy justified its use in these experiments to track the internalisation and intracellular trafficking of the IT.

When interpreting the confocal microscopy presented here it is therefore important to consider that the conjugation of both saporin and OKT10-SAP to Alexa Fluor 488 may also have affected the internalisation characteristics of the toxin/IT. Conjugation of these proteins to a fluorescent label with a different structure and via a different chemical reaction followed by subsequent internalisation studies may be able to determine whether the internalisation and trafficking of the saporin/IT seen in the present study was independent of the fluorophore.

The original aim of this work was to utilise this confocal assay to investigate the effects of pharmacological inhibitors on the SA-mediated increase in endolysosomal escape of SAP-AF and OKSAP-AF. However, a few of major problems prevented this work from continuing successfully. The first of these was the lack of success in successfully performing semi-quantitative analysis of the confocal imagery. Analysis of the imagery was limited because, due to the non-adherent nature of the cells being investigated and the long periods between imaging time points, it was not possible to image the same cells at each time point. Therefore, as described in Appendix B, an attempt was made to develop an analysis protocol to determine the extent of endolysosomal escape that had occurred at each time point by estimating the approximate number of cells in each image and then measuring the average area of relevant fluorescent signal per cell. This was confounded by inter-experimental variations in cytosolic fluorescent intensity in cells where endolysosomal escape had occurred. This was either due to variations in the amount of endocytosed SAP-AF or differences in the effect of SA on endolysosomal escape between experiments. This variation meant that it was necessary to set the fluorescent thresholds used to define cytosolic fluorescence from background levels independently with each experiment. Setting these thresholds introduced substantial subjective user bias and made it impossible to determine the viability of the analysis to detect small changes in cytosolic fluorescence between experiments. For these technical reasons the analysis was therefore abandoned.

The second problem that arose whilst attempting to use confocal microscopy to investigate the effects of pharmacological inhibitors on endolysosomal escape was that when tested only chloroquine was capable of abrogating the increase in endolysosomal escape of SAP-AF seen in Daudi cells treated with 5 μg/ml of SA. Both chlorpromazine and EIPA had no observable abrogatory effect upon the observed endolysosomal escape. This is in contrast to the effect of these inhibitors on the augmentation of saporin cytotoxicity by SA, where they both showed near complete abrogation of inhibition. These results suggested that either there was a disconnect between the effects of SA on endolysosomal escape and the effect exerted on cytotoxicity or that the requirement for to use SA at a concentration of 5 μg/ml to visualise endolysosomal escape by confocal microscopy was somehow responsible. At this increased concentration it is possible that augmentation might occur via a different mechanism, perhaps through internalisation of SA

through transient permeabilisation of the plasma membrane. Alternatively, it may be that maximum sub-toxic concentration of these inhibitors was insufficient to prevent the augmentative activity at this concentration of SA. To try to determine a reason for this discrepancy the abrogatory effect of these inhibitors was examined on the augmentation of saporin and OKT10-SAP cytotoxicity by 5 µg/ml of SA using the XTT assay. The results of these experiments showed a reduction in the abrogatory effect of every inhibitor tested except chloroquine when compared to their effects on the augmentation of cytotoxicity by 1 µg/ml of SA.

In cells treated with 5 µg/ml of SA, chlorpromazine showed almost no abrogation of the SA-mediated augmentation of saporin and OKT10-SAP cytotoxicity in both Daudi and HSB-2 cells. This was in contrast to the near complete abrogation of augmentation by chlorpromazine when SA was used at the lower concentration of 1 µg/ml in both cell lines. Similarly, there was a reduction in the abrogatory effect of EIPA on augmentation in Daudi cells, and a complete loss of abrogation in HSB-2 cells with the higher concentration of SA. These results suggest that the higher concentration of SA is responsible for the failure of these inhibitors to prevent the increased endolysosomal escape of SAP-AF that was seen by confocal microscopy. In addition, the increase in SA concentration also resulted in a reduction in the inhibitory effect of both cytochalasin D and bafilomycin A1 on the augmentation of both saporin and OKT10-SAP cytotoxicity in both cell lines. As all of the inhibitors were used at their maximum sub-toxic concentration it was not possible to increase the concentration in an attempt to counteract the effects of the higher concentration of SA. The outcome of these studies showed that it was not possible to investigate the effect of these inhibitors on endolysosomal escape using this confocal microscopic assay.

It was therefore necessary to develop a more sensitive assay capable of detecting any endolysosomal escape that may occur in cells treated with 1 µg/ml of SA. Ideally such an assay would be capable of analysing a larger number of cells and be more easily quantifiable than traditional microscopy techniques. These criteria could be met by high throughput imaging flow cytometers such as ImageStream which combine the sensitivity and quantifiability of flow cytometry with the imagery of microscopy. However, access to this technology was not possible during this study. Therefore, the alternative option of a flow cytometric assay was employed. Preliminary attempts to differentiate between cells in which endolysosomal escape had occurred and those where it had not based on the overall fluorescent signal within the cell were unsuccessful. A literature search uncovered a rarely utilised method of using the measurement of fluorescent pulse width in order to provide a degree of information on the spatial distribution of a fluorescent label within the cell. This method, termed pulse shape analysis, was investigated to determine whether or not it could differentiate between endolysosomal fluorescence and cytosolic fluorescence.

Initial studies described in this chapter investigated whether pulse shape analysis could track the internalisation of SAP-AF and OKSAP-AF. Incubation of both Daudi and HSB-2 cells with SAP-AF or OKSAP-AF resulted in a time dependent reduction in FITC-W accompanied by an increase in FITC-H. This corresponds to the endocytosis of the fluorescent conjugate from its initial, diffuse surface bound location which has a high FITC-W and low FITC-H. As the toxin is internalised into endosomal compartments its spatial distribution is reduced, reducing the FITC-W of the cell, and the local concentration increased leading to an increase in the fluorescence of the point of maximum fluorescence within the cell and therefore an increase in FITC-H. These results demonstrate the capability for pulse shape analysis to provide limited spatial data from flow cytometry.

Following on from this, experiments were performed to determine whether or not pulse shape analysis could be used to differentiate between cells in which endolysosomal escape had occurred and those where it had not. Treatment of SAP-AF and OKSAP-AF loaded cells with 5 μg/ml of SA, which had been demonstrated by microscopy to cause increased endolysosomal escape was used as a positive control. A significant increase in the median FITC-W was observed after 24 hours in cells treated with this concentration of SA when compared to untreated control cells. This encouraging result suggested that analysis of pulse width could be developed and used as an assay to assess endolysosomal escape. Further use of this assay determined that a significant increase in FITC-W was seen after 24 hours in Daudi cells and 48 hours in HSB-2 cells treated with 1 μg/ml of SA. Although it was not possible to confirm this by confocal microscopy it was inferred from this data that 1 μg/ml of SA did bring about an increase in the endolysosomal escape SAP-AF and OKSAP-AF. This increase in endolysosomal escape was not seen by confocal microscopy, either because the level of escaped toxin within each cell was below the sensitivity limit of the microscope's detector or because it was not possible to determine a difference from the small number of cells recorded in a cell field. The non-augmentative concentration of 0.1 μg/ml of SA was also tested. At this concentration no increase in FITC-W was observed up to 48 hours after initial exposure. These results add further evidence that increased endolysosomal escape is at least one if not the main mechanism by which SA increases saporin cytotoxicity.

The use of pulse width analysis to investigate the escape of toxins and immunotoxins from the lumen of endolysosomal vesicular structure offers several advantages over traditional methods. By providing a direct assessment of endolysosomal escape, in contrast to methods that rely on measuring the cytotoxic effect of the escaped toxin, pulse width analysis allows for specific measurement of the efficacy of endolysosomal escape enhancers. With the capability for flow cytometry to measure thousands of cells a minute a quantitative assessment of these enhancers is possible at the single cell level without the requirement for complex microscopic image analysis

and potential cell selection bias. Whilst pulse shape analysis has a number of advantages, there are also several limitations that need to be taken into consideration. The use of pulse width flow cytometry needed to be used in conjunction with fluorescence microscopy to confirm that any changes in pulse width were genuinely due to endolysosomal escape and not the result of trafficking of the fluorescent toxin to different endosomal compartments or movement of the endolysosomal organelles within the cell. The particular cell type distribution of endolysosomal vesicles within the cell might also determine the sensitivity of pulse width analysis for detection of endolysosomal escape. This was obvious when making a comparison between the HSB-2 and Daudi cell lines. In HSB-2 cells no significant increase in the number of cells undergoing endolysosomal escape was seen with 1 μg/ml of SA until 48 hours after the start of treatment. This is in contrast to the 24 hours observed for Daudi cells. In HSB-2 cells the endolysosomal vesicles were widely distributed throughout the cell in comparison to a much more clustered pattern observed in Daudi cells. This wider spread of vesicles resulted in a broader range of FITC-W within the cell population after they were exposed to SAP-AF or OKSAP-AF for 24 hours. This may consequently have reduced the sensitivity of the assays ability to detect significant changes in the numbers of cells showing an increased FITC-W.

Experiments were then performed to investigate the effect of pharmacological inhibitors on the endolysosomal escape of SAP-AF and OKSAP-AF in Daudi and HSB-2 cells. The aim of this work was to confirm that the effect of these inhibitors on the augmentation of saporin and OKT10-SAP cytotoxicity is due to an inhibition of the action of SA to enhance the endolysosomal escape of the toxin.

Treatment with chlorpromazine completely prevented the endolysosomal escape of SAP-AF and OKSAP-AF in Daudi and HSB-2 cells exposed to 1 μg/ml of SA. This result reflects the near complete abrogation of the SA-mediated augmentation of cytotoxicity at this concentration by chlorpromazine. This suggests that the abrogatory effect of chlorpromazine on the augmentation of cytotoxicity is due to its inhibition of the endolysosomal escape of the toxin. As previously discussed, it is not possible to conclude from this work whether or not this is due entirely to its effect on CME. At the higher concentration of 5 μg/ml, chlorpromazine showed no effect on the increase in FITC-W in Daudi cells. This result agrees with XTT cytotoxicity assay data that show no effect of this agent on the augmentation of cytotoxicity by this concentration of SA and with confocal microscopy where chlorpromazine unable to prevent the endolysosomal escape of SAP-AF in cells treated with 5 μg/ml of SA.

EIPA completely abrogated the increase in FITC-W in both Daudi and HSB-2 cells loaded with SAP-AF and treated with 1 μg/ml of SA and a significant abrogation was also measured in Daudi cells

loaded with OKSAP-AF at this concentration of SA. These results agree with the complete abrogation of augmentation of cytotoxicity by EIPA and also suggest that the effect of EIPA on augmentation is due, at least in part, to its effect on endolysosomal escape. In both Daudi and HSB-2 cells loaded with OKSAP-AF and in Daudi cells containing SAP-AF, treated with 5 µg/ml of SA, EIPA only inhibited the increase in FITC-W observed by 6 hours with no reduction in FITC-W observed after 48 hours. This suggests that EIPA reduced the rate of endolysosomal escape and therefore extended the duration of SA exposure required before an increase in the median FITC-W could be measured. In XTT assays with 5 µg/ml of SA a partial abrogation of the augmentation of cytotoxicity was observed with EIPA and this may be due to this reduction in the rate of endolysosomal escape leading to a delay in the cytotoxic effect of the saporin. Interestingly, in contrast to its effect in cells loaded with OKSAP-AF, EIPA completely abrogated the increase in FITC-W in HSB-2 cells loaded with SAP-AF and treated with 5 µg/ml of SA. This result partially agrees with the corresponding cytotoxicity experiments where the augmentation of saporin was greatly, but not completely abrogated.

In Daudi cells no significant abrogation in the increase in FITC-W by cytochalasin D was observed with either SAP-AF or OKSAP-AF at either concentration of SA tested. This is likely due to its effect on Daudi cell size as this agent also increased the FITC-W of control cells and was shown to increase the forward scatter of these cells. In HSB-2 cells a complete abrogation of the increase in FITC-W was observed in cells loaded with either SAP-AF or OKSAP-AF and treated with 1 µg/ml SA. These results concur with the effect of cytochalasin D on the SA-mediated augmentation of cytotoxicity and suggest that actin polymerisation may be involved in the endolysosomal escape of these conjugates, most likely through inhibition of the internalisation and trafficking of SA to the endolysosomal compartment.

The complete inhibition by chloroquine of the 1 µg/ml of SA-mediated increase in FITC-W in Daudi and HSB-2 cells with either SAP-AF or OKSAP-AF was also consistent with the effect of this agent on the augmentation of cytotoxicity. In addition, the partial abrogation of the increase in FITC-W observed in Daudi cells with 5 µg/ml was also in agreement with both its partial abrogation of cytotoxicity augmentation and the inhibition of SAP-AF endolysosomal escape observed by confocal microscopy with this concentration of SA. The effect of bafilomycin A1, the other inhibitor of endosomal acidification used in this study, was less straightforward. In Daudi cells incubated with OKSAP-AF, treatment with bafilomycin A1 increased FITC-W in the absence of SA. This was shown by confocal microscopy to be due to a dispersal of OKSAP-AF containing vesicles throughout the cell in the presence of bafilomycin A1 and highlights the need for fluorescent microscopy to be used alongside pulse shape analysis flow cytometry to exclude other causes of FITC-W changes wherever this is possible. In addition, the inability of bafilomycin A1 to

significantly reduce the SA-mediated increase in FITC-W in HSB-2 cells containing SAP-AF did not correspond with the effect of the inhibitor in XTT cytotoxicity assays. In contrast, bafilomycin A1 almost completely abrogated the augmentation of saporin cytotoxicity with 1 µg/ml of SA. The reason for this discrepancy is uncertain want warrants further investigation. However, despite this isolated result the overall conclusion from these studies was that prevention of endosomal acidification inhibits the SA-mediated increase in FITC-W and therefore endolysosomal escape and the augmentation of cytotoxicity.

The results of these studies investigating the effect of various pharmacological agents on the SA-mediated increase in endolysosomal escape of SAP-AF and OKSAP-AF has demonstrated that the inhibitory effects of these agents on the augmentation of saporin and OKT10-SAP cytoxicity is likely, in part at least, due to the result of their effect on SA-mediated endolysosomal escape. The link between these effects for each of the tested pharmacological agents further confirms one of the mechanism(s) behind the augmentation of saporin/IT cytotoxicity by SA is increased endolysosomal escape. However, there may be additional mechanisms at play such as lysosomal membrane permeabilisation (LMP) and release of proteolytic enzymes into the cytosol that may also contribute to cell death that this project has not examined[342].

The work presented here builds upon previously published work with fluorescently labelled saporin and saporin based targeted toxins [152,343] and presents a number of novel findings. The pulse width analysis method used in this current project offered a greater level of sensitivity for the endolysosomal escape of saporin than previously used microscopic methods and allowed the detection of endolysosomal escape in cells exposed to lower concentrations of SA than was observed in previously published work. The improved sensitivity also enabled the effects of inhibitors of endocytosis on the endolysosomal escape of saporin to be investigated which had not been possible with confocal microscopic methods. In addition, the higher throughput and ease of quantification of these results facilitated the correlation between the effect of these pharmacological inhibitors on the endolysosomal escape of saporin and IT in the presence of SA and their effect on the cytotoxicity of these compounds.

As discussed earlier in the context of cytotoxicity assays, future work to expand upon the pulse shape analysis studies presented here should include the use of genetic knockdown of specific genes relating to endocytic processes. This would allow for a more precise determination of the involvement of these processes in the augmentation of endolysosomal escape and the subsequent effects on cytotoxicity augmentation by saponins. Pulse shape analysis also provides the opportunity to investigate the effect of increased endolysosomal escape on apoptosis. Multi-colour flow cytometry combining this endolysosomal escape assay with a fluorescent assay for

apoptosis such as annexin V/PI[344], fluorochrome-labelled inhibitors of caspases to detect caspase-3[345] or potentiometric dyes that detect reduced mitochondrial potential[346] could directly investigate the effect of increased FITC-W on the activation of apoptotic mechanisms.

Chapter 5 Discussion

The overall aim of this project was to investigate and test the hypothesis that saponins augment the cytotoxicity of saporin and saporin based ITs by enhancing the endolysosomal escape of the saporin or IT into the cytoplasm of the target cell. This would increase the number of toxin molecules with access to target ribosomes per unit time thus delivering increased protein synthesis inhibition and subsequent ribotoxic stress resulting in apoptotic death. It is speculated that this enhancement of saporin endolysosomal escape is dependent on the internalisation of both saponin and saporin into the cell and their trafficking as cargo to the lumen of a common endolysosomal compartment. Here saponin is thought to increase the efficiency of the endolysosomal escape of the saporin or IT which may occur due to a direct permeabilisation effect of saponin on the endolysosomal membrane or alternatively may result from a pH dependent association between saporin and the saponin into a complex that takes on membrane disruptive properties thus allowing the toxin to escape into the cytosol. The experiments performed during this were study aimed at investigating the mechanisms by which SA is internalised and trafficked to the endolysosomal compartment, either by defined endosomal pathways or as a part of a membrane repair mechanism in response to SA mediated plasma membrane damage. In addition, the role of endolysosomal luminal acidification in the augmentation of saporin or IT cytotoxicity was also investigated. Alongside these experiments that quantified the augmentation of saporin or IT cytotoxicity by SA, studies were also conducted to determine the effect of the saponin as an enhancer of endolysosomal escape using by confocal microscopy and a novel flow cytometric assay.

The results presented earlier in this thesis suggest that SA is likely internalised into the cell and that this is a requirement for its augmentation of saporin cytotoxicity. However, the work described here has only gone part way determining the precise mechanism(s) or pathway(s) involved in this internalisation. It allows us to conclude that membrane damage and subsequent repair processes are probably not involved in the internalisation of SA as no membrane damage from exposure to the augmentative concentration of 1 µg/ml of SA was observed. There was also no evidence for the membrane repair associated processes of lysosomal exocytosis or MEND occurring in cells exposed to this augmentative but sub-lytic concentration of SA. Studies involving pharmacological inhibitors of CME or macropinocytosis demonstrated near complete abrogation of the SA-mediated augmentation of saporin and IT cytotoxicity with both types of inhibitor. This finding suggests that the internalisation of SA is necessary for the augmentation of cytotoxicity, but due to other diverse effects of both of these inhibitory agents it is not possible to discern which particular processes are involved in the internalisation of SA. The involvement of actin in

the internalisation and initial trafficking of SA was also investigated using a selective pharmacological inhibitor. The partial abrogation of the SA-mediated augmentation of saporin or IT cytotoxicity in Daudi cells and the complete abrogation of this effect in HSB-2 cells with actin inhibitors indicates that saponin is likely internalised by an actin-dependent endocytic pathway. The requirement for the trafficking of any subsequently internalised SA in the augmentation of saporin/IT cytotoxicity was investigated by pharmacological disruption of microtubule assembly using nocadazole. Nocadazole did not affect the augmentation of saporin/IT cytotoxicity by SA suggesting that microtubule dependent trafficking of SA is not required for augmentation to occur.

The abrogation of the augmentation of saporin or IT cytotoxicity by the inhibitors of endosomal acidification, chloroquine and bafilomycin A1, indicates that a low endosomal pH is a prerequisite for augmentation. To investigate the suggestion that an acidic endosomal lumen is necessary because a pH dependent association between saponin and the RIP is needed for the endolysosomal escape of the toxin to occur, the effect of SA on the cytotoxicity of the RIP gelonin was measured. The cytotoxicity of gelonin, which has previously been shown not to be associated with saponins at low pH[152], was however augmented by the presence of SA. This suggests that a pH dependent association may not be required for the SA-mediated augmentation of RIP cytotoxicity. This finding therefore throws into some doubt the absolute necessity for an acidic endolysosomal lumen for augmentation.

The present study describes an increase in the endolysosomal escape of fluorescently conjugated saporin and OKT10-SAP in response to treatment of cells with 5 µg/ml SA was observed by confocal microscopy. The development of a more sensitive and more easily quantifiable flow cytometric assay to assess endolysosomal escape showed that endolysosomal escape of the toxin was also increased in the presence of the augmentative but non-cell membrane permeabilising concentration of 1 µg/ml of SA. Comparisons between the effects of the pharmacological inhibitors of endocytic processes on the SA-mediated augmentation of saporin and IT cytotoxicity and the SA-mediated increase in endolysosomal escape showed that there was a good correlation between the two parameters. This strongly suggests that increasing endolysosomal escape of the toxin is at least one of the contributory mechanisms by which SA augments saporin cytotoxicity, though it should be kept in mid that there may be others operating in parallel that this study has not revealed.

The limitations to the experiments performed in this study and the caveats associated with the presented results have been discussed in the previous results chapters where relevant. It is also important to note that in the work presented here in this study, certain inferences have been

made about the internalisation and trafficking of SA. These conclusions were made based on the assumption that for SA to mediate an increase in the endolysosomal escape of saporin or IT it must be trafficked to the same endolysosomal compartment within the cell as the toxin. On this principle, the effects of different pharmacological inhibitors of endocytic processes on the SA mediated increase in endolysosomal escape were inferred to be due to their effects on the endocytosis and trafficking of SA from the cell plasma membrane to the endolysosomal compartment. In order to make any firm conclusions about the internalisation of the saponins contained in SA it will be necessary to directly track their intracellular location.

The first possibility would be to develop a polyclonal or monoclonal antibody specific to a defined saponin species such as SA1641. Such antibodies could then be used to probe the intracellular location of the saponin by fluorescent or confocal microscopy. This would enable more direct studies to investigate the mechanisms involved in the internalisation and trafficking of the saponin in question. Observing the effects of pharmaceutical inhibitors of different endocytic processes such as chlorpromazine or EIPA on the internalisation of the saponin would likely provide insights into the pathways involved in its endocytosis. A more precise alternative approach, as previously discussed in Chapter 4 would be to use of gene knockout techniques to disable precise endocytic pathways. This would provide a more specific method than offered by pharmacological agents that have other off-target activities. Visualisation of the intracellular location of the saponin would also enable co-localisation studies to be performed by fluorescence microscopy. Co-localisation with specific markers of endosomal compartments such as LAMP-1 and EEA1 would also enable confirmation of whether or not saponins are trafficked to an endolysosomal compartment. In addition to this, co-localisation studies with fluorescently labelled saporin and IT would determine whether these are trafficked to, and therefore accumulate within, the same intracellular compartment as the saponin thus providing evidence for the hypothesis that necessitates co-localisation of saponin with saporin. In addition to fluorescence microscopy, the development of an anti-saponin antibody would also facilitate the use of immunogold staining techniques for electron microscopy. This would allow for more precise studies on the intracellular location of internalised saponins. This would be of particular value in a further, more detailed investigation of the potential involvement of membrane repair processes in saponin internalisation and for determining whether saponins are internalised in fluid phase directly into the endosomal lumen or are incorporated into the plasma and endosomal membranes, following a non-covalent association with cholesterol in the outer leaflet of the plasma membrane[347]. The downside to this approach is that these techniques require cells to be fixed and permeabilised and thus cannot be used in live cell imaging studies. This means that it would not be possible to track saponins in real time as a part of an investigation into the

endolysosomal escape of the toxin to the cytosol. A further complication is the likely possibility that permeabilisation of the cells under investigation could result in internalised saponins being washed out from their intracellular location. Additional to the intracellular localisation of saponins, development of an anti-saponin antibody would also be of value in developing an ELISA-based method to provide an independent confirmation of the SPR data published by Weng and co-workers[152] which purported to show a pH dependent association between the saponin SA1641 and the toxin saporin. A number of attempts have been made by this laboratory to raise polyclonal and monoclonal antibodies against SA1641 but unfortunately none were successful and a different antibody raising strategy may need to be adopted. Antibodies have previously been successfully raised against several other species of triterpenoid saponin including saikosaponin-a[348,349] and bacopaside I[350] and so further attempts should be made to pursue this line of work.

An alternative to the development of an antibody against saponin species would be to label the particular saponin with a fluorescent probe such as the Alexa Fluor 488 used in the present study to label saporin and OKT10-SAP. This approach would also allow for fluorescent microscopic analysis of saponin internalisation and for co-localisation studies with endosomal markers and fluorescently labelled toxin and IT. In addition, the direct labelling of the saponin would also allow its use in live cell microscopic imaging studies. There are a small number of previous studies involving the fluorescent labelling of other steroidal saponins[222,351] which suggest that the labelling of a triterpenoid saponin such as SA1641 may be achievable. The potential drawback of fluorescently labelling the saponin is the effect that the conjugation could have on its biological properties that includes potential modification to the way in which it traffics in the cell. This is especially pertinent because of the small size of the saponin molecule in relation to the size of available fluorescent probes. The molecular weight of even a small fluorescent probe such as FITC (389.4 g/mol) is a significant fraction of the molecular weight of SA1641 (1641 g/mol). This increases the risk that conjugation will destroy or hinder access to biologically active sites of the saponin molecule potentially affecting its internalisation and routing within the cell together with its biological activity to augment the endolysosomal escape of saporin and IT into the cytosol and thus their cytotoxic activity. Only additional empirical investigations of this will be able to validate the value of this approach for future studies.

Another possible option for tracking the internalisation and trafficking of saponin into cells is offered by Raman confocal microscopy which incorporates a Raman spectrometer into an optical microscope system. Raman spectroscopy measures the frequency changes in a proportion of the light scattered off of a molecule. This change, known as Raman scattering, is dependent on the vibrational states of the molecule and produces a spectral emission that is unique to each

individual molecule based on its chemical bonds[352,353]. Specific molecules can therefore be identified through their unique spectral pattern. Combining Raman spectroscopy with confocal microscopy allows for the intracellular localisation of the molecule of interest[354,355]. This technique could therefore potentially be applied to follow the internalisation and intracellular trafficking of saponin. Because this technique is non-destructive it allows for live cell imaging that obviates the need to chemically modify the saponin through conjugation to a fluorophore. This overcomes the potential problem that conjugation may introduce the intracellular trafficking and biological properties of the saponin. In addition, Raman microscopy combined with high resolution microscopic fluorescence imaging[356] can be used to identify the compartments into which saponins are trafficked and their co-localisation with fluorescently labelled toxin or IT. This approach may therefore offer the best option for future research into this topic.

The studies described in this thesis were aimed at paving the way to an understanding of the mechanisms of augmentation as an important contribution to the long-term end goal of developing saponins as enhancers for clinical use. The aim therefore is to increase the immunologically specific cytotoxic effect of a saporin-based IT, therefore expanding the therapeutic window and allowing patients to be treated at lower doses thus reducing unwanted side effects. Towards this goal further work is needed to investigate the augmentation of immunotoxin cytotoxicity in situations closer to the intended clinical application. This could begin with the use of relevant primary cells which more accurately represent the tissue of origin than immortalised cell lines and should be followed by *in vivo* studies in appropriate animal models of human cancers. Currently there is only very limited evidence for the *in vivo* efficacy of saponins to augment the cytotoxicity of targeted toxins or immunotoxins. A study published by Bachran and co-workers investigated the effect of SA saponins on the anti-tumour activity of the targeted toxin SA2E in a murine model of mammary adenocarcinoma[357]. In this study BALB/c mice were subcutaneously injected with TSA murine mammary adenocarcinoma cells transfected with human EGFR-and the effect of SA2E with and without SA on the size of resulting tumours was measured. Subcutaneous application of SA2E and SA significantly augmented the anti-tumour activity of the targeted toxin when compared to treatment with either alone. Other small studies have looked at the anti-tumour effect of SE and SA1641 in the same murine model but did not compare this to the effect of the targeted toxin alone and therefore offered no insight into the augmentative effect of the SA1641 saponin[152,358]. The anti-tumour effect of a dianthin-EGF targeted toxin in combination with the saponin SO1861, derived from soapwort, has also been investigated in murine models involving xenografted HCT116 human colon carcinoma cells in nu/nu mice[359]. This combination therapy significantly reduced tumour volumes when compared to mock treated controls but this study also lacked targeted toxin only control groups

and therefore it was not possible to evaluate the augmentative effect of the SO1861 saponin. However, a more recent study by Bhargava and co-workers compared the efficacy of the targeted toxin dianthin-EGF used with and without SO1861 in CD-1 nu/nu mice xenografted with BxPC-3 human pancreatic carcinoma cells[360]. In this study combination treatment with the targeted toxin and saponin resulted in a 13-fold increase in efficacy over treatment with the targeted toxin alone as measured by reduction in tumour volume. This limited study offers promising results about the efficacy of targeted toxins and saponins used in combination *in vivo* but relies on only small numbers of animals in each treatment group (5 animals/group). Additional work is therefore needed with larger well controlled treatment group in order to make a statistically robust analysis of the augmentative activity of the saponins used *in vivo*.

The use of saponins as augmentative agents for immunotoxin therapies is faced with a number of potential barriers that might hinder their clinical application. Saponins have poor oral bioavailability[361] and therefore require parenteral administration. Saponins are haemolytic[202] and the intravenous and subcutaneous delivery of a triterpenoid saponin in mice and dogs demonstrated hepatotoxic effects and splenic enlargement[362]. Such toxicities would likely prove dose limiting clinically. Triterpenoid saponins are known to form complexes with cholesterol and other lipids[363] and it is possible that free plasma cholesterol and cholesterol in cell membranes would act as a sink for circulating saponins thus reducing their bioavailability and potentially narrowing their therapeutic window as augmentative agents.

Adding further complication, the SA-mediated augmentation of saporin based immunotoxin cytotoxicity has been shown to be largely non-immunospecific[196]. Because of this, concomitant treatment with an IT and saponin combination would likely increase the off-target toxicities of immunotoxin treatment and thereby prevent the desired widening of the therapeutic window. This problem could potentially be overcome in a number of ways including a scheduled timed separation between doses of saponin and IT or modifications to the delivery of saponins in order to target them to the tumour site only. Holmes and co-workers showed that immunospecific augmentation of IT cytoxicity by SA could be achieved by separating the IT and SA exposures as long as the cells were exposed to the IT first, followed by the SA[196]. Combination treatment delivered in this way would allow the IT to reach, bind to and be internalised by the target antigen expressing cells before subsequent treatment with a saponin is used to enhance the toxicity of the internalised IT. Alternatively, the specific targeting of saponin to the tumour cells would reduce the effects of the saponin for off-target cells. This could be achieved by conjugation of the saponin directly to the IT thereby ensuring delivery of both saponin and IT only to targeted tumour cells. Careful molecular engineering would be needed to ensure that such a double

conjugation did not affect the binding or toxicity of the IT or the augmentative activity of the saponin. Recombinant molecular engineering would only partially solve this matter as the saponin moiety would always require chemically conjugating to the IT which itself could be produced as a chimeric recombinant protein[364]. In the future, immunoliposomes may be developed further as a viable drug targeting system and may offer an ideal delivery system for saponins[365,366]. For localised solid tumours, the intratumoural injection of saponin following systemic or intratumoural administration of the IT could be used to limit off-target toxicities but this approach is not feasible for diffuse liquid tumours such as leukaemia.

The present study opens up scope for future work building upon the results presented here. Whilst the development of saponins as augmentative agents for immunotoxin therapies requires significant further research, there is promise that they may help to achieve more effective treatments of solid and haematological malignancies.

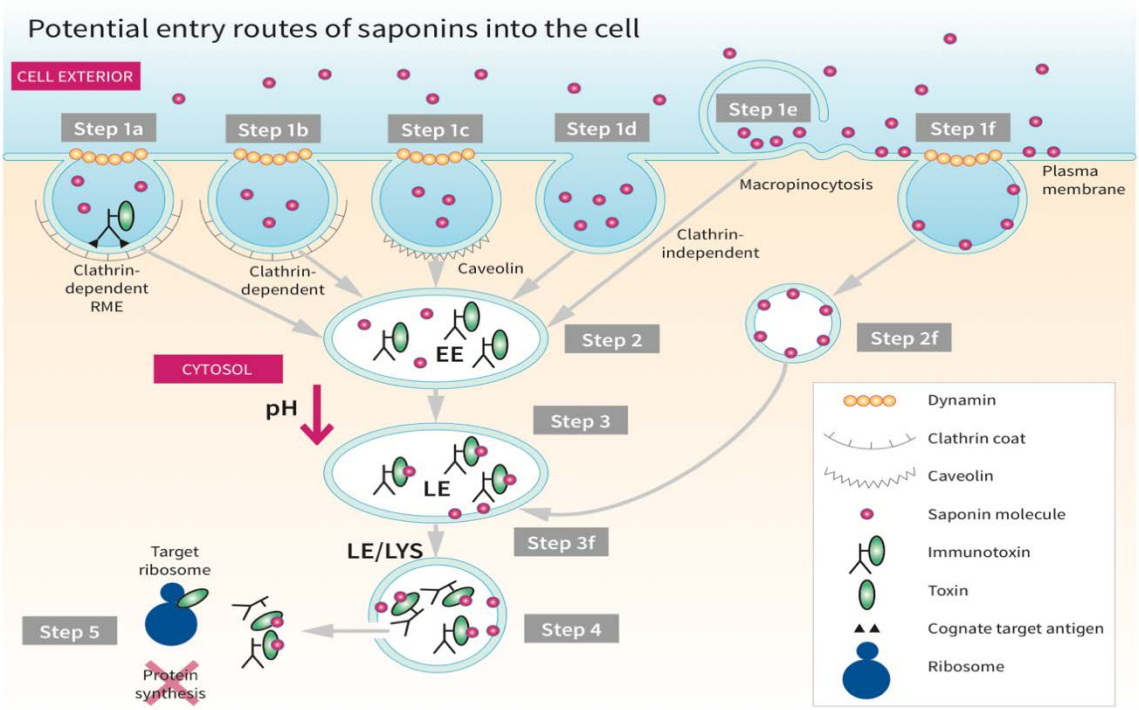

Figure 44. Summary of the Possible Mechanisms by which Saponin Augments the Cytotoxicity of Saporin Based Immunotoxins

The work performed in this thesis investigated the hypothesis that the mechanism by which SA augments the cytotoxicity of saporin and saporin based ITs involves the internalisation of SA into the cell and it's trafficking to the same endolysosomal compartment as the toxin or IT. Here it facilitates the endolysosomal escape of the toxin into the cytosol where its toxic activity can occur.

The various possible endocytic routes by which saponins might enter the cell are shown.

In (1a) and (1b) saponins from the cell exterior are internalised by CME. This could occur either in the lumen of the same vesicle that is internalised following clathrin-dependent receptor-mediated endocytosis following binding of the antibody component of immunotoxin to cognate antigen (1a) or independently from target antigen vesicles (1b). In this study, the pharmacological inhibition of CME was shown to abrogate the increase in both the SA mediated endolysosomal escape of IT and the augmentation of its cytotoxicity. Caveolae (1c) may also provide the point of access for internalisation, particularly as a consequence of SA induced membrane damage resulting in MEND, as may clathrin/caveolin-independent uncoated vesicles (1d). However, no evidence of caveolae were found in this study in response to plasma membrane challenge with the augmentative concentration of SA. An alternative mechanism for fluid phase uptake of saponin may be through macropinocytosis (1e). Similarly to CME, pharmacological inhibition of macropinocytosis abrogated the augmentation of both the endolysosomal escape and cytotoxicity of IT by SA. This made it difficult to draw firm conclusions about the roles of these pathways. Once internalised by one or more of these pathways it was suggested that saponin is trafficked through the early (EE) (2) and late (LE) (3) endosome to the endolysosomal compartments (LE/LYS) (4) alongside the IT. Here it facilitates the endolysosomal escape of the toxin into the cytosol in a pH dependent manner (5). The requirement for a low endolysosomal pH in this process was confirmed here with two pharmacological inhibitors of endosomal acidification. The use of confocal microscopy and pulse shape analysis flow cytometry showed that SA increased the endolysosomal escape of the IT into the cytoplasm. The correlation between the effects of different inhibitors on the augmentation of IT cytotoxicity by SA and the SA mediated endolysosomal escape of the IT provides further evidence that this is the mechanism by which augmentation of cytotoxicity occurs.

Appendix A siRNA Knockdown

A.1 Introduction

As is discussed in detail in section 4.3, many of the pharmacological agents used in the experiments detailed in sections 4.2.1 and 4.2.9 have a number of off-target effects. These make it difficult to determine the exact effect each agent is having on the augmentation process, especially when multiple inhibitors of different endosomal pathways are able to completely abrogate this augmentation. It was proposed that gene knockdown studies with siRNA targeting process specific proteins would provide a better picture of the mechanism of SA induced endolysosomal escape and some preliminary work is presented here.

A.2 Methods

A.2.1 Transfection with Fluorescent siRNA and Fluorescent Analysis of Transfection

To investigate the optimum ratio of siRNA and INTERFERin to transfect U937 pro-monocytic myeloid leukaemia cells [367], a transfection study was performed with the fluorescently labelled transfection indicator siGLO. The U937 cell line was selected based on previously published work demonstrating the use of INTERFERin in this line[368]. Cells were obtained from the European Collection of Cell Cultures (ECACC, Porton Down, Salisbury, UK). Cells were seeded into a 96 well plate on the day of transfection at $2x10^4$ cells per well in 50 µl of R10. siGLO was diluted in RPMI-1640 to 20 nM and 50 nM and complexed with 1:50 or 1:25 of INTERFERin for 15 min at room temperature. 50 µl of siGLO and INTERFERin mixture was added to each well with 50 µl siGLO alone used as a control. After 4 hours 100 µl R10 was added to each well and the plates were incubated for 24 h at 37°C in 7% CO_2. After 24 hours cells were extracted from wells, washed with RPMI-1640 and read on a Cytoflex flow cytometer and SP8 confocal microscope.

A.2.2 Transfection

To investigate the efficacy of siRNA transfection via INTERFERin and subsequent knockdown, U937 cells were transfected with siRNA targeting the housekeeping gene cyclophilin B. Cells were plated into a 12 well plate at $5x10^5$ cells per well in 500 µl R10. Cyclophilin B siRNA pools and non-targeting siRNA sequences, for use as a negative control, were complexed with INTERFERin at 1:25 for 15 minutes in RPMI-1640 before 200 µl was added to each well. After 6 hours of

incubation at 37°C in 7% CO_2 1 ml of R10 was added to each well and the plates were incubated for a further 72 h before cells were harvested for protein extraction.

A.2.3 Protein Extraction and Quantification

Whole cell lysates of transfected and untreated control cells were prepared to analyse the effectiveness of protein knockdown. Cells were collected and centrifuged at 470 g for 5 min, media was aspirated, and cells were washed in RPMI-1640. RIPA Buffer (0.15 M NaCl, 1% NP40, 0.5% sodium deoxycholate, 0.1% SDS, 0.05 M Tris pH 8.0 in dH_2O) with a protease inhibitor cocktail was added to the cell pellet at 30 µl per $2x10^6$ cells. Pelleted cells were mixed with the RIPA buffer with a pipette before being incubated on ice for 30min Lysed cells were then centrifuged for 30 min at 13,000 rpm in a Sanyo Microcentaur (~9500 g). The supernatant was collected and stored at 4°C. The protein concentration of the supernatant was measured using a bicinchoninic acid (BCA) protein assay kit (Thermo Fisher Scientific) as detailed in the manufacturer's instructions.

A.2.4 Gel Electrophoresis and Western Blotting

From the previously calculated protein concentration, the volume of whole cell lysate containing 30 µg of protein was calculated and added to 2.5 µl 1 M DTT, 7.5 µl 4x RunBlue LDS Sample Buffer and dH_2O to a total volume of 30 µl. Samples were heated for 5 min at 95°C in a water bath before being added to wells of a 12% SDS gel and separated by SDS-PAGE. Proteins were electroblotted onto Protran 0.45µl Nitrocellulose transfer membrane (GE Healthcare) in transfer buffer (25 mM tris, 200 mM glycine, 20 % Ethanol in dH_2O). This membrane was probed with rabbit anti-cyclophilin B primary antibodies at a 1:1000 dilution in tris saline buffer (100 mM tris, 1.5 M NaCl, 0.1% Tween-20 in dH_2O) containing 3% BSA overnight at 4°C before being washed and probed for 1 h with an appropriate HRP-conjugated secondary. Enhanced chemiluminescent substrate was added to the nitrocellulose as directed by the manufacturer and was imaged on a Chemidoc XRS chemiluminescence detection system.

A.3 Results

A.3.1 Optimisation of Transfection

In order to determine the optimum ratio of siRNA to the lipofection reagent INTERFERin U937 cells were treated with the fluorescent transfection indicator siGLO complexed with INTERFERin at

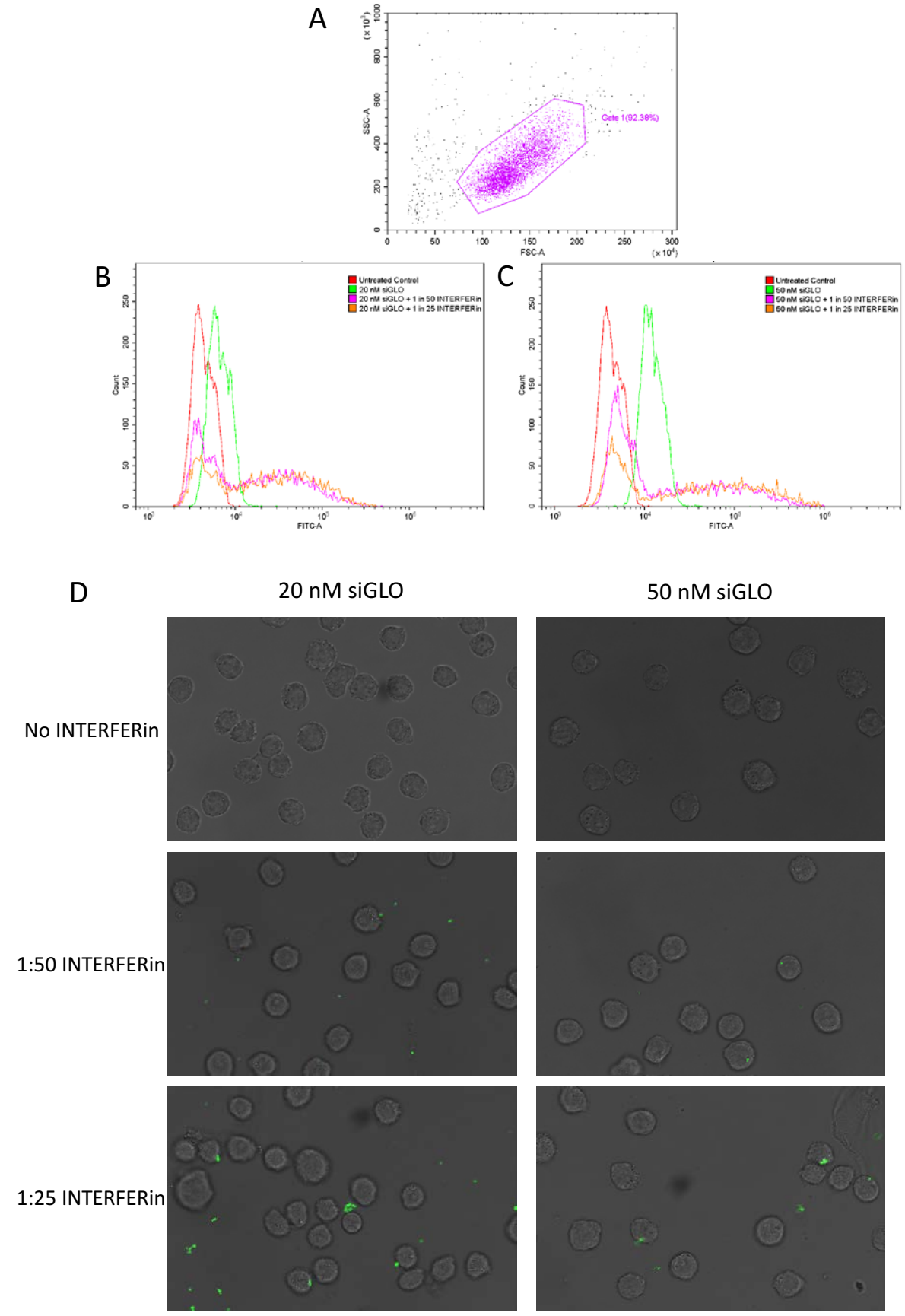

Figure 45 Optimisation of Transfection of U937 Cells with siGLO

Forward and side scatter dot plot showing gating of untreated control U937 cells (A). Histograms showing fluorescence intensity of U937 cells treated with 20 nM (B) or 50

nM (C) of siGLO in the absence or presence of INTERFERin at a ratio of 1:50 or 1:25 as measured by flow cytometry. Histograms showing untreated control cells are shown for comparison. Cells in B and C fell within the gating defined in A. (D) Confocal microscopy images showing U937 cells treated with 20 nM or 50 nM of siGLO in the absence or presence of INTERFERin at a ratio of 1:50 or 1:25. Images show brightfield images with siGLO shown in green.

a ratio of 1:50 and 1:25. After 24 hours, flow cytometric measurement of cell fluorescence by flow cytometry of cells treated with siGLO alone showed an increase in mean fluorescence compared to untreated control cells (Figure 44B & C). Increased fluorescence was recorded in cells treated with siGLO and INTERFERin when compared to those treated with siGLO alone. This increase in fluorescence was dependent on the ratio of INTERFERin to siGLO used.

Confocal microscopic imaging of U937 cells treated with siGLO in the absence of INTERFERin showed no fluorescent signal. In cells treated with siGLO complexed with INTERFERin fluorescence was observed in extracellular clumps with intracellular fluorescence only observed in a small number of cells treated with 50 nM siGLO and a 1:25 ratio of INTERFERin. These results indicate that transfection of U937 cells with siGLO by INTERFERin was unsuccessful

A.3.2 Knockdown of Cyclophilin B by siRNA

Transfections of U937 cells with a pool of siRNA targeting the housekeeping protein cyclophilin B were performed. After 72 hours, no reduction in the cyclophilin B levels of cell lysate was measured by western blot (Figure 45) confirming that knockdown of this protein was not successful.

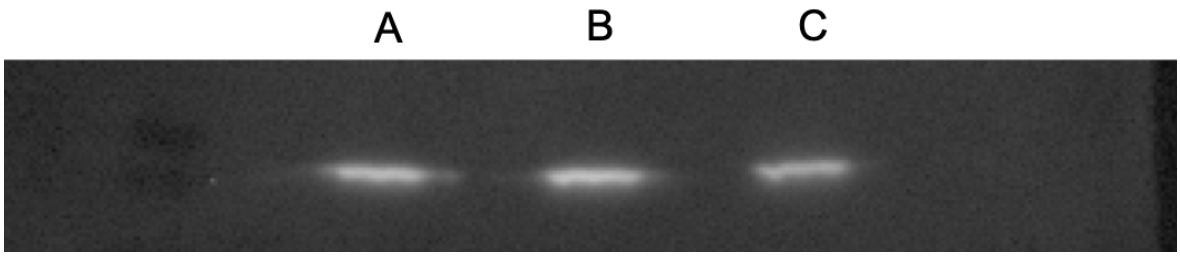

Figure 46 Western Blot Showing Cyclophilin B

Western blot probed with antibody targeting the 21kDa housekeeping protein cyclophilin B. Bands shown fall between 20 and 25kDa and represent protein extractions from untreated control U937 cells (A), cells treated with non-targeting siRNA (B) and cells treated with siRNA targeting cyclophilin B (C).

Appendix B Semi-Quantitative Analysis of Confocal Microscopy

B.1 Introduction

In section 4.2.4.2 it was shown that confocal microscopy could be used to record the endolysosomal escape of SAP-AF and OKSAP-AF into the cytosol. In order to better investigate the effect of SA on this endolysosomal escape, an attempt was made to perform a semi-quantitative analysis of these images by determining the average area of Alexa Fluor 488 (AF488) fluorescence per cell. As the labelled toxin escapes into the cytosol, the area of the cell that which exhibits fluorescence will increase.

This process was partially automated using the FIJI distribution of ImageJ[369] in order to extract data from all of the approximately 300 to 500 cells within a cell field image. First the number of cells in each field was estimated by determining the total area of fluorescence corresponding to the nuclear stain Hoechst 33342 and dividing this by the average area of a nucleus which was calculated manually from the average of ten nuclei in each image. The area of Alexa Fluor 488 fluorescence was then determined. In order to differentiate between background fluorescence, cytosolic fluorescence and intravesicular fluorescence, a threshold gate was determined based on fluorescence intensity. This excluded the lower intensity background and the high intensity intravesicular fluorescence. Exclusion of vesicular fluorescence was necessary to reduce the impact of variations in vesicular distribution upon the analysis. The calculated area of fluorescence was then divided by the number of cells to give an approximate area per cell.

B.2 Methods

Daudi cells were prepared for confocal microscopy and imaged as described in section 2.3.11. Images acquired at 0 and 24 h after the addition of SA were analysed as described here.

To estimate the number of cells in each field the following work flow was applied:

1. The .lif image files generated by the Leica TCS SP8 confocal microscope were imported into FIJI.

2. Images were split into the three separate recorded channels (bright field, Hoechst and AF488) and the Hoechst 33342 channel was selected for further processing.

3. Each Z-stack of 21 planes was combined into a single maximum projection image.
4. Ten cell nuclei, chosen at random were then drawn around free-hand by the user and the mean area of a nucleus was determined.
5. To remove any background signal, the intensity of the image was reduced by 3, a value determined previously to be representative of background intensity.
6. To compensate for the variable fluorescent intensity within the nucleus, images had a median filter applied, replacing each pixel with the median value in its 2x2 neighbourhood.
7. The total area of Hoechst 33342 fluorescence falling within an intensity threshold between 20 and 255 was calculated
8. This area was divided by the previously estimated mean nuclear area to provide an estimated count of cells in the image.

To estimate the total area occupied by cytosolic SAP-AF in each field the following work flow was applied:

1. The .lif image files generated by the Leica TCS SP8 confocal microscope were imported into FIJI.
2. Images were split into the three separate recorded channels and the AF488 channel was selected for further processing.
3. Each Z-stack of 21 planes was combined into a single maximum projection image.
4. The background AF488 signal was estimated by the user and this value was subtracted from the image.
5. To differentiate between the high intensity signal of SAP-AF contained within the endolysosome and the low intensity signal of SAP-AF in the cytosol a threshold range was determined by the user to include cytosolic SAP-AF but exclude endolysosomal SAP-AF.
6. The total area of AF488 signal within this threshold range was measured across the cell field.
7. The total area of AF488 signal representing cytosolic SAP-AF was then divided by the estimated cell count to provide an approximate area of fluorescent signal per cell.

Thanks to Dr David Chatelet at the Biomedical Imaging Unit in Southampton General Hospital for his assistance in developing this method and his work creating a macro for FIJI to automate this analysis.

B.3 Results

Analysis of confocal microscopy images from several independent experiments showed an increase in the average area of cytosolic AF488 channel fluorescence per cell over 24 hours in both untreated Daudi cells and those treated with SA. Treatment of cells 5 µg/ml of SA increased the average area of cytosolic fluorescence after 24 hours compared to untreated control cells at the same time point. No increase in the area of cytosolic fluorescence was observed in cells treated with 1 µg/ml of SA compared to untreated control cells after 24 hours (Figure 46).

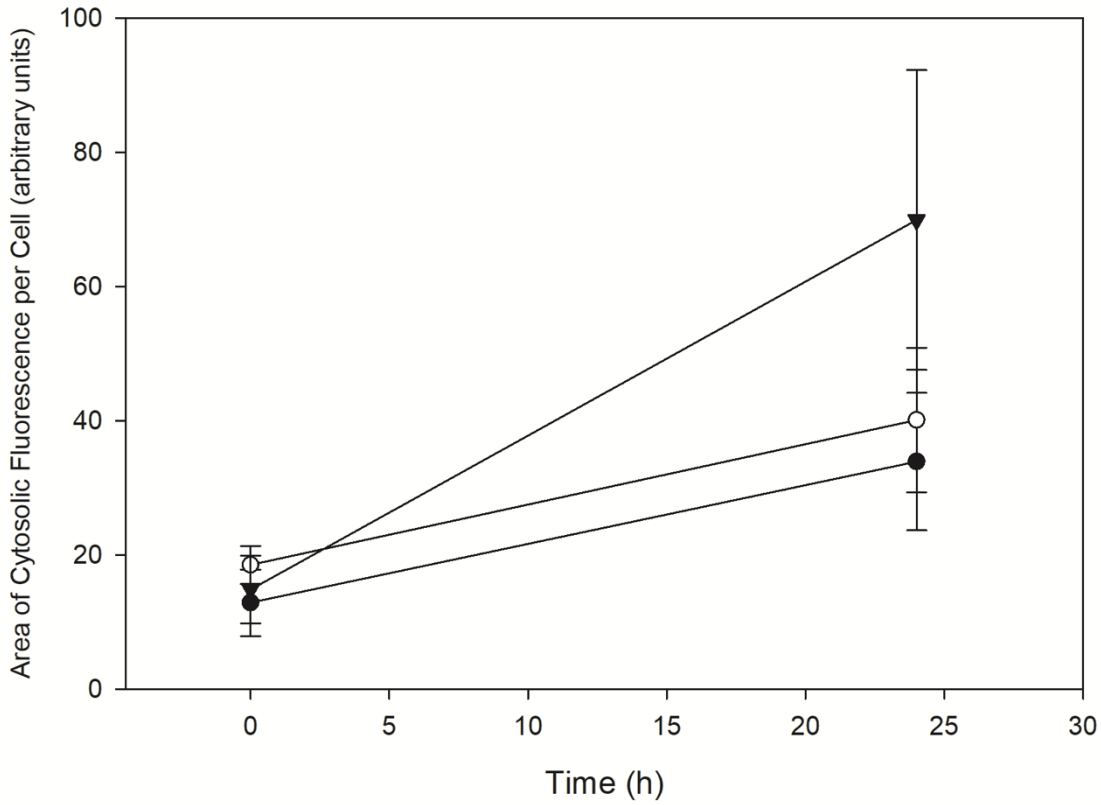

Figure 47 Effect of SA on the Average Area of Cytosolic Fluorescence in SAP-AF Containing Daudi Cells

Daudi cells preincubated with SAP-AF for 24 hours were treated with 1 or 5µg/ml of SA or mock treated with R10. Live cell confocal images taken after 0 and 24 hours. Images were analysed to determine the average area of cytosolic AF488 fluorescence per cell at each time point. An increased area of cytosolic fluorescence indicated increased escape of SAP-AF into the cytosol.

Appendix C Comparison of the XTT Cytotoxicity Assay and PI Influx as Measures of Cell Viability

C.1 Introduction

The XTT cytotoxicity assay was used throughout this study to evaluate the effect of saporin and IT on cell viability and the augmentation of this effect by SA. As described in section 2.3.2 this assay assesses cellular metabolic activity as a measure of cell viability. Because reduced metabolic activity does not confirm cell death, an alternative measure of cell viability was tested to confirm these results. PI is a membrane impermeant fluorescent DNA/RNA binding stain that is generally excluded from viable cells but can penetrate the damaged membranes of non-viable cells. A comparison was made between the XTT assay and the internalisation of PI, as measured by flow cytometry, as assays to investigate the cytotoxicity of OKT10-SAP in the absence and presence of 1 µg/ml of SA.

C.2 Methods

C.2.1 Investigation of OKT10-SAP Cytotoxicity by XTT Assay

Daudi cells were plated in clear 96 well plates (Nunc) at a density of 50000 cells per well in phenol free R10. OKT10-SAP at varying concentrations between $1x10^{-7}$ M and $1x10^{-15}$ M was added to the wells in the presence or absence of 1 µg/ml SA. Each concentration of IT was tested in quadruplicate. Plates were incubated for 48h at 37°C before cytotoxicity was measured by XTT assay as described in section 2.3.2.

C.2.2 Investigation of OKT10-SAP Cytotoxicity by PI Cell Permeabilisation Assay

Daudi cells were plated in 24 well plates at $2.5x10^5$ cells per cell. OKT10-SAP at varying concentrations between $1x10^{-7}$ M and $1x10^{-15}$ M was added to the wells in the presence or absence of 1 µg/ml SA. After incubation for 48h at 37°C, cells were extracted from wells and added to flow tubes. Samples were centrifuged at 470 g for 5 min, the supernatant was aspirated off and 200 µl 5 µg/ml PI in DMEM or DMEM with 10 mM EGTA was added. Samples were read on a Cytoflex flow cytometer (Beckman Coulter) and results analysed with CytExpert software. Cells with a fluorescence on the PE filter (585/42 band pass) 2 logs greater than the mean fluorescence of control cells were considered permeabilised. The number of permeabilised cells was expressed as a percentage of total cells.

C.3 Results

The cytotoxic effect of OKT10-SAP on Daudi cells was observed by both the XTT cytotoxicity assay and PI influx (Figure 47). Both of these assays were also able to show the augmentative effect of SA on OKT10-SAP cytotoxicity. However, there were differences between the levels of cytotoxicity recorded by each assay. By XTT assay an EC_{50} for OKT10-SAP alone was measured at $3x10^{-10}$ M and the addition of 1 µg/ml of SA reduced this EC_{50} to $4x10^{-13}$ M (Figure 47D). In comparison when the cytotoxicity of OKT10-SAP both alone and in the presence of 1 µg/ml of SA was measured by the PI membrane permeabilisation assay, an EC_{50} was not achieved (Figure 47A & B). At the highest concentration tested an average of 9.2% of cells were measured as being permeabilised. Treatment with both OKT10-SAP at $1x10^{-7}$ M and 1 µg/ml of SA increased the percentage of permeabilised cells to 48.5% (Figure 47C).

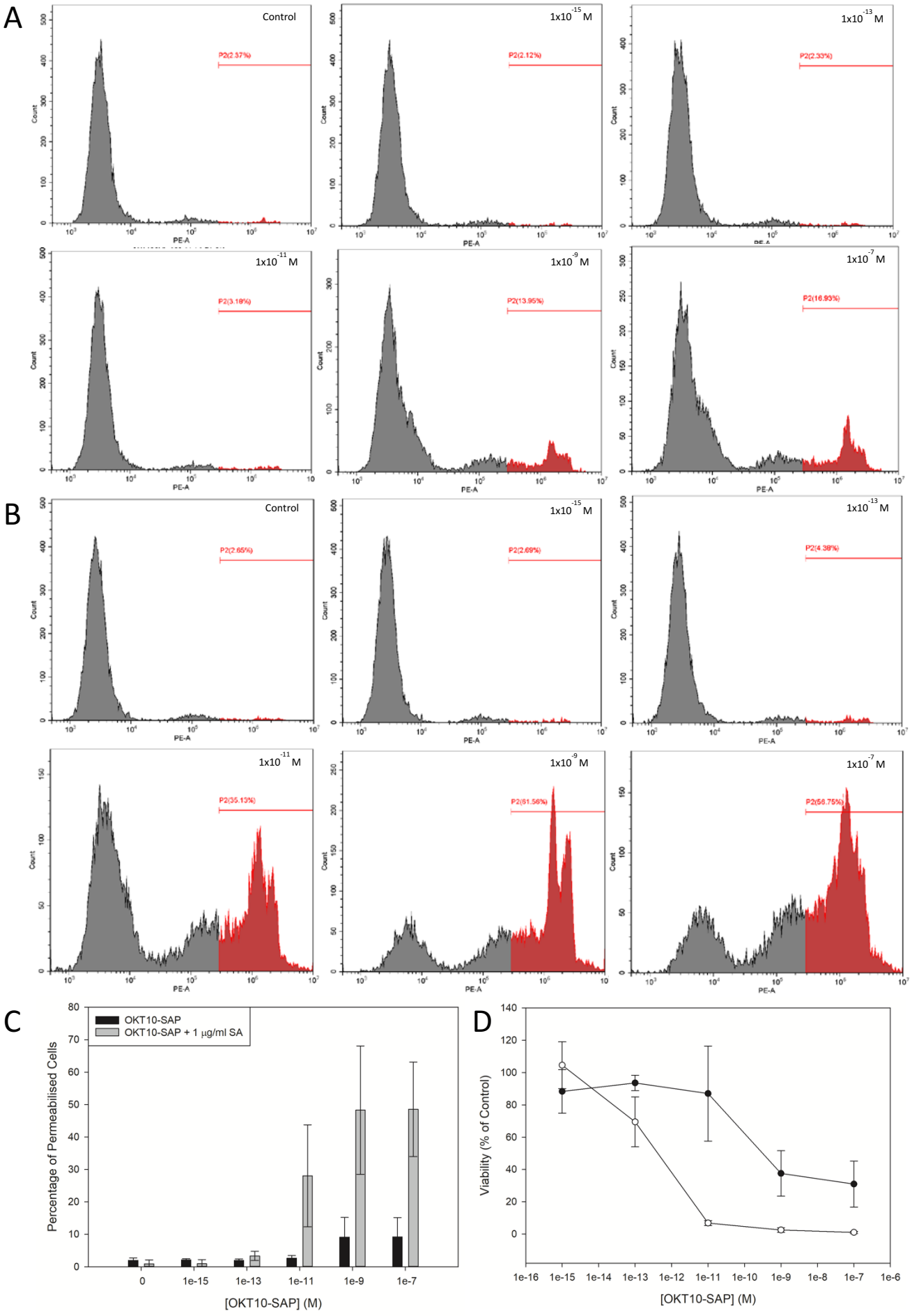
A
Control
1x10 -15 M
1x10 -13 M
1x10 -11 M
1x10 -9 M
1x10 -7 M
P2(2.37%)
P2(2.12%)
P2(2.33%)
P2(3.18%)
P2(13.95%)
P2(16.93%)
B
Control
1x10 -15 M
1x10 -13 M
1x10 -11 M
1x10 -9 M
1x10 -7 M
P2(2.65%)
P2(2.69%)
P2(4.38%)
P2(35.13%)
P2(61.56%)
P2(58.75%)
Count
PE-A
C
OKT10-SAP
OKT10-SAP + 1 µg/ml SA
Percentage of Permeabilised Cells
0
1e-15
1e-13
1e-11
1e-9
1e-7
[OKT10-SAP] (M)
D
Viability (% of Control)
1e-16
1e-15
1e-14
1e-13
1e-12
1e-11
1e-10
1e-9
1e-8
1e-7
1e-6
[OKT10-SAP] (M)

Figure 48 Comparison of XTT Cytotoxicity Assay and PI Membrane Permeabilisation Assay

Histograms showing PE filter fluorescence in Daudi cells treated with a range of OKT10-SAP concentrations between $1x10^{-15}$ and $1x10^{-7}$ M both alone (A) and in the presence of 1 µg/ml of SA (B). Control cells, untreated with OKT10-SAP are shown for comparison. Gating for permeabilised cells was set at 2 logs above control cells. (C) Graph showing the percentage of permeabilised Daudi cells treated with OKT10-SAP or OKT10-SAP and 1 µg/ml of SA. Each bar is the mean of 2 independent experiments and the error bars one standard deviation either side of this mean. (D) Dose-response curves determined by XTT assay for Daudi cells treated with OKT10-SAP in the absence (●) or presence (○) of 1 µg/ml of SA. Each datum point is the mean of 2 independent experiments and the error bars one standard deviation either side of this mean.

List of References

1. Goodman LS, Wintrobe MM. Nitrogen mustard therapy; use of methyl-bis (beta-chloroethyl) amine hydrochloride and tris (beta-chloroethyl) amine hydrochloride for Hodgkin's disease, lymphosarcoma, leukaemia and certain allied and miscellaneous disorders. J Am Med Assoc. 1946 Sep 21;132:126–32.

2. Malhotra V, therapy MPCB, 2003. Classical chemotherapy: mechanisms, toxicities and the therapeutic window. Taylor & Francis 2014 Oct 27;2(sup1):1–3.

3. Zhang H, Chen J. Current status and future directions of cancer immunotherapy. J Cancer. 2018 Apr 20;9(10):1773–81.

4. Iqbal N, Iqbal N. Imatinib: a breakthrough of targeted therapy in cancer. Chemother Res Pract. Hindawi; 2014;2014(2):357027–9.

5. Rosenberg SA, Lotze MT, Muul LM, Leitman S, Chang AE, Ettinghausen SE, Matory YL, Skibber JM, Shiloni E, Vetto JT. Observations on the systemic administration of autologous lymphokine-activated killer cells and recombinant interleukin-2 to patients with metastatic cancer. N Engl J Med. 1985 Dec 5;313(23):1485–92.

6. Rosenberg SA, Spiess P, Lafreniere R. A new approach to the adoptive immunotherapy of cancer with tumor-infiltrating lymphocytes. Science. American Association for the Advancement of Science; 1986 Sep 19;233(4770):1318–21.

7. Rohaan MW, van den Berg JH, Kvistborg P, Haanen JBAG. Adoptive transfer of tumor-infiltrating lymphocytes in melanoma: a viable treatment option. Journal for ImmunoTherapy of Cancer; 2018 Oct 1;:1–16.

8. Gross G, Waks T, Eshhar Z. Expression of immunoglobulin-T-cell receptor chimeric molecules as functional receptors with antibody-type specificity. Proceedings of the National Academy of Sciences of the United States of America. National Academy of Sciences; 1989 Dec 1;86(24):10024–8.

9. Irving BA, Weiss A. The cytoplasmic domain of the T cell receptor ζ chain is sufficient to couple to receptor-associated signal transduction pathways. Cell. Cell Press; 1991 Mar 8;64(5):891–901.

10. Brocker T. Chimeric Fv-zeta or Fv-epsilon receptors are not sufficient to induce activation or cytokine production in peripheral T cells. Blood. 2000 Sep 1;96(5):1999–2001.

11. Park JR, DiGiusto DL, Slovak M, Wright C, Naranjo A, Wagner J, Meechoovet HB, Bautista C, Chang W-C, Ostberg JR, Jensen MC. Adoptive Transfer of Chimeric Antigen Receptor Re-directed Cytolytic T Lymphocyte Clones in

Patients with Neuroblastoma. Molecular Therapy. The American Society of Gene Therapy; 2016 Sep 15;15(4):825–33.

12. Finney HM, Lawson AD, Bebbington CR, Weir AN. Chimeric receptors providing both primary and costimulatory signalling in T cells from a single gene product. J Immunol. 1998 Sep 15;161(6):2791–7.

13. Acuto O, Michel F. CD28-mediated co-stimulation: a quantitative support for TCR signalling. Nat Rev Immunol. Nature Publishing Group; 2003 Dec;3(12):939–51.

14. Zhong X-S, Matsushita M, Plotkin J, Rivière I, Sadelain M. Chimeric Antigen Receptors Combining 4-1BB and CD28 Signalling Domains Augment PI3kinase/AKT/Bcl-XL Activation and CD8∓ T Cell–mediated Tumor Eradication. Molecular Therapy. Nature Publishing Group; 2009 Nov 13;18(2):413–20.

15. Moeller M, Kershaw MH, Cameron R, Westwood JA, Trapani JA, Smyth MJ, Darcy PK. Sustained antigen-specific antitumor recall response mediated by gene-modified CD4+ T helper-1 and CD8+ T cells. Cancer Res. American Association for Cancer Research; 2007 Dec 1;67(23):11428–37.

16. Grupp SA, Maude SL, Shaw PA, Aplenc R, Barrett DM, Callahan C, Lacey SF, Levine BL, Melenhorst JJ, Motley L, Rheingold SR, Teachey DT, Wood PA, Porter D, June CH. Durable Remissions in Children with Relapsed/Refractory ALL Treated with T Cells Engineered with a CD19-Targeted Chimeric Antigen Receptor (CTL019). Blood. American Society of Hematology; 2015 Dec 3;126(23):681–1.

17. Kochenderfer JN, Dudley ME, Kassim SH, Somerville RPT, Carpenter RO, Stetler-Stevenson M, Yang JC, Phan GQ, Hughes MS, Sherry RM, Raffeld M, Feldman S, Lu L, Li YF, Ngo LT, Goy A, Feldman T, Spaner DE, Wang ML, Chen CC, Kranick SM, Nath A, Nathan D-AN, Morton KE, Toomey MA, Rosenberg SA. Chemotherapy-Refractory Diffuse Large B-Cell Lymphoma and Indolent B-Cell Malignancies Can Be Effectively Treated With Autologous T Cells Expressing an Anti-CD19 Chimeric Antigen Receptor. Journal of Clinical Oncology. 2015 Feb 20;33(6):540–9.

18. Schuster SJ, Svoboda J, Chong EA, Nasta SD, Mato AR, Anak Ö, Brogdon JL, Pruteanu-Malinici I, Bhoj V, Landsburg D, Wasik M, Levine BL, Lacey SF, Melenhorst JJ, Porter DL, June CH. Chimeric Antigen Receptor T Cells in Refractory B-Cell Lymphomas. N Engl J Med. 2017 Dec 28;377(26):2545–54.

19. Beavis PA, Slaney CY, Kershaw MH, Gyorki D, Neeson PJ, Darcy PK. Reprogramming the tumor microenvironment to enhance adoptive cellular therapy. Seminars in Immunology. Elsevier Ltd; 2016 Feb 1;28(1):64–72.

20. Moon EK, Wang LC, Dolfi DV, Wilson CB, Ranganathan R, Sun J, Kapoor V, Scholler J, Pure E, Milone MC, June CH, Riley JL, Wherry EJ, Albelda SM. Multifactorial T-cell Hypofunction That Is Reversible Can Limit the Efficacy of

Chimeric Antigen Receptor-Transduced Human T cells in Solid Tumors. Clin Cancer Res. 2014 Aug 13;20(16):4262–73.

21. Sotillo E, Barrett DM, Black KL, Bagashev A, Oldridge D, Wu G, Sussman R, Lanauze C, Ruella M, Gazzara MR, Martinez NM, Harrington CT, Chung EY, Perazzelli J, Hofmann TJ, Maude SL, Raman P, Barrera A, Gill S, Lacey SF, Melenhorst JJ, Allman D, Jacoby E, Fry T, Mackall C, Barash Y, Lynch KW, Maris JM, Grupp SA, Thomas-Tikhonenko A. Convergence of Acquired Mutations and Alternative Splicing of CD19 Enables Resistance to CART-19 Immunotherapy. Cancer Discov. 2015 Dec 3;5(12):1282–95.

22. Maude SL, Frey N, Shaw PA, Aplenc R, Barrett DM, Bunin NJ, Chew A, Gonzalez VE, Zheng Z, Lacey SF, Mahnke YD, Melenhorst JJ, Rheingold SR, Shen A, Teachey DT, Levine BL, June CH, Porter DL, Grupp SA. Chimeric Antigen Receptor T Cells for Sustained Remissions in Leukemia. http://dxdoiorg/101056/NEJMoa1407222. Massachusetts Medical Society; 2014 Oct 15.

23. Brudno JN, Kochenderfer JN. Toxicities of chimeric antigen receptor T cells: recognition and management. Blood. 2016 Jun 30;127(26):3321–30.

24. Ehrlich P. Collected studies on immunity. New York: J. Wiley & Sons; 1906.

25. Schwartz RS. Paul Ehrlich's magic bullets. Vol. 350, The New England journal of medicine. 2004. 2 p.

26. Köhler G, MILSTEIN C. Continuous cultures of fused cells secreting antibody of predefined specificity. Nature. Nature Publishing Group; 1975 Aug 1;256(5517):495–7.

27. Khazaeli MB, Conry RM, LoBuglio AF. Human immune response to monoclonal antibodies. J Immunother Emphasis Tumor Immunol. 1994 Jan 1;15(1):42–52.

28. Badger CC, Anasetti C, Davis J, Bernstein ID. Treatment of Malignancy with Unmodified Antibody. PIR. Karger Publishers; 1987;6(5-6):419–34.

29. Riechmann L, Clark M, Waldmann H, Winter G. Reshaping human antibodies for therapy. Nature. Nature Publishing Group; 1988 Mar 24;332(6162):323–7.

30. Gul N, van Egmond M. Antibody-Dependent Phagocytosis of Tumor Cells by Macrophages: A Potent Effector Mechanism of Monoclonal Antibody Therapy of Cancer. Cancer Res. 2015 Nov 30;75(23):5008–13.

31. Green MC, Murray JL, Hortobagyi GN. Monoclonal antibody therapy for solid tumors. Cancer Treatment Reviews. Elsevier; 2000 Aug 1;26(4):269–86.

32. Schrama D, Reisfeld RA, Becker JC. Antibody targeted drugs as cancer therapeutics. Nature Reviews Drug Discovery 2006 5:2. Nature Publishing Group; 2006 Feb 1;5(2):147–59.

33. Seidel UJE, Schlegel P, Lang P. Natural killer cell mediated antibody-dependent cellular cytotoxicity in tumor immunotherapy with therapeutic antibodies. Front Immunol. Frontiers; 2013;4:76.

34. Smyth MJ, Cretney E, Kelly JM, Westwood JA, Street SEA, Yagita H, Takeda K, Dommelen SLHV, Degli-Esposti MA, Hayakawa Y. Activation of NK cell cytotoxicity. Molecular Immunology. 2005 Feb;42(4):501–10.

35. Warmerdam PA, Nabben NM, van de Graaf SA, van de Winkel JG, Capel PJ. The human low affinity immunoglobulin G Fc receptor IIC gene is a result of an unequal crossover event. J Biol Chem. American Society for Biochemistry and Molecular Biology; 1993 Apr 5;268(10):7346–9.

36. Li X, Wu J, Ptacek T, Redden DT, Brown EE, Alarcon GS, Ramsey-Goldman R, Petri MA, Reveille JD, Kaslow RA, Kimberly RP, Edberg JC. Allelic-Dependent Expression of an Activating Fc Receptor on B Cells Enhances Humoral Immune Responses. Science Translational Medicine. 2013 Dec 18;5(216):216ra175–5.

37. Morel PA, Ernst LK, Metes D. Functional CD32 Molecules on Human NK Cells. Leuk Lymphoma. 2009 Jul;35(1-2):47–56.

38. Ravetch JV, Bolland S. IgG Fc receptors. Annu Rev Immunol. 2001;19:275–90.

39. Koenderman L. Inside-Out Control of Fc-Receptors. Front Immunol. 2019 Mar 21;10:875–11.

40. Clynes RA, Towers TL, Presta LG, Ravetch JV. Inhibitory Fc receptors modulate in vivo cytoxicity against tumor targets. Nature Medicine 2009 15:10. Nature Publishing Group; 2000 Apr 1;6(4):443–6.

41. Dall'Ozzo S, Tartas S, Paintaud G, Cartron G, Colombat P, Bardos P, Watier H, Thibault G. Rituximab-dependent cytotoxicity by natural killer cells: influence of FCGR3A polymorphism on the concentration-effect relationship. Cancer Res. 2004 Jul 1;64(13):4664–9.

42. de Haij S, Jansen JHM, Boross P, Beurskens FJ, Bakema JE, Bos DL, Martens A, Verbeek JS, Parren PWHI, van de Winkel JGJ, Leusen JHW. In vivo cytotoxicity of type I CD20 antibodies critically depends on Fc receptor ITAM signaling. Cancer Res. American Association for Cancer Research; 2010 Apr 15;70(8):3209–17.

43. Gül N, Babes L, Siegmund K, Korthouwer R, Bögels M, Braster R, Vidarsson G, Hagen ten TLM, Kubes P, van Egmond M. Macrophages eliminate circulating tumor cells after monoclonal antibody therapy. J Clin Invest. 2014 Jan 16;124(2):812–23.

44. Church AK, VanDerMeid KR, Baig NA, Baran AM, Witzig TE, Nowakowski GS, Zent CS. Anti-CD20 monoclonal antibody-dependent phagocytosis of chronic lymphocytic leukaemia cells by autologous macrophages. Clin Exp Immunol. 2015 Oct 28;183(1):90–101.

45. Minard-Colin V, Xiu Y, Poe JC, Horikawa M, Magro CM, Hamaguchi Y, Haas KM, Tedder TF. Lymphoma depletion during CD20 immunotherapy in mice is mediated by macrophage FcγRI, FcγRIII, and FcγRIV. Blood. 2008 Aug 15;112(4):1205–13.

46. Bindon CI, Hale G, Brüggemann M, Waldmann H. Human monoclonal IgG isotypes differ in complement activating function at the level of C4 as well as C1q. Journal of Experimental Medicine. 1988 Jul 1;168(1):127–42.

47. Schroeder HW Jr., Cavacini L. Structure and function of immunoglobulins. Journal of Allergy and Clinical Immunology. 2010 Feb;125(2):S41–S52.

48. Zipfel PF, Skerka C. Complement regulators and inhibitory proteins. Nat Rev Immunol. Nature Publishing Group; 2009 Sep 4;9(10):729–40.

49. Golay J, Cittera E, Di Gaetano N, Manganini M, Mosca M, Nebuloni M, van Rooijen N, Vago L, Introna M. The role of complement in the therapeutic activity of rituximab in a murine B lymphoma model homing in lymph nodes. Haematologica. 2006 Feb;91(2):176–83.

50. Di Gaetano N, Cittera E, Nota R, Vecchi A, Grieco V, Scanziani E, Botto M, Introna M, Golay J. Complement Activation Determines the Therapeutic Activity of Rituximab In Vivo. J Immunol. 2003 Jul 21;171(3):1581–7.

51. Shan D, Ledbetter JA, Press OW. Signaling events involved in anti-CD20-induced apoptosis of malignant human B cells. Cancer Immunol Immunother. Springer-Verlag; 2000 Feb 23;48(12):673–83.

52. Hofmeister JK, Cooney D, Coggeshall KM. Clustered CD20 Induced Apoptosis: Src-Family Kinase, the Proximal Regulator of Tyrosine Phosphorylation, Calcium Influx, and Caspase 3-Dependent Apoptosis. Blood Cells, Molecules, and Diseases. 2000 Apr;26(2):133–43.

53. Lenz H-J. Cetuximab in the management of colorectal cancer. Biologics. 2007 Jun;1(2):77–91.

54. Sunada H, Magun BE, Mendelsohn J, MacLeod CL. Monoclonal antibody against epidermal growth factor receptor is internalized without stimulating receptor phosphorylation. Proceedings of the National Academy of Sciences of the United States of America. National Academy of Sciences; 1986 Jun 1;83(11):3825–9.

55. Kiyota A, Shintani S, Mihara M, Nakahara Y, Ueyama Y, Matsumura T, Tachikawa T, Wong DTW. Anti-epidermal growth factor receptor monoclonal antibody 225 upregulates p27(KIP1) and p15(INK4B) and induces G1 arrest in oral squamous carcinoma cell lines. OCL. Karger Publishers; 2002;63(1):92–8.

56. Tandon AK, Clark GM, Chamness GC, Ullrich A, McGuire WL. HER-2/neu oncogene protein and prognosis in breast cancer. Journal of Clinical Oncology. 1989 Aug;7(8):1120–8.

57. Claret FX. Trastuzumab: updated mechanisms of action and resistance in breast cancer. 2012 Jun 15;:1–6.

58. Tanimoto K. Hypoxia-inducible factor-1 polymorphisms associated with enhanced transactivation capacity, implying clinical significance. Carcinogenesis. 2003 Jun 19;24(11):1779–83.

59. Wood JM, Bold G, Buchdunger E, Cozens R, Ferrari S, Frei J, Hofmann F, Mestan J, Mett H, O'Reilly T, Persohn E, Rösel J, Schnell C, Stover D, Theuer A, Towbin H, Wenger F, Woods-Cook K, Menrad A, Siemeister G, Schirner M, Thierauch K-H, Schneider MR, Drevs J, Martiny-Baron G, Totzke F, Marmé D. PTK787/ZK 222584, a Novel and Potent Inhibitor of Vascular Endothelial Growth Factor Receptor Tyrosine Kinases, Impairs Vascular Endothelial Growth Factor-induced Responses and Tumor Growth after Oral Administration. Cancer Res. American Association for Cancer Research; 2000 Apr 15;60(8):2178–89.

60. Kazazi-Hyseni F, Beijnen JH, Schellens JHM. Bevacizumab. The Oncologist. 2010 Aug 31;15(8):819–25.

61. Los M, Roodhart JML, Voest EE. Target practice: lessons from phase III trials with bevacizumab and vatalanib in the treatment of advanced colorectal cancer. The Oncologist. 2007 Apr;12(4):443–50.

62. Pardoll DM. The blockade of immune checkpoints in cancer immunotherapy. Nature Publishing Group. Nature Publishing Group; 2012 Apr 1;12(4):252–64.

63. Walunas TL, Lenschow DJ, Bakker CY, Linsley PS, Freeman GJ, Green JM, Thompson CB, Bluestone JA. CTLA-4 can function as a negative regulator of T cell activation. Immunity. 1994 Aug;1(5):405–13.

64. Linsley PS, Brady W, Urnes M, Grosmaire LS, Damle NK, Ledbetter JA. CTLA-4 is a second receptor for the B cell activation antigen B7. Journal of Experimental Medicine. 1991 Sep 1;174(3):561–9.

65. Linsley PS, Greene JL, Brady W, Bajorath J, Ledbetter JA, Peach R. Human B7-1 (CD80) and B7-2 (CD86) bind with similar avidities but distinct kinetics to CD28 and CTLA-4 receptors. Immunity. Cell Press; 1994 Dec 1;1(9):793–801.

66. Kane LP, Andres PG, Howland KC, Abbas AK, Weiss A. Akt provides the CD28 costimulatory signal for up-regulation of IL-2 and IFN-gamma but not TH2 cytokines. Nat Immunol. 2001 Jan;2(1):37–44.

67. Pagès F, Ragueneau M, Rottapel R, Truneh A, Nunes J, Imbert J, Olive D. Binding of phosphatidyl-inositol-3-OH kinase to CD28 is required for T-cell signalling. Nature. Nature Publishing Group; 1994 May 1;369(6478):327–9.

68. Tivol EA, Borriello F, Schweitzer AN, Lynch WP, Bluestone JA, Sharpe AH. Loss of CTLA-4 leads to massive lymphoproliferation and fatal multiorgan tissue destruction, revealing a critical negative regulatory role of CTLA-4. Immunity. 1995 Nov;3(5):541–7.

69. Waterhouse P, Penninger JM, Timms E, Wakeham A, Shahinian A, Lee KP, Thompson CB, Griesser H, Mak TW. Lymphoproliferative Disorders with Early Lethality in Mice Deficient in Ctla-4. Science. American Association for the Advancement of Science; 1995 Nov 10;270(5238):985–8.

70. Peggs KS, Quezada SA, Chambers CA, Korman AJ, Allison JP. Blockade of CTLA-4 on both effector and regulatory T cell compartments contributes to the antitumor activity of anti–CTLA-4 antibodies. Journal of Experimental Medicine. 2009 Aug 3;206(8):1717–25.

71. Ramagopal UA, Liu W, Garrett-Thomson SC, Bonanno JB, Yan Q, Srinivasan M, Wong SC, Bell A, Mankikar S, Rangan VS, Deshpande S, Korman AJ, Almo SC. Structural basis for cancer immunotherapy by the first-in-class checkpoint inhibitor ipilimumab. Proceedings of the National Academy of Sciences of the United States of America. 2017 May 23;114(21):E4223–32.

72. Selby MJ, Engelhardt JJ, Quigley M, Henning KA, Chen T, Srinivasan M, Korman AJ. Anti-CTLA-4 Antibodies of IgG2a Isotype Enhance Antitumor Activity through Reduction of Intratumoral Regulatory T Cells. Cancer Immunology Research. 2013 Jul 10;1(1):32–42.

73. Camacho LH. CTLA-4 blockade with ipilimumab: biology, safety, efficacy, and future considerations. Cancer Med. 2015 Jan 25;4(5):661–72.

74. Keir ME, Liang SC, Guleria I, Latchman YE, Qipo A, Albacker LA, Koulmanda M, Freeman GJ, Sayegh MH, Sharpe AH. Tissue expression of PD-L1 mediates peripheral T cell tolerance. Journal of Experimental Medicine. Rockefeller University Press; 2006 Apr 17;203(4):883–95.

75. Nishimura H, Okazaki T, Tanaka Y, Nakatani K, Hara M, Matsumori A, Sasayama S, Mizoguchi A, Hiai H, Minato N, Honjo T. Autoimmune dilated cardiomyopathy in PD-1 receptor-deficient mice. Science. American Association for the Advancement of Science; 2001 Jan 12;291(5502):319–22.

76. Agata Y, Kawasaki A, Nishimura H, Ishida Y, Tsubata T, Yagita H, Honjo T. Expression of the PD-1 antigen on the surface of stimulated mouse T and B lymphocytes. Int Immunol. 1996 May;8(5):765–72.

77. Freeman GJ, Long AJ, Iwai Y, Bourque K, Chernova T, Nishimura H, Fitz LJ, Malenkovich N, Okazaki T, Byrne MC, Horton HF, Fouser L, Carter L, Ling V, Bowman MR, Carreno BM, Collins M, Wood CR, Honjo T. Engagement of the Pd-1 Immunoinhibitory Receptor by a Novel B7 Family Member Leads to Negative Regulation of Lymphocyte Activation. Journal of Experimental Medicine. 2000 Oct 2;192(7):1027–34.

78. Latchman Y, Wood CR, Chernova T, Chaudhary D, Borde M, Chernova I, Iwai Y, Long AJ, Brown JA, Nunes R, Greenfield EA, Bourque K, Boussiotis VA, Carter LL, Carreno BM, Malenkovich N, Nishimura H, Okazaki T, Honjo T, Sharpe AH, Freeman GJ. PD-L2 is a second ligand for PD-1 and inhibits T cell activation. Nat Immunol. 2001 Mar;2(3):261–8.

79. Hui E, Cheung J, Zhu J, Su X, Taylor MJ, Wallweber HA, Sasmal DK, Huang J, Kim JM, Mellman I, Vale RD. T cell costimulatory receptor CD28 is a primary target for PD-1–mediated inhibition. Science. 2017 Mar 30;355(6332):1428–33.

80. Yokosuka T, Takamatsu M, Kobayashi-Imanishi W, Hashimoto-Tane A, Azuma M, Saito T. Programmed cell death 1 forms negative costimulatory microclusters that directly inhibit T cell receptor signaling by recruiting phosphatase SHP2. Journal of Experimental Medicine. 2012 Jun 4;209(6):1201–17.

81. Bengsch B, Johnson AL, Kurachi M, Odorizzi PM, Pauken KE, Attanasio J, Stelekati E, McLane LM, Paley MA, Delgoffe GM, Wherry EJ. Bioenergetic Insufficiencies Due to Metabolic Alterations Regulated by the Inhibitory Receptor PD-1 Are an Early Driver of CD8 + T Cell Exhaustion. Immunity. 2016 Aug;45(2):358–73.

82. Wherry EJ. T cell exhaustion. Nature Publishing Group. Nature Publishing Group; 2011 Jun 1;131(6):492–9.

83. Wei SC, Duffy CR, Allison JP. Fundamental Mechanisms of Immune Checkpoint Blockade Therapy. Cancer Discov. 2018 Sep 4;8(9):1069–86.

84. Im SJ, Hashimoto M, Gerner MY, Lee J, Kissick HT, Burger MC, Shan Q, Hale JS, Lee J, Nasti TH, Sharpe AH, Freeman GJ, Germain RN, Nakaya HI, Xue H-H, Ahmed R. Defining CD8+ T cells that provide the proliferative burst after PD-1 therapy. Nature. Nature Publishing Group; 2016 Aug 2;537(7620):417–21.

85. Di Giacomo AM, Biagioli M, Maio M. The emerging toxicity profiles of anti-CTLA-4 antibodies across clinical indications. Semin Oncol. 2010 Oct;37(5):499–507.

86. Wang DY, Johnson DB, Davis EJ. Toxicities Associated With PD-1/PD-L1 Blockade. Cancer J. 2018 Jan;24(1):36–40.

87. Larkin J, Chiarion-Sileni V, Gonzalez R, Grob JJ, Cowey CL, Lao CD, Schadendorf D, Dummer R, Smylie M, Rutkowski P, Ferrucci PF, Hill A, Wagstaff J, Carlino MS, Haanen JB, Maio M, Marquez-Rodas I, McArthur GA, Ascierto PA, Long GV, Callahan MK, Postow MA, Grossmann K, Sznol M, Dreno B, Bastholt L, Yang A, Rollin LM, Horak C, Hodi FS, Wolchok JD. Combined Nivolumab and Ipilimumab or Monotherapy in Untreated Melanoma. N Engl J Med. 2015 Jul 2;373(1):23–34.

88. Postow MA, Chesney J, Pavlick AC, Robert C, Grossmann K, McDermott D, Linette GP, Meyer N, Giguere JK, Agarwala SS, Shaheen M, Ernstoff MS, Minor D, Salama AK, Taylor M, Ott PA, Rollin LM, Horak C, Gagnier P, Wolchok JD, Hodi FS. Nivolumab and Ipilimumab versus Ipilimumab in Untreated Melanoma. N Engl J Med. 2015 May 21;372(21):2006–17.

89. MD FSH, MD VC-S, MD PRG, MD PJ-JG, MD PPR, MD CLC, MD CDL, MD PDS, MD PJW, MD RD, MD PFF, MD MS, MD AH, MD DH, MD PIM-R, PhD JJ, MD JR,

FRCP JL, MD PJDW. Nivolumab plus ipilimumab or nivolumab alone versus ipilimumab alone in advanced melanoma (CheckMate 067): 4-year outcomes of a multicentre, randomised, phase 3 trial. Lancet Oncology. Elsevier Ltd; 2018 Oct 11;:1–14.

90. Chae YK, Arya A, Iams W, Cruz MR, Chandra S, Choi J, Giles F. Current landscape and future of dual anti-CTLA4 and PD-1/PD-L1 blockade immunotherapy in cancer; lessons learned from clinical trials with melanoma and non-small cell lung cancer (NSCLC). J Immunother Cancer. BMJ Specialist Journals; 2018 Dec 1;6(1):39.

91. Gu L, Khadaroo PA, Su H, Kong L, Chen L, Wang X, Li X, Zhu H, Zhong X, Pan J, Chen M. The safety and tolerability of combined immune checkpoint inhibitors (anti-PD-1/PD-L1 plus anti-CTLA-4): a systematic review and meta-analysis. BMC Cancer. BioMed Central; 2019 Dec 1;19(1):1–10.

92. Ellerman D. Bispecific T-cell engagers_ Towards understanding variables influencing the in vitro potency and tumor selectivity and their modulation to enhance their efficacy and safety. Methods. Elsevier; 2019 Feb 1;154:102–17.

93. Haas C, Krinner E, Brischwein K, Hoffmann P, Lutterbüse R, Schlereth B, Kufer P, Baeuerle PA. Mode of cytotoxic action of T cell-engaging BiTE antibody MT110. Immunobiology. Elsevier; 2009 Jun;214(6):441–53.

94. Kantarjian H, Stein A, Gökbuget N, Fielding AK, Schuh AC, Ribera J-M, Wei A, Dombret H, Foà R, Bassan R, Arslan Ö, Sanz MA, Bergeron J, Demirkan F, Lech-Maranda E, Rambaldi A, Thomas X, Horst H-A, Brüggemann M, Klapper W, Wood BL, Fleishman A, Nagorsen D, Holland C, Zimmerman Z, Topp MS. Blinatumomab versus Chemotherapy for Advanced Acute Lymphoblastic Leukemia. N Engl J Med. 2017 Mar 2;376(9):836–47.

95. Bargou R, Leo E, Zugmaier G, Klinger M, Goebeler M, Knop S, Noppeney R, Viardot A, Hess G, Schuler M, Einsele H, Brandl C, Wolf A, Kirchinger P, Klappers P, Schmidt M, Riethmüller G, Reinhardt C, Baeuerle PA, Kufer P. Tumor regression in cancer patients by very low doses of a T cell-engaging antibody. Science. 2008 Aug 15;321(5891):974–7.

96. Reichert JM. Monoclonal antibodies in the clinic. Nature Biotechnology 2001 19:9. 2001 Sep;19(9):819–22.

97. Witzig TE, Gordon LI, Cabanillas F, Czuczman MS, Emmanouilides C, Joyce R, Pohlman BL, Bartlett NL, Wiseman GA, Padre N, Grillo-López AJ, Multani P, White CA. Randomized Controlled Trial of Yttrium-90–Labeled Ibritumomab Tiuxetan Radioimmunotherapy Versus Rituximab Immunotherapy for Patients With Relapsed or Refractory Low-Grade, Follicular, or Transformed B-Cell Non-Hodgkin's Lymphoma. Journal of Clinical Oncology. American Society of Clinical Oncology; 2016 Sep 21;20(10):2453–63.

98. Larson SM, Carrasquillo JA, Cheung N-KV, Press OW. Radioimmunotherapy of human tumours. Nat Rev Cancer. Nature Publishing Group; 2015 Jun 1;15(6):347–60.

99. Cheson BD. Radioimmunotherapy of non-Hodgkin lymphomas. Blood. American Society of Hematology; 2003 Jan 15;101(2):391–8.

100. Green DJ, Press OW. Whither Radioimmunotherapy: To Be or Not To Be? Cancer Res. American Association for Cancer Research; 2017 May 1;77(9):2191–6.

101. Axworthy DB, Reno JM, Hylarides MD, Mallett RW, Theodore LJ, Gustavson LM, Su F, Hobson LJ, Beaumier PL, Fritzberg AR. Cure of human carcinoma xenografts by a single dose of pretargeted yttrium-90 with negligible toxicity. Proceedings of the National Academy of Sciences of the United States of America. National Academy of Sciences; 2000 Feb 15;97(4):1802–7.

102. Bakhtiar R. Antibody drug conjugates. Biotechnology Letters. Springer Netherlands; 2016 Jun 20;38(10):1655–64.

103. Peters C, Brown S. Antibody-drug conjugates as novel anti-cancer chemotherapeutics. Bioscience Reports. 2015 Jul 7;35(4):e00225–5.

104. Verma S, Miles D, Gianni L, Krop IE, Welslau M, Baselga J, Pegram M, Oh D-Y, Diéras V, Guardino E, Fang L, Lu MW, Olsen S, Blackwell K. Trastuzumab Emtansine for HER2-Positive Advanced Breast Cancer. http://dxdoiorg/101056/NEJMoa1209124. Massachusetts Medical Society; 2012 Nov 7;367(19):1783–91.

105. Teo EC-Y, Chew Y, Phipps C. A review of monoclonal antibody therapies in lymphoma. Crit Rev Oncol Hematol. 2016 Jan;97:72–84.

106. Moolten FL, Cooperband SR. Selective Destruction of Target Cells by Diphtheria Toxin Conjugated to Antibody Directed against Antigens on the Cells. Science. American Association for the Advancement of Science; 1970 Jul 3;169(3940):68–70.

107. Alewine C, Hassan R, Pastan I. Advances in anticancer immunotoxin therapy. The Oncologist. AlphaMed Press; 2015 Feb;20(2):176–85.

108. Pavlovskis OR, Iglewski BH, Pollack M. Mechanism of action of Pseudomonas aeruginosa exotoxin A in experimental mouse infections: adenosine diphosphate ribosylation of elongation factor 2. Infect Immun. American Society for Microbiology; 1978 Jan 1;19(1):29–33.

109. Collier RJ. Effect of diphtheria toxin on protein synthesis: Inactivation of one of the transfer factors. Journal of Molecular Biology. 1967 Apr;25(1):83–98.

110. Nour-Imene Zahaf, Gudula Schmidt. Bacterial Toxins for Cancer Therapy. Toxins. Multidisciplinary Digital Publishing Institute; 2017 Aug;9(8):236–11.

111. Stirpe F. Ribosome-inactivating proteins. Toxicon. 2004 Sep;44(4):371–83.

112. Bergan J, Lingelem ABD, Simm R, Skotland T, Sandvig K. Shiga toxins. Toxicon. Elsevier Ltd; 2012 Nov 1;60(6):1085–107.

113. Endo Y, Mitsui K, Motizuki M, Tsurugi K. The mechanism of action of ricin and related toxic lectins on eukaryotic ribosomes. The site and the characteristics of the modification in 28 S ribosomal RNA caused by the toxins. J Biol Chem. American Society for Biochemistry and Molecular Biology; 1987 Apr 25;262(12):5908–12.

114. Endo Y, Tsurugi K. The RNA N-glycosidase activity of ricin A-chain. The characteristics of the enzymatic activity of ricin A-chain with ribosomes and with rRNA. J Biol Chem. American Society for Biochemistry and Molecular Biology; 1988 Jun 25;263(18):8735–9.

115. Montanaro L, Sperti S, Mattioli A, Testoni G, Stirpe F. Inhibition by ricin of protein synthesis in vitro. Inhibition of the binding of elongation factor 2 and of adenosine diphosphate-ribosylated elongation factor 2 to ribosomes. Biochemical Journal. Portland Press Ltd; 1975 Jan;146(1):127–31.

116. Olsnes S, Fernandez-Puentes C, Carrasco L, Vazquez D. Ribosome inactivation by the toxic lectins abrin and ricin. Kinetics of the enzymic activity of the toxin A-chains. Eur J Biochem. 1975 Dec 1;60(1):281–8.

117. Eiklid K, Olsnes S, Pihl A. Entry of lethal doses of abrin, ricin and modeccin into the cytosol of HeLa cells. Exp Cell Res. 1980 Apr;126(2):321–6.

118. Brinkmann U, Mansfield E, Pastan I. Effects of BCL-2 overexpression on the sensitivity of MCF-7 breast cancer cells to ricin, diphtheria and Pseudomonas toxin and immunotoxins. Apoptosis. 1997;2(2):192–8.

119. Narayanan S, Surolia A, Karande AA. Ribosome-inactivating protein and apoptosis: abrin causes cell death via mitochondrial pathway in Jurkat cells. Biochem J. Portland Press Limited; 2004 Jan 1;377(Pt 1):233–40.

120. Griffiths GD, Leek MD, Gee DJ. The toxic plant proteins ricin and abrin induce apoptotic changes in mammalian lymphoid tissues and intestine. J Pathol. John Wiley & Sons, Ltd; 1987 Mar;151(3):221–9.

121. Gan YH, Peng SQ, Liu HY. Molecular mechanism of apoptosis induced by ricin in HeLa cells. Acta Pharmacol Sin. 2000 Mar;21(3):243–8.

122. Bolognesi A, Tazzari PL, Olivieri F, Polito L, Falini B, Stirpe F. Induction of apoptosis by ribosome-inactivating proteins and related immunotoxins. Int J Cancer. Wiley Subscription Services, Inc., A Wiley Company; 1996 Nov 4;68(3):349–55.

123. Sikriwal D, Ghosh P, Batra JK. Ribosome inactivating protein saporin induces apoptosis through mitochondrial cascade, independent of translation inhibition. Int J Biochem Cell Biol. 2008;40(12):2880–8.

124. Hu RG, Zhai QW, Liu WY, Liu XY. An insight into the mechanism of cytotoxicity of ricin to hepatoma cell: Roles of Bcl-2 family proteins, caspases, Ca2+-dependent proteases and protein kinase C. Journal of Cellular Biochemistry. John Wiley & Sons, Ltd; 2001 Jan 1;81(4):583–93.

125. Iordanov MS, Pribnow D, Magun JL, Dinh TH, Pearson JA, Chen SL, Magun BE. Ribotoxic stress response: activation of the stress-activated protein kinase JNK1 by inhibitors of the peptidyl transferase reaction and by sequence-specific RNA damage to the alpha-sarcin/ricin loop in the 28S rRNA. Molecular and Cellular Biology. American Society for Microbiology; 1997 Jun 1;17(6):3373–81.

126. Smith WE, Kane AV, Campbell ST, Acheson DWK, Cochran BH, Thorpe CM. Shiga Toxin 1 Triggers a Ribotoxic Stress Response Leading to p38 and JNK Activation and Induction of Apoptosis in Intestinal Epithelial Cells. Infect Immun. 2003 Mar 1;71(3):1497–504.

127. Tournier C, Hess P, Yang DD, Xu J, Turner TK, Nimnual A, Bar-Sagi D, Jones SN, Flavell RA, Davis RJ. Requirement of JNK for Stress- Induced Activation of the Cytochrome c-Mediated Death Pathway. Science. American Association for the Advancement of Science; 2000 May 5;288(5467):870–4.

128. Fujii J, Matsui T, Heatherly DP, Schlegel KH, Lobo PI, Yutsudo T, Ciraolo GM, Morris RE, Obrig T. Rapid apoptosis induced by Shiga toxin in HeLa cells. Infect Immun. American Society for Microbiology Journals; 2003 May;71(5):2724–35.

129. Shih S-F, Wu Y-H, Hung C-H, Yang H-Y, Lin J-Y. Abrin Triggers Cell Death by Inactivating a Thiol-specific Antioxidant Protein. J Biol Chem. American Society for Biochemistry and Molecular Biology; 2001 Jun 15;276(24):21870–7.

130. Komatsu N, Nakagawa M, Oda T, Muramatsu T. Depletion of Intracellular NAD+ and ATP Levels during Ricin-Induced Apoptosis through the Specific Ribosomal Inactivation Results in the Cytolysis of U 937 Cells. J Biochem (Tokyo). The Japanese Biochemical Society; 2000;128(3):463–70.

131. Barbieri L, Brigotti M, Perocco P, Carnicelli D, Ciani M, Mercatali L, Stirpe F. Ribosome-inactivating proteins depurinate poly(ADP-ribosyl)ated poly(ADP-ribose) polymerase and have transforming activity for 3T3 fibroblasts. FEBS Letters. 2003 Feb 22;538(1-3):178–82.

132. Bagga S, Seth D, Batra JK. The Cytotoxic Activity of Ribosome-inactivating Protein Saporin-6 Is Attributed to Its rRNA N-Glycosidase and Internucleosomal DNA Fragmentation Activities. J Biol Chem. 2003 Feb 14;278(7):4813–20.

133. Day PJ, Lord JM, Roberts LM. The deoxyribonuclease activity attributed to ribosome-inactivating proteins is due to contamination. Eur J Biochem. 1998 Dec 1;258(2):540–5.

134. Lombardi A, Bursomanno S, Lopardo T, Traini R, Colombatti M, Ippoliti R, Flavell DJ, Flavell SU, Ceriotti A, FABBRINI MS. Pichia pastoris as a host for secretion of toxic saporin chimeras. FASEB J. Federation of American Societies for Experimental Biology; 2009 Sep 28.

135. Olsnes S, Pihl A. Different biological properties of the two constituent peptide chains of ricin a toxic protein inhibiting protein synthesis. Biochemistry. 1973.

136. Maras B, Ippoliti R, De Luca E, Lendaro E, Bellelli A, Barra D, Bossa F, Brunori M. The amino acid sequence of a ribosome-inactivating protein from Saponaria officinalis seeds. Biochem Int. 1990 Aug;21(5):831–8.

137. Savino C, Federici L, Ippoliti R, Lendaro E. The crystal structure of saporin SO6 from Saponaria officinalis and its interaction with the ribosome. FEBS …. 2000.

138. Fermani S, Falini G, Ripamonti A, Polito L, Stirpe F, Bolognesi A. The 1.4Å structure of dianthin 30 indicates a role of surface potential at the active site of type 1 ribosome inactivating proteins. Journal of Structural Biology. 2005 Feb;149(2):204–12.

139. Newton DL, Wales R, Richardson PT, Walbridge S, Saxena SK, Ackerman EJ, Roberts LM, Lord JM, Youle RJ. Cell surface and intracellular functions for ricin galactose binding. J Biol Chem. American Society for Biochemistry and Molecular Biology; 1992 Jun 15;267(17):11917–22.

140. Lord JM, Roberts LM, Robertus JD. Ricin: structure, mode of action, and some current applications. FASEB J. 1994 Feb;8(2):201–8.

141. van Deurs B, Tønnessen TI, Petersen OW, Sandvig K, Olsnes S. Routing of internalized ricin and ricin conjugates to the Golgi complex. J Cell Biol. 1986 Jan;102(1):37–47.

142. Spooner RA, Watson PD, Marsden CJ, Smith DC, Moore KAH, Cook JP, Lord JM, Roberts LM. Protein disulphide-isomerase reduces ricin to its A and B chains in the endoplasmic reticulum. Biochem J. Portland Press Limited; 2004 Oct 15;383(Pt 2):285–93.

143. Bellisola G, Fracasso G, Ippoliti R, Menestrina G, Rosén A, Soldà S, Udali S, Tomazzolli R, Tridente G, Colombatti M. Reductive activation of ricin and ricin A-chain immunotoxins by protein disulfide isomerase and thioredoxin reductase. Biochemical Pharmacology. 2004 May;67(9):1721–31.

144. Stevenson J, Huang EY, Olzmann JA. Endoplasmic Reticulum–Associated Degradation and Lipid Homeostasis. Annu Rev Nutr. 2016 Jul 17;36(1):511–42.

145. Sandvig K, Skotland T, van Deurs B, Klokk TI. Retrograde transport of protein toxins through the Golgi apparatus. Histochemistry and cell …. 2013.

146. Rapak A, Falnes PO, Olsnes S. Retrograde transport of mutant ricin to the endoplasmic reticulum with subsequent translocation to cytosol. Proceedings of the National Academy of Sciences of the United States of America. 1997 Apr 15;94(8):3783–8.

147. Cavallaro U, Nykjaer A, Nielsen M. α2-Macroglobulin Receptor Mediates Binding and Cytotoxicity of Plant Ribosome-Inactivating Proteins. European journal of …. 1995.

148. Chan W-L, Shaw P-C, Tam S-C, Jacobsen C, Gliemann J, Nielsen MS. Trichosanthin Interacts with and Enters Cells via LDL Receptor Family Members. Biochemical and Biophysical Research Communications. 2000 Apr;270(2):453–7.

149. Bagga S, Hosur MV, Batra JK. Cytotoxicity of ribosome-inactivating protein saporin is not mediated through α 2-macroglobulin receptor. FEBS Letters. 2003 Mar 28;541(1-3):16–20.

150. Vago R, Marsden CJ, Lord JM, Ippoliti R, Flavell DJ, Flavell SU, Ceriotti A, Fabbrini MS. Saporin and ricin A chain follow different intracellular routes to enter the cytosol of intoxicated cells. FEBS Journal. 2005 Sep 7;272(19):4983–95.

151. Thakur M, Weng A, Pieper A, Mergel K, Mallinckrodt von B, Gilabert-Oriol R, Görick C, Wiesner B, Eichhorst J, Melzig MF, Fuchs H. Macromolecular interactions of triterpenoids and targeted toxins: Role of saponins charge. International Journal of Biological Macromolecules. Elsevier B.V; 2013 Oct 1;61:285–94.

152. Weng A, Thakur M, Mallinckrodt von B, Beceren-Braun F, Gilabert-Oriol R, Wiesner B, Eichhorst J, Böttger S, Melzig MF, Fuchs H. Saponins modulate the intracellular trafficking of protein toxins. Journal of Controlled Release. Elsevier B.V; 2012 Nov 28;164(1):74–86.

153. Stirpe F, Gasperi-Campani A, Barbieri L, Falasca A, Abbondanza A, Stevens WA. Ribosome-inactivating proteins from the seeds of Saponaria officinalis L. (soapwort), of Agrostemma githago L. (corn cockle) and of Asparagus officinalis L. (asparagus), and from the latex of Hura crepitans L. (sandbox tree). Biochemical Journal. Portland Press Limited; 1983 Dec 15;216(3):617–25.

154. Ferreras JM, Barbieri L, Girbés T, Battelli MG, Rojo MA, Arias FJ, Rocher MA, Soriano F, Mendéz E, Stirpe F. Distribution and properties of major ribosome-inactivating proteins (28 S rRNA N-glycosidases) of the plant Saponaria officinalis L. (Caryophyllaceae). Biochim Biophys Acta. 1993 Oct 19;1216(1):31–42.

155. Santanché S, Bellelli A, Brunori M. The unusual stability of saporin, a candidate for the synthesis of immunotoxins. Biochemical and Biophysical Research Communications. 1997 May 8;234(1):129–32.

156. Bolognesi A, Tazzari PL, Tassi C, Gromo G, Gobbi M, Stirpe F. A comparison of anti-lymphocyte immunotoxins containing different ribosome-inactivating proteins and antibodies. Clin Exp Immunol. Wiley-Blackwell; 1992 Sep;89(3):341–6.

157. Thorpe PE, Brown AN, Bremner JA, Foxwell BM, Stirpe F. An immunotoxin composed of monoclonal anti-Thy 1.1 antibody and a ribosome-inactivating protein from Saponaria officinalis: potent antitumor effects in vitro and in vivo. J Natl Cancer Inst. 1985 Jul;75(1):151–9.

158. Polito L, Bortolotti M, Pedrazzi M, Bolognesi A. Immunotoxins and Other Conjugates Containing Saporin-S6 for Cancer Therapy. Toxins. 2011 Dec;3(12):697–720.

159. Polito L, Bortolotti M, Mercatelli D, Battelli M, Bolognesi A. Saporin-S6: A Useful Tool in Cancer Therapy. Toxins. Multidisciplinary Digital Publishing Institute; 2013 Oct;5(10):1698–722.

160. Flavell DJ, Flavell SU, Boehm DA, Emery L, Noss A, Ling NR, Richardson PR, Hardie D, Wright DH. Preclinical studies with the anti-CD19-saporin immunotoxin BU12-SAPORIN for the treatment of human-B-cell tumours. British Journal of Cancer. Nature Publishing Group; 1995 Dec 1;72(6):1373–9.

161. Flavell DJ, Noss A, Pulford KA, Ling N, Flavell SU. Systemic therapy with 3BIT, a triple combination cocktail of anti-CD19, -CD22, and -CD38-saporin immunotoxins, is curative of human B-cell lymphoma in severe combined immunodeficient mice. Cancer Res. 1997 Nov 1;57(21):4824–9.

162. Flavell DJ, Cooper S, Okayama K, Emery L, Flavell SU. Comparison of the performance of anti-CD7 and anti-CD38 bispecific antibodies and immunotoxins for the delivery of saporin to a human T-cell acute lymphoblastic leukemia cell line. Hematological Oncology. John Wiley & Sons, Ltd; 1995 Jan 1;13(4):185–200.

163. Flavell DJ, Boehm DA, Noss A, Warnes SL, Flavell SU. Therapy of human T-cell acute lymphoblastic leukaemia with a combination of anti-CD7 and anti-CD38-SAPORIN immunotoxins is significantly better than therapy with each individual immunotoxin. British Journal of Cancer. 2001 Feb;84(4):571–8.

164. Falini B, Bolognesi A, Flenghi L, Tazzari PL, Broe MK, Stein H, Dürkop H, Aversa F, Corneli P, Pizzolo G. Response of refractory Hodgkin's disease to monoclonal anti-CD30 immunotoxin. Lancet. 1992 May 16;339(8803):1195–6.

165. Bonardi MA, Bell A, French RR, Gromo G, Hamblin T, Modena D, Tutt AL, Glennie MJ. Initial experience in treating human lymphoma with a combination of bispecific antibody and saporin. Int J Cancer Suppl. 1992;7:73–7.

166. French RR, Hamblin TJ, Bell AJ, Tutt AL, Glennie MJ. Treatment of B-cell lymphomas with combination of bispecific antibodies and saporin. Lancet. 1995 Jul 22;346(8969):223–4.

167. French RR, Bell AJ, Hamblin TJ, Tutt AL, Glennie MJ. Response of B-cell lymphoma to a combination of bispecific antibodies and saporin. Leuk Res. 1996 Jul;20(7):607–17.

168. Kreitman RJ. Immunotoxins for targeted cancer therapy. AAPS J. Springer-Verlag; 2006;8(3):E532–51.

169. Flavell DJ. Countering immunotoxin immunogenicity. Nature Publishing Group; 2016 May 6;114(11):1177–9.

170. Hassan R, Miller AC, Sharon E, Thomas A, Reynolds JC, Ling A, Kreitman RJ, Miettinen MM, Steinberg SM, Fowler DH, Pastan I. Major cancer regressions in mesothelioma after treatment with an anti-mesothelin immunotoxin and immune suppression. Science Translational Medicine. American Association for the Advancement of Science; 2013 Oct 23;5(208):208ra147–7.

171. Cizeau J, Grenkow DM, Brown JG, Entwistle J, MacDonald GC. Engineering and Biological Characterization of VB6-845, an Anti-EpCAM Immunotoxin Containing a T-cell Epitope-depleted Variant of the Plant Toxin Bouganin. Journal of Immunotherapy. 2009 Jul;32(6):574–84.

172. He X-H, Shaw P-C, Xu L-H, Tam S-C. Site-directed polyethylene glycol modification of trichosanthin: Effects on its biological activites, pharmacokinetics, and antigenicity. Life Sciences. Pergamon; 1999 Feb 26;64(14):1163–75.

173. Stone MJ, Sausville EA, Fay JW, Headlee D, Collins RH, Figg WD, Stetler-Stevenson M, Jain V, Jaffe ES, Solomon D, Lush RM, Senderowicz A, Ghetie V, Schindler J, Uhr JW, Vitetta ES. A phase I study of bolus versus continuous infusion of the anti-CD19 immunotoxin, IgG-HD37-dgA, in patients with B-cell lymphoma. Blood. 1996 Aug 15;88(4):1188–97.

174. Sausville EA, Headlee D, Stetler-Stevenson M, Jaffe ES, Solomon D, Figg WD, Herdt J, Kopp WC, Rager H, Steinberg SM. Continuous infusion of the anti-CD22 immunotoxin IgG-RFB4-SMPT-dgA in patients with B-cell lymphoma: a phase I study. Blood. 1995 Jun 15;85(12):3457–65.

175. Kreitman RJ, Stetler-Stevenson M, Margulies I, Noel P, Fitzgerald DJP, Wilson WH, Pastan I. Phase II trial of recombinant immunotoxin RFB4(dsFv)-PE38 (BL22) in patients with hairy cell leukemia. J Clin Oncol. 2009 Jun 20;27(18):2983–90.

176. Lynch TJ Jr, Lambert JM, Coral F, Shefner J, Wen P, Blattler WA, Collinson AR, Ariniello PD, Braman G, Cook S, Esseltine D, Elias A, Skarin A, Ritz J. Immunotoxin therapy of small-cell lung cancer: a phase I study of N901-blocked ricin. Journal of Clinical Oncology. 1997 Feb;15(2):723–34.

177. Avarbock AB, Loren AW, Park JY, Junkins Hopkins JM, Choi J, Litzky LA, Rook AH. Lethal vascular leak syndrome after denileukin diftitox administration to a patient with cutaneous gamma/delta T?cell lymphoma and occult cirrhosis. Am J Hematol. Wiley Subscription Services, Inc., A Wiley Company; 2008 Jul;83(7):593–5.

178. LoRusso PM, Lomen PL, Redman BG, Poplin E, Bander JJ, Valdivieso M. Phase I study of monoclonal antibody-ricin A chain immunoconjugate Xomazyme-

791 in patients with metastatic colon cancer. Am J Clin Oncol. 1995 Aug;18(4):307–12.

179. Smallshaw JE, Ghetie V, Rizo J, Fulmer JR, Trahan LL, Ghetie M-A, Vitetta ES. Genetic engineering of an immunotoxin to eliminate pulmonary vascular leak in mice. Nature Biotechnology 2001 19:9. Nature Publishing Group; 2003 Mar 10;21(4):387–91.

180. Weldon JE, Xiang L, Zhang J, Beers R, Walker DA, Onda M, Hassan R, Pastan I. A Recombinant Immunotoxin against the Tumor-Associated Antigen Mesothelin Reengineered for High Activity, Low Off-Target Toxicity, and Reduced Antigenicity. Molecular Cancer Therapeutics. 2013 Jan 13;12(1):48–57.

181. Olsen E, Duvic M, Frankel A, Kim Y, Martin A. Pivotal phase III trial of two dose levels of denileukin diftitox for the treatment of cutaneous T-cell lymphoma. Journal of Clinical …. 2001;19(2):376–88.

182. Vallera D, Kreitman R. Immunotoxins Targeting B cell Malignancy—Progress and Problems With Immunogenicity. Biomedicines. Multidisciplinary Digital Publishing Institute; 2019 Mar;7(1):1–6.

183. Kreitman RJ, Dearden C, Zinzani PL, Delgado J, Karlin L, Robak T, Gladstone DE, le Coutre P, Dietrich S, Gotic M, Larratt L, Offner F, Schiller G, Swords R, Bacon L, Bocchia M, Bouabdallah K, Breems DA, Cortelezzi A, Dinner S, Doubek M, Gjertsen BT, Gobbi M, Hellmann A, Lepretre S, Maloisel F, Ravandi F, Rousselot P, Rummel M, Siddiqi T, Tadmor T, Troussard X, Yi CA, Saglio G, Roboz GJ, Balic K, Standifer N, He P, Marshall S, Wilson W, Pastan I, Yao N-S, Giles F. Moxetumomab pasudotox in relapsed/refractory hairy cell leukemia. Leukemia. Springer US; 2018 Aug 4;:1–10.

184. Pirker R, FitzGerald DJ, Hamilton TC, Ozols RF, Laird W, Frankel AE, Willingham MC, Pastan I. Characterization of immunotoxins active against ovarian cancer cell lines. J Clin Invest. American Society for Clinical Investigation; 1985 Sep 1;76(3):1261–7.

185. Ravel S, Colombatti M, Casellas P. Internalization and intracellular fate of anti-CD5 monoclonal antibody and anti-CD5 ricin A-chain immunotoxin in human leukemic T cells. Blood. American Society of Hematology; 1992 Mar 15;79(6):1511–7.

186. Casellas P, Bourrie BJ, Gros P, Jansen FK. Kinetics of cytotoxicity induced by immunotoxins. Enhancement by lysosomotropic amines and carboxylic ionophores. J Biol Chem. American Society for Biochemistry and Molecular Biology; 1984 Aug 10;259(15):9359–64.

187. Colombatti M, Dell'Arciprete L, Chignola R, Tridente G. Carrier Protein-Monensin Conjugates: Enhancement of Immunotoxin Cytotoxicity and Potential in Tumor Treatment. Cancer Res. American Association for Cancer Research; 1990 Mar 1;50(5):1385–91.

188. Fuchs H, Weng A, Gilabert-Oriol R. Augmenting the Efficacy of Immunotoxins and Other Targeted Protein Toxins by Endosomal Escape Enhancers. Toxins. 2016 Jul;8(7):200–28.

189. Chignola R, Anselmi C, Serra MD, Franceschi A, Fracasso G, Pasti M, Chiesa E, Lord JM, Tridente G, Colombatti M. Self-potentiation of Ligand-Toxin Conjugates Containing Ricin A Chain Fused with Viral Structures. J Biol Chem. American Society for Biochemistry and Molecular Biology; 1995 Oct 6;270(40):23345–51.

190. Fitzgerald D, Padmanabhan R, Pastan I. Adenovirus-induced release of epidermal growth factor and pseudomonas toxin into the cytosol of KB cells during receptor-mediated endocytosis. Cell. 1983;32(2):607–17.

191. Flavell DJ, Warnes SL, Bryson CJ, Field SA, Noss AL, Packham G, Flavell SU. The anti-CD20 antibody rituximab augments the immunospecific therapeutic effectiveness of an anti-CD19 immunotoxin directed against human B-cell lymphoma. Br J Haematol. Blackwell Publishing Ltd; 2006 Jul;134(2):157–70.

192. Flavell DJ, Warnes S, Noss A, Flavell SU. Host-mediated antibody-dependent cellular cytotoxicity contributes to the in vivo therapeutic efficacy of an anti-CD7-saporin immunotoxin in a severe combined immunodeficient mouse model of human T-cell acute lymphoblastic leukemia. Cancer Res. 1998 Dec 15;58(24):5787–94.

193. Flavell DJ, Warnes SL, Noss AL, Flavell SU. Anti-CD7 antibody and immunotoxin treatment of human CD7(+)T-cell leukaemia is significantly less effective in NOD/LtSz-scid mice than in CB.17 scid mice. British Journal of Cancer. Nature Publishing Group; 2000 Dec;83(12):1755–61.

194. Flavell DJ, Warnes S, Holmes SE, Flavell SU. The TLR3 agonist poly inosinic:cytidylic acid significantly augments the therapeutic activity of an anti-CD7 immunotoxin for human T-cell leukaemia. In preparation. 2018.

195. Weng A, Thakur M, Beceren-Braun F, Bachran D, Bachran C, Riese SB, Jenett-Siems K, Gilabert-Oriol R, Melzig MF, Fuchs H. The toxin component of targeted anti-tumor toxins determines their efficacy increase by saponins. Molecular Oncology. Elsevier B.V; 2012 Jun 1;6(3):323–32.

196. Holmes SE, Bachran C, Fuchs H, Weng A, Melzig MF, Flavell SU, Flavell DJ. Triterpenoid saponin augmention of saporin-based immunotoxin cytotoxicity for human leukaemia and lymphoma cells is partially immunospecific and target molecule dependent. Immunopharmacology and Immunotoxicology. 2014 Oct 16;37(1):42–55.

197. Bachran D, Schneider S, Bachran C, Urban R, Weng A, Melzig MF, Hoffmann C, Kaufmann AM, Fuchs H. Epidermal growth factor receptor expression affects the efficacy of the combined application of saponin and a targeted toxin on human cervical carcinoma cells. Int J Cancer. 2009 Dec 17;127(6):1453–61.

198. Vincken J-P, Heng L, de Groot A, Gruppen H. Saponins, classification and occurrence in the plant kingdom. Phytochemistry. 2007 Feb;68(3):275–97.

199. Oleszek WA. Chromatographic determination of plant saponins. Journal of chromatography A. 2002;967(1):147–62.

200. Van Dyck S, Flammang P, Meriaux C, Bonnel D, Salzet M, Fournier I, Wisztorski M. Localization of secondary metabolites in marine invertebrates: contribution of MALDI MSI for the study of saponins in Cuvierian tubules of H. forskali. PLOS ONE. Public Library of Science; 2010 Nov 10;5(11):e13923.

201. Liu HW, Li JK, Zhang DW, Zhang JC. Two new steroidal compounds from starfish Asterias amurensis Lutken. Journal of Asian …. 2008.

202. Sparg SG, Light ME, van Staden J. Biological activities and distribution of plant saponins. Journal of Ethnopharmacology. 2004 Oct;94(2-3):219–43.

203. Abe I, Rohmer M, Prestwich GD. Enzymatic cyclization of squalene and oxidosqualene to sterols and triterpenes. Chemical Reviews. 1993.

204. Haralampidis K, Trojanowska M, Osbourn AE. Biosynthesis of Triterpenoid Saponins in Plants. In: Dutta NN, Hammar F, Haralampidis K, Karanth NG, König A, Krishna SH, Kunze G, Nagy E, Orlich B, Osbourn AE, Raghavarao KSMS, Riedel K, Sahoo GC, Schomäcker R, Srinivas ND, Trojanowska M, editors. History and Trends in Bioprocessing and Biotransformation. Berlin, Heidelberg: Springer Berlin Heidelberg; 2002. pp. 31–49. (Advances in Biochemical Engineering/Biotechnology; vol. 75).

205. Hostettmann K, Marston A. Saponins. Cambridge University Press; 2005. 1 p.

206. Mahato SB, Pal BC, Nandy AK. Structure elucidation of two acylated triterpenoid bisglycosides from cunn. Tetrahedron. 1992 Jan;48(32):6717–28.

207. Lorent J, Le Duff CS, Quetin-Leclercq J. Induction of highly curved structures in relation to membrane permeabilization and budding by the triterpenoid saponins, α-and δ-Hederin. Journal of biological …. 2013.

208. Keukens E, de Vrije T, van den Boom C. Molecular basis of glycoalkaloid induced membrane disruption. … et Biophysica Acta (BBA …. 1995;1240(2):216–28.

209. Li XX, Davis B, Haridas V, Gutterman JU, Colombini M. Proapoptotic triterpene electrophiles (avicins) form channels in membranes: cholesterol dependence. Biophysical Journal. Elsevier; 2005 Apr;88(4):2577–84.

210. Armah CN, Mackie AR, Roy C, Price K, Osbourn AE. The membrane-permeabilizing effect of avenacin A-1 involves the reorganization of bilayer cholesterol. Biophysical Journal. 1999;76(1):281–90.

211. NISHIKAWA M, NOJIMA S, AKIYAMA T, SANKAWA U, INOUE K. Interaction of Digitonin and Its Analogs with Membrane Cholesterol. J Biochem (Tokyo). The Japanese Biochemical Society; 1984 Oct 1;96(4):1231–9.

212. Smith WS, Baker EJ, Holmes SE, Koster G, Hunt AN, Johnston DA, Flavell SU, Flavell DJ. Membrane cholesterol is essential for triterpenoid saponin augmentation of a saporin-based immunotoxin directed against CD19 on human lymphoma cells. BBA - Biomembranes. Elsevier B.V; 2017 May 1;1859(5):993–1007.

213. Segal R, Milo-Goldzweig I. The susceptibility of cholesterol-depleted erythrocytes to saponin and sapogenin hemolysis. Biochimica et Biophysica Acta (BBA)- …. 1978;512(1):223–6.

214. Hu M, Konoki K, Tachibana K. Cholesterol-independent membrane disruption caused by triterpenoid saponins. Biochimica et Biophysica Acta (BBA)-Lipids …. 1996;1299(2):252–8.

215. Bangham AD, Horne RW. Action of saponin on biological cell membranes. Vol. 196, Nature. 1962. 2 p.

216. Glauert. Action of saponin on biological cell membranes. Nature. 1962 May 13;:1–3.

217. Seeman P, Cheng D, Iles GH. STRUCTURE OF MEMBRANE HOLES IN OSMOTIC AND SAPONIN HEMOLYSIS. J Cell Biol. Rockefeller University Press; 1973 Feb 1;56(2):519–27.

218. Segal R, Mansour M, Zaitschek DV. Effect of ester groups on the haemolytic action of some saponins and sapogenins. Biochemical Pharmacology. 1966;15(10):1411–6.

219. Gauthier C, Legault J, Girard-Lalancette K, Mshvildadze V, Pichette A. Haemolytic activity, cytotoxicity and membrane cell permeabilization of semi-synthetic and natural lupane- and oleanane-type saponins. Bioorganic & Medicinal Chemistry. Elsevier Ltd; 2009 Mar 1;17(5):2002–8.

220. Melzig MF, Bader G, Loose R. Investigations of the mechanism of membrane activity of selected triterpenoid saponins. Planta Med. 2001;67(1):43–8.

221. Takechi M, Uno C, Tanaka Y. Structure-activity relationships of synthetic saponins. Phytochemistry. 1996;41(1):121–3.

222. Wang Y, Zhang Y, Zhu Z, Zhu S, Li Y, Li M, Yu B. Exploration of the correlation between the structure, hemolytic activity, and cytotoxicity of steroid saponins. Bioorganic & Medicinal Chemistry. 2007 Apr;15(7):2528–32.

223. Takechi M, Shimada S, Tanaka Y. Structure-activity relationships of the saponins dioscin and dioscinin. Phytochemistry. 1991;30(12):3943–4.

224. Chwalek M, Plé K, Voutquenne-Nazabadioko L. Synthesis and Hemolytic Activity of Some Hederagenin Diglycosides. Chem Pharm Bull. The Pharmaceutical Society of Japan; 2004;52(8):965–71.

225. Woldemichael GM, Wink M. Identification and biological activities of triterpenoid saponins from Chenopodium quinoa. J Agric Food Chem. 2001 May;49(5):2327–32.

226. Voutquenne L, Lavaud C, Massiot G, Men-Olivier LL. Structure-Activity Relationships of Haemolytic Saponins. Pharmaceutical Biology (Formerly International Journal of Pharmacognosy). 2002 Jun 1;40(4):253–62.

227. Hebestreit P, Melzig MF. Cytotoxic activity of the seeds from Agrostemma githago var. githago. Planta Med. © Georg Thieme Verlag Stuttgart · New York; 2003 Oct;69(10):921–5.

228. Melzig MF, Hebestreit P, Gaidi G. Structure-activity-relationship of saponins to enhance toxic effects of agrostin. Planta …. 2005.

229. Heisler I, Sutherland M, Bachran C, Hebestreit P, Schnitger A, Melzig MF, Fuchs H. Combined application of saponin and chimeric toxins drastically enhances the targeted cytotoxicity on tumor cells. Journal of Controlled Release. 2005 Aug;106(1-2):123–37.

230. Hebestreit P, Weng A, Bachran C, Fuchs H, Melzig MF. Enhancement of cytotoxicity of lectins by Saponinum album. Toxicon. 2006 Mar;47(3):330–5.

231. Böttger S, Westhof E, Siems K, Melzig MF. Structure–activity relationships of saponins enhancing the cytotoxicity of ribosome- inactivating proteins type I (RIP-I). Toxicon. Elsevier Ltd; 2013 Oct 1;73(C):144–50.

232. Gilabert-Oriol R, Thakur M, Haussmann K, Niesler N, Bhargava C, Görick C, Fuchs H, Weng A. Saponins from Saponaria officinalis L. Augment the Efficacy of a Rituximab-Immunotoxin. Planta Med. 2016 Jul 8;:1–8.

233. Gilabert-Oriol R, Mergel K, Thakur M, Mallinckrodt von B, Melzig MF, Fuchs H, Weng A. Real-time analysis of membrane permeabilizing effects of oleanane saponins. Bioorganic & Medicinal Chemistry. Elsevier Ltd; 2013 Apr 15;21(8):2387–95.

234. Weng A, Bachran C, Fuchs H, Melzig MF. Soapwort saponins trigger clathrin-mediated endocytosis of saporin, a type I ribosome-inactivating protein. Chemico-Biological Interactions. 2008 Nov;176(2-3):204–11.

235. Weng A, Bachran C, Fuchs H, Krause E, Stephanowitz H, Melzig MF. Enhancement of saporin cytotoxicity by Gypsophila saponins—More than stimulation of endocytosis. Chemico-Biological Interactions. 2009 Oct;181(3):424–9.

236. Bachran D, Schneider S, Bachran C, Weng A, Melzig MF, Fuchs H. The Endocytic Uptake Pathways of Targeted Toxins Are Influenced by

Synergistically Acting GypsophilaSaponins. Mol Pharmaceutics. 2011 Dec 5;8(6):2262–72.

237. Bachran C, Sutherland M, Heisler I, Hebestreit P, Melzig MF, Fuchs H. The saponin-mediated enhanced uptake of targeted saporin-based drugs is strongly dependent on the saponin structure. Experimental Biology and Medicine. 2006 Apr;231(4):412–20.

238. Sigismund S, Woelk T, Puri C, Maspero E, Tacchetti C, Pietro Transidico, Di Fiore PP, Polo S. Clathrin-independent endocytosis of ubiquitinated cargos. Proceedings of the National Academy of Sciences of the United States of America. National Acad Sciences; 2005 Feb 22;102(8):2760–5.

239. Pirie CM, Hackel BJ, Rosenblum MG, Wittrup KD. Convergent Potency of Internalized Gelonin Immunotoxins across Varied Cell Lines, Antigens, and Targeting Moieties. J Biol Chem. 2011 Feb 4;286(6):4165–72.

240. de Duve C, de Barsy T, Poole B, Trouet A, Tulkens P, Van Hoof F. Commentary. Lysosomotropic agents. Biochemical Pharmacology. 1974 Sep 15;23(18):2495–531.

241. Bowman EJ, Siebers A, Altendorf K. Bafilomycins: a class of inhibitors of membrane ATPases from microorganisms, animal cells, and plant cells. Proceedings of the National Academy of Sciences of the United States of America. National Academy of Sciences; 1988 Nov 1;85(21):7972–6.

242. Huotari J, Helenius A. Focus Review Endosome maturation. The EMBO Journal. Nature Publishing Group; 2011 Aug 31;30(17):3481–500.

243. Schmid EM, Ford MGJ, Burtey A, Praefcke GJK, Peak-Chew S-Y, Mills IG, Benmerah A, McMahon HT. Role of the AP2 β-Appendage Hub in Recruiting Partners for Clathrin-Coated Vesicle Assembly. Hughson F, editor. PLoS Biol. Public Library of Science; 2006 Aug 15;4(9):e262–17.

244. Damke H, Baba T, Warnock DE, Schmid SL. Induction of mutant dynamin specifically blocks endocytic coated vesicle formation. J Cell Biol. The Rockefeller University Press; 1994 Nov 2;127(4):915–34.

245. Praefcke GJK, McMahon HT. The dynamin superfamily: universal membrane tubulation and fission molecules? Nat Rev Mol Cell Biol. 2004 Feb;5(2):133–47.

246. Elkin SR, Lakoduk AM, Schmid SL. Endocytic pathways and endosomal trafficking: a primer. Wien Med Wochenschr. Springer Vienna; 2016 Feb 9;166(7-8):196–204.

247. Wang LH, Rothberg KG, Anderson RG. Mis-assembly of clathrin lattices on endosomes reveals a regulatory switch for coated pit formation. J Cell Biol. Rockefeller University Press; 1993 Dec 1;123(5):1107–17.

248. Vercauteren D, Vandenbroucke RE, Jones AT, Rejman J, Demeester J, De Smedt SC, Sanders NN, Braeckmans K. The Use of Inhibitors to Study Endocytic Pathways of Gene Carriers: Optimization and Pitfalls. Molecular Therapy. Nature Publishing Group; 2009 Nov 13;18(3):561–9.

249. Ivanov AI. Pharmacological inhibition of endocytic pathways: is it specific enough to be useful? Methods Mol Biol. Totowa, NJ: Humana Press; 2008;440(Chapter 2):15–33.

250. Mayor S, Parton RG. Clathrin-independent pathways of endocytosis. Cold Spring Harbor …. 2014.

251. Cheng JPX, Nichols BJ. Caveolae: One Function or Many? Trends in Cell Biology. Elsevier Ltd; 2016 Mar 1;26(3):177–89.

252. Shvets E, Ludwig A, Nichols BJ. News from the caves: update on the structure and function of caveolae. Current Opinion in Cell Biology. 2014.

253. Lim JP, Gleeson PA. Macropinocytosis: an endocytic pathway for internalising large gulps. Immunology and Cell Biology. 2011.

254. Sallusto F, Cella M, Danieli C, Lanzavecchia A. Dendritic cells use macropinocytosis and the mannose receptor to concentrate macromolecules in the major histocompatibility complex class II compartment: downregulation by cytokines and bacterial products. Journal of Experimental Medicine. Rockefeller University Press; 1995 Aug 1;182(2):389–400.

255. Racoosin EL, Swanson JA. Macropinosome maturation and fusion with tubular lysosomes in macrophages. J Cell Biol. Rockefeller University Press; 1993 Jun 1;121(5):1011–20.

256. Doherty GJ, McMahon HT. Mechanisms of Endocytosis. Annu Rev Biochem. 2009 Jun;78(1):857–902.

257. Corrotte M, Almeida PE, Tam C, Castro-Gomes T, Fernandes MC, Millis BA, Cortez M, Miller H, Song W, Maugel TK, Andrews NW. Caveolae internalization repairs wounded cells and muscle fibers. eLife. 2013 Sep 17;2:206–30.

258. Idone V, Tam C, Goss JW, Toomre D, Pypaert M, Andrews NW. Repair of injured plasma membrane by rapid Ca 2+-dependent endocytosis. J Cell Biol. 2008 Mar 10;180(5):905–14.

259. Bi GQ, Alderton JM, Steinhardt RA. Calcium-regulated exocytosis is required for cell membrane resealing. J Cell Biol. Rockefeller University Press; 1995 Dec 15;131(6):1747–58.

260. Reddy A, Caler EV, Andrews NW. Plasma membrane repair is mediated by Ca 2+-regulated exocytosis of lysosomes. Cell. 2001.

261. Tam C, Idone V, Devlin C, Fernandes MC, Flannery A, He X, Schuchman E, Tabas I, Andrews NW. Exocytosis of acid sphingomyelinase by wounded cells promotes endocytosis and plasma membrane repair. J Cell Biol. 2010 Jun 14;189(6):1027–38.

262. Holopainen JM, Angelova MI, Kinnunen PK. Vectorial budding of vesicles by asymmetrical enzymatic formation of ceramide in giant liposomes. Biophysical Journal. 2000 Feb;78(2):830–8.

263. Fra AM, Williamson E, Simons K, Parton RG. Detergent-insoluble glycolipid microdomains in lymphocytes in the absence of caveolae. J Biol Chem. 1994 Dec 9;269(49):30745–8.

264. Miller H, Castro-Gomes T, Corrotte M, Tam C, Maugel TK, Andrews NW, Song W. Lipid raft–dependent plasma membrane repair interferes with the activation of B lymphocytes. J Cell Biol. Rockefeller University Press; 2015 Dec 21;211(6):1193–205.

265. Lariccia V, Fine M, Magi S, Lin M-J, Yaradanakul A, Llaguno MC, Hilgemann DW. Massive calcium-activated endocytosis without involvement of classical endocytic proteins. J Gen Physiol. Rockefeller University Press; 2011 Jan;137(1):111–32.

266. Corrotte M, Fernandes MC, Tam C, Andrews NW. Toxin Pores Endocytosed During Plasma Membrane Repair Traffic into the Lumen of MVBs for Degradation. Traffic. 2012 Jan 24;13(3):483–94.

267. Luisoni S, Suomalainen M, Boucke K, Tanner LB, Wenk MR, Guan XL, Grzybek M, Coskun Ü, Greber UF. Co-option of Membrane Wounding Enables Virus Penetration into Cells. Cell Host and Microbe. Elsevier Inc; 2015 Jul 8;18(1):75–85.

268. Nagahama M, Takehara M, Takagishi T, Seike S, Miyamoto K, Kobayashi K. Cellular Uptake of Clostridium botulinum C2 Toxin Requires Acid Sphingomyelinase Activity. Infect Immun. American Society for Microbiology; 2017 Apr;85(4):e00966–16.

269. Weng A, Bachran D, G rick C, Bachran C, Fuchs H, Melzig M. A Simple Method for Isolation of GypsophilaSaponins for the Combined Application of Targeted Toxins and Saponins in Tumor Therapy. Planta Med. © Georg Thieme Verlag KG Stuttgart · New York; 2009 May 18;75(13):1421–2.

270. Klein E, Klein G, Nadkarni JS, Nadkarni JJ, Wigzell H, Clifford P. Surface IgM-kappa specificity on a Burkitt lymphoma cell in vivo and in derived culture lines. Cancer Res. American Association for Cancer Research; 1968 Jul;28(7):1300–10.

271. Adams RA, Flowers A, Davis BJ. Direct implantation and serial transplantation of human acute lymphoblastic leukemia in hamsters, SB-2. Cancer Res. American Association for Cancer Research; 1968 Jun;28(6):1121–5.

272. Scudiero DA, Shoemaker RH, Paull KD, Monks A. Evaluation of a soluble tetrazolium/formazan assay for cell growth and drug sensitivity in culture using human and other tumor cell lines. Cancer Res. 1988.

273. Roehm NW, Rodgers GH, Hatfield SM, Glasebrook AL. An improved colorimetric assay for cell proliferation and viability utilizing the tetrazolium salt XTT. Journal of Immunological Methods. 1991 Sep;142(2):257–65.

274. Reynolds ES. THE USE OF LEAD CITRATE AT HIGH pH AS AN ELECTRON-OPAQUE STAIN IN ELECTRON MICROSCOPY. J Cell Biol. The Rockefeller University Press; 1963 Apr 1;17(1):208–12.

275. Lock JT, Parker I, Smith IF. A comparison of fluorescent Ca2+ indicators for imaging local Ca2+ signals in cultured cells. Cell Calcium. 2015 Dec;58(6):638–48.

276. Kölzer M, Werth N, Sandhoff K. Interactions of acid sphingomyelinase and lipid bilayers in the presence of the tricyclic antidepressant desipramine. FEBS Letters. Wiley-Blackwell; 2004 Jan 21;559(1-3):96–8.

277. Beckmann N, Sharma D, Gulbins E, in KBF, 2014. Inhibition of acid sphingomyelinase by tricyclic antidepressants and analogons. frontiersinorg

.

278. Kornhuber J, Tripal P, Reichel M, Terfloth L, Bleich S, Wiltfang J, Gulbins E. Identification of new functional inhibitors of acid sphingomyelinase using a structure-property-activity relation model. J Med Chem. 2008 Jan 24;51(2):219–37.

279. Ishizaki J, Yokogawa K, Hirano M, Nakashima E, Sai Y, Ohkuma S, Ohshima T, Ichimura F. Contribution of lysosomes to the subcellular distribution of basic drugs in the rat liver. Pharm Res. 1996 Jun;13(6):902–6.

280. Hurwitz R, Ferlinz K, Sandhoff K. The tricyclic antidepressant desipramine causes proteolytic degradation of lysosomal sphingomyelinase in human fibroblasts. Biol Chem Hoppe-Seyler. 1994 Jul;375(7):447–50.

281. Mazzucchelli GD, Cellier NA, Mshviladzade V, Elias R, Shim Y-H, Touboul D, Quinton L, Brunelle A, Laprévote O, De Pauw EA, De Pauw-Gillet M-CA. Pores Formation on Cell Membranes by Hederacolchiside A1 Leads to a Rapid Release of Proteins for Cytosolic Subproteome Analysis. Journal of proteome …. American Chemical Society; 2008 Mar 14.

282. Abe H, Konishi H, Komiya H, Arichi S. Effects of saikosaponins on biological membranes. 3. Ultrastructural studies on effects of saikosaponins on the cell surface. Planta Med. 1981 Aug;42(4):356–63.

283. Clapham DE. Calcium Signaling. Cell. 2007 Dec;131(6):1047–58.

284. Hoeflich KP, Ikura M. Calmodulin in action: diversity in target recognition and activation mechanisms. Cell. 2002 Mar 22;108(6):739–42.

285. Machaca K. Ca2+ signaling, genes and the cell cycle. Cell Calcium. Elsevier Ltd; 2011 May 1;49(5):323–30.

286. Parsons PG, Musk P, Goss PD, Leah J. Effects of calcium depletion on human cells in vitro and the anomalous behavior of the human melanoma cell line MM170. Cancer Res. 1983 May;43(5):2081–7.

287. Humeau J, Pedro JMB-S, Vitale I, Nuñez L, Villalobos C, Kroemer G, Senovilla L. Calcium signaling and cell cycle: progression or death. Cell Calcium. Elsevier Ltd; 2017 Jul 25;:1–43.

288. Lynch K, Fernandez G, Pappalardo A, Peluso JJ. Basic fibroblast growth factor inhibits apoptosis of spontaneously immortalized granulosa cells by regulating intracellular free calcium levels through a protein kinase Cdelta-dependent pathway. Endocrinology. 2000 Nov;141(11):4209–17.

289. Voccoli V, Tonazzini I, Signore G, Caleo M, Cecchini M. Role of extracellular calcium and mitochondrial oxygen species in psychosine-induced oligodendrocyte cell death. Nature Publishing Group; 2014 Nov 11;5(11):e1529–10.

290. Rizzuto R, Pinton P, Ferrari D, Chami M, Szabadkai G, Magalhães PJ, Virgilio FD, Pozzan T. Calcium and apoptosis: facts and hypotheses. Oncogene. Nature Publishing Group; 2003 Nov 24;22(53):8619–27.

291. Bootman MD, Collins TJ, Peppiatt CM, Prothero LS, MacKenzie L, De Smet P, Travers M, Tovey SC, Seo JT, Berridge MJ, Ciccolini F, Lipp P. Calcium signalling—an overview. Seminars in Cell and Developmental Biology. 2001 Feb;12(1):3–10.

292. Carriedo SG, Yin HZ, Sensi SL, Weiss JH. Rapid Ca2+ entry through Ca2+-permeable AMPA/Kainate channels triggers marked intracellular Ca2+ rises and consequent oxygen radical production. J Neurosci. 1998 Oct 1;18(19):7727–38.

293. Orrenius S, Zhivotovsky B, Nicotera P. Regulation of cell death: the calcium-apoptosis link. Nat Rev Mol Cell Biol. 2003 Jul;4(7):552–65.

294. Kornhuber J, Tripal P, Reichel M, Mühle C, Rhein C, Muehlbacher M, Groemer TW, Gulbins E. Functional Inhibitors of Acid Sphingomyelinase (FIASMAs): a novel pharmacological group of drugs with broad clinical applications. Cell Physiol Biochem. 2010;26(1):9–20.

295. Andrews NW, Almeida PE, Corrotte M. Damage control: cellular mechanisms of plasma membrane repair. Trends in Cell Biology. Elsevier Ltd; 2014 Dec 1;24(12):734–42.

296. Vines A, McBean GJ, Blanco-Fernández A. A flow-cytometric method for continuous measurement of intracellular Ca2+ concentration. Cytometry. John Wiley & Sons, Ltd; 2010 Sep 24;77A(11):1091–7.

297. Koivusalo M, Welch C, Hayashi H, Scott CC, Kim M, Alexander T, Touret N, Hahn KM, Grinstein S. Amiloride inhibits macropinocytosis by lowering submembranous pH and preventing Rac1 and Cdc42 signaling. J Cell Biol. 2010 Feb 22;188(4):547–63.

298. El-Sayed A, Harashima H. Endocytosis of Gene Delivery Vectors: From Clathrin-dependent to Lipid Raft-mediated Endocytosis. Molecular Therapy. 2013 Jun;21(6):1118–30.

299. Hoebeke J, Van Nijen G, De Brabander M. Interaction of oncodazole (R 17934), a new antitumoral drug, with rat brain tubulin. Biochemical and Biophysical Research Communications. 1976 Mar 22;69(2):319–24.

300. Schliwa M. Action of cytochalasin D on cytoskeletal networks. J Cell Biol. Rockefeller University Press; 1982 Jan;92(1):79–91.

301. Smith W, Johnston D, Holmes S, Wensley HJ, Flavell S, Flavell D. Augmentation of Saporin-Based Immunotoxins for Human Leukaemia and Lymphoma Cells by Triterpenoid Saponins: The Modifying Effects of Small Molecule Pharmacological Agents. Toxins. Multidisciplinary Digital Publishing Institute; 2019 Feb;11(2):127–21.

302. Granger E, McNee G, Allan V, Woodman P. The role of the cytoskeleton and molecular motors in endosomal dynamics. Seminars in Cell and Developmental Biology. Elsevier Ltd; 2014 Jul 1;31:20–9.

303. Bayer N, Schober D, Prchla E, Murphy RF, Blaas D, Fuchs R. Effect of bafilomycin A1 and nocodazole on endocytic transport in HeLa cells: implications for viral uncoating and infection. J Virol. 1998 Dec;72(12):9645–55.

304. Togo T. Disruption of the plasma membrane stimulates rearrangement of microtubules and lipid traffic toward the wound site. Journal of Cell Science. The Company of Biologists Ltd; 2006 Jul 1;119(Pt 13):2780–6.

305. Rabinovitch M. Professional and non-professional phagocytes: an introduction. Trends in Cell Biology. 1995 Mar;5(3):85–7.

306. Merrifield CJ, Perrais D, Zenisek D. Coupling between Clathrin-Coated-Pit Invagination, Cortactin Recruitment, and Membrane Scission Observed in Live Cells. Cell. Elsevier Inc; 2005 May 20;121(4):593–606.

307. Mooren OL, Galletta BJ, Cooper JA. Roles for Actin Assembly in Endocytosis. Annu Rev Biochem. 2012 Jul 7;81(1):661–86.

308. Gilabert-Oriol R, Thakur M, Mallinckrodt von B, Bhargava C, Wiesner B, Eichhorst J, Melzig M, Fuchs H, Weng A. Reporter Assay for Endo/Lysosomal

Escape of Toxin-Based Therapeutics. Toxins. Multidisciplinary Digital Publishing Institute; 2014 May;6(5):1644–66.

309. Kang K, Lee SB, Yoo J-H, Nho CW. Flow cytometric fluorescence pulse width analysis of etoposide-induced nuclear enlargement in HCT116 cells. Biotechnology Letters. 2010 Apr 29;32(8):1045–52.

310. Ramdzan YM, Polling S, Chia CPZ, Ng IHW, Ormsby AR, Croft NP, Purcell AW, Bogoyevitch MA, Ng DCH, Gleeson PA, Hatters DM. Tracking protein aggregation and mislocalization in cells with flow cytometry. Nature Methods 2012 9:5. Nature Publishing Group; 2012 May 1;9(5):467–70.

311. Chia PZC, Ramdzan YM, Houghton FJ, Hatters DM, Gleeson PA. High-Throughput Quantitation of Intracellular Trafficking and Organelle Disruption by Flow Cytometry. Traffic. John Wiley & Sons, Ltd (10.1111); 2014 May 1;15(5):572–82.

312. Fang C, Li T, Li Y, Xu GJ, Deng QW, Chen YJ, Hou YN, Lee HC, Zhao YJ. CD38 produces nicotinic acid adenosine dinucleotide phosphate in the lysosome. J Biol Chem. American Society for Biochemistry and Molecular Biology; 2018 May 25;293(21):8151–60.

313. ZOCCHI E, FRANCO L, GUIDA L, Piccini D, Tacchetti C, De Flora A. NAD+-dependent internalization of the transmembrane glycoprotein CD38 in human Namalwa B cells. FEBS Letters. 1996 Nov 4;396(2-3):327–32.

314. Soraj Al M, He L, Peynshaert K, Cousaert J, Vercauteren D, Braeckmans K, De Smedt SC, Jones AT. siRNA and pharmacological inhibition of endocytic pathways to characterize the differential role of macropinocytosis and the actin cytoskeleton on cellular uptake of dextran and cationic cell penetrating peptides octaarginine (R8) and HIV-Tat. Journal of Controlled Release. Elsevier B.V; 2012 Jul 10;161(1):132–41.

315. Ogiso T, Iwaki M, Mori K. Fluidity of human erythrocyte membrane and effect of chlorpromazine on fluidity and phase separation of membrane. Biochim Biophys Acta. 1981 Dec 7;649(2):325–35.

316. Murata T, Maruoka N, Omata N, Takashima Y, Fujibayashi Y, Yonekura Y, Wada Y. A comparative study of the plasma membrane permeabilization and fluidization induced by antipsychotic drugs in the rat brain. Int J Neuropsychopharm. 2006 Sep 18;10(05):289–7.

317. Giocondi MC, Mamdouh Z, Le Grimellec C. Benzyl alcohol differently affects fluid phase endocytosis and exocytosis in renal epithelial cells. Biochim Biophys Acta. 1995 Mar 22;1234(2):197–202.

318. Marshak DR, Lukas TJ, Watterson DM. Drug-protein interactions: binding of chlorpromazine to calmodulin, calmodulin fragments, and related calcium binding proteins. Biochemistry. 1985 Jan 1;24(1):144–50.

319. Walenga RW, Opas EE, Feinstein MB. Differential effects of calmodulin antagonists on phospholipases A2 and C in thrombin-stimulated platelets. J Biol Chem. 1981 Dec 10;256(23):12523–8.

320. Wells A, Ware MF, Allen FD, Lauffenburger DA. Shaping up for shipping out: PLCgamma signaling of morphology changes in EGF-stimulated fibroblast migration. Cell Motil Cytoskeleton. 1999 Dec;44(4):227–33.

321. Amyere M, Payrastre B, Krause U, Van Der Smissen P, Veithen A, Courtoy PJ. Constitutive macropinocytosis in oncogene-transformed fibroblasts depends on sequential permanent activation of phosphoinositide 3-kinase and phospholipase C. Mol Biol Cell. 2000 Oct;11(10):3453–67.

322. Masson M, Spezzatti B, Chapman J, Battisti C, Baumann N. Calmodulin antagonists chlorpromazine and W-7 inhibit exogenous cholesterol esterification and sphingomyelinase activity in human skin fibroblast cultures. Similarities between drug-induced and Niemann-Pick type C lipidoses. J Neurosci Res. Wiley-Blackwell; 1992 Jan;31(1):84–8.

323. Lange Y, Ye J, Steck TL. Activation Mobilizes the Cholesterol in the Late Endosomes-Lysosomes of Niemann Pick Type C Cells. Gasset M, editor. PLOS ONE. Public Library of Science; 2012 Jan 20;7(1):e30051–12.

324. Lagana A, Vadnais J, Le PU, Nguyen TN, Laprade R, Nabi IR, Noel J. Regulation of the formation of tumor cell pseudopodia by the Na(+)/H(+) exchanger NHE1. Journal of Cell Science. 2000 Oct;113 (Pt 20):3649–62.

325. Lee E, Knecht DA. Visualization of actin dynamics during macropinocytosis and exocytosis. Traffic. 2002 Mar;3(3):186–92.

326. Heuser J. The role of coated vesicles in recycling of synaptic vesicle membrane. Cell Biol Int Rep. 1989 Dec;13(12):1063–76.

327. Dutta D, Donaldson JG. Search for inhibitors of endocytosis. Cellular Logistics. 2014 Oct 27;2(4):203–8.

328. Boucrot E, Saffarian S, Massol R, Kirchhausen T, Ehrlich M. Role of lipids and actin in the formation of clathrin-coated pits. Exp Cell Res. 2006 Dec;312(20):4036–48.

329. Fujimoto LM, Roth R, Heuser JE, Schmid SL. Actin assembly plays a variable, but not obligatory role in receptor-mediated endocytosis in mammalian cells. Traffic. 2000 Feb;1(2):161–71.

330. Baravalle G, Schober D, Huber M, Bayer N, Murphy RF, Fuchs R. Transferrin recycling and dextran transport to lysosomes is differentially affected by bafilomycin, nocodazole, and low temperature. Cell Tissue Res. 2005 Apr;320(1):99–113.

331. Mellman I, Fuchs R, Helenius A. Acidification of the endocytic and exocytic pathways. Annu Rev Biochem. 1986;55(1):663–700.

332. Redmann M, Benavides GA, Berryhill TF, Wani WY, Ouyang X, Johnson MS, Ravi S, Barnes S, Darley-Usmar VM, Zhang J. Inhibition of autophagy with bafilomycin and chloroquine decreases mitochondrial quality and bioenergetic function in primary neurons. Redox Biology. Elsevier B.V; 2017 Apr 1;11:73–81.

333. Yuan N, Song L, Zhang S, Lin W, Cao Y, Xu F, Fang Y, Wang Z, Zhang H, Li X, Wang Z, Cai J, Wang J, Zhang Y, Mao X, Zhao W, Hu S, Chen S, Wang J. Bafilomycin A1 targets both autophagy and apoptosis pathways in pediatric B-cell acute lymphoblastic leukemia. Haematologica. Haematologica; 2015 Mar;100(3):345–56.

334. Lippincott-Schwartz J, Fambrough DM. Cycling of the integral membrane glycoprotein, LEP100, between plasma membrane and lysosomes: kinetic and morphological analysis. Cell. 1987 Jun 5;49(5):669–77.

335. Chapman RE, Munro S. Retrieval of TGN proteins from the cell surface requires endosomal acidification. The EMBO Journal. 1994 May 15;13(10):2305–12.

336. Pearse BM, Robinson MS. Clathrin, adaptors, and sorting. Annu Rev Cell Biol. 1990;6(1):151–71.

337. Wang JTH, Teasdale RD, Liebl D. Macropinosome quantitation assay. MethodsX. 2014;1:36–41.

338. Peterson JR, Mitchison TJ. Small Molecules, Big Impact: A History of Chemical Inhibitors and the Cytoskeleton. Chemistry & Biology. Cell Press; 2002 Dec 1;9(12):1275–85.

339. Signoretto E, Honisch S, Briglia M, Faggio C, Castagna M, Lang F. Nocodazole Induced Suicidal Death of Human Erythrocytes. Cell Physiol Biochem. 2016;38(1):379–92.

340. Ma L, Ouyang Q, Werthmann GC, Thompson HM, Morrow EM. Live-cell Microscopy and Fluorescence-based Measurement of Luminal pH in Intracellular Organelles. Front Cell Dev Biol. Frontiers; 2017 Aug 21;5:357–18.

341. Chen LB. Mitochondrial membrane potential in living cells. Annu Rev Cell Biol. 1988;4:155–81.

342. Boya P, Kroemer G. Lysosomal membrane permeabilization in cell death. Oncogene. Nature Publishing Group; 2008 Oct 27;27(50):6434–51.

343. Gilabert-Oriol R, Thakur M, Mallinckrodt von B, Hug T, Wiesner B, Eichhorst J, Melzig MF, Fuchs H, Weng A. Modified Trastuzumab and Cetuximab Mediate Efficient Toxin Delivery While Retaining Antibody-Dependent Cell-Mediated Cytotoxicity in Target Cells. Mol Pharmaceutics. 2013 Nov 4;10(11):4347–57.

344. Rieger AM, Nelson KL, Konowalchuk JD, Barreda DR. Modified Annexin V/Propidium Iodide Apoptosis Assay For Accurate Assessment of Cell Death. JoVE. 2011;(50):1–4.

345. Darzynkiewicz Z, Pozarowski P, Lee BW, Johnson GL. Fluorochrome-labeled inhibitors of caspases: convenient in vitro and in vivo markers of apoptotic cells for cytometric analysis. Methods Mol Biol. 2011;682:103–14.

346. Wallberg F, Tenev T, Meier P. Analysis of Apoptosis and Necroptosis by Fluorescence-Activated Cell Sorting. Cold Spring Harb Protoc. 2016 Apr 1;2016(4):pdb.prot087387.

347. Lorent JH, Quetin-Leclercq J, Mingeot-Leclercq M-P. The amphiphilic nature of saponins and their effects on artificial and biological membranes and potential consequences for red blood and cancer cells. Org Biomol Chem. 2014 Sep 15;12(44):8803–22.

348. Zhu S, Shimokawa S, Shoyama Y, Tanaka H. A novel analytical ELISA-based methodology for pharmacologically active saikosaponins. Fitoterapia. 2006 Feb;77(2):100–8.

349. Zhu S-H, Shimokawa S-I, Tanaka H, Shoyama Y. Development of an Assay System for Saikosaponin a Using Anti-saikosaponin a Monoclonal Antibodies. Biological and Pharmaceutical Bulletin. The Pharmaceutical Society of Japan; 2004;27(1):66–71.

350. Phrompittayarat W, Putalun W, Tanaka H, Wittaya-Areekul S, Jetiyanon K, Ingkaninan K. An enzyme-linked immunosorbant assay using polyclonal antibodies against bacopaside I. Analytica Chimica Acta. 2007 Feb;584(1):1–6.

351. Yamada R, Takeshita T, Hiraizumi M, Shinohe D, Ohta Y, Sakurai K. Fluorescent analog of OSW-1 and its cellular localization. Bioorganic & Medicinal Chemistry Letters. Elsevier Ltd; 2014 Apr 1;24(7):1839–42.

352. Raman CV, KRISHNAN KS. A New Type of Secondary Radiation. Nature. Nature Publishing Group; 1928 Mar 1;121(3048):501–2.

353. Smith R, Wright KL, Ashton L. Raman spectroscopy: an evolving technique for live cell studies. Analyst. Royal Society of Chemistry; 2016;141(12):3590–600.

354. Zoladek A, Pascut F, Patel P, Notingher I. Development of Raman Imaging System for time-course imaging of single living cells. Journal of Spectroscopy. Hindawi; 2010;24(1-2):131–6.

355. Klein K, Gigler AM, Aschenbrenner T, Monetti R, Bunk W, Jamitzky F, Morfill G, Stark RW, Schlegel J. Label-Free Live-Cell Imaging with Confocal Raman Microscopy. Biophysical Journal. Biophysical Society; 2012 Jan 18;102(2):360–8.

356. Krauß SD, Petersen D, Niedieker D, Fricke I, Freier E, El-Mashtoly SF, Gerwert K, Mosig A. Colocalization of fluorescence and Raman microscopic images for

the identification of subcellular compartments: a validation study. Analyst. Royal Society of Chemistry; 2015;140(7):2360–8.

357. Bachran C, Dürkop H, Sutherland M, Bachran D, Müller C, Weng A, Melzig MF, Fuchs H. Inhibition of Tumor Growth by Targeted Toxins in Mice is Dramatically Improved by Saponinum Album in a Synergistic Way. Journal of Immunotherapy. 2009 Sep 1;32(7):713–25.

358. Thakur M, Mergel K, Weng A, Mallinckrodt von B, Gilabert-Oriol R, Dürkop H, Melzig MF, Fuchs H. Targeted tumor therapy by epidermal growth factor appended toxin and purified saponin: An evaluation of toxicity and therapeutic potential in syngeneic tumor bearing mice. Molecular Oncology. Elsevier B.V; 2013 Jun 1;7(3):475–83.

359. Mallinckrodt BV, Thakur M, Weng A, Gilabert-Oriol R, Dürkop H, Brenner W, Lukas M, Beindorff N, Melzig MF, Fuchs H. Dianthin-EGF is an effective tumor targeted toxin in combination with saponins in a xenograft model for colon carcinoma. Future Oncology. 2014 Nov;10(14):2161–75.

360. Bhargava C, Dürkop H, Zhao X, Weng A, Melzig MF, Fuchs H. Targeted dianthin is a powerful toxin to treat pancreatic carcinoma when applied in combination with the glycosylated triterpene SO1861. Molecular Oncology. 2017 Sep 15;11(11):1527–43.

361. Gao S, Basu S, Yang Z, Deb A, Hu M. Bioavailability challenges associated with development of saponins as therapeutic and chemopreventive agents. Curr Drug Targets. 2012 Dec;13(14):1885–99.

362. Maes L. Intravenous and Subcutaneous Toxicity and Absorption Kinetics in Mice and Dogs of the Antileishmanial Triterpene Saponin PX-6518. Molecules. Multidisciplinary Digital Publishing Institute; 2013 Apr;18(4):4803–15.

363. Wojciechowski K, Orczyk M, Gutberlet T, Geue T. Complexation of phospholipids and cholesterol by triterpenic saponins in bulk and in monolayers. BBA - Biomembranes. Elsevier B.V; 2016 Feb 1;1858(2):363–73.

364. Cristina Della P, Castagna M, Lombardi A, Barison E, Tagliabue G, Ceriotti A, Koutris I, Di Leandro L, Giansanti F, Vago R, Ippoliti R, Flavell SU, Flavell DJ, Colombatti M, FABBRINI MS. Systematic comparison of single-chain Fv antibody-fusion toxin constructs containing Pseudomonas Exotoxin A or saporin produced in different microbial expression systems. Microb Cell Fact. BioMed Central; 2015 Feb 13;14(1):19–17.

365. Orciani M, Cavaletti G, Fino V, Mattioli-Belmonte M, Tredici G, Bruni P, Di Primio R. Exploiting CD38-mediated endocytosis for immunoliposome internalization. Anti-Cancer Drugs. 2008 Jul 1;19(6):599–605.

366. Alavizadeh SH, Soltani F, Ramezani M. Recent Advances in Immunoliposome-Based Cancer Therapy. Current Pharmacology Reports. Current Pharmacology Reports; 2016 Apr 26;:1–13.

367. Sundström C, Nilsson K. Establishment and characterization of a human histiocytic lymphoma cell line (U-937). Int J Cancer. John Wiley & Sons, Ltd; 1976 May 15;17(5):565–77.

368. Xu X, Padilla MT, Li B, Wells A, Kato K, Tellez C, Belinsky SA, Kim KC, Lin Y. MUC1 in macrophage: contributions to cigarette smoke-induced lung cancer. Cancer Res. American Association for Cancer Research; 2014 Jan 15;74(2):460–70.

369. Schindelin J, Arganda-Carreras I, Frise E, Kaynig V, Longair M, Pietzsch T, Preibisch S, Rueden C, Saalfeld S, Schmid B, Tinevez J-Y, White DJ, Hartenstein V, Eliceiri K, Tomancak P, Cardona A. Fiji: an open-source platform for biological-image analysis. Nature Methods 2012 9:5. Nature Publishing Group; 2012 Jun 28;9(7):676–82.